Closed Loop Wet Scrubber System for Maritime Application

Dynamic Modelling and System Integration

Enri Elmazi

TU Delft

Challenge the future

CLOSED LOOP WET SCRUBBER SYSTEM FOR MARITIME APPLICATION

DYNAMIC MODELLING AND SYSTEM INTEGRATION

by

Enri Elmazi

in partial fulfilment of the requirements for the degree of

Master of Science
in Marine Technology

at the Delft University of Technology,
to be defended publicly on Tuesday March 31, 2020 at 10:45 AM.

Student number:	4747038
Thesis number:	SDPO.20.004.m.
MTI report number:	AO 164

Thesis committee:

Ir. K. Visser	TU Delft, Chairman
Dr.Ir. P. de Vos	TU Delft, Daily Supervisor
Ir. B.T.W. Mestemaker	Royal IHC , Daily Supervisor
Assoc. Prof. Dr.Ir. C.A. Infante Ferreira	TU Delft, External Committee Member

Dedicated to my family.
To Shkëlqim, Mirela and Matea

Enri Elmazi

SUMMARY

The maritime sector is important for the facilitation and growth of global trade. Currently, about 90% of the goods are transported by ships and as a result, the number of ships has risen, increasing the emissions related to shipping. Pollution caused by exhaust gas, especially the sulphur oxide emission, from marine diesel engines has become a global concern in recent years. Therefore, the International Maritime Organisation limited marine fuel sulphur content in both Emission Control Areas to 0.1%w/w since 2015 and globally to 0.5%w/w since January 1^{st}, 2020. It is anticipated, that the newly implemented IMO regulations will help to mitigate negative impact of ship emissions on public health and the environment in the coastal areas.

The wet scrubber system is a reliable technology for flue gas desulphurisation in marine applications and can achieve a sulphur dioxide removal efficiency of 98%. The operating costs are low, however the capital cost for installation are high and a scrubber system requires space for installation while maintaining ship's stability. Wet scrubber systems operating in a closed loop and using caustic soda may operate without discharge to the sea and thus are allowed to operate in ports. The use of caustic soda also makes it possible to use the scrubber in areas with low seawater alkalinity. However, scrubber systems generally operate at 100%, even when the engine operates at low load. This results in an increase of the fuel consumption and carbon dioxide emissions.

The main objectives of this research are to examine the influence of water evaporation on the sulphur dioxide removal efficiency and the (response of the scrubber) effect of dynamic loads on the scrubber efficiency. A dynamic model of a closed loop wet scrubber operating with fresh water and caustic soda also known as sodium hydroxide was created and verified. The scrubber model consists of three resistance elements, namely the venturi scrubber, the tower scrubber with a packed bed and the demister and two volume elements (lower and upper) to connect the resistance elements. The absorption of SO_2 is mainly taking place in the packed bed and the two phase flow of exhaust gas and scrubbing liquid was modelled in this section. The Nerst film theory was used and extended to a two film theory in which the exhaust gas and scrubbing liquid phases come into contact through an interface and exchange both heat and mass. The gas flow in the packed bed could be modelled with a combination of resistance and volume elements as this phase is compressible. The liquid flow and liquid film thickness in the packed bed were modelled based on the conservation of mass and the liquid holdup theory developed by Billet and Schultes. A feedback control system controls the scrubbing liquid flow based on the sulphur dioxide to carbon dioxide ratio. The system includes a time constant to account for the inertia of the scrubber's pump and pipe system. The verified model was integrated with engine data and used to run several static and dynamic simulations.

The inclusion of evaporation in the packed bed leads to an increase of the scrubber efficiency in all engine loads. The extra vapour added dilutes the gas phase and reduces the mass fraction of sulphur dioxide. When evaporation is included in the analysis, the sulphur dioxide to carbon dioxide ratio leaving the scrubber is 1.88, equal to a fuel sulphur content of 0.043% on a mass base (from 3.5% in the fuel) for 100% engine load. When evaporation is not included in the analysis the previous values are 2.3 and 0.053% respectively. To increase the precision concerning the amount of water that evaporates, a higher discretisation of the packed bed is required.

High engine load fluctuations and/or high input frequencies lead to overshoots and higher liquid supply, in order to keep the scrubber system efficient. In the transition from 25% MCR to 100% MCR the liquid supply exceeds the nominal value of 94 kilogram per second by by 5.3 kilogram per second (or by 5.6%). In the transition between 75% MCR to 100% MCR, for the frequency of 50 seconds the liquid supply is equal to 92.9 kilogram per second. Increasing the input frequency 5 times results in an increase of the liquid supply to 96.1 kilogram per second. The sulphur dioxide to carbon dioxide ratio leaving the scrubber was always below the ECA sulphur limit and was fluctuating around the set point, but most of the time below it. A combination of feed forward and feedback and/or a more advanced control may result in a more stable control of the scrubber, but this has to be investigated.

The model functions, but more research is required for the venturi and the demister models, but also for the packed bed model. In the venturi a three phase flow is required and in the demister an analytical and dimensional analysis is required. Also, the packed bed model needs to be further developed to include the condensation effect and a more precise approach for the liquid phase.

Further research can be done on the integration of the model with a diesel engine and SCR model. Also, seawater can be examined as a scrubbing liquid as this may reduce the operational costs of the scrubber. Finally, because space requirements of the scrubber are high, a structured packed bed could be an alternative to the dumped and reduce the space occupied by the wet scrubber.

ACKNOWLEDGEMENTS

With the completion of this project a wonderful journey ends. It was a journey of efforts, failures and achievements, sadness and joy, but most importantly an invaluable lesson. On this journey I was not alone. I had people who supported me and never left me alone. I am grateful that I had the honour and pleasure to meet them and I would like to thank them for everything.

First and foremost, I would like to thank my supervisor, Rear Admiral (ME, ret) ir. Klaas Visser, for his interest, valuable help and guidance during the project. Thank you dr. ir Peter de Vos, for your support these years at the university and for introducing me to ir. Benny Mestemaker to find a thesis topic. Also, I am grateful to dr. ir Carlos Infante Ferreira for the careful proof reading of my work and his valuable suggestions. I would also like to thank Anouk de Goede-Oosterhoff for her administrative support and all the academic staff of the department of Maritime and Transportation Technology at TU Delft for their lectures and passing on their knowledge to me.

My special thanks to my daily supervisor Benny, for helping me find this amazing thesis topic, for the motivational support and introducing me to the world of modelling and simulations. I am grateful to the New Fuel and Drives team of Royal IHC: Bernardete, Henrik and Lindert, who were always there for me. Thank you, all guys, in IHC MTI B.V., for making me feel like home since the first day. Grazie mille Pietro, for the entertaining coffee breaks.

I am grateful to my professors from the department of Mechanical Engineering of University of Thessaly, prof. Vasilis Bontozoglou and prof. Nikos Andritsos, for supporting me during my master's application and providing helpful material for this project.

"Good friends are hard to find, harder to leave and impossible to forget." (G. Randlof). Thank you, Giovanni, Karina and Zhongwei, for the amazing Saturday night dinners, for introducing me to your culture and travelling with me around Netherlands exploring the beauties of this country. I want to thank Stamatis and Nicole, for being by my side, for the amazing moments while having BBQs, watching movies, studying, moving house and enjoying good food and drinks. Thank you, George, for motivating me to follow a healthy diet, joining the gym and our lunches and coffee breaks in IHC. Distance means so little when friendship means so much and Giannis (in the USA), Vangelis (in Scotland), Dimitris (in Greece) and Kostas (in Greece) proved that to be true. There are friends, there is family and there are friends that become family. Eris, my best friend and Alexandros, my cousin and best friend, you supported a lot the last years and most of the times without even realising it. You are the brothers that I chose.

Last, but certainly not least, I would like to thank my family, my father Shkëlqim, my mother Mirela and of course my little sister Matea, for their wholehearted support and love. Family is the Alpha and the Omega in life and you are my life-giving power. Words and actions are not enough to describe how much I adore you. Only God knows. Thank you.

One journey ends and another begins. New destinations, challenges and adventures. What the future holds, unknown. But that may be its beauty. One thing is for sure: "People's dreams never end" (Eiichiro Oda).

Enri Elmazi
Delft, March 2020

CONTENTS

List of Figures

List of Tables

1

INTRODUCTION

"Fillimi i mbarë është gjysma e punës"
Translation: "Well begun, is half done"

Albanian proverb

1.1. RESEARCH RELEVANCE AND BACKGROUND

The maritime industry plays a fundamental role in the facilitation and globalisation of trade. The growing world population has increased the demand for liabilities and consequently increased the demand for shipping services. Around 90% of international cargo is carried by ships [18]. The increase in the global-scale trade led to an increase in the number of ships [19]. As a result, the sulphur oxide (SO_X) emissions increased. Attracting less attention compared to other modes of transportation, shipping contributes about 5-8% of global SO_X emissions [20, 21]. However, ships are the most energy efficient and cost effective form of freight transportation.

Ship's emissions impose a limit on the future of diesel engines which are the most efficient method for vessel propulsion. Sulphur oxides are one of the primary air pollutants from vessels having extensive and proven damage to human health [22]. In 2005, the International Maritime Organisation (IMO) issued legislation limiting the SO_X emissions from vessels to improve air quality. Today, the global sulphur cap on fuel is 0.5% (since January 1^{st}, 2020). There are Emission Controls Areas, where this limit is even lower, 0.1% (since January 1^{st}, 2015). According to MARPOL Annex VI, the sulphur limit can be achieved if vessels are using more expensive low sulphur fuel, or invest in abatement technologies.

Research has been done focusing on the different strategies to comply with the regulations. These strategies include application of reduction technologies on board and using alternative fuels. One of the main directions is the environmental and health impact of the new policies in coastal areas. The other directions approach the legislation from the ship owners/ship operators perspective. Creating tools for selecting technologies related to compliance based on widely used financial appraisal criteria. These criteria calculate the abatement costs based on shipowners' optimal decision making in choosing between low sulphur fuel or investing in a sulphur scrubber. The size of the vessel, the operational area and the remaining operational lifetime of the vessel are some of the most frequently used criteria to decide between low sulphur fuel or a scrubber.

The wet scrubber technology has been applied in industry for decades. Much research has been done in this area. Flagiello et al. [22] carried out small scale experiments for power plant applications using seawater as scrubbing liquid. A structure packed column (height 0.16 m) is used, in atmospheric conditions, with liquid-to-gas ratio between 1.06 and 3.44 $\frac{kg}{kg}$. Sulphur dioxide (SO_2) concentration were in the range 500–2000 ppmv. The synthetic flue-gas was prepared by mixing SO_2 (2% in nitrogen (N_2)) with either N_2 (99.999%)

or air, supplied by in high-pressure cylinders. Brown et al. [23] in order to improve the scrubber, nozzle characteristics and placement, created a Computational Fluid Dynamics (CFD) model that uses lime slurry spray in tube of 24inch diameter. Brogren et al. [24] developed models based on the penetration theory to calculate the dynamic absorption rate of sulphur dioxide into a droplet of limestone slurry. Hatamipour et al. [25] studied the reactive absorption of SO_2 by seawater in a spray tower experimentally and mathematically. They focused on the importance of liquid film formation on the walls of the scrubber and the liquid droplets hydrodynamics and its effect on the performance of the equipment.

For maritime applications, the research mainly focused on the financial perspective. Ship's diesel engines and wet scrubber systems are big and expensive devices. Therefore, experiments are in small scale and in steady state conditions. Tang et al. [26] developed a prediction model for the desulphurisation efficiency of on board magnesium base seawater scrubber. The exhaust gasses contain about 200 ppmv in SO_2 and are the product of the combustion of heavy fuel oil (HFO) with sulphur content of 1% w/w. They used statistical approach to examine liquid to gas ratio, pH value and superficial velocity on the desulphurisation efficiency. The results showed that the liquid to gas ratio and the pH are the key parameters influencing the desulphurisation efficiency while the superficial velocity has limited effect. The highest efficiency reached was 95.6%. Zhu et al. [27] carried out shipboard trial to investigate the efficacy of a magnesium based exhaust gas cleaning system (Mg-EGCS) and the life cycle cost analysis method was utilised to evaluate the economic benefit of Mg-EGCS. The results of life cycle cost analysis indicated that the Mg-EGCS could bean economical approach for fulfilling the convention. The cost of the additional fuel consumption and the chemicals was around 1% of the total fuel cost. Boscarato et al. [28] examined the effect of the catalyst in a system that uses a monolithic Pt/Al_2O_3 oxidation catalyst and seawater scrubber for the simultaneous removal of nitrogen oxides and sulphur oxides. The presence of catalyst before the scrubber allowed reduction of both NO_X and SO_X. The examined system showed significant efficiency for all target pollutants for fuel sulphur content up to 0.4%. IMO NO_X Tier III could be achievable with high sulphur content fuels. Yang et al. [29] proposed a method for removal of NO_X and SO_2 from simulated ship emissions by wet scrubbing using electrolysed seawater. The results showed that the main factors influencing the removal of NO_X are available chlorine concentration, seawater pH, the gas flow rates and O_2 concentration in flue gas. Dashliborun et al. [30] investigated CO_2 capture performance into aqueous alkanolamine solution, in structured and dumped packed bed scrubbers, on offshore floating vessels, in a systematic study using a hexapod robot with six-degree-of-freedom. The experimental results showed that deviation from the vertical position of the packing material reduced the efficiency of mass transfer. In all the tests, the structured performance was better than the dumped.

The research for maritime scrubbers is done mostly by wet scrubber manufacturers. The focus is on open loop scrubber with seawater, closed loop scrubber with fresh water and sodium hydroxide and on hybrid systems that operate either seawater, with fresh water and NaOH or seawater and NaOH. The scope is normally limited in 100% engine operation and the findings are not publicly available. Wet scrubbers, can meet the strict ECA sulphur limit in all engine loads. The closed loop does not have the side effects of the open loop (discharges at sea) or the low sulphur fuel (more black carbon than HFO at lower engine loads). But, when the engine operates in at low load, the scrubber keeps operating at 100% of its potential, increasing fuel consumption.

At TU Delft, a first attempt to model a wet scrubber for maritime applications was carried out by Brouwer [31]. The objective was to create a dynamic model and to show the applicability of the model in the analysis and preliminary design of a system. The dynamic analysis examines the changes in the liquid feed composition and liquid flow. The amount of NaOH injected to the system varies in the dynamic analysis. The control system used is feedforward, meaning that the signal for the required liquid supply is taken before the gasses enter the scrubber system. The sulphur dioxide over carbon dioxide ratio is calculated at the exit of the scrubber. During a transient from high to low engine load an overshoot was observed for some seconds and the amount of SO_2 leaving the scrubber was higher than the limit. This was caused by the liquid entering at the top of the scrubber was controllrd according to the gas conditions leaving the engine. Therefore, Brouwer proposed an alternative control system to be used. A case study was done to show the possibilities and the limitations of the scrubber. A dimension optimisation occurred from this study. In the analysis done only the packed bed section was examined. The influence of the other sections of the scrubber were not taken into account. The packed bed used had diameter of 2.5 meters which is in accordance with the commercial

scrubbers. The 10 meters height of the packed bed section was larger than the commercial packing materials. The majority of the commercially available scrubbers are around 8 meters in height and that includes the lower volume, the packed bed, the upper volume and the demister section. The designed model used fresh water but the evaporation effect is not taken into account. Brouwer recommends to investigate the effect of evaporation in a future research.

1.2. OBJECTIVE AND RESEARCH QUESTIONS

Sulphur oxides have a significant impact on the environment and human well being. The other sectors took drastic measures to reduce sulphur oxide emissions, but the maritime sector did not followed the same pace. This resulted in being considered one of the most polluting sectors nowadays. To reduce sulphur oxide emissions from ships, operators can use very low sulphur fuel oil (VLSFO), which is more expensive than HFO. A study submitted to IMO by Germany and Finland indicates that VLSFO produces more black carbon than HFO [32]. An alternative that is gaining ground the last two years are wet scrubbers. More vessel operators are retrofitting their vessels with scrubbers [33]. The closed loop scrubber was chosen, as it can operate in areas with low seawater alkalinity and has no discharges in the sea. The scrubbing liquid is fresh water with NaOH. Fresh water is stored in water tanks reducing the available space on vessels. Wet scrubbers are designed to operate at 100% of their potential even when the engine operates at lower loads. The power required for the operation of the wet scrubber is provided by the diesel engine. When a scrubber operates fuel consumption is increased due to the operation of water pumps and a slight increase of back pressure. Therefore, it is important to examine the influence of dynamic loads on scrubber operations.

The objective of this thesis is to cover the knowledge gap regarding the influence of:

- water evaporation and
- dynamic loads

on the operation of a closed loop wet scrubber systems for maritime applications.

The primary research questions derived from the above objective are:

1. How does the water evaporation affect the removal efficiency?
2. How fast can the scrubber respond to transient loads?

The secondary questions are:

1. What is the current legislation for SO_X in maritime sector and what is the importance of their application?
2. What are the available systems for SO_X removal?
3. What is financially more viable, a scrubber or low sulphur fuel?
4. Can the proposed model meet the strict SECA sulphur cap?
5. Is the gas coming out of the packed bed fully saturated or not? Is there a need to include a demister and how much water evaporates and needs to be replenished?
6. What is the SO_X removal in transient conditions?
7. What is the buffer capacity of the water flow for the SO_X absorption at different engine loads?

1

1.3. THESIS OUTLINE

The sources of sulphur oxides and the impact on the environment and humans are examined in chapter 2. In this chapter, emphasis is given on the maritime sector, focusing on its share in the SO_X emissions; legislation to reduce SO_X emissions; possible SO_X reduction methods and an estimation about the future. Chapter 3, deals with wet scrubber technology, its advantages and disadvantages, the pollutants removed, the effect of the discharging scrubber wash water on marine environment and the economic viability of using this system. In chapter 4, the modelling approach for the gas and liquid phase will be discussed. Chapter 5, provides the model development and the governing phenomena in the scrubber system. Chapter 6, provides the inputs of the model and the verification analysis. In chapter 7, the scrubber model will be integrated in a complete system and static and dynamic analysis will be carried out. Finally, in chapter 8 the conclusions are given with recommendations for future work.

2

SULPHUR OXIDE EMISSIONS

"We cannot solve our problems with the same thinking
we used when we created them"

Albert Einstein

2.1. BRIEF HISTORY OF ATMOSPHERIC POLLUTION

Anthropogenic air pollution has its roots since the ancient times with the appearance of humans [34]. The Roman philosopher Seneca describes with aversion the situation of Rome's atmosphere which incurred by chimneys and other unpleasant emissions [35]. In the 13^{th} century humans started to use coal in the lime kiln. According to Te Brake [36] the situation became even worse at the beginning of the next century in densely populated areas such as London. In his book "The Age of Smoke", Frank Uekoetter [37] states that the problem was abated over the next few centuries until the industrial revolution (usage of steam engine that was fuelled by coal) where severe emissions reached high levels and became a severe problem in big cities. The first national legislation appeared on 1880 in USA focusing on industries, in mobile and maritime sources.

In the 20^{th}, the technology's progress, the improvement of legislation and the increase of public awareness, played a decisive role in the air pollution control [38]. Filters and other devices started to be applied, but the most important contributor was the substitution of coal by other fuels that produce less smoke; and steam engine by the electric generator. Moreover, the optimisation of gas treatment devices and the improvement of chemical engineering in the field of analysis, design and process control, played a significant role in the treatment of exhaust gas. In this day and age, a big part of the of atmospheric pollution is related to the usage of fuels for industrial purposes, for transport and for electricity production for households [38]. The regions that face the greatest problem are the large industrial urban areas because of their high energy requirements. Earth's population is on increase and consequently there is a greater need for energy. Is estimated that in the near future, the issues of air pollution will be due to the continuous increase of fossil and nuclear fuels usage. Abatement technologies are an efficient method to deal with air pollution, but it is a temporary solution. For this reason, it is imperative to focus on sustainable, zero-emission sources of energy.

2.2. SOURCES OF SULPHUR OXIDES

Sulphur oxides (SO_X) are chemical compounds created by the combustion of sulphur or any other compound that contains sulphur. Among all chemical compounds containing sulphur, sulphur dioxide (SO_2) is the component of greatest concern. Sulphur dioxide make up 95% of the total sulphur oxide emissions [39]. Sulphur dioxide is used as an indicator for the group of gaseous SO_X, because it is in elevated concentration compared to all the others. All fossil fuels contain sulphur. Tiwary and Colls [40] explain that the content of different fuels in sulphur is not the same, proposing the following categorisation:

- Sulphur content of oil and its by-products lies in the range between 0.1% (paraffin) and 3% (heavy fuel oil) in the form of sulphides and thiols. The processed oil and gasoline contain less than 0.05% sulphur.
- Petrol contain a small amount of sulphur in the contex of total mass emission. Although, an odour problem may arise when converted to hydrogen sulphide on catalytic converter.
- In coal, sulphur appears mostly as flakes of iron pyrites (F_eS_2), and ranges from 0.1 - 4%.
- Natural gas, initially when extracted for the well may have 40% (H_2S), but before distribution is subject to chemical processing so as to be sulphur free.

The sources of SO_X can classified in two general categories:

1. Natural sources
2. Anthropogenic sources

2.2.1. NATURAL SOURCES

Natural sources are considered all the sources that are not caused by human activity. Even though separation in this sense is not always easy or obvious, it helps a lot to consider it. Examples are erupting volcanoes and forest or green area fires, which among the other elements, release SO_2. Hot springs are another natural source of SO_X and sulphuric gasses in general [41]. However, the natural sources are not considered to be a major concern as they are part of natural equilibrium. The natural sources of sulphur are outweighed by the anthropogenic [42].

2.2.2. ANTHROPOGENIC SOURCES

Anthropogenic pollution is inextricably linked with man kind evolution, both in terms of growth of population, in energy consumption and technological development. Man made sources are negatively contributing to the air quality [42]. SO_X emissions are regulated on a mass based percentage of the fuel, because sulphur is a fuel based atom. Almost all the anthropogenic sulphur contribution in the atmosphere originates from fossil fuel combustion. Depending on the fuel (crude/distillates) the amounts may vary. Sulphur dioxide is formed according to the reaction:

$$CH_3 - SH + 3O_2 \longrightarrow SO_2 + CO_2 + 2H_2O \tag{2.1}$$

Oxidisation of SO_2 to sulphur trioxide (SO_3) takes place during the combustion process and in the exhaust channels. Sulphur trioxide, is a highly hygroscopic molecule and a reaction with water (from the flue gasses) will lead to the formation of sulphuric acid (H_2SO_4) [43]. At temperatures higher than 800°C and in the presence of vanadium of iron oxides, chemical conversion will increase [42]. Fuel oil with elevated vanadium concentration can convert 20% -30% of sulphur to SO_3 [40].

When released into the ambient, SO_2 reacts photochemically with oxygen in proportion 1-2‰/$_{hour}$ under the presence of ultraviolet radiation (UVR) and will form SO_3. The following reaction will take place:

$$2SO_2 + O_2 \xrightarrow{\text{UVR}} 2SO_3 \tag{2.2}$$

$$SO_3 + H_2O + \longrightarrow H_2SO_4 \tag{2.3}$$

The newly formed SO_3 will instantly absorb moisture to create H_2SO_4 in the form of microscopic drops (aerosol). An increase of the conversion of the order of 15% is observed in presence of high humidity or fog [42].

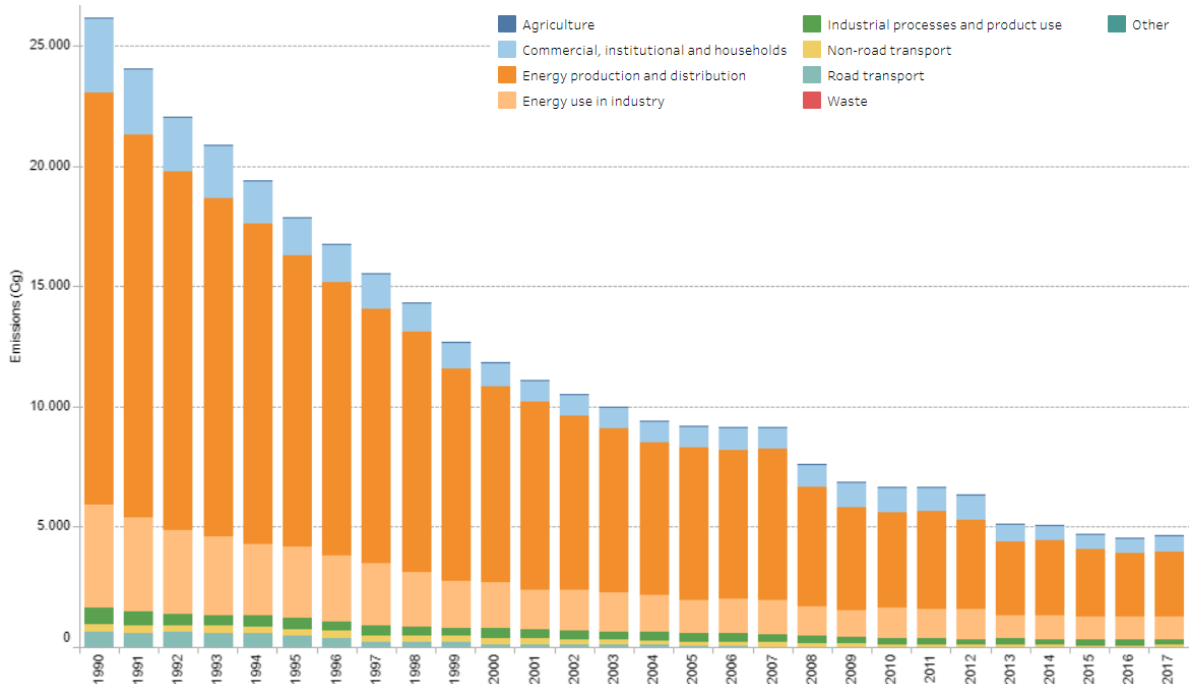

Figure 2.1: SO_X emissions (in Gg) by sector in the period 1990-2017 [1].

Anthropogenic sources, in turn can be classified into two major categories a) mobile and b) stationary sources. In the stationary anthropogenic source, the principal sources of sulphur are industrial activities (e.g. metallurgical plant and refining processes) and services of general interest (e.g. power plants burning coal or fuel combustion mainly for electricity production). In the member countries of the European Environment Agency (EEA-33), even though the immobile SO_X emissions have been reduced for more than 75% since 1990, they still contribute to more than the half SO_X emissions (Figure 2.1) [2]. European industrial sector is reported to be less sulphur emission intensive and economic crisis seems to be another reason for that reduction due to lower economic activity that are the result of lower demands in industrial goods and energy [44].

Mobile sources of pollution can be characterised as sources that produce their own energy required to move from the one place to the other. Cars, are the most representative subject of road sources. Non-road sources include ships, aeroplanes, that can move in different levels (sea, land, sky) and use different combustion processes and fuels. In developed countries diesel vehicles are the main mobile sources of pollution. The improvement of technology and new stricter legislation forces toward an improvement in fuel quality and application of emission mitigation equipment (SCR, scrubbers) to alleviate the harmful pollutants. In the EEA, between 1990 and 2016, the transport sector significantly reduced emissions of several pollutants, among them SO_X (63% reduction). In areas with large ports there is also significant contribution from ships.

An increase in the global SO_2 emissions (stationary and mobile) from 4 million tonnes (mt) to 150 mt was observed for the period 1860 - 1990. The USA and Europe had a gradually increasing trend until 1970 where SO_X emissions reached their peak. After that time they measures were taken to reduce them. Globally, SO_X contribute around 24 mt/year in the atmospheric pollution. National Emission Ceilings Directive (NECD) and the Gothenburg Protocol under the Convention on Long-range Transboundary Air Pollution (CLRTAP) set emission ceilings to European countries for the ambient air pollution [2]. All the EU-28 countries have reduced their SO_X emissions below the level of NECD and UNECE/CLRTAP Gothenburg protocol [45], a 91% decrease in SO_X emission. In 2016, the total emissions in EEA were almost 4.7 mt, which was decrease in the

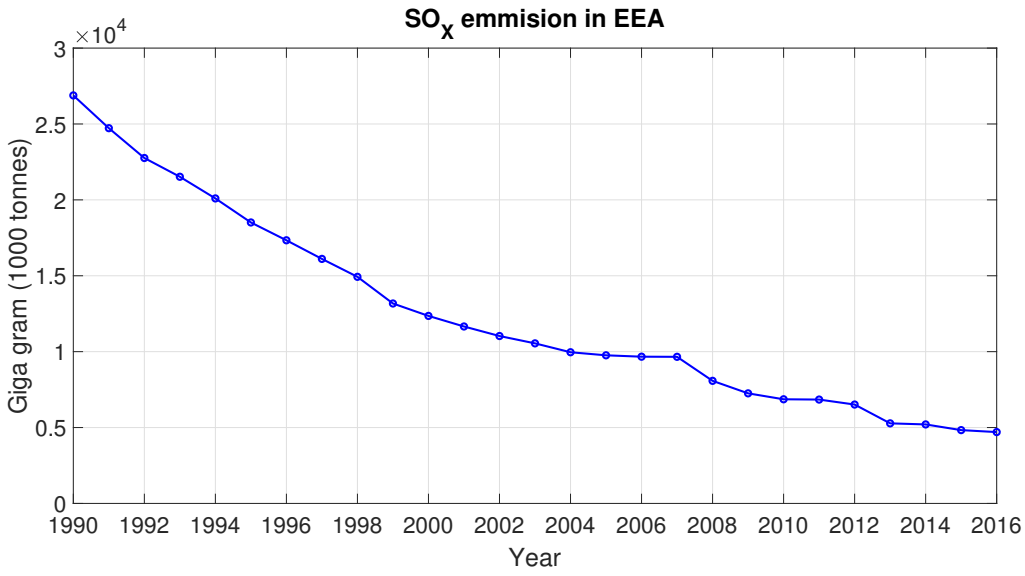

Figure 2.2: Emission trends of the air pollutant SO_X [2].

order of 82% compared to the values of 1990 (Figure 2.2).

To comply with the legislation set by national and international organisations the following measures were taken:

- ***Fuel Switching:*** The last years has been a trend in all sectors (energy production, industry and domestic) to switch from high sulphur fuels (solid or liquid) to low/zero sulphur fuels (e.g. natural gas).
- ***Abatement equipment:*** In sectors that use fuels with high content of sulphur, flue gas desulphurisation equipment needs to be installed.
- ***Improvements in energy efficiency:*** Improvement in energy efficiency has an outcome in reducing energy demand and thus a reduction of sulphur emissions.
- ***Sulphur content of fuel:*** Emission legislation is a significant step that leads the way toward sulphur reduction.

Application of legislation is of paramount importance to mitigate and if possible to eliminate the negative effects of sulphur oxides. Their impact the last centuries is severe and it is not affecting only human beings, but also the environment in the broader sense.

2.3. IMPACT OF SULPHUR OXIDES ON THE ENVIRONMENT

Inorganic sulphide particles, sulphuric acid and other sulphates are typically measured to be between 5 - 20% of the total amount of particles in an urban area [41]. The most disreputable and disastrous group of atmospheric pollutants are associated with the sulphur element. The impact of SO_2 can be more intense if they are combined with other pollutants, especially particulate matter, as the reaction speed depends on relative humidity, the amount of sunlight intensity and air temperature, and the presence of other chemical compounds (hydrocarbons and NO_2) [41]. In the stratosphere, SO_2 oxidises to sulphuric acid, which with the soot particles from aircraft exhaust promote heterogeneous chemical reaction cycles that destroy ozone (O_3) [46]. Sulphur oxides are associated with significant effects in the chemistry of the atmosphere, problems to human health, flora, fauna, civil structures and probably are also contributing to climate change [41].

2.3.1. IMPACT ON HUMANS

Researches have shown that SO_2 is soluble and is easily absorbed in the upper respiratory tract. In humans, lower perception limit for taste and smell is 0.3 ppmv and 0.5 ppmv respectively [38]. In concentration higher than 1 ppm, partial bronchoconstriction is noted which causes variations in the breathing and the pulse frequency. When concentration is above 5 ppm it causes breathing problems such as spasmodic reactions, while in concentration higher than 10 ppm it irritates the eyes, the nasal cavity (causing nosebleed) and the throat (cough) [38]. The ability of SO_2 to irritate the eyes increases three to four times when conditions favour the formation of sulphuric acid. In the presence of particulates, SO_2 can penetrate deep into the lungs and cause severe health problems. The elderly, children and individuals with asthma and bronchitis are more sensitive compared to the rest of the population [38]. Long lasting exposure of human beings in low SO_2 concentrations can cause death [38, 41, 46].

Several incidents of atmospheric pollution, that have been recorded in big cities around the world, were the result of elevated level of SO_2 in combination with favourable conditions for sulphuric acid formation. All these incidents had a common characteristic that was respiratory problems. Many patients were hospitalised and some died. It is worth noting some hazardous events occurred in Donora 1948 and London [41].

2.3.2. IMPACT ON FAUNA

There is a lack of bibliography concerning the impact of SO_X on fauna. The impacts of SO_2 on animals, for short-term periodic exposure, are similar to humans. Although, animals seem to be less sensitive than humans. However, in densely populated areas animals lifespan is shorter compered to them who live in areas without industrial activity or sparsely populated areas [41]. One of the main impacts of the SO_X emissions is acid deposition (acid rain or snow). Acid deposition has increased the acidity of many lakes making them unable to support fish life, destroying the aquatic ecosystems [38]. Also, some plants thrive on higher acidity, it reduces the biodiversity and with this the animals that can live in a certain area.

2.3.3. IMPACT ON FLORA

The early history of pollution from SO_2 is linked with the damage on vegetation and can be acute (direct) or chronic. The damages can be created either by the extensive exposure on low concentration of SO_2 or in short exposure on higher concentration [38]. The sensitivity of vegetation to SO_2 may vary. Some trees and shrubs start to change their colour to yellow due to short exposure at SO_2 concentrations between 0.3 to 0.5 ppmv. Exposure in lower concentration but for longer periods may cause the leaves to fall and severe damage to some seeds. It is also possible that the growth of plants will be delayed even with a low concentration of sulphur in the atmosphere [41]. The major effects on green plants are the loss of chlorophyll (chlorosis) and the tissue collapse of many of the leaf cells (plasmolysis). Frequently, in areas with minerals roasting activity, where sulphur concentration is high, vegetation is completely destroyed [38]. There are also other studies that are concentrated on the combined effects of acid deposition (half of these deposition are sulphur based) and ozone on plants [47].

The main question that arises is if there are sufficient methods to reduce sulphur oxide emissions so as to eliminate their negative effects and gradually bring the atmospheric conditions back to pre-industrial levels.

2.4. METHODS USED FOR SULPHUR EMISSION REDUCTION

The two major strategies for the pollution control from SO_X are:

1. the usage of sulphur free or low sulphur fuels and
2. the removal of SO_X from the exhausts gasses.

Each one of the above approaches, provides many methods that have been investigated. Based on the work of Cooper and Alley [38], the most well-known processes will be described briefly in the following subsections.

2.4.1. FUEL DESULPHURISATION

Crude oil's content on sulphur ranges between 1% - 3%, which means it is mostly acidic. Generally consumers prefer to use clean fuels, with low sulphur content. Therefore, a lot of refineries have installed hydrodesulphurization (HDS) units following the catalytic reaction:

$$R - S + H_2 \longrightarrow H_2S + R \tag{2.4}$$

where R, is the organic-functional group.

Up to 1975, H_2S from the desulphurisation unit was normally mixed with the gas fuels of the refineries and SO_2 was produced from the combustion. Thus, there was just a redistribution of the source and not overall SO_X reduction in the atmosphere. To deal with this issue, sulphur recovery methods were created that use the Claus process [38]. According to this process, part of H_2S is combusted to SO_2 (equation 2.5). Then, both compounds are combined with a catalyst for simultaneous oxidisation (equation 2.6). The reactions that take place are:

$$H_2S + \frac{3}{2}O_2 \longrightarrow H_2O + SO_2 \tag{2.5}$$

$$2H_2S + SO_2 \longrightarrow 2H_2O + 3S \tag{2.6}$$

The elemental sulphur is separated as a by-product and the amount of H_2S and SO_2 emissions from the refinery is significantly reduced [38].

2.4.2. EXHAUST GAS AFTER TREATMENT

Depending on the SO_2 concentration, the removal techniques can be divided:

1. *High concentration techniques*, an example of this process is smelting of sulphur-containing minerals (around 10% sulphur), where a current of high SO_2 concentration is produced . In the presence of catalyst (Vanadium, Va) oxidation of SO_2 to gas SO_3 takes place and then absorption of SO_3 in water to form H_2SO_4 [38].
2. *Low or middle concentration technique* (SO_2 concentration < 2000 ppm or 0.2%). In this scenario, flue gas desulphurisation is carried out. In turn, this technique can be divided in two main methods, the throwaway method and regenerative method. In the *throwaway* method, sulphur is removed from the exhaust fumes. The most common processes of the throwaway method are: limestone scrubbing, lime scrubbing, dual alkali system, lime-spray drying and dry scrubbing. In the *regenerative* method the retrieved sulphur can be used again in the process. The regenerative method is more expensive than the throwaway method and is chosen when there are space limitation and limited product disposal options. The most know process is called Wellman Lord (W-L process). Other known methods are: MgO process, Citrate scrubbing process and Westvaco process [38].

2.5. MARITIME SULPHUR OXIDE EMISSIONS

In the 21^{st} century, impact on the environment is a crucial issue. The pollution control measures taken the last years contribute to the reduction of global SO_X emissions from all sources. Although, the progress made from the maritime industry hasn't proceeded in the same pace as in the other sectors and could diminish all the progress made from the inland activities [48]. There is a growing awareness of the increasing contribution made on air quality by the national and international shipping sector. In the last few decades, the maritime industry bloomed reaching its climax in May 20^{th}, 2008 when the Baltic Dry Index hit a record of 11,793 [49]. The increase in the global-scale trade had as an outcome the number of vessels to increase, which in turn increased the SO_X impact on the coastal areas [50]. Besides primary inland pollution, special attention is placed on the pollution from vessels as they account 5 - 8% globally [51].

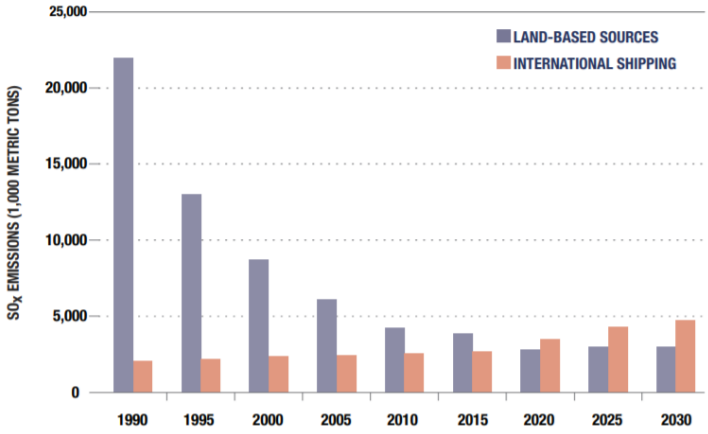

Figure 2.3: Estimation of SO_X emission from the maritime sector compared to land-based activities for 25 EU countries [3]. This estimation refer only to ships in the international trade and do not include inland shipping and harbours.

Sulphur oxide emissions from vessels were not high compared to other sectors. Ships transport large quantities of necessary goods across the world, they are the most sustainable and energy efficient means of transportation compared to all the others (aviation, railway, road trucks) [52, 53]. However, SO_X emissions from international shipping exceeds road transportation [54]. The maritime industry is now considered to be one of the main contributors of SO_X emissions in the transport sector, especially in regions with intense vessel traffic. If no measures were taken, then according to an estimation of European Commission in 2005 (see Figure 2.3), the combined SO_X ship emissions for 25 EU member countries would be higher than the land-based [3]. The prediction of International Council on Clean Transportation (ICCT) for 2050 is that SO_X emissions will rise more than 18% [3]. These predictions were done before 2005 and do not include the IMO regulations. The purpose was to show the trends if no measures were taken.

Figure 2.4a displays that for the EEA countries, an essential reduction is observed the last decades.Athough, maritime impact is still significant. In 2016 (Figure 2.4b), the share of the international shipping in EEA was 11%.

2.5.1. SOURCES AND IMPACT OF SULPHUR OXIDES

Vessel's emissions are anthropogenic mobile emission sources. All the power required on ships for propulsion and other functions is generated though the main and auxiliary engines. These prime movers are in most of the cases diesel engines as they offer some significant advantages such as being insensitive to fuel quality, are reliable and efficient. A disadvantage is that exhaust gasses from marine diesel engines are the main source of emissions from vessels and have a significant contribution to air pollution. This drawback of diesel engine is also the major threat to their future use in marine propulsion [56].

Sulphur oxide emissions from vessels are the result burning of sulphur compounds in the marine fuel used on board. Stapersma [56] states that SO_X emissions are directly linked to the fuel sulphur content. The fuel

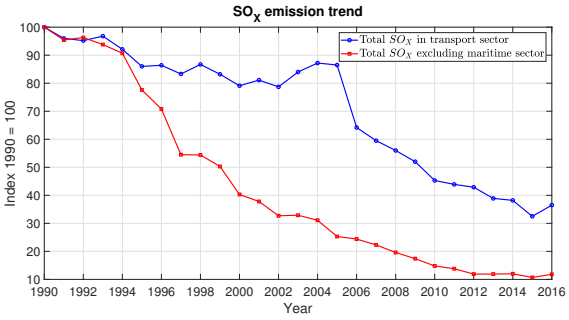

(a) Overall SO_X emission from the transport sector in the EEA countries for the time period 1990 - 2016 [55]

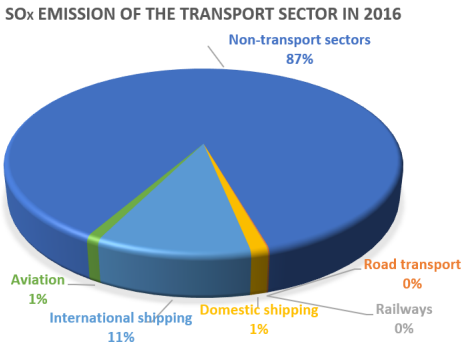

(b) SO_X emission from the transport sector in the EEA countries in 2016 [55]

Figure 2.4: sulphur oxide emissions from the transport sector in the EEA.

used on vessels can be categorised in grades, based on the properties described in ISO 8217. Generally, lower fuel grades (e.g. lower quality fuels) have a higher fuel sulphur content. These low quality fuels are the left over waste for the refining process after all other useful components have been removed. The maritime sector consumes mostly low grade fuels such as heavy fuel oil (HFO) and marine diesel oil (MDO), due to a lower fuel price.

Formation of SO_X in the exhaust gasses is caused by the oxidation of the elemental sulphur in the fuel into sulphur monoxide (SO), SO_2 and SO_3 during the combustion process. When referring to SO_X emissions in diesel engine exhaust gasses, this mostly consists SO_2 and a small amount of SO_3 [56]. Typically, the amount of SO_3 is 5% of the amount of SO_X [57].

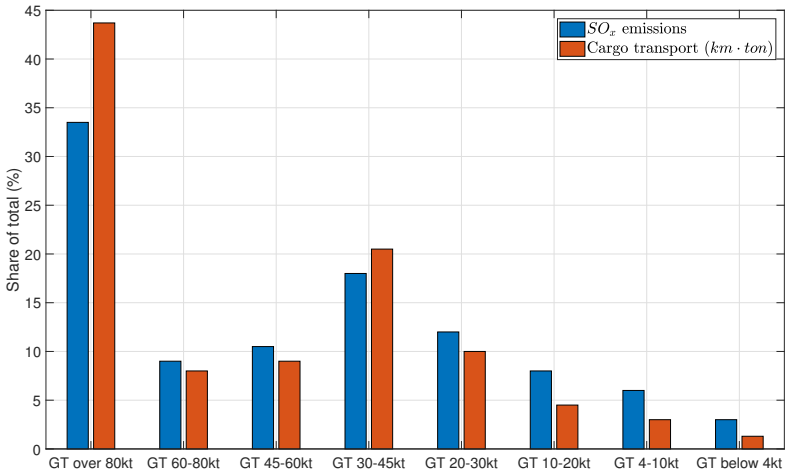

Figure 2.5: Shares of global SO_X emissions and transport work (payload; $km \cdot ton$) in 2015 classified in terms of size categories of ships (measured gross tonnage, GT) [4]

The fuel consumption of the vessel is affected by its sailing speed. Recently, the average operational speeds have been reduced [58]. This in response to the high fuel prices which represent the main element of the operational cost and the low freight markets [59]. Vessel operators, operate their vessels between 15% to 40% of their total power. This strategy saves energy through the hull resistance to speed relation, but it increases the specific fuel consumption of the engine [60]. At a lower load the mechanical efficiency and the thermodynamic cycle efficiency may be lower. Sulphur oxides is directly related to the specific fuel consumption. Therefore, the specific fuel consumption is about 10% higher at low load, resulting in a

specific increase of SO_X emissions with the same percentage [61].

Considering the size, vessels equal to or greater than 80000 GT constitute the 6.8% of all the IMO registered vessels but they contribute 33% to shipping emissions and they carry around 44% of all maritime cargo (see Figure 2.5). Vessels smaller than 10000 GT compose around 88% of the global fleet but their contribution on the total SO_X emissions is the least [4]. They have the lowest average travel distance and the smaller engines (low power engines). Container ships, cargo carriers and tanker's emit about 87% of all maritime SO_X emissions [4].

2.5.2. AREAS FACING THE GREATEST PROBLEM FROM SULPHUR OXIDES POLLUTION

Colvile et al. [46], claim that shipping on its own cannot cause excessive SO_X concentrations in the atmosphere without the contribution of land based sources. In sensitive areas, close to harbours the presence of shipping-related emissions amplifies the inland SO_X sources and makes the situation unfavourable [62]. Measures demonstrated that in the ports of the USA, ship manoeuvring is responsible for 10% of SO_2 [63]. In the North Sea and the English Channel, at a distance of 50 nautical miles from the coast, it has been estimated that around 90% of the total SO_2 emissions come from ships [57]. Ship emissions close to land affect soils, rivers and lakes in those areas [64].

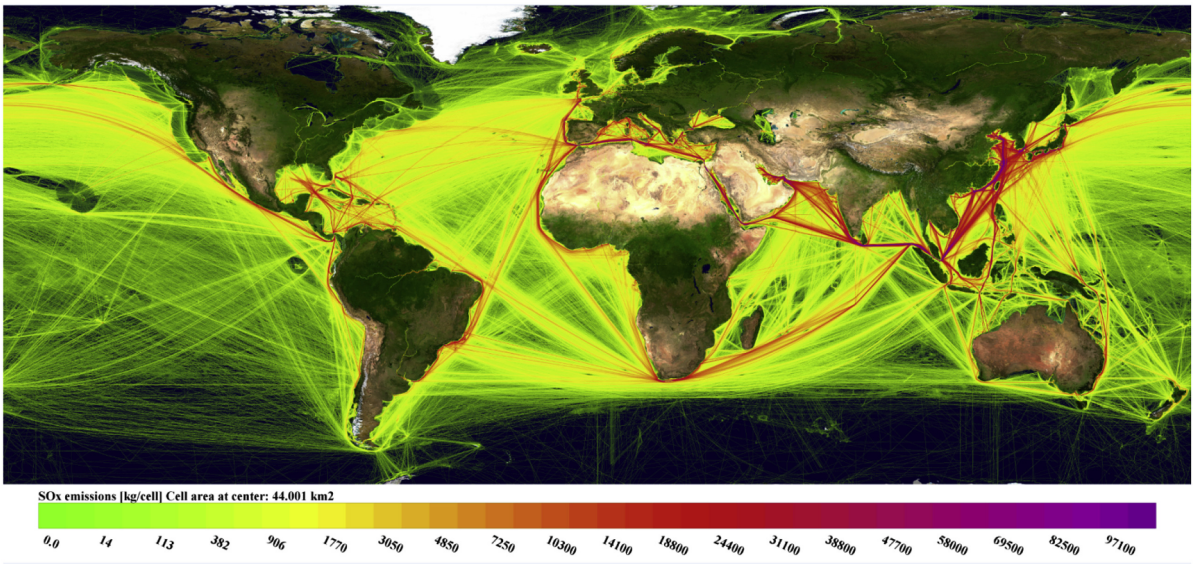

Figure 2.6: Geographical distribution of SO_X emissions from shipping in the year 2015 [4]

Johansson et al. [4], based on real data collected from vessels and the route that they follow, created a model about the major pollutants from ships. The results of this research are that the areas facing the greatest problem of SO_X emissions from international shipping are the Eastern and Southern China Seas, the seas in south-eastern and southern Asia, the Red Sea, the Mediterranean, the North Atlantic near the European coast, the Gulf of Mexico and the Caribbean Sea, and along the western coast of North America . In another, more detailed geographical analysis measured within a circle of 10 km, Johansson et al. [4], concluded that the highest SO_X emission densities are in ascending order from Rotterdam, Los Angeles, Shanghai, Antwerp, Hong Kong and Singapore. Figure 2.6 presents the global distribution of the SO_X emissions. The effects of the legislation introduced in the ECA's are visible even if these areas have a high ship traffic.

2.5.3. LEGISLATION AND EMISSION CONTROL OF SULPHUR OXIDES FROM SHIPS

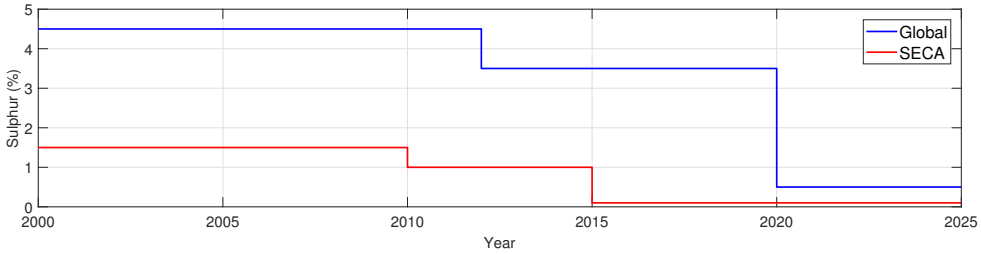

Figure 2.7: MARPOL Annex IV SO_X emission limits globally and in the ECA's [5].

Shipping is by nature an international activity and thus it is of vital importance that regulations on issues such as air pollution to be a subject of global decisions. All these motivated the regulating power of the shipping industry, the International Maritime Organisation (IMO), to issue some restricted legislation for the SO_X emissions from vessels to improve the air quality and protect the environment. Regulations concerning SO_X emission came into force on 2005, under Annex VI, Chapter 3 (Requirements for control of emissions from ships) and especially Regulation 14 of the International Convention for the Prevention of Pollution from Ships (also known as the MARPOL Convention) which include also PM emission. So far there is no explicit regulation concerning PM emissions. Ever since, the new regulations are tightening SO_X limit [65]. The Emission Control Areas (ECA), which have more stringent regulations. The SO_X limits introduced by IMO during the years in the ECA's and throughout the world are presented in Figure 2.7. All vessels, regardless of their contraction date are subject to these rules [57].

Since January 1^{st} 2020 the global SO_X emission limit went down from 3.5% to 0.5% w/w. The ECA's has more stringent limit of 0.1% w/w since 2015 [5]. Compliance with the new limit can be achieved by limiting the maximum fuel sulphur content. Fuel oil suppliers already provide the market with fuels that can meet the more stringent limits of 0.1% for clients that operate their vessels in the already-established ECA's [66]. Refineries can offer low sulphur blend fuel oils by blending heavy fuel oil with fuel oils with very low sulphur content to achieve the required value. Additives may also be added to improve other properties. The fuel oil blends which are suitable to meet the ECA sulphur limit, can also meet the 2020 limit.But, these blends are more expensive than heavy fuel oil. Vessels can also switch to alternative fuels such as liquefied natural gas (LNG), bio-fuels and marine gas oil (MGO), that are low enough or zero in sulphur [67].

An alternative method to reduce the sulphur emissions from vessels is to install an exhaust gas cleaning systems. Scrubbers are the most applied exhaust gas cleaning system on vessels. The waste streams should not discharged in the ports, harbours and estuaries unless the it can be proved by the ship that these streams have no adverse impact in the ecosystem [68].

The last years many companies around the world are trying to invent new technologies so as to carry out the desulphurisation of the fuel on board. Hielscher and Technoveritas that are using the Ultrasound-assisted oxidative desulphurisation (UAOD) that is an established method that accelerates the oxidation reaction [69, 70]. Green Framework has developed a system named De-Sul. This system extracts sulphur from HFO through a pre-treatment by forcing sulphur molecules to stick to the heavier and thicker particles of HFO and then filter them out [71]. The above mentioned companies and others that specialise in the field of desulphurisation claim that can achieve the global sulphur gap that IMO imposed. Although, none of them has yet received the accreditation required to be installed on board and to be considered an equivalent method to reduce SO_X emissions.

2.5.4. THE SIGNIFICANCE OF THE 2020 SULPHUR CAP FOR THE NEXT YEARS

Since January 2020, the global limit of SO_X emissions has been reduced to 0.5% w/w and both large and small vessels should comply with the new regulations. The new limit will have a significant health and environmental benefits, especially for the populations living close to ports, coastal regions and areas that are close to major shipping routes.

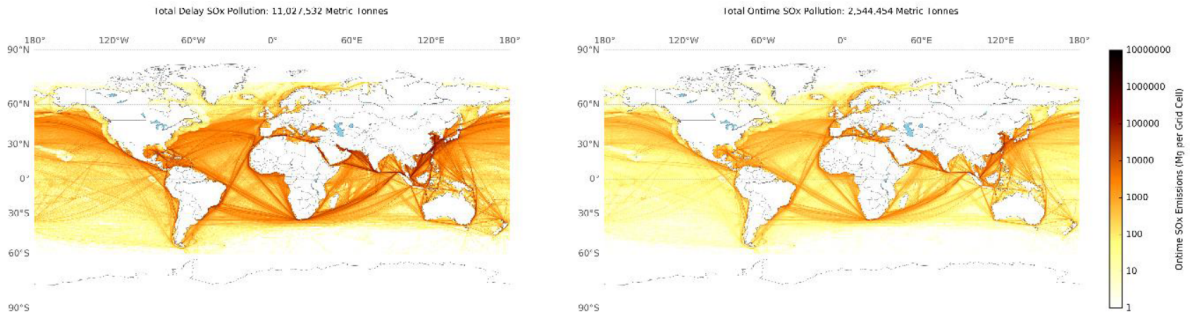

Figure 2.8: Annual shipping inventories of SO_X under the delay scenario (left) and under the scenario of being applied on 2020 (right) [6]

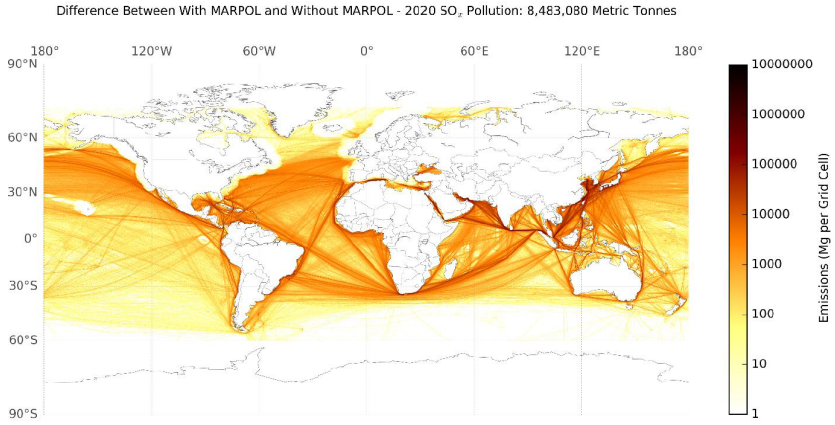

Figure 2.9: Annual shipping inventories [6]

Limiting SO_X emissions from ships will progressively partially reverse the negative effects that this pollutant has caused all these years. The areas that will mostly benefit are the coastal communities and them close to high marine traffic. For total recovery all the anthropogenic sectors that produce SO_X have to annihilate their emissions. Some damages already created will be smoothed out in the long run [46]. Anti-pollution measures will improve air quality and result in a cleaner environment. In 2016, Finland, submitted to IMO a study, addressing the impacts of SO_X emissions from ships on the human health. According to this study, if no action is taken to reduce the SO_X from vessels by 2020, then in the time period 2020-2025 more than 570,000 people would die from the air pollution maritime sector [66]. Figure 2.8 shows the geospatially distribution of the SO_X for the year 2020 for the case that the regulation is applied in 2020 and for the case that it would be postponed to 2025. Figure 2.9 provides the difference between these two predictions. In the SECA's there is no significant difference in the SO_X emissions between the two scenarios. These areas have already applied more stringent regulation since 2015 and their sulphur cap is lower than the global maximum of 2020.

Sulphur emission reduction will aggravate global warming [62, 72]. Lindstad et al. [61] showed that SO_X reduction will contribute to global warming, as it reduces the cooling effect of SO_X in the atmosphere. The reduction of SO_X by 2020 will increase in the percentage of CO_2 emissions per kWh.

3

MARITIME SULPHUR OXIDES EMISSION REDUCTION TECHNOLOGIES

"É melhor prevenir do que remediar"
Translation: "It is better to prevent than to mend"

Portuguese proverb

3.1. INTRODUCTION

IMO legislation applied since January 1^{st} 2020, forces ship owners and ship operators to drastically reduce vessel's SO_X emissions worldwide. In ECA's the rules are tighter. Sulphur emission depend on fuel sulphur content. Compliance with the regulations has put ship owners in a dilemma, to select new engines such as LNG, to switch to low sulphur fuels or install emission after treatment equipment [73]. Liquefied natural gas requires not only new engines, but also a complete fuel supply and storage system. In an existing vessel, the option to substitute the engine with a new type (LNG) is not financially viable. The solutions that can be implemented are either combustion a low sulphur fuel or employ a scrubber on board, that washes out the exhaust gasses. Using low sulphur fuels means minor adaptions to the existing engine and fuels supply system, but the price of low sulphur fuels is higher than heavy fuel oil.

Application of an exhaust gas cleaning system, i.e. scrubbers, is a possible alternative to low sulphur fuels to reduce the total emission of SO_X and considerably reduces emissions of other polluting particles [57]. According to the IMO regulation ships can continue to use HFO, if they install a scrubber to desulphurise the exhaust gasses [74]. Scrubbers are large devices and when they are retrofitted on a vessel, space has to be designed for fast and easy installation [75]. Two main types of scrubbers can be used on vessels: a wet or a dry scrubber. In the wet scrubbing technology, SO_X is dissolved in the water and removed from the exhaust gasses. The alkalinity of the wash water neutralises the SO_X emissions. While in the dry scrubbing technology, SO_X is absorbed by the dry chemical compound. The scrubber technology and the advantages and disadvantages that it offers will be discussed in this chapter.

3.2. WET SCRUBBERS

Wet scrubbers can use seawater as the cleaning medium (open loop) or fresh water with $NaOH$ (closed loop). There are also closed loop scrubbers operating with seawater and $NaOH$. Normally they have the same layout whether the system is open loop, closed loop or hybrid. Most of the times, they consist of a venturi scrubber, a tower scrubber and a demister.

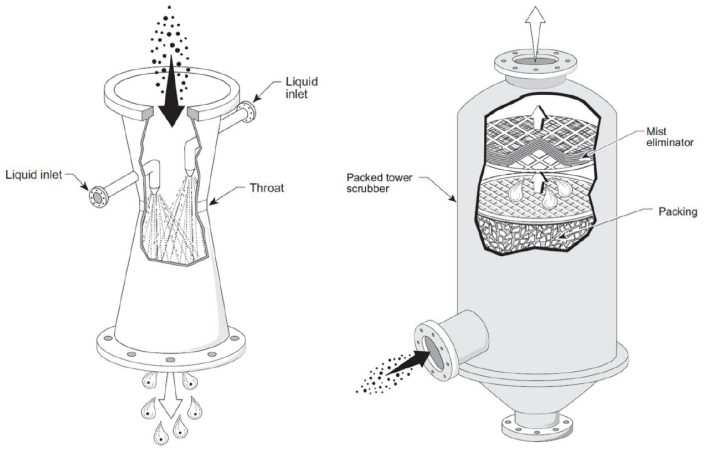

Figure 3.1: Venturi scrubber (left) and tower scrubber (right) [7]

VENTURI SCRUBBER

Figure 3.1 shows a venturi scrubber which may be used as the first stage of a scrubbing system [76]. Although, not all scrubbers have a venturi. The water injected in the venturi is dispersed (water atomisation) and mixed with the exhaust gas because of the high exhaust gas velocity. Turbulent conditions prevail in this part and the kinetic energy of the exhaust gasses is the diving force of the mixing process [7, 75]. The removal efficiency of SO_X is not high due to the limited time and space that the SO_X emissions have for absorption in water. In maritime applications, it serves two main purposes: cooling the exhaust gasses before entering the tower scrubber and removing a considerable part of particulate matter [76]. The lower gas temperature results in a lower gas volume flow and thus longer duration in the tower scrubber. The lower temperature also increases the absorption capability of the scrubbing liquid.

TOWER SCRUBBER

The second stage of the marine scrubber is the tower scrubber (Figure 3.1). For the open and closed loop system, the exhaust gas temperature leaving the scrubber tower is 10°C - 15°C higher than the seawater temperature [8]. To increase the removal efficiency, the tower is filled with packed bed that increase the water - gas contact area and reduces the gas velocity in the scrubber [7]. The packed bed can be structured or dumped. Structured packing is more efficient than dumped because it has higher specific area. Due to more complicated manufacturing procedure, the structured packing is more expensive than dumped [76]. Another factor affecting the efficiency of the scrubber is the alkalinity of water. Ülpre et al. [77] claim that water alkalinity of 1300 μmole/L can remove SO_X efficiently. If the value is higher then it can remove more SO_X, but for values lower than 1000 μmole/L it becomes inefficient [77].

DEMISTER

The demister is placed in the process after the tower scrubber. Its function is to remove the moisture from the exhaust stream, reducing this way the water consumption which is important especially for the closed loop system. A non appropriate demister design may lead to clogging and soot emissions which in turn can create high back pressure in the exhaust. The problem can be solved by a combination of practices: a new demister design; demister cleaning system (nozzles); and the application of venturi before the tower [8].

3.2.1. OPEN LOOP SCRUBBERS

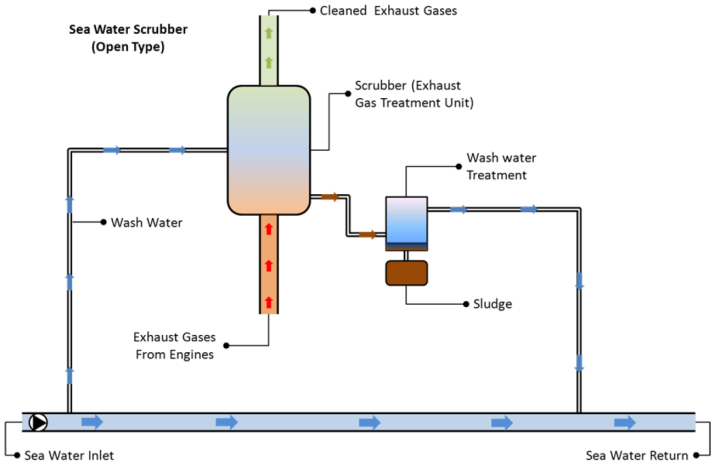

Figure 3.2: Schematic description of an open loop scrubber [8]

The simplest scrubbing system is the open loop scrubber (Figure 3.2), that uses seawater as scrubbing liquid [78]. No other consumable is required for the operation [53]. In the open loop system, seawater is pumped on-board, it is sprayed in the scrubber where it washes out (captures SO_X) the exhaust gasses and then is discharged back to the sea. During this procedure H_2SO_4 is formed as the SO_X come into contact with water particles [77]. Flow rates of seawater in the scrubber are approximately 45 m^3/MWh [57, 79]. The scrubbed water is drained at the bottom of scrubber and prior discharging it to the sea, it passes through a water treatment system to remove the sludge. The water treatment system are normally cyclonic separators or fluctuation systems [75]. The sludge, which generally consists of particulate fuel impurities and carbon particles, is stored in the sludge tank. The absorbed SO_X is not collected but is discharged in the sea. Seawater's alkalinity is used to buffer the SO_X gasses acidity [80]. The alkalinity of seawater is due to bicarbonates (HCO_3^-) and carbonates (CO_3^{-2}). The discharged water is acidic but this is mitigated by the alkalinity of seawater in the vicinity of the discharge nozzle which dilutes it an brings the pH back to ambient levels [77]. If the initial buffering capacity is consumed the pH of the wash water can take a value of 3 [80]

The produced SO_X from the combustion of fuels are dissolved and removed by the scrubbing water. Initially SO_2 is dissolved in water and produces sulphurous acid (H_2SO_3). This is then ionised to bi-sulphate (HSO_3) and HSO_3 is ionised to sulphate (SO_3^{-2}). In the presence of oxygen in seawater SO_3^{-2} is oxidised to sulphate (SO_4^{-2}) [57, 75]. The complete chemical procedure is given below:

$$SO_2 + H_2O \longrightarrow H_2SO_3 \tag{3.1}$$

$$H_2SO_3 \longrightarrow H^+ + HSO_3^- \tag{3.2}$$

$$HSO_3^- \longrightarrow H^+ + SO_3^{-2} \tag{3.3}$$

$$SO_3^{-2} + \frac{1}{2}O_2 \longrightarrow SO_4^{-2} \tag{3.4}$$

Similarly, SO_3 in presence of water will form H_2SO_4, which reacts with water to form hydrogen sulphate (HSO_4^-). Then HSO_4^- and water will form SO_4^{-2} [57, 75]. Analytically the reactions are the following:

$$SO_3 + H_2O \longrightarrow H_2SO_4 \tag{3.5}$$

$$H_2SO_4 + H_2O \longrightarrow HSO_4^- + H_3O^+ \tag{3.6}$$

$$HSO_4^- + H_2O \longrightarrow SO_4^{-2} + H_3O^+ \tag{3.7}$$

This technology is similarly efficient as using low sulphur fuels. The removal rate is around 98%. This means that after scrubbing the sulphur emissions will be equivalent to those of a 0.1% sulphur fuel even if the fuel used has a sulphur content of 3.5% [57]. The energy consumption of an open loop scrubber is 2 - 3 % of the nominal engine power [80].

SEA WATER ALKALINITY

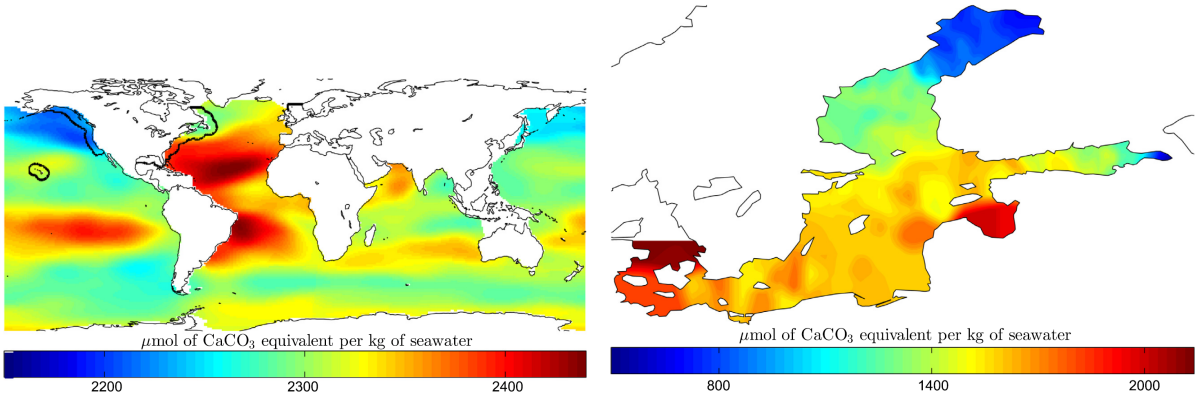

(a) Estimation of global seawater alkalinity based on seawater salinity [81]

(b) Estimation of Baltic Sea seawater alkalinity based on seawater salinity [81]

Figure 3.3: Sea water alkalinity estimation

The pH recovery of the discharged water depends partially on the chemical composition of seawater and on the quantity of dilution. Seawater alkalinity is normally estimated based on calcium carbonate $CaCO_3$ equivalent, because calcium carbonate (a slightly soluble alkaline) is common in seawater. The pH buffering capacity of seawater derives from carbonate (CO_3^{2-}) and bicarbonate (HCO_3^-) ions [77].

Globally seawater alkalinity is in the range of 2000 to 2400 μmole/kg (Figure 3.3a). However, there are areas like the Baltic Sea where alkalinity is lower than 800 μmole/kg (Figure 3.3b) [77]. Generally seawater alkalinity is lower on the surface, because CO_2 is absorbed from the atmosphere and contributes to the production of carbonic acid [82]. To comply with the regulations in areas with low alkalinity, the scrubber must be operated either with larger seawater volumetric flow or by using an additive such as caustic soda.

3.2.2. CLOSED LOOP SCRUBBERS

Closed loop scrubbers are systems that use fresh water with caustic soda ($NaOH$) as scrubbing liquid [53]. The scrubbing liquid can also be seawater and $NaOH$. $NaOH$ is used to increase the alkalinity of the fresh water that has a pH value between 7.5 - 8.5 before entering the scrubber. $NaOH$ is stored in 50% in a aqueous solution [57, 83]. The scrubbing liquid is cooled with seawater that flows in the heat-exchanger to reduce the temperature of the fresh water entering the scrubber and consequently reduce water consumption by minimising the water evaporation [53]. Fresh water is pumped from a buffer tank, where it mixes with $NaOH$, passes through a heat-exchanger and then enters the scrubber. In the scrubber, the scrubbing liquid comes into contact with SO_X to absorb and neutralise them.

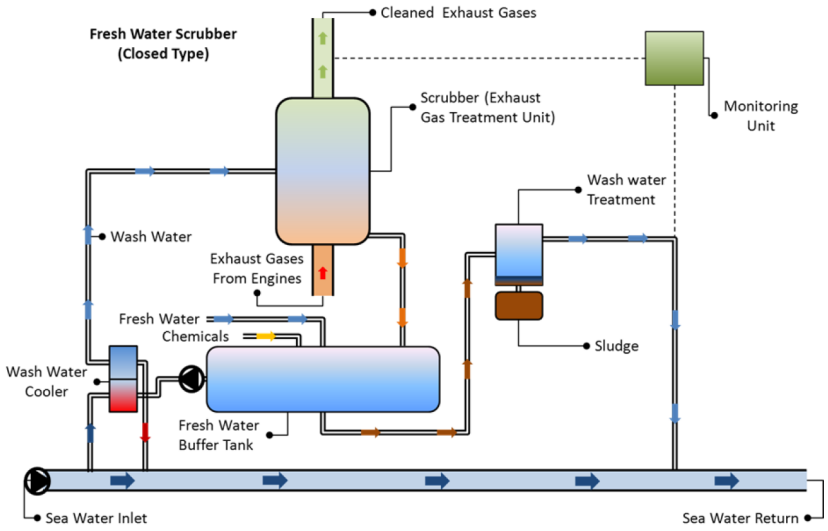

Figure 3.4: Schematic description of an closed loop scrubber [8]

The used wash water is drained from the scrubber is transported to the buffer tank where is treated and sludge removal takes place. Black water containing sludge goes to the sludge tank and clean water is returned back to the scrubbing cycle. The produced sludge mainly consists of particulate matter, but also contains Nickel(Ni) and Vanadium (V). The presence of heavy metals and hydrocarbons makes sludge a hazardous material [75]. The amount of water that evaporates in the scrubber and the one that is taken away as black water with the sludge is recovered. An amount of water is discharged from the vessel but it is small compared to open loop systems (approximately 0.1 to 0.3 m^3/MWh). Closed loop systems can periodically operate without any discharge in the sea [80].

The chemical reactions in the scrubber converts SO_X to sodium sulphate (Na_2SO_4) [57, 75]. There are two cases, one for SO_2 (equations 3.8 - 3.10) and one for SO_3 (equations 3.11 & 3.12).

$$Na^+ + OH^- + SO_2 \longrightarrow NaHSO_3 \tag{3.8}$$

$$2Na^+ + 2OH^- + SO_2 \longrightarrow Na_2SO_3 \tag{3.9}$$

$$2Na^+ + 2OH^- + SO_2 + \frac{1}{2}O_2 \longrightarrow Na_2SO_4 \tag{3.10}$$

$$SO_3 + H_2O \longrightarrow H_2SO_4 \tag{3.11}$$

$$2NaOH + H_2SO_4 \longrightarrow Na_2SO_4 + 2H_2O \tag{3.12}$$

One of the advantages of the closed loop systems is that they can operate in areas where the alkalinity of seawater is low and the scrubbing process in open loop mode is not efficient. Closed loop can be used when high cleaning efficiency is required. By adjusting amount of NaOH entering the buffer tank the pH value is also controlled. In closed loop the liquid flow is lower leading to less corrosion [83]. The operational cost of the closed loop system is higher than the open loop because it uses $NaOH$ (0.8€/kg) [26], monitoring tools and there is the cost of discharging the sludge tank at the harbour.

The efficiency of a closed loop system is about 98% [53, 57]. This efficiency can be affected by the temperature of seawater. High seawater temperature will increase the fresh water consumption (increase evaporation) as the efficiency of the heat exchanger will be reduced. Relative humidity of the air is also important for the efficiency because the air leaving the scrubber is fully saturated and if the atmospheric air is dry them the scrubber will require more scrubbing liquid to operate efficiently. In normal operations the circulation rate of fresh water and $NaOH$ is 35 m^3/MWh [83]. The dosage of $NaOH$ rate is approximately 15 ℓ/MWh of

engine power to scrub a 2.7% sulphur fuel to an equivalent of 0.1% [57]. The energy consumption of a closed loop scrubber is about 2% of the engine power output [80].

3.2.3. HYBRID SCRUBBERS

The hybrid scrubber (Figure 3.5) is a combination of both the open loop and the closed loop system. When operating in open loop it uses seawater and in closed loop the wash water can be either seawater or fresh water [80]. The hybrid scrubber can operate in the closed loop mode in port and other areas in which the discharge of scrubber wash water is prohibited or in areas with low alkalinity. In closed loop mode, the amount of sludge generated is small and thus there is no need to be disposed to port, reducing the operational cost. When allowed it can switch to open loop mode. Except from the advantage of the reducing cost from sludge deposition, another asset of hybrid system is that the water accumulated in the buffer tank can be discharged in the open sea and the tank can be filled up again for the operation in the next harbour.

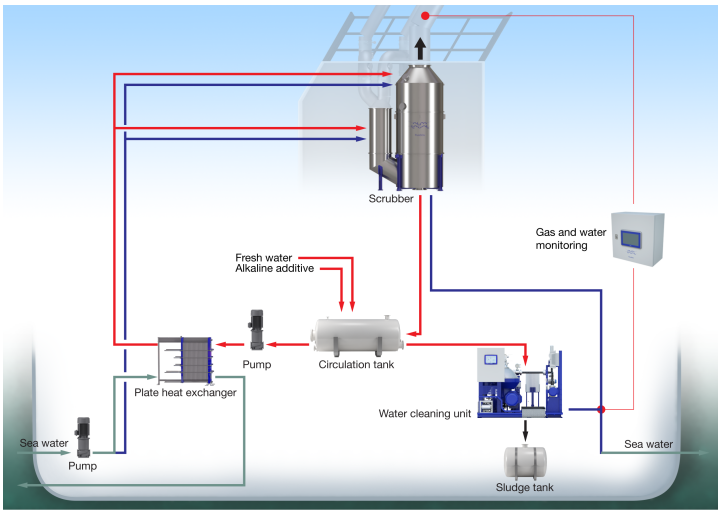

Figure 3.5: Schematic description of the hybrid Pure SO_X scrubber of Alfa Laval

3.3. DRY SCRUBBERS

In the dry scrubber the exhaust gasses get into contact with calcium hydroxide ($Ca(OH)_2$) [76]. $Ca(OH)_2$, also known as limestone, is the most common absorbent used for marine applications [75]. Another absorbent that can be used is bicarbonate ($NaHCO_3$), known also as baking soda [26]. $Ca(OH)_2$ is in the form of spherical granules (Figure 3.6b) or pellet with a diameter between 2 to 8 mm and a bulk density of 800 kg/m^3 [53]. SO_X will be bonded to the molecules of $Ca(OH)_2$ and form calcium sulphate ($CaSO_3$). The absorbent rate of consumption is approximately $40 kg/MWh$ [57]. The complete chemical reactions are the following:

$$SO_2 + Ca(OH)_2 \longrightarrow CaSO_3 + H_2O \tag{3.13}$$

$$2CaSO_3 + O_2 \longrightarrow 2CaSO_4 \tag{3.14}$$

$$SO_2 + Ca(OH)_2 + \frac{1}{2}O_2 \longrightarrow CaSO_4 + H_2O \tag{3.15}$$

$$SO_3 + Ca(OH)_2 + H_2O \longrightarrow CaSO_4 + 2H_2O \tag{3.16}$$

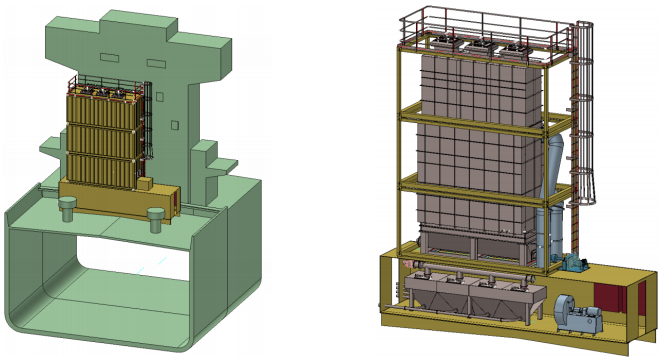

(a) Size of dry scrubber compared to the accommodation area of a vessel (left), dry scrubber (right) [Couple Systems, 2019 [84]].

(b) Calcium hydroxide granulate [85]

Figure 3.6: Dry scrubber and spherical granule size.

Application of dry scrubbers on vessels has several advantages as it requires only electric energy and $Ca(OH)_2$ to operate. The operational temperature is in the range of 240°C to 450°C [57]. The high operational temperatures makes dry scrubber a convenient option for cooperation with a selective catalytic reduction system (SCR) [75]. Dry scrubber can be placed before the SCR, clean the exhaust fumes from sulphur and then the gasses are entering the SCR preventing catalyst poisoning. The spherical shape of the granulates provides the maximum allowed surface for contact of $Ca(OH)_2$ and the exhaust gasses to result in a more efficient absorption. The outcome of this reaction is the formation of gypsum ($CaSO_4$) [57]. This byproduct can be reused in industrial applications (power plants, cement plants, steel plants and agricultural companies) [75].

The efficiency of dry scrubbers is up to 99%, making it capable to meet the IMO requirements [57, 75]. The investment cost is lower than that of a wet scrubber. It has no discharges to marine environment as the used granules are disposed in harbours. The main disadvantages compared to wet scrubbers come when considering the running cost of the equipment and the required space that occupies on the vessel (Figure 3.6a) [57]. Dry scrubber is 8 - 10 times larger than the wet scrubber [26].

3.4. POLLUTANTS REMOVED BY SCRUBBERS

Wet scrubbers are mainly used to remove SO_X from the exhaust gasses. Except from SO_X there are other particles that the wet scrubber can reduce, namely::

- *Particulate matter:* when removing SO_X also particulate matter is taken off the exhaust gasses. If a venturi pre-scrubber is installed then, the removal of PM is more efficient. The removal efficiency is between 70 - 80%, but mainly for the coarser part of particulate emissions [75].
- *Nitrogen oxides:* The wet scrubber cannot remove all the nitrogen oxides, only NO_2. The removal efficiency is small, around 5 - 10% NO_2 is removed. For more effective removal of NO_X a selective catalytic reduction system is required [75].
- *Carbon oxides:* some CO_2 emissions can be taken of by the wet scrubber but this requires the pH of the wash water to be higher than 10 (more $NaOH$ is required). On the other hand, dry scrubbers have a CO_2 removal efficiency of maximum 15%. Wet scrubber cannot remove any CO or HC emissions [75].

3.5. IMPACT OF SCRUBBER DISCHARGES AT SEA

The number of ports and governments prohibiting the discharge of scrubber wash water is increasing the last years. The reason is the negative effects of the discharged water in the local marine environment. The discharged wash water of the scrubber reduces the pH of seawater, making it more acidic. According to the IMO MEPC 59/24/Add.1 Annex 9, Method 1, the wash water should reach a pH greater than 6.5 at the discharge point. An exception is in case of manoeuvring and transit, where a maximum pH difference of 2 is allowed between the ship's inlet and discharge. Method 2 indicates that during commissioning of the unit(s) after installation, the discharged wash water plume should be measured externally from the ship (at rest in a harbour) and the discharge pH at the ship's overboard pH monitoring point will be recorded if the plume at a distance of 4 meters from the discharge point equals or exceeds a pH of 6.5 [80].

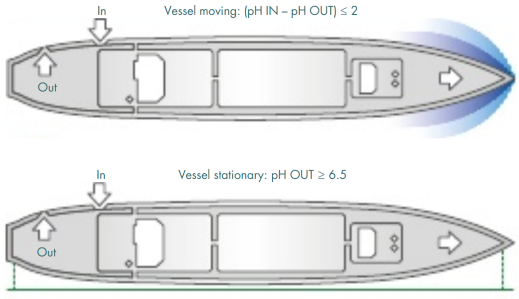

(a) Measurement of position pH – Method 1 [85].

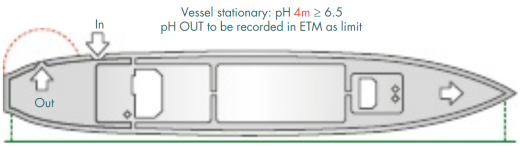

(b) Measurement of position pH – Method 2 [85].

Figure 3.7: IMO pH measurement methods for the wet scrubber discharges.

There are contradicting opinions about the discharges of the wet scrubber. Koski et al. [78] and Bockman et al. [86] claim that scrubbing technology is not solving the problem but shifting it, as the scrubber discharge water is finally discharged back to the sea and is highly acidic (pH around 3). A lot of marine animals and algae have calcified external skeletons, carbonate bodies covering their cells, or carbonate encrusted cell walls and surfaces. The calcium carbonate of calcified tissue appears mainly in the two crystalline forms of calcite and aragonite, the latter being a little more soluble and begins to solute when pH values are 6.3 or less [87]. It is important to have a rapid recovery of the discharged water pH, because it can harm marine organisms. Normally these organism are used to pH fluctuations, but exposure of them for long time in low pH values can be harmful for their well being [82]. Recession of the pH value will have also an impact on other aspects of seawater chemistry: solubility of various compounds; chemical form of metals; charge and other characteristics of amphoteric substances[82].

Discharged wash water contain in addition to sulphur also several chemical compounds like cadmium (Cd), vanadium (V), nickel (Ni), lead (Pb) and Polycyclic Aromatic Hydrocarbons (PAHs). When these substances are at high concentrations, the European Commission characterises them as priority substances that need to be minimised [88]. Discharging these metals and PAHs to the sea could be problematic. These metals, when exist individually and at low concentrations do not have any effect in maritime microorganisms (plankton), but when they mix with scrubber discharges, even at low concentrations, they affect their mortality [78]. U.S. EPA [80] claims that the concentrations of these substances and the pH decrease, in ports and high traffic shipping lines can be higher than the standards.

Other researches support that the dilution at the discharge point is expected to significantly reduce their levels below any environmental limit and thus there is almost no effect of the scrubber operation in ports or coastal waters [75]. If rapid dilution of scrubber discharge water is ensured then the impact can be minimal [78]. Recently CE Delft launched its study about open loop scrubbers, addressing the issue of their impact within port areas, stating their insignificant impact on water quality, in comparison to future EU standards for priority substances in the water [89]. It should also kept in mind that the amount sulphur discharged from wet scrubbers is negligible compered to the total amount of sea [90].

3.6. FINANCIAL ESTIMATION

The available pollution abatement technologies (scrubbers) are able to meet the rigid environmental regulation. Ship owners have to choose the best option for them to comply with the legislation. To come to a decision, most attention is paid on the financial aspect, as fuel cost is normally half of the operational expenses (OPEX) of the vessel [91]. Applying sulphur regulation, also requires a positive "net" effect, meaning that the benefits have to exceed costs [10]. On this aspect the opinions are again divided. Regardless of the option of the shipowner, the additional cost (capital and operating cost) cannot be excluded [92, 93].

By switching to marine gasoil ($MGO < 0.1\%S$) or very low sulphur fuel oil (VLSFO $0.1 < S < 0.5\%$) the vessel operator does not have the investment costs of scrubber. Although, MGO and VLSFO appreciation can be non profitable [94], making this option inappropriate for medium and long term investment [92]. Moreover, VLSFO will require engine modifications, because evaporates at lower temperatures [95]. Natural VLSFO is rare [77] and the refining processes of desulphurisation is an expensive procedure, demanding higher energy consumption at refineries [74], thus increasing the price of distillates. Furthermore, there is a probability that refineries will not be able to meet the high demands of the maritime sector for VLSFO [94]. Analyst of International Energy Agency (IEA) estimate that the IMO rules will drastically reduce HFO use in marine sector up to 75% [9] and increase the demand for VLSFO (Figure 3.8).

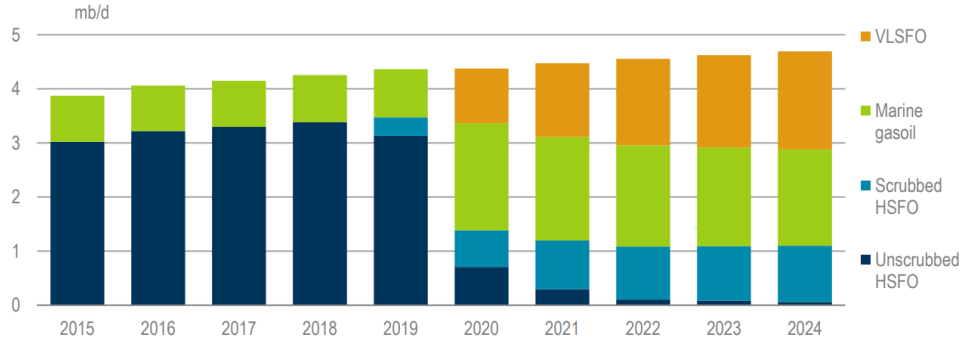

Figure 3.8: Bunker oil demand prognosis [9]

Scrubber installation is a multi-million euro upfront capital expenditure (CAPEX) that include the purchase of the unit and waste water storage tank, the loss of income for the period of retrofit in dry dock [10, 94] and the permanent loss of cargo space on deck [92]. Retrofitting an existing vessel with a scrubber is about 40% more expensive than installing the scrubber in a new-build vessel [10]. The advantage of using a scrubber is that vessel will continue to operate on HFO. Normally the price of HFO is 75% of the crude oil price [74] making the scrubber an attractive option compared to the high cost distillate fuels. The price of HFO may plummet in case of switching to VLSFO [10], but if the demand for scrubber continues to rise then the price of HFO can be resilient in changes. Halff et al. [94] state that even if the orders of scrubber have been increased, still the demand is low compared to the actual number of vessels. IMO has set multiple targets for the protection of environment (NO_X and GHG reduction) and wet scrubbers are not suitable to achieve these reduction levels. By the time the regulation come into force and the first increase of the VLSFO price will be observed, the number of scrubbers on vessels is expected to increase (Figure 3.9). Clarksons research [33] sees 12% of the global tonnage equipped with scrubber at the beginning of 2020, a number that will rise to 19% by the end of 2020. A view shared by the Lloyd's list [96] that predict that round 4000 vessel will be equipped by scrubbers by the end of the year and points out that the queue for scrubber retrofits is large and a third of scrubber orders will miss IMO cap deadline.

For the existing small vessels, Lindstand et al. [74] propose distillates, while they support that scrubber and HFO to be a more attractive option for large vessels. Ülpre et al. [77] and Lindstad and Eskeland [97] consider HFO and a scrubber system as a cheaper alternative compared to LSFO. When the fuel prices are high, scrubbers appear to be more competitive relative to VLSFO [10]. For vessels with lifespan of less that 4 years scrubbers are not a viable financial option, but for new-built vessels they recommend scrubber employment as a more profitable option (Figure 3.10) [10, 92]. In the analysis does not include vessels operating in LNG.

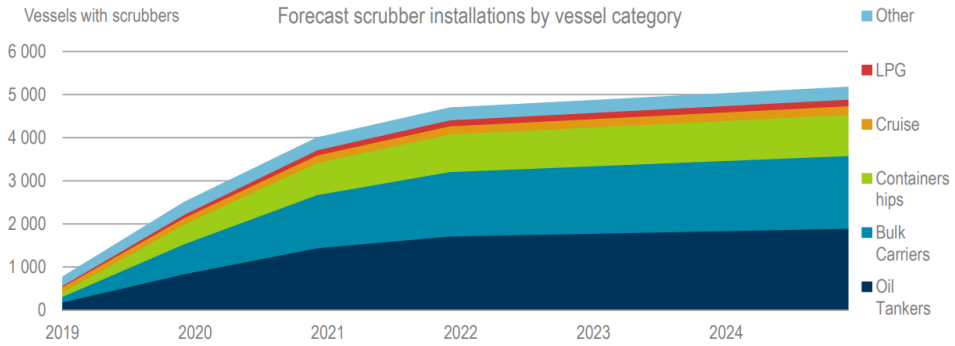

Figure 3.9: Forecast of scrubber installation by vessel category [9]

Ship with high fuel consumption, container vessels, ferries and other long distant transports vessels are the expected candidates [95]. Fuel consumption is consumption per km is a function of the square of vessel speed and when scrubbers are installed it encourages the vessels to operate at higher speeds and the excess fuels consumption is rewarded by the better utilisation of the engine and the scrubber system [74].

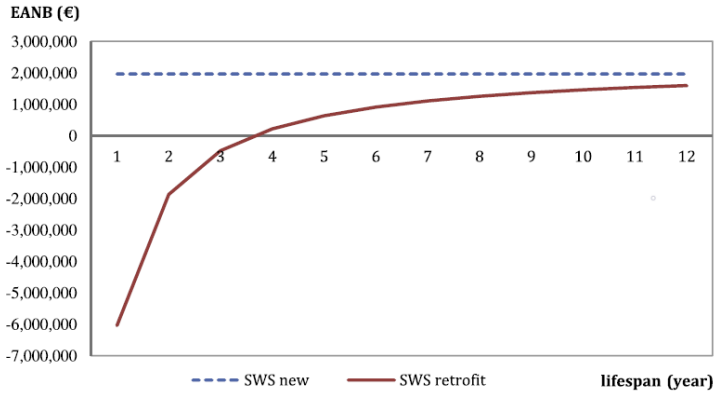

Figure 3.10: Sensitivity of seawater scrubber's equivalent annual net benefit to retrofit's remaining lifespan [10].

In the analysis to follow the low sulphur fuels that will be examined are (MGO) and VLSFO and the high sulphur fuel is IFO-380. The chosen scrubber system that will be examined are open loop and closed loop separately. The data used for the scrubber case are average values from different scrubbers are based on offers received by Royal IHC [98]. The proposed dredger has 3 engines of 2 MW operating in 80% engine load and specific fuel consumption of 200 g/kWh. Two of the engines are used for the vessel's propulsion for about 5000 hours per year and the third is used for running the dredging pump for 3000 hours per year. The average price of a scrubber is 1500000€ and the average total installation cost is 1500000€ (includes installation, design, cutting the hull, documentation, piping, electrical, control and supervision). So, the total CAPEX is 3000000€.

A 10-year financial estimation is made for the open loop, closed loop, VLSFO the MGO case. The annual cost is assumed to be calculated at the end of the year. The reference year is 2019, but for the cash flow it is assumed that the scrubber is installed at the end of 2018 so as to be available on January 1^{st} 2019. Fuel prices are based on estimates of Skandinaviska Enskilda Banken (SEB) for the relative difference between MGO and HFO [99] (see Appendix A). As a reference fuel value is taken the Global 20 Ports average Price for MGO on 20 May 2019 which is 624.2€/ton [100] and is assumed to be constant the next 10 years. For the price of VLSFO predictions of SEB will be used based on the price difference between MGO and VLSFO over the years. NaOH price has fluctuations and the future price is also unpredictable. So, for this reason the price of 19 May 2019, which is 0.8€/ℓ, is used for the calculations and is assumed to be constant the coming years.

When the vessels operates on MGO or VLSFO the considered fuel expenses are only them of the fuel

Table 3.1: Inputs of the financial estimation

Engine Properties	**Value**	**Unit**	**Scrubber Cost**	**Value**	**Unit**
Engine power (MCR)	2000	kW	Purchase	1500000	€/year
sfc (at max power)	200	g/kWh	Installation	1500000	€/year
Engine load	0.8				
Propulsion operational time	5000	h/year	CAPEX	3000000	€/year
Dredge pump operational time	3000	h/year			
Scrubber Properties			**Individual costs**		
Open loop power consumption	200	kW	NaOH	0.8	€/ℓ
Closed loop power consumption	175	kW	MGO	624.2	€/ton
NaOH consumption for 3.5%S	125	ℓ/h			

combustion in the main engine. No scrubber is installed so there is no excess fuel consumption. The fuel cost (FC) of MGO is 2596663.5 $\frac{€}{year}$, is not changing in the 10-year estimation (see Appendix A) and is calculated according to equation 3.17. In a similar way is calculated the price of VLSFO and the result of 2019 are given in equation 3.18. The difference compared to MGO is the price of VLFSO is changing during the years because their difference is increasing.

$$FC_{MGO} = P_{0.8MCR} \cdot sfc \cdot t_{tot} \cdot C_{MGO} = 0.8 \cdot 2000kW \cdot 200\frac{g}{kWh} \cdot 13000hr \cdot 549.08\frac{€}{ton} \tag{3.17}$$

$$FC_{VLSFO} = P_{0.8MCR} \cdot sfc \cdot t_{tot} \cdot C_{MGO} = 0.8 \cdot 2000kW \cdot 200\frac{g}{kWh} \cdot 13000hr \cdot 468.6\frac{€}{ton} \tag{3.18}$$

By using a scrubber, operational costs comparing to the IFO, increase due to scrubber's high power requirements and as a consequence increase in fuel consumption. Compensation comes by continue combusting IFO-380. In this case, the total fuel cost is the cost of normally combusted IFO-380 plus the extra fuel cost for operating the scrubber. Equations 3.19-3.21 provide the fuel consumption of IFO-380 alone, of open and closed loop. The example is only for year 2019. In Table 3.2 are given analytically the results of each year together with the annual cost of NaOH (equation3.22). In Table 3.2, the terms MGO, IFO, VLSFO and NaOH refer to their individual yearly costs, while the terms OL_{IFO} and CL_{IFO} refer to the extra fuel cost (IFO) due to the operation of open loop and closed loop scrubber respectively. Finally, the terms $OL+IFO$ and $CL+IFO+NaOH$ refer to the total cost of the open loop and closed loop scrubber respectively, including fuel and additives for their operation.

$$FC_{IFO-380} = P_{0.8MCR} \cdot sfc \cdot t_{tot} \cdot C_{IFO-380} = 0.8 \cdot 2000kW \cdot 200\frac{g}{kWh} \cdot 13000hr \cdot 325.51\frac{€}{ton} \tag{3.19}$$

$$FC_{open} = P_{open} \cdot sfc \cdot t_{open} \cdot C_{IFO-380} = 200kW \cdot 200\frac{g}{kWh} \cdot 5000hr \cdot 325.51\frac{€}{ton} \tag{3.20}$$

$$FC_{closed} = P_{closed} \cdot sfc \cdot t_{closed} \cdot C_{IFO-380} = 175kW \cdot 200\frac{g}{kWh} \cdot 5000hr \cdot 325.51\frac{€}{ton} \tag{3.21}$$

$$FC_{NaOH} = Load_{engine} \cdot NaOH_{nom} \cdot t_{NaOH} \cdot C_{NaOH} = 0.8 \cdot \frac{125}{3}\frac{\ell}{h} \cdot 13000hr \cdot 0.4\frac{€}{\ell} \tag{3.22}$$

Table 3.2: Operational costs of the examined systems for the decade 2019 - 2028

Year	IFO	OL_{IFO}	CL_{IFO}	NaOH	MGO	VLSFO	OL+IFO	CL+IFO+NaOH	Unit
2018	0	3000000	3000000	0	0	0	3000000	3000000	€/year
2019	1666626	80126	70110	346667	2596663	2261850	1746753	2083404	€/year
2020	922597	44356	38811	346667	2596663	2261850	966952	1308075	€/year
2021	1294612	62241	54461	346667	2596663	2261850	1356853	1695739	€/year
2022	1480619	71184	62286	346667	2596663	2224649	1551803	1889571	€/year
2023	1573623	75655	66198	346667	2596663	2187447	1649278	1986487	€/year
2024	1666626	80126	70110	346667	2596663	2150246	1746753	2083404	€/year
2025	1666626	80126	70110	346667	2596663	2075843	1746753	2083404	€/year
2026	1666626	80126	70110	346667	2596663	2038641	1746753	2083404	€/year
2027	1666626	80126	70110	346667	2596663	2001440	1746753	2083404	€/year
2028	1666626	80126	70110	346667	2596663	2001440	1746753	2083404	€/year

Another conclusion deriving from Table 3.2 is that the yearly operational costs of the scrubber, are lower of that of MGO and VLSFO, but the scrubber has an initial investment cost. To determine which option is more viable in the 10-year approach, the Net Present Value (NPV) is applied with and interest rate of 5% based on the proposal of the European Commission [101]. NPV indicates that the most financially advantageous option is open loop with a cost of 12678096.1€, followed by VLSFO, then the closed loop with a cost of 17813962.2€ and finally MGO with a total cost of 20050747.2€. The VLSFO can meet the global sulphur cap but it cannot meet the SECA's requirements that the scrubber system is able to comply with. Analytically the application on NPV is given in Appendix A.

Even though NPV is a widely applied and accepted method it does not give an indication of the time period of when the one investment becomes more profitable compared to the other. For that reason an analysis was made based on the cash flow and the difference in the yearly expenses of the scrubber and MGO. Again, MGO is used as the reference. The return on investment of the scrubber is provided in Figure 3.11. As it can be seen by the middle of 2020 both scrubbing systems become more advantageous compared to MGO even though MGO had a zero initial investment and the scrubber had an investment of 3000000€.

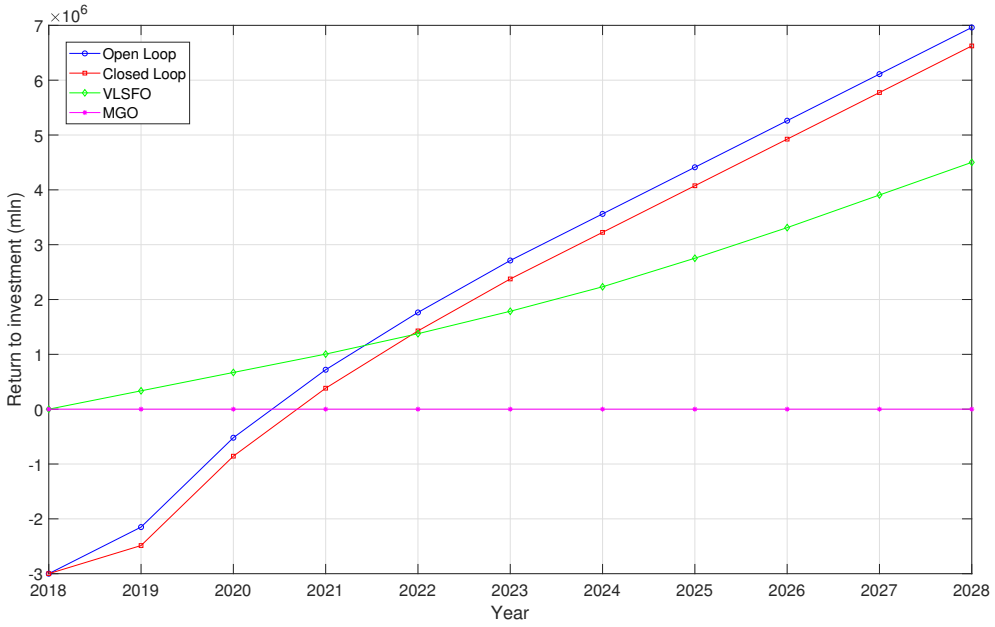

Figure 3.11: Payback time of the scrubber system and VLSFO compared to MGO

Both financial analysis converge that the scrubber is a better financial option to deal with the new legislation. In NVP method, VLSFO seems to be more profitable, but considering that with the closed loop system the vessel can operate in SECA, gives it an advantage compared to VLSFO. Moreover, a study submitted to IMO by Finland and Germany [32], indicates that new blends with 0.5% sulphur content can contain large amounts of aromatic compounds and increase black carbon emissions. Although, this analysis is just an estimation based on a hypothetical dredger and predictions for the future value of the fuels, so there is an error rate. However, it provides a base where the ship owner can start an analysis and considering the remaining operational years of the vessels, can estimate which option is more favourable.

3.7. CONCLUSIONS

IMO regulation for the global sulphur cap is already in force and the ship operators need to decide how they are going to deal with it. In the analysis carried out in this chapter, it was shown that the abatement technologies to deal with SO_X pollution in maritime sector are more than one. There is the option to replace the diesel engine with another engine that can combusts a sulphur free fuel (e.g. LNG), but this is an expensive option for the vessels that are already operating. It mostly appeal to new build ships. Then there is the option to keep diesel engines and either apply low sulphur fuels or a scrubber. Among the wet scrubber and the dry scrubber the most appropriate for marine applications is the wet scrubber. A dry scrubber is 8 - 10 times larger than a wet scrubber and has higher operational cost. Thus, a wet scrubber is more appropriate as space is of paramount importance for vessels.

Comparing MGO and a wet scrubber, it was shown that both these options achieve the same sulphur oxide emission reduction. For for large ships or for ships with long lifespan, the financial analysis indicates that MGO has higher cost and is more suitable for small vessels or vessels with short lifespan. In the case of the wet scrubber, there are 2 options. The hybrid case was not examined as it requires to know the operational areas of the vessel and the time spend in each one. Open loop seem more simple and has lower operational cost as it uses seawater, but in areas with low seawater alkalinity it is not efficient and also many countries with high sea traffic have prohibited the scrubber discharges in their waters. By having a bit higher operational cost for NaOH, a shipowner can opt for a closed loop which solves the problems of open loop and also offers the advantage of increasing the efficiency by controlling the amount of NaOH in the wash water. In the following chapters, the modelling of closed loop scrubber will be carried out.

4

MODELLING APPROACH

"If I had nine hours to chop down a tree,
I'd spend the first six sharpening my axe."

Abraham Lincoln

4.1. INTRODUCTION

Modelling is an activity, a cognitive activity in which the thoughts are used to create models and describe how devices or objects of interest behave [102]. The multitude parameters affecting the performance and operation of scrubber, make experimental analysis time and financial consuming. Absorbers are by nature massive devices, that are feed sometimes by larger sources and all the systems require considerable setups. On the other hand, simulation by using mathematical modelling is economical and fast method to reach sufficient conclusions for both static and dynamic conditions. In the scrubber technology, dynamic simulations are important to determine process responses such as load variations and liquid feed changes. So far, liquid feed is constant in most cases regardless of the engine load leading to unnecessary power consumption of the water supply pump.

Modelling of an scrubber system is not a recent endeavour. Previous research regarding scrubber modelling focused on stationary industrial applications for particulate matter capture. The basic principles can also be applied for SO_X absorption. Maritime scrubbers gained popularity the last years due to the sulphur limits imposed by IMO as they allow ship operators to continue operating their vessels with cheap heavy fuel oil. Research related to wet scrubbers is mainly performed by scrubber manufacturers. Their focus is concentrated in the reduction of sulphur oxides in the gas flow. In the closed loop scrubbers it is important the investigation of evaporation and consumption of water, because they use fresh water as scrubbing liquid. The fresh water has to be carried or made on board.

A dynamic model of a closed loop wet scrubber operating with fresh water and caustic soda will be created for future integration to a diesel engine model. The scrubber model consists of three resistance elements, namely the venturi scrubber, the tower scrubber with a packed bed and the demister and two volume elements (lower and upper) to connect the resistance elements. The absorption of SO_2 is mainly taking place in the packed bed and the two phase flow of exhaust gas and scrubbing liquid was modelled in this section. The gas flow in the packed bed could be modelled with a combination of resistance and volume elements as this phase is compressible. The liquid flow and liquid film thickness in the packed bed will be modelled based on the conservation of mass and the liquid holdup theory. A feedback control system controls the scrubbing liquid flow based on the sulphur dioxide to carbon dioxide ratio.

4.2. OVERALL SYSTEM

To investigate the influence of the scrubber system on diesel engine and simulate real dynamic load conditions, the dynamic model of the scrubber is built for a future integration with a diesel engine model. The inputs to the scrubber system are exhaust gasses from the diesel engine, scrubbing water from the pump and the ambient conditions (Figure 4.1). For easier future integration with the diesel engine model the scrubber system will be modelled as a combination of resistance and volume elements. Diesel B model developed by TU Delft belongs to the category of the high order Mean Value First Principle (MVFP) models, and follows the resistance and volume element approach. The scrubber model will be approached as an resistance element, together with the diesel engine inputs and the pump system and for the ambient block volume element approach will be adopted. Diesel engine and pump will provide to the scrubber mass flow, temperature and composition while the ambient conditions will provide pressure as input. The outputs of the wet scrubber system are mass flow, temperature and composition of the exhaust gasses to ambient. Moreover, the wet scrubber will add back pressure to the diesel engine increasing the fuel consumption. The aim is that the wet scrubber will not operate in full load continuously, but will follow the load of the main engine while complying the to sulphur oxide emission limits.

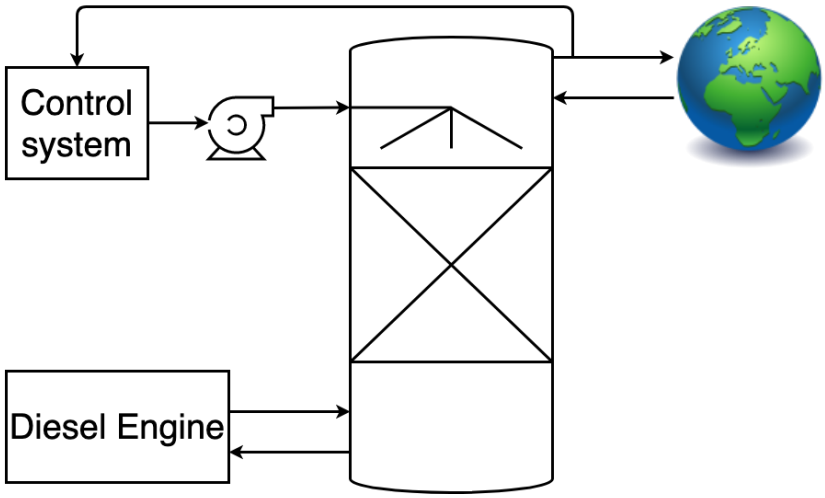

Figure 4.1: Overall approach of the involved systems

Exhaust gasses enter the scrubber at the bottom of the tower and follow an upward movement due to the pressure difference with the ambient. A pump supplies water at the top of the scrubber and the liquid dispenser ensures a uniform distribution of flow in the column cross-section. The dispenser is followed by the packed bed. Finally, the bottom of the column acts as a fluid collection vessel, with the gas dispensing system slightly higher. The complete wetting of the packed bed with the liquid and the good distribution of the two phases in the cross sections of packed bed are essential for the process to function effectively. Particular difficulties occur if the liquid supply is too low and also if the speeds of the two phases are high resulting in flooding. Flooding conditions are not taken into account in this thesis.

4.3. CONTROL SYSTEM

The most important evaluation criteria for the wet scrubber operation is the reduction of sulphur dioxide and the amount of liquid supplied. The purpose of the control system is to keep the amount of the sulphur dioxide to carbon dioxide ratio $\left(\frac{ppmvSO_2}{y_{CO_2}}\right)$ bellow the SECA limit and at the same time reduce the liquid supply from the pump as much as possible. To do so the feedback approach is adopted. The value of the sulphur dioxide to carbon dioxide ratio is measured before the outlet of the scrubber and the signal is provided to a PI controller that provides the pump the information for the required liquid flow in the scrubber. The overall system is given in Figure 4.1.

The principle of this open loop strategy is to calculate the require amount of scrubbing liquid flow rate so as the exhaust gas leaving the scrubber to have less sulphur dioxide than the SECA's demands. The setpoint for the PI controller is decided to be 75% of the SECA limit value.

$$\left.\frac{ppmvSO_2}{y_{CO_2}}\right|_{setpoint} = 0.75 \cdot 4.3 \tag{4.1}$$

The steady state error is the setpoint minus the sulphur dioxide to carbon dioxide ratio. The error becomes non dimensional by dividing it with the setpoint and then is feed to the controller (Figure 4.2).

$$e(t) = \left.\frac{ppmvSO_2}{y_{CO_2}}\right|_{setpoint} - \left.\frac{ppmvSO_2}{y_{CO_2}}\right|_{scrubber} \tag{4.2}$$

A time constant of 2 seconds is meant to imitate the inertia of the system (pump and pipes). The signal from the pump response is multiplied with the nominal value of the liquid supply that was found in the previous chapter and the output is provided to the scrubber.

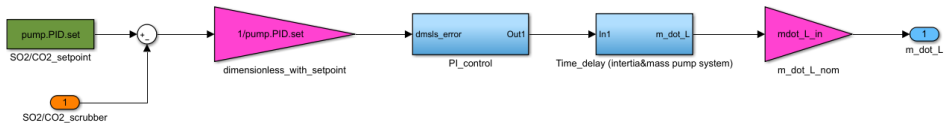

Figure 4.2: Water supply control system

4.4. MODELLING APPROACH

In chemical engineering, devices can be classified as open or closed systems. An closed system is the one that no substance enters or leaves the device and no substance penetrates the system boundaries. Inside the system there are various changes but there is no mass exchange with the environment. If a substance crosses the boundaries of a system then the system is characterised as an open system [103]. Scrubbers are considered open system.

Chemical process devices can also be classified according to how they operate, namely continuous and batch operation. For continuous operation, the inflow and outflow of material streams is continuous and constant. As a result, the devices operate in a steady state conditions, that is the conditions at each point of the device remain unchanged over time. Batch-fed deivices, where conditions inside it change gradually over time are less common [104]. Maritime absorbers are characterised by continuous process.

Continuous devices are distinguished in lumped and distributed systems. In the first, the two phases come in contact, alternate components and separate, a process that is repeated at each step (different operating conditions exist at different steps). Perfect mixing is characterising these processes. In the second, the two phases are in continuous contact without interfering with successive separations. Packed columns, which allows good dispersion and liquid/gas contact, are the most common example of a distributed device. The distinction between distributed and lumped process is crucial to how they are designed. The distributed are designed based on the assumption that the output currents of each step are in thermodynamic equilibrium. Lumped processes continuously maintain a divergence from phase equilibrium and are designed using mass transfer coefficients [104, 105]. In the wet scrubber some parts of it will be approached as lumped and other as combination of both lumped and distributed processes. The packed bed for example will be modelled as a distribute system with several lumps.

4.5. GAS PHASE MODEL APPROACH

The gas phase of the scrubber device will be modelled as a combination of a resistance and volume elements (Figure 4.3). Each of these elements calculates a different set of variables.

(a) Volume element (b) Resistance element

Figure 4.3: Resistance and volume elements of the gas phase

4.5.1. VOLUME ELEMENT

In a volume element, the inputs are the gas mass inflow and outflow of the control volume, the temperature and the composition, while the output is the pressure of the control volume (Figure 4.3a). The total mass balance (conservation of mass) is integrated to obtain the mass in the control volume (equation 4.3). Integration of the energy balance (first law of thermodynamics) provides the temperature of the control volume (equation 4.4). Generally the volume element acts as an integrator [106]. Knowing the temperature and the net mass of the control volume, the ideal gas law can be applied to calculate the pressure in the control volume (equation 4.5).

$$\frac{dm^g}{dt} = \dot{m}^g_{in} - \dot{m}^g_{out} = \dot{m}^g_{net,cv} \tag{4.3}$$

$$\frac{d(m^g \cdot u^g)}{dt} = \dot{m}^g_{in} \cdot h^g_{in} - \dot{m}^g_{out} \cdot h^g_{out} + \dot{Q}^g - \dot{W}^g \tag{4.4}$$

$$p^g_{cv} = \frac{m^g_{net,cv} \cdot R \cdot T^g_{cv}}{V^g_{cv}} \tag{4.5}$$

Some assumptions made for the volume element are:

- The terms of potential and kinetic energy are small compared to the enthalpy changes and thus they are neglected [104].
- Shaft work does not change/exist because these kind of devices rarely have moving parts. Also, work flow is already included in the enthalpy.

The governing equation for each case that the volume elements are used will be provided in the corresponding chapters.

4.5.2. RESISTANCE ELEMENT

While the volume element is used to calculate the pressure of the control volume, the resistance element (Figure 4.3b) is used to calculate of the mass outflow of the control volume. A resistance element can be modelled as an orifice (Figure 4.4) because there is no mass accumulation [106]. In the case of a steady and incompressible flow the momentum equation is given by equation 4.6.

$$\frac{p^g_{in}}{\rho^g \cdot g} + \frac{(v^g_{in})^2}{2 \cdot g} = \frac{p^g_{out}}{\rho^g \cdot g} + \frac{(v^g_{g,out})^2}{2 \cdot g} + \frac{p^g_{loss}}{\rho^g \cdot g} \tag{4.6}$$

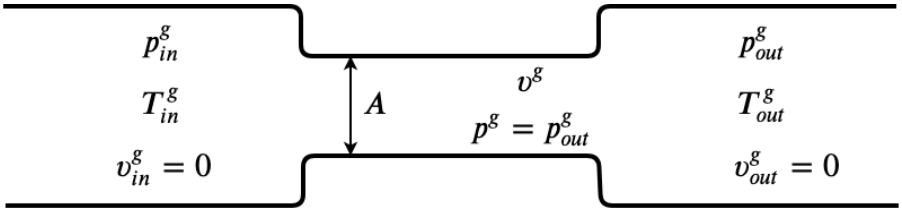

Figure 4.4: Orifice representation

The pressure in the throat is assumed to be equal to the pressure after the throat ($p^g = p^g_{out}$). Along the orifice there is a pressure loss (p^g_{loss}) that represents the losses of the gas phase at the entrance of the resistance. It is commonly written as:

$$p^g_{loss} = \zeta \cdot \frac{\rho^g \cdot v^2}{2} \tag{4.7}$$

Assuming that the downstream velocity in the volume is zero [106] and by combining equations 4.6 and equation 4.7 the velocity in the throat is:

$$v^g = \sqrt{\frac{2 \cdot (p^g_{in} - p^g_{out})}{(1+\zeta) \cdot \rho^g}} \tag{4.8}$$

The ideal gas law provides the density of the gas phase.

$$\rho^g \approx \rho^g_{in} = \frac{p^g_{in}}{R \cdot T^g_{in}} \tag{4.9}$$

In a resistance element the mass flow is calculated by:

$$\dot{m}^g = \rho^g \cdot A_{eff} \cdot v^g \tag{4.10}$$

The effective area of the flow is smaller than the geometric area A and is equal to $A_{eff} = \varepsilon \cdot A$. Where ε is the void fraction. By implementing the equations 4.8 and 4.9 in equation 4.10 and by applying simple rearrangement of the terms, results in the following expression for the mass flow:

$$\dot{m}^g = \frac{A_{eff}}{\sqrt{(1+\zeta)}} \cdot \frac{p^g_{in}}{\sqrt{R \cdot T^g_{in}}} \cdot \sqrt{2} \cdot \sqrt{1 - \frac{p^g_{out}}{p^g_{in}}} \tag{4.11}$$

Although the above analysis is valid for incompressible flow. The flow of the ideal gas (and in this case the exhaust gasses) is anything but incompressible according to White [14] and so the isentropic relations have to be used. Following the analysis of Stapersma [107], the mass flow equation needs to be transformed in the following:

$$\dot{m}^g = \frac{A_{eff}}{\sqrt{(1+\zeta)}} \cdot \frac{p^g_{in}}{\sqrt{R \cdot T^g_{in}}} \cdot \Psi \tag{4.12}$$

The term Ψ is a function of pressure ratio π ($\pi = \frac{p_{in}}{p_{out}}$) and the ratio specific heats γ ($\gamma = \frac{c_p}{c_v}$). It is worth mentioning that the critical pressure ratio π_{crit} is given by equation 4.13

$$\pi_{crit} = \left(\frac{\gamma+1}{2}\right)^{\frac{\gamma}{\gamma-1}} \tag{4.13}$$

Three characteristic cases can be observed. They are provided below:

$$\Psi = \sqrt{2} \cdot \sqrt{1 - \frac{1}{\pi}} \qquad \text{for incompressible flow}$$

$$\Psi = \sqrt{\frac{2 \cdot \gamma}{\gamma - 1}} \cdot \sqrt{\left(\frac{1}{\pi}\right)^{\frac{2}{\gamma}} - \left(\frac{1}{\pi}\right)^{\frac{\gamma+1}{\gamma}}} \qquad \text{for } \pi < \pi_{crit}\text{, compressible flow}$$

$$\Psi = \sqrt{\gamma \cdot \left(\frac{2}{\gamma+1}\right)^{\frac{\gamma+1}{\gamma-1}}} \qquad \text{for } \pi > \pi_{crit}\text{, compressible flow}$$

4

4.6. WET SCRUBBER SECTIONS APPROACH

Figure 4.5 shows the scrubber and its separation in smaller sections, namely the venturi; the lower volume, the packed bed, the upper volume and the demister. The approach that will be followed is to model all these parts individually and connect them to each other in order to create a system whose part/subsystems will interact to each other.

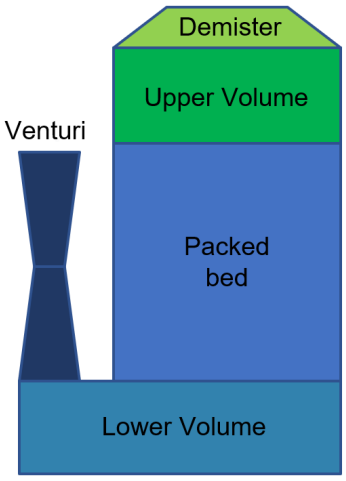

Figure 4.5: Parts composing the wet scrubber system.

The venturi, packed bed and the demister will be modelled as a resistance elements and the upper and lower volume will be modelled as a volume element (Figure 4.6). All the parts will be approached as lumped systems, with the properties being evenly distributed throughout the volume. The packed bed section, where SO_X and evaporation mainly occur will be approached as a combination of distributed and lumped system. The liquid flows in the packed bed section and has no interaction with the gas phase of the other sections. Liquid model will be discussed later.

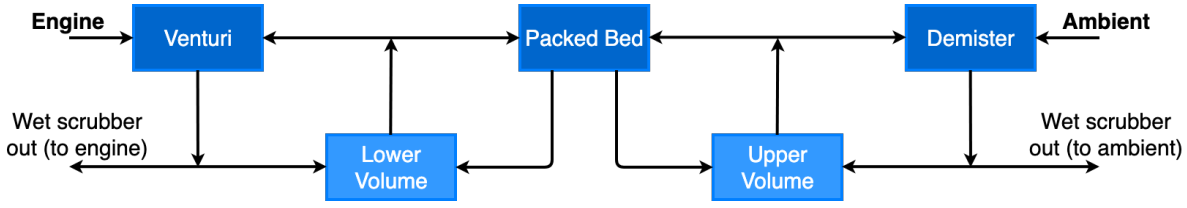

Figure 4.6: Sections of the wet scrubber as resistance (upper row of blocks) and volume (lower row of blocks) elements.

4.7. PACKED BED APPROACH

The purpose of the absorption columns is to combine uniformity in radial direction and low dispersion in axial. This behaviour is achieved by the use of packing material. The liquid disperses over the packed bed and moves downward, in the form of a film in contact with the material wall. The gaseous phase moves upward through the channels / openings leaving the packing material and the wet film. Considering the gas phase, the entire packed bed section is modelled as resistance element. To obtain more accurate results for the removal efficiency of sulphur oxides and the evaporation of water in the scrubber the packed bed will be modelled as a distributed system composed by smaller lumped system. Therefore, the gas phase of the packed bed will be a combined system of resistance and volume elements Figure 4.7.

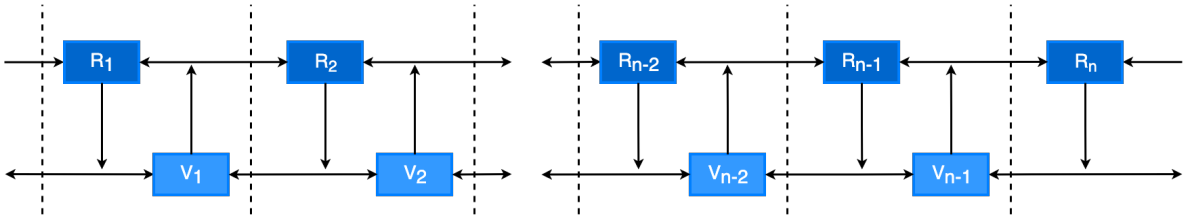

Figure 4.7: Packed bed gas phase discretisation to resistance and volume element

The packed bed will be divided in smaller pieces where liquid and gas flow come into contact exchanging heat and mass transfer. The properties of both phases in the packed bed section will vary with respect to the axial direction of the packed bed. In the same section the properties will be the same regardless if the substance is in the centre of the packing material or close to the walls of the scrubber. Each phase will be an autonomous control volume.

4.7.1. CONTROL VOLUME APPROACH

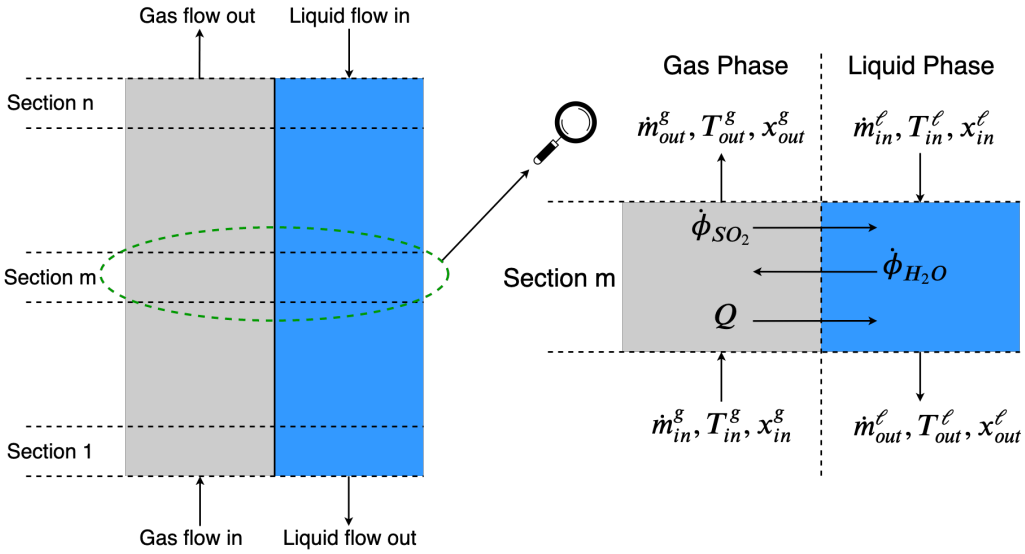

Figure 4.8: Packed bed presentation in n-sections (left) and detailed presentation of a random section m (right)

The created stack of sections is given in Figure 4.8. The liquid (denoted by blue) is fed to the top of the column and flows down due to gravity, while the gas (denoted in grey) is fed to the bottom and moves upward due to hyper-pressure. In each of these sections coexists liquid and gas. The rate of mass transfer from the gas phase to the liquid phase is proportional to the interface created by the two phases and proportional to the deviation of the concentration from the equilibrium value (i.e. the maximum solubility of the gas in the liquid). Solubility maximisation is achieved by reducing the temperature while maximising the liquid gas

interface by choosing the appropriate contact device. Often the absorption towers are filled with packing material so that the fluid flows over it in the form of a thin film thus obtaining an extended interface. The packing material improves water distribution and creates a high water-air interface [104].

In a random section m (Figure 4.8 right) gas and liquid flow come into contact and there is a simultaneous mass and heat transfer. Each phase has its own control volume and the properties of each phase are calculated there. In the control volume there is a two directional flow. There are the axial flows of the fluids but there is also the radial mass flow of sulphur dioxide from the gas to the liquid phase (ϕ_{SO_2}) due to absorption and the radial flow of water from the liquid to the gas phase (ϕ_{H_2O}) due to evaporation. There is also radial heat transfer ($\dot{Q}$) from gas to liquid. The gas control volume m, has as inputs mass flow, temperature and composition from the control volume m-1. The outflow are the same properties but with new values that derive from the calculations in control volume m. The outflow of control volume m is the inflow of the control volume m+1. The same applies to the liquid phase control volume m, but now the input are the properties from control volume m+1 and the outflow of m is the inflow for control volume m-1.

4.8. LIQUID PHASE MODEL

The liquid entering the scrubber in the closed loop mode, is stored in the water tank and is circulated by pumps. Liquid flow enters the scrubber at the top of the scrubber tower, more specifically in the upper volume, between the demister and the packed bed. Before entering the packed bed, liquid is distributed uniformly. Once, entering the scrubber the movement of the liquid is governed by gravity alone. The pressure difference is not affecting the vertical movement of the liquid because the scrubber is an open system and the pressure of water is assumed to be atmospheric everywhere in the scrubber tower. The approach that was used in the gas phase with resistance and volume elements cannot be applied in the case of liquid, as these models require a pressure drop. Thus, an alternative way to model the liquid phase needs to be introduced.

In the model of the liquid phase, only the packed bed part will be examined, because this is the area where the mass transfer is carried out and there are the major interactions between the two phases. In the venturi, the high speed of gas creates conditions for water atomisation and there is a mixture of the gas phase and the liquid phase which is in the form of both droplets and liquid film making the approach challenging. The size of the droplets varies and is difficult to be estimated. It is assumed that the venturi part contribute only as a normal part for the gas phase to flow. In the lower volume, the water falling from the packed bed is in the form of droplets, not evenly distributed and because of the big diameter of the scrubber there is not significant interaction of the two phases and thus can be neglected. In the upper volume the water enters just before the packed bed and the gas that flows in this part is in most of the cases saturated in water vapour. Also the droplets falling from the condensation in the demister are not significant compared to the total size of the upper volume. In the demister there is no extra water injected. The steam is condensed in this part and the water droplets formed do not create conditions that will affect the mass transfer or temperature in this area of the scrubber.

Considering that the pressure of the liquid in the scrubber is constant the one thing to be defined in the model for the liquid phase is mass balance of the control volume of the packed bed.

$$\frac{dm^{\ell}_{pb}}{dt} = \dot{m}^{\ell}_{pb,in} - \dot{m}^{\ell}_{pb,out} - \dot{\Phi}_{H_2O} = \dot{m}^{\ell}_{pb,cv} \tag{4.14}$$

The total amount of liquid mass in the control volume is:

$$m^{\ell}_{pb,cv} = \rho^{\ell} \cdot V^{\ell}_{pb,cv} \tag{4.15}$$

In this stage, is important to define the liquid volume by using introducing the assumption for the liquid phase. The void fraction created by the packed bed is occupied by both the gas and the liquid phase. This void areas have irregular shape and orientation. It is assumed that the empty space of the packing can be replaced, for theoretical considerations, by vertical flow channels through which the liquid flows evenly distributed downwards and the gas flows upwards in counterflow. The geometrical shape cannot defined by the surface area or the volume alone. In the model is assumed that deviation of the real flow behaviour

from the vertical flow channels in mass transfer columns can be expressed by specific shape constant. An important shape constant is the specific surface area α. Specific surface area, is the area of the packing in contact with liquid per cubic meter packed volume. Together with the void fraction, ε they define the hydraulic diameter d_h [108]:

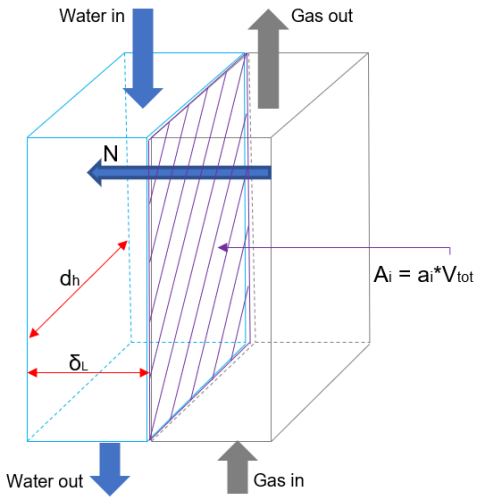

Figure 4.9: Wet surface area crated by the gas and liquid film

$$d_h = 4 \cdot \frac{\varepsilon}{\alpha} \tag{4.16}$$

In the devices that have packing material the interface between the two phases (liquid-gas) is difficult to determine and strongly dependent on the phase conditions of the two phases. From the definition of the specific surface area, the wet surface area (sometimes also referred as interface area A_i) in the packed bed can be defined. It is the product of the specific surface area an the total volume of the packed bed.

$$A_w = \alpha \cdot V_{pb,tot} \tag{4.17}$$

The liquid is assumed to flow down and come into contact with the gas in one straight area which is the wet surface area. Hydraulic diameter can be used as the width of the liquid film. The film except from a width it also has a thickness, δ^{ℓ}. Now that the major dimensions of the liquid film are defined, the mass of the liquid in the control volume (equation 4.15) can be rewritten as:

$$m_{cv}^{\ell} = \rho^{\ell} \cdot A_w \cdot \delta^{\ell} \tag{4.18}$$

Substituting the last equation in the relation of the mass balance 4.14 :

$$\frac{d\left(\rho^{\ell} \cdot A_w \cdot \delta^{\ell}\right)}{dt} = \dot{m}_{in}^{\ell} - \dot{m}_{out}^{\ell} - \dot{\Phi}_{H_2O} \tag{4.19}$$

In the left side of 4.19, the term A_w has no time dependency and is constant because is the product of two constant variables. Also, it is assumed that the liquid density is independent of temperature and pressure (incompressible liquid). The variable δ^{ℓ} has a time dependency because the film thickness depends on the amount of water flow in in the scrubber at every single moment. So, relation 4.19 is written as:

$$\frac{d\delta^{\ell}(t)}{dt} = \frac{\dot{m}_{in}^{\ell} - \dot{m}_{out}^{\ell} - \dot{\Phi}_{H_2O}}{\rho^{\ell} \cdot A_w} \tag{4.20}$$

The mass flow in the control volume is the product of the density of the fluid, the vertical surface (vs) of the flow direction and the speed of the flow:

$$\dot{m}_{cv} = \rho^{\ell} \cdot A_{vs} \cdot v_{cv}^{\ell} \tag{4.21}$$

The vertical area in the flow direction is equal to the hydraulic diameter times the film thickness.

$$A_{vs} = d_h \cdot \delta^{\ell} \tag{4.22}$$

The only unknown until now is the velocity of the control volume. For the determination of the velocity, the empirical formula from Billet and Schultes [108] for the liquid holdup in packing materials will be used. The liquid holdup is the amount of liquid per volume of packed bed.

$$h^{\ell} = \left(12 \cdot \frac{\mu^{\ell}}{g \cdot \rho^{\ell}} \cdot v_s^{\ell} \cdot \alpha^2\right)^{1/3} \tag{4.23}$$

This relation is applied to loading conditions up to the loading point of the two phase counterflow. In this thesis this conditions will not be exceed as it is assumed no flooding. The velocity in the above relation (v_s) is the velocity of the liquid with reference to empty column cross section, and is referred in the bibliography as the superficial velocity. The packing material occupies some of the space in the packed bed section. The free volume for the flow is thus smaller than the geometrical volume of the packed bed section. The free volume for the flow is the product of the void of the packed bed and the total volume of the packed bed:

$$V_f = \varepsilon \cdot V_{pb.tot} \tag{4.24}$$

In the void volume for the flow one part of it is occupied by the gas phase and another by the liquid phase. The total volume of the gas phase is in the control volume is:

$$V_{pb,cv}^{g} = (\varepsilon - h^{\ell}) \cdot V_{pb.tot} \tag{4.25}$$

And the total volume of the liquid phase is:

$$V_{pb,cv}^{\ell} = h^{\ell} \cdot V_{pb.tot} \tag{4.26}$$

The volume of the liquid can be obtained by by assuming that the liquid phase flow is a liquid film with a straight wet area (A_w) and a film thickness of δ^{ℓ}. Thus, the volume of the liquid film is $V_{pb,cv}^{\ell} = A_w \cdot \delta^{\ell}$. By using this relation and doing rearrangement of the term of equation 4.26, the liquid hold up can be calculated.

$$h^{\ell} = \frac{A_w \cdot \delta^{\ell}}{V_{pb.tot}} \tag{4.27}$$

From equation 4.27 the value of liquid hold up can be calculated. Then the value of h^{ℓ} will be used to to equation 4.23 so as to calculate the velocity of the liquid for the case that the scrubber is empty (without packing material), v_s. For the model the required velocity is that of the control volume in the presence of packed bed and the gas. The liquid mass flow from the cross sectional area of the empty scrubber (A_{sc}) is equal to that of the scrubber with the packed bed.

$$v_s^{\ell} \cdot A_{sc} = v_{cv}^{\ell} \cdot d_h \cdot \delta^{\ell} \tag{4.28}$$

Finally by doing rearrangement of the terms of the above equation:

$$v_{cv}^{\ell} = \frac{v_s^{\ell} \cdot A_{sc}}{d_h \cdot \delta^{\ell}} \tag{4.29}$$

Due to the assumption of the perfect mixing the liquid velocity in the control volume is equal to that leaving the control volume. So, the mass flow out of the control volume is given in equation 4.30. The entire approach can be found in Figure 4.10.

$$\dot{m}_{cv}^{\ell} = \rho^{\ell} \cdot d_h \cdot \delta^{\ell} \cdot v_{cv}^{\ell} \tag{4.30}$$

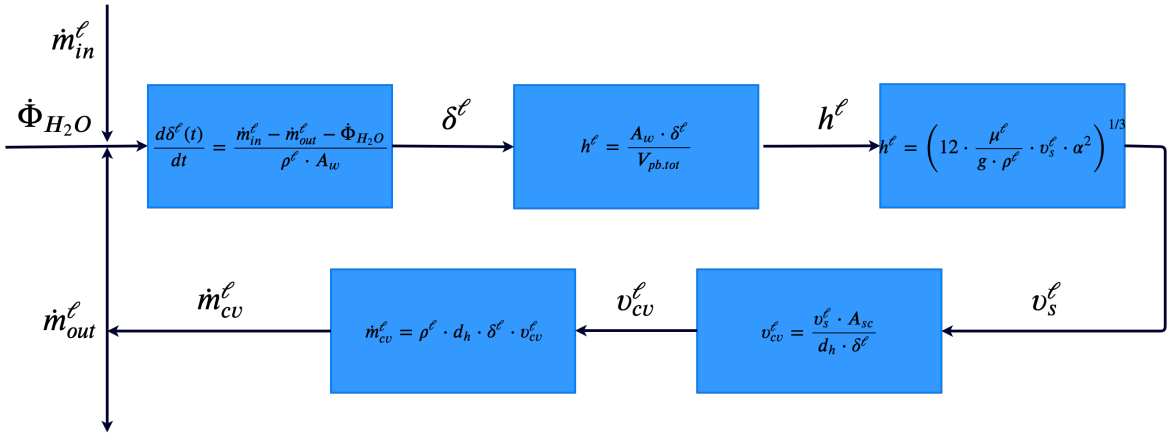

Figure 4.10: Wet surface area crated by the gas and liquid film

In the calculations of the packed bed is convenient to work with mole flow instead of mass flow due to the chemical reaction, absorption and evaporation process. Also in the case of the packed bed the term of the amount of water evaporated should be added in the mole balance. More analytically that will be described in the next chapter.

4.9. COMPOSITION AND MAIN ASSUMPTIONS

Exhaust gas composition is important to determine the thermodynamic properties of the gas phase. Composition is highly influenced by the fuel used and the engine operation conditions. For this thesis the composition used the same used in the Diesel B model with some adjustments. One of the main assumptions concerning the exhaust gasses is that they do not contain nitrogen oxides. The amount of nitrogen oxides is low in the exhaust gasses and thus will not taken into account but they are important for future integration with an selective catalytic reduction system. The exhaust gas are consists of nitrogen (N_2), oxygen (O_2), argon (Ar), carbon dioxide (CO_2), water (H_2O) and sulphur dioxide (SO_2). The composition vector is given below:

$$[N_2 \quad O_2 \quad Ar \quad CO_2 \quad H_2O \quad SO_2]$$

Liquid composition is also mainly fresh water. Sodium hydroxide is in small quantities and there is also the product of the reaction of SO_2 with the hydroxides of the sodium hydroxide. The thermodynamic properties of the liquid phase will the calculated as being pure water, because the other two substances are in small quantities compared to the total amount of water and their influence is insignificant. The composition vector of the liquid phase is the following:

$$[H_2O \quad OH^- \quad SO_3^{2-}]$$

Apart from the assumptions for each part there are also some general assumptions made for the entire model:

- There are no deposits in the packed bed, so the flow area and the heat transfer are not affected by depositions.
- Two cases of evaporation can be distinguished: liquid film and droplets. The surface in the packed bed is much larger than that of the walls of the scrubber and also the packed bed covers a significant part of this walls surface. Thus evaporation will be examined in the packed bed where is mainly in liquid film form. Throughout the report the liquid film evaporation will be adopted.
- The exhaust gasses can be approached as ideal gasses [109]. Specific internal energy and enthalpy is a function of temperature only
- Mass transfer is positive for transfer from the gas phase to the liquid phase. Only SO_2 is transferred from the gas to the liquid phase and no other substance. Exhaust gasses contain an amount of water vapour produced during fuel combustion. It is assumed that this amount is not transferred to the liquid phase.

- NaOH will not included in the evaporation for two major reasons: 1) From the total amount of liquid that entering the scrubber only a small amount evaporates. Condensation is not taken into account. The amount of NaOH is small compared to the total amount of water so the NaOH evaporation is negligible. 2) The evaporation temperature of NaOH is above 1000°C. and the conditions in the scrubber never exceed this temperature.
- Liquid volume is assumed to be independent of temperature and pressure. The density of the liquid phase is assumed to be constant as the pressure is atmospheric and the variations are very small. So, for incompressible liquid $c_p = c_v$.
- Perfect mixing is assumed, meaning that the properties leaving the control volume are the same with them in the control volume.
- Ambient properties that are the inputs for the scrubber are in atmospheric condition

5

MODEL DEVELOPMENT

"Science is about knowing,
engineering is about doing."

Henry Petroski

5.1. INTRODUCTION

This chapter provides an explanation of the techniques used to develop the model of the wet scrubber. As previously explained, the wet scrubber model is composed by 5 parts, namely the venturi, the upper and lower volume, the packed bed and the demister.

The packed bed is the most complex part of the scrubber. It is the part where mainly heat and mass transfer between gas and liquid is carried out. In the packed bed, sulphur oxides are absorbed in the liquid phase and react chemically with NaOH, while water evaporates. For the other parts of the scrubber, only the gas phase model will be provided and is assumed that is no interaction with the liquid phase. The approaches described in the previous chapter will be adopted and adjusted for each part, of the gas and liquid phase.

5.2. VENTURI

The exhaust gasses enter the wet scrubber in the venturi. The venturi will be approached as a resistance element (there is a pressure drop, $P_{vent,in} > P_{vent,out}$) and no mass accumulation occurs [106]. It is assumed that the pressure drop in the venturi is the 10% of the total pressure drop in the scrubber system. The venturi model in Simulink is provided in Figure 5.1.

The venturi scrubber is capable of removing up to 75% of the particulate matter emission [83, 85]. Particulate matter emissions of diesel engines are less than 1% of the total exhaust gas flow [56], therefore the effect of their removal is negligible and will be neglected in this research. Other emissions are not influenced in the venturi scrubber. In the venturi, there is no mass accumulation, because the resident time of gasses and liquid in this section is small and the water droplets are of considerable size to be trapped in the gas phase, so they drop due to gravity.

The gas phase is accelerated and creates a turbulent flow. This conditions leads to the atomisation of the sprayed water and a decrease of the exhaust gas temperature. The exact diameter of the water droplets varies and is challenging to be calculated.

The velocity in the inlet and outlet of the venturi is assumed to be zero. The pressure in the venturi throat is equal to the pressure in the outlet. The mass flow is calculated according to equation 5.1. An analytical explanation of this expression is provided in 4.5.2.

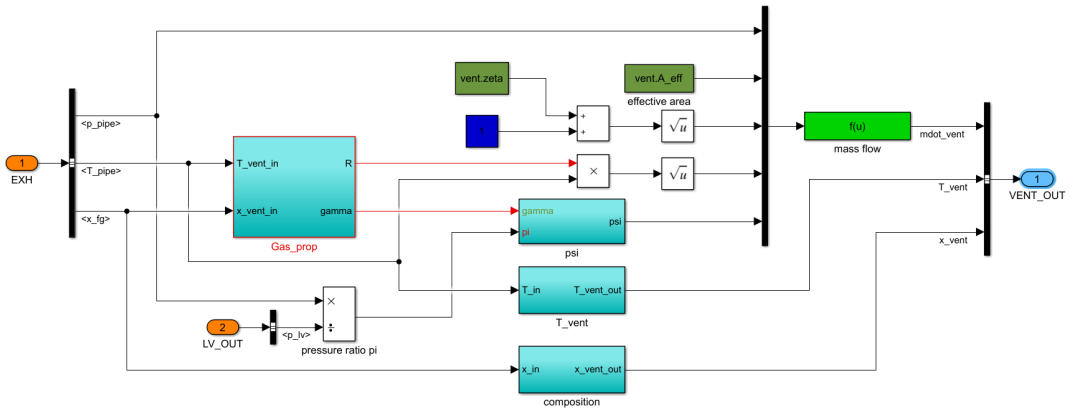

Figure 5.1: The inside of the Simulink block of the venturi model.

$$\dot{m}_{vent,out} = \frac{A_{eff,vent}}{\sqrt{(1+\zeta_{vent})}} \cdot \frac{p_{vent,in}}{\sqrt{R_{vent,in} \cdot T_{vent,in}}} \cdot \Psi \tag{5.1}$$

Where the effective area is $A_{eff,vent} = \varepsilon_{vent} \cdot A_{vent}$. The void fraction is assumed to have a value of $\varepsilon_{vent} = 0.9$, $A_{vent} = \pi \cdot \frac{d_{vent}^2}{4}$ and $\zeta = 0.2$. The gas is consider to be ideal and the density is provided according to the ideal gas law (Equation 5.2).

$$\rho_{vent,in} = \frac{p_{vent,in}}{R_{vent,in} \cdot T_{vent,in}} \tag{5.2}$$

A small amount of SO_X is removed by the venturi and is around 5-15% of the amount that enters the system [38]. One of the major contributions of the venturi pre-scrubber is to cool the exhaust gasses that enter the packed bed. The exact calculation of the temperature drop in the venturi quite challenging is out of the scope of this thesis. Heat transfer is mainly by conduction and convection. Both these methods require the knowledge of the liquid-gas interface. The shape and size of the droplet is random and demanding to be calculated, making the liquid-gas interface difficult to calculate. The venturi effect in the wet scrubber system will not examined and will be approached as a simple resistance element.

5.3. UPPER AND LOWER VOLUME

Both the upper and lower volume are approached as volume elements (Figure 5.2). The analysis to follow is for the lower volume which also applies for the upper volume. For the lower volume the mass balance is:

$$\frac{dm_{lv}}{dt} = \dot{m}_{lv,in} - \dot{m}_{lv,out} = \dot{m}_{lv,net} \tag{5.3}$$

By applying the first law of thermodynamics in the lower volume:

$$\frac{dU}{dt} = \dot{m}_{lv,in} \cdot h_{lv,in} - \dot{m}_{lv,out} \cdot h_{lv,out} + \dot{Q}_{lv} - \dot{W}_{lv} \tag{5.4}$$

As stated in the chapter 4.5.1, the gravitational and potential energy is neglected, there are no movable parts. Another assumption made is that the wet scrubber is an adiabatic device. This assumption is generally applied in devices such as cooling towers where gas and liquids come into contact [105]. The change of internal energy in the control volume is:

$$\frac{dU_{lv,cv}}{dt} = \frac{d(m_{lv,cv} \cdot u_{lv,cv})}{dt} = m_{lv,cv} \cdot \frac{du_{lv,cv}}{dt} + u_{lv,cv} \cdot \frac{dm_{lv,cv}}{dt} \tag{5.5}$$

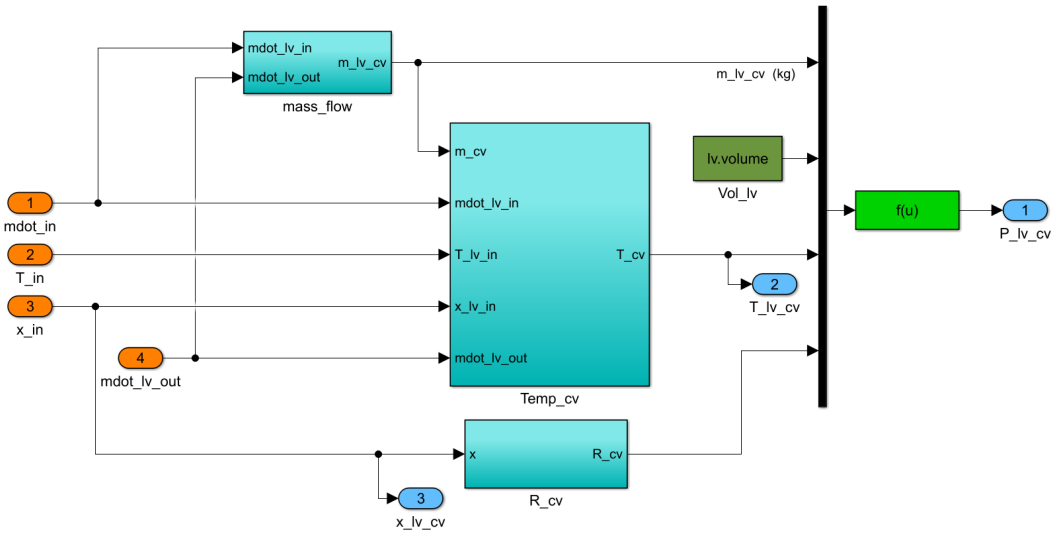

Figure 5.2: The inside of the Simulink block of the lower volume model.

Internal energy energy of an ideal gas is dependent on the temperature, $du = c_v \cdot dT$. By applying all the above in the first thermodynamic law (equation 5.4) and making the mandatory rearrangements it results:

$$\dot{m}_{lv,net} \cdot c_v \cdot \frac{dT_{lv,cv}}{dt} = \dot{m}_{lv,in}(h_{lv,in} - u_{lv,cv}) - \dot{m}_{lv,out}(h_{lv,out} - u_{lv,cv}) \tag{5.6}$$

Now that the temperature is known the pressure of the lower volume can be calculated using the ideal gas law.The approach for the upper volume is the same as the one for the lower volume.

$$p_{lv,cv} = \frac{m_{lv} \cdot R_{lv} \cdot T_{lv,cv}}{V_{lv,cv}} \tag{5.7}$$

5.4. DEMISTER

The last part of the wet scrubber is the demister (Figure 5.3). In the demister water condensation might occur, which has two functions. The gasses leaving the scrubber in most of the cases will be saturated in water making them heavy and making it difficult for upward movement. This will create something like a "water spray - mist" on the upper decks and an unpleasant condition for the people there. Second, the water condensation saves water for the exhaust cleaning process in the vessel. The gas leaving the demister should have a relative humidity of 100% [110].

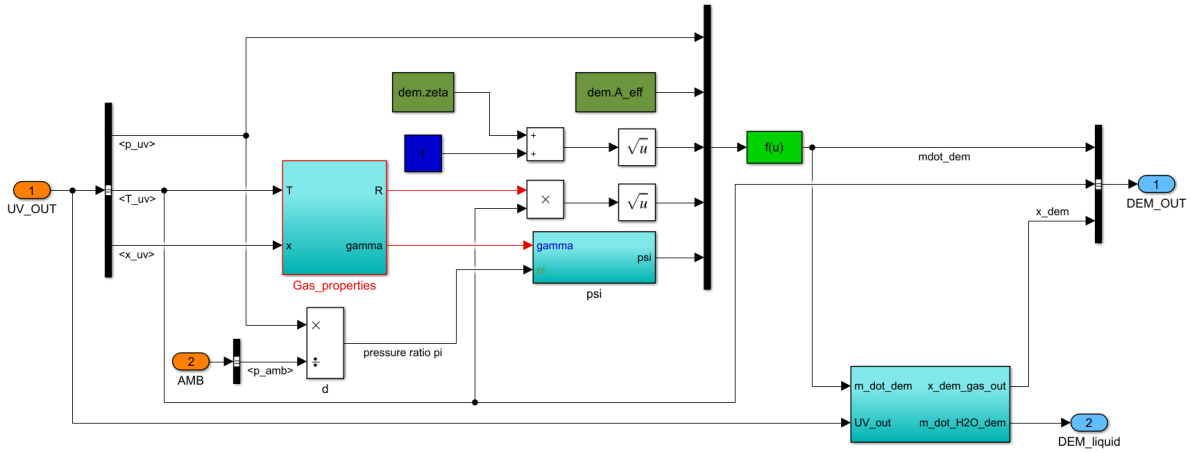

Figure 5.3: The inside of the Simulink block of the demister model.

The mass rate of the gasses leaving the demister to the ambient is:

$$\dot{m}_{dem,out} = \frac{A_{eff,dem}}{\sqrt{(1+\zeta_{dem})}} \cdot \frac{p_{demt,in}}{\sqrt{R_{dem,in} \cdot T_{dem,in}}} \cdot \Psi \tag{5.8}$$

The effective area of the demister is $A_{eff,dem} = \varepsilon_{dem} \cdot A_{dem}$. The values of the void fraction in the demister are in the range of 97-99% [110]. In this thesis is assumed to have a value of $\varepsilon_{dem} = 0.98$. The value of ζ is 0.2. The gas density is obtained from the ideal gas law (Equation 5.9).

$$\rho_{dem,in} = \frac{p_{dem,in}}{R_{dem,in} \cdot T_{dem,in}} \tag{5.9}$$

5.5. PACKED BED

The desulphurisation of the exhaust gas mainly occurs in the packed bed. The same holds true for the evaporation of scrubbing liquid (e.g. water). In the packed bed is more convenient to work with mole units for the case of mass transfer and the species balance, because of the chemical reaction. Chemical reactions are easier to be approached with use of moles instead of mass. Although, the calculations of the thermodynamic properties and heat transfer, will be carried out with mass units (Appendix B.1). Specific blocks are created in the Simulink model in particular places for the conversion of mass to moles and the conversion of mass fraction to molar fraction, and the opposite. The remaining of this chapter will deal with the physics and chemistry in the packed bed.

5.5.1. MASS TRANSFER

When a system contains two or more constituents whose concentrations vary from point to point, then the natural tendency is to transfer mass to minimise the differences in concentration within the system. Mass transfer, is the transfer of a component from a region in which there is a high concentration of the component to a region of low concentration. There are other physical processes that can lead to mass transfer, such as the existence of a temperature gradient (Soret effect), pressure diffusion, and differences created by external forces (gravity, magnetic fields, etc.). In many of the mass transfer processes there is also a simultaneous heat and/or momentum transfer [111].

FICK'S LAW

The driving force for molecular diffusion is the concentration gradient (see Figure 5.4). As an analogy to Fourier's law of heat conduction, Fick proposed a similar relation for the diffusion in a binary mixture A and B. This relation is known as Fick's 1^{st} law of diffusion. The molar flux relative to the average molar velocity of the binary mixture (not limited to equilibrium and isothermal conditions) is:

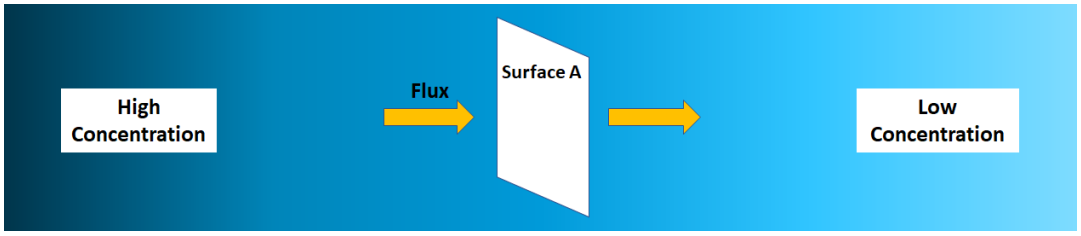

Figure 5.4: Diffusion through a surface, in one direction due to concentration difference

$$j_A = -D_{AB} \cdot c \cdot \nabla y_A \tag{5.10}$$

And for constant concentration in the control volume (as is the case for ideal gasses in isobars and isothermal conditions) and in one direction:

$$j_A = -D_{AB} \frac{\mathrm{d}c_A}{\mathrm{d}x} \qquad \left[\frac{mole}{m^2 \cdot s}\right] \tag{5.11}$$

Despite the seemingly analogous behaviour to heat transfer, mass transfer is more complex. In mass transfer there is always molecular diffusion and convection. Convective mass transfer involves mass transfer between two non-miscible fluids moving and separated by an interface. The specific molar flow of component A (from a surface parallel to the direction of flow) at constant coordinates (Figure 5.5) is given by the empirical relation:

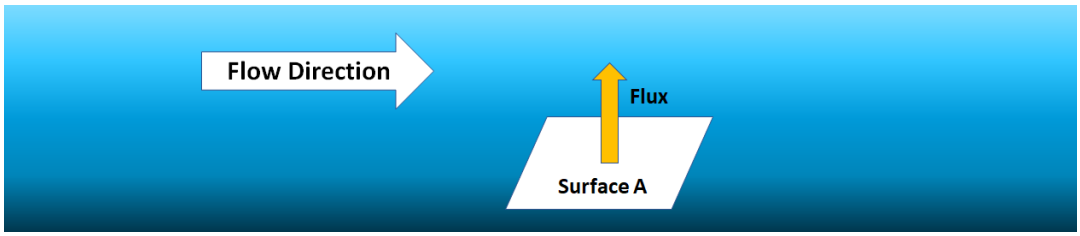

Figure 5.5: Convective mass transfer in a surface parallel to the flow.

$$N_A = k_c \Delta c_A \qquad \left[\frac{mole}{m^2 \cdot s}\right] \tag{5.12}$$

Where k_c is the mass transfer coefficient and Δc_A is the concentration difference of A, between the interface of the two fluids and the bulk concentration.

Convective mass transfer is not an independent mechanism, but rather a combination of molecular transport with the variations in the concentration range caused by macroscopic motion. In most cases, the problem is extremely complex and complete resolution is difficult. For this reason, quantitative descriptions of transfer rates are summarised based on semi-empirical correlations.

The specific flow of component A is given by Fick's law. Mass convection cannot be analysed in relation to simple mass diffusion is because fluid motion strongly influences the concentration distribution of c_A, in a way that is usually challenging to predict in theory. Qualitatively it can be understood that macroscopic motion increases mass transfer. The higher the velocity of a fluid the less it will be saturated. However, according to the above relation of Fick's law, a small concentration near the interface, together with a high concentration of saturation on the interface, results in a high concentration gradient and hence an increased mass transfer rate [111].

The specific molar flow of component A from interface to the bulk of fluid (relative to constant coordinates), usually due to the combination of convection and diffusion, as a linear function of the total pushing force, is approached according to the relationship:

$$N_A = k_c \cdot (c_{As} - c_A) \tag{5.13}$$

where c_{As} is the concentration of A on the liquid - gas interface and c_A is the concentration of A on the bulk fluid. The "ratio constant" k_c is the convective mass transfer coefficient, and the above relation can be considered as its definition. The inference factor conceals all the challenges to explain in details the velocity and concentration fields. Therefore, it is not a thermophysical property of the fluid, but is also highly dependent on the flow conditions, fluid properties and geometry of the system [108]. The value of the mass transfer coefficient is calculated by semi-empirical correlations with appropriate two-dimensional numbers. These correlations are the result of a combination of dimensional analysis and experimental measurements. The above methodology for analysing convective mass transfer problems has many proportions with the analysis of corresponding heat transfer problems.

FILM THEORY

To correlate empirical mass transfer coefficients with fluid flow rate and type, it is important to define the type of flow. The analysis would simple, if there were theoretical methods (and physical models) that could predict this behaviour in the best possible way. Significant efforts have been made for more than 100 years to

develop theories for interpreting the mechanism of turbulent mass transfer.

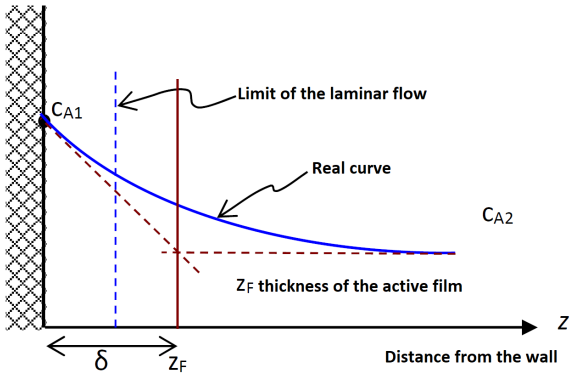

Figure 5.6: The film theory of Nerst and Lewis

The film theory is the simplest and oldest model developed by Nernst (1904) and Lewis (1918). When a fluid flows next to a wall, the model assumes that there is a thin laminar-film layer near the surface. This thin film is not found experimentally, but is a hypothetical film and is similar to the laminar layer that the turbulent flow creates around the flat plate. It is assumed that the total resistance to mass transfer lies only in the thin hypothetical film in which the transport is controlled by molecular diffusion. The thin film theory assumes that the concentration follows the dotted line up to z_F (or δ, thickness of the "active" film) and that the transfer from c_{A1} to c_{A2} is by molecular means (Figure 5.6).

The wet scrubber is a separation column in which mass transfer takes place between the two phases (gas and liquid) across an interface. The interface is created by the opposite direction of the flows of these two phases and is perpendicular to the flow direction. Since the absorption of gasses takes place between two contacting phases it is possible to extend the film theory into a two film theory. The two film theory suggests that each film (liquid and gas phase) represent a mass transfer resistance. At the interface created by these fluids, the concentrations of the two phases are in equilibrium. But this does not mean that they are the equal (see Figure 5.7).

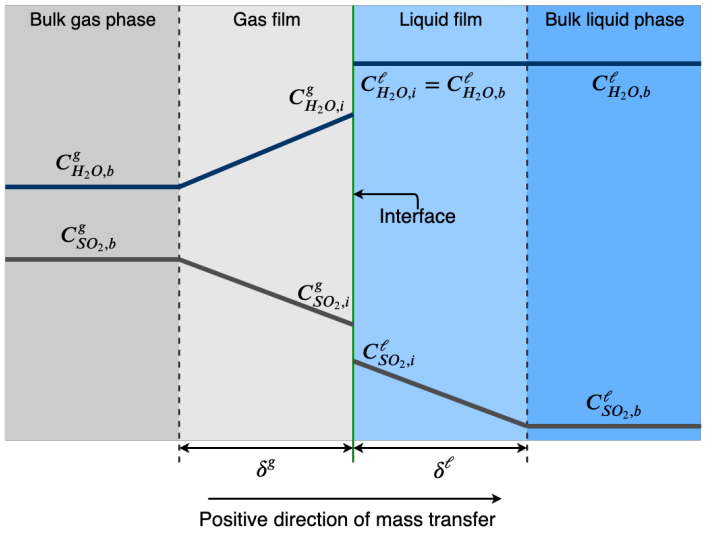

Figure 5.7: Concentrations for the case of pure absorption of SO_2 and H_2O in the bulk and film region of the gas and liquid phase.

In the Figure 5.7, the molar concentration of SO_2 and H_2O in the liquid and gas phase are presented. Two regions can be recognised in each phase, the bulk and the stagnant film region. The bulk (denoted by b) of both the gas and liquid phase is well mixed, meaning that the composition is uniform and thus there is

no resistance to mass transfer. The stagnant film region exist next to the interface and imposes a resistance in the mass transfer. In the bulk of gas phase the molar concentration of SO_2 is $c^g_{SO_2,b}$ and at the interface (denoted by i) is $c^g_{SO_2,i}$. The SO_2 in the gas phase diffuses into the gas film and into the interface. Then is absorbed by the liquid film. At the interface the concentrations are in equilibrium, but not equal, imposing an additional resistance to mass transfer. SO_2 is diluted in the gas phase resulting in low mass transfer rates, therefore this assumption is generally accepted. The concentration in the interface of the liquid phase is $c^\ell_{SO_2,i}$ and in the bulk is $c^\ell_{SO_2,b}$.

The flux of SO_2 in the gas phase is equal to that of the liquid phase. The films have a thickness of δ^g and δ^ℓ respectively,

$$J_{SO_2} = \frac{D^g_{SO_2}}{\delta^g} \cdot \left(c^g_{SO_2,b} - c^g_{SO_2,i}\right) = \frac{D^\ell_{SO_2}}{\delta^\ell} \cdot \left(c^\ell_{SO_2,i} - c^\ell_{SO_2,b}\right) \tag{5.14}$$

As stated the thickness of the film is difficult to be calculated and thus the terms $\frac{D^g_{SO_2}}{\delta^g}$ and $\frac{D^\ell_{SO_2}}{\delta^\ell}$ by the terms k^g_c and k^ℓ_c respectively. Equation 5.14 then is converted to:

$$J_{SO_2} = k^g_c \cdot \left(c^g_{SO_2,b} - c^g_{SO_2,i}\right) = k^\ell_c \cdot \left(c^\ell_{SO_2,i} - c^\ell_{SO_2,b}\right) \tag{5.15}$$

For this analysis, it is useful to convert the concentrations to mole fractions. This can be done by the correlations that connect these properties,

$$c_{SO_2} = \frac{n_{SO_2}}{V} \xrightarrow[(V=\frac{m}{\rho})]{(n_{SO_2}=y_{SO_2}\cdot n_{tot})} c_{SO_2} = \frac{y_{SO_2} \cdot n_{tot} \cdot \rho}{m} \tag{5.16}$$

In equation 5.16, the definition of molecular mass can be recognised, $M = \frac{m}{n_{tot}}$. By imposing this definition and rearranging the terms equation 5.16 becomes:

$$c_{SO_2} = \frac{y_{SO_2} \cdot \rho}{M} \tag{5.17}$$

By substituting the terms of concentration in equation 5.15 with the relation of equation 5.17, the molar flux can be written in terms of mole fraction:

$$J_{SO_2} = k^g_c \cdot \left(y^g_{SO_2,b} - y^g_{SO_2,i}\right) \cdot \frac{\rho^g}{M^g} = k^\ell_c \cdot \left(y^\ell_{SO_2,i} - y^\ell_{SO_2,b}\right) \frac{\rho^\ell}{M^\ell} \tag{5.18}$$

The products $k^g_c \cdot \frac{\rho^g}{M^g}$ and $k^\ell_c \cdot \frac{\rho^\ell}{M^\ell}$ are substituted and are equal to k^g_y and k^ℓ_y. Then 5.18 is written us:

$$J_{SO_2} = k^g_y \cdot \left(y^g_{SO_2,b} - y^g_{SO_2,i}\right) = k^\ell_y \cdot \left(y^\ell_{SO_2,i} - y^\ell_{SO_2,b}\right) \tag{5.19}$$

MODEL OF CHEMICAL ABSORPTION OF SO_2 IN SOLUTION OF $NaOH$ AND WATER

The analysis made was only for pure absorption. It did not include the chemical absorption of SO_2 in the liquid phase in the presence of NaOH. Therefore, the analysis has to be extended to include also the chemical absorption of SO_2 with NaOH. NaOH is assumed to have broken down to Na^+ and OH^-. The reactions that take place are the following:

$$SO_2 + OH^- \longrightarrow HSO_3^- \tag{5.20}$$

$$HSO_3^- + OH^- \longrightarrow SO_3^{-2} + H_2O \tag{5.21}$$

The overall reaction is:

$$SO_2 + 2 \cdot OH^- \longrightarrow SO_3^{-2} + H_2O \tag{5.22}$$

According to Dean [112], the first reaction (equation 5.20) is fast, with a rate constant at 25°C being 10^9 mole/s. The second reaction, that engages only proton transfer is faster [113]. Thus, it can be assumed that both reaction can be considered instantaneous (compared to the rate of diffusional processes), irreversible, with excess of OH^-, an assumption that is in line with Dean and Vazquez.

Another model needs to be introduced to cover the case for the chemical reaction and absorption of SO_2. This model includes only the liquid phase, as it is in the liquid phase where the reactions takes place. In the gas phase, the situation remains the same, because is assumed that the liquid that evaporates is pure water.

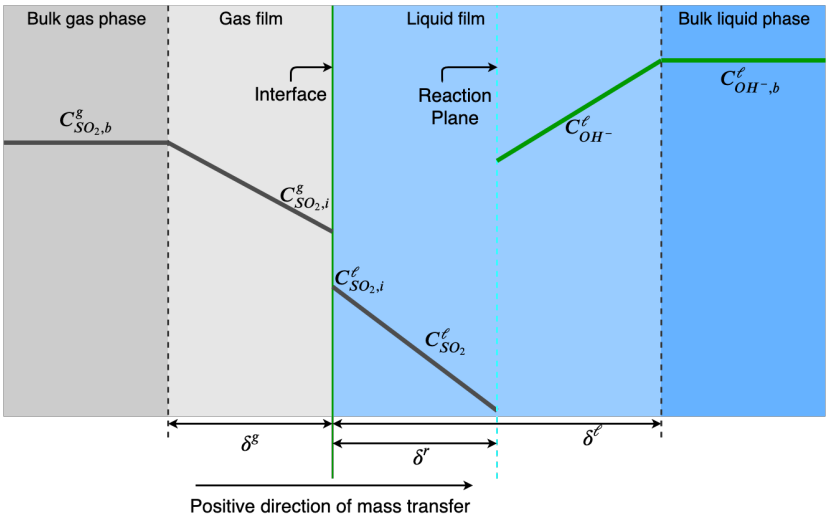

Figure 5.8: Concentrations of the substances that are engaged in the instantaneous reaction

A model introduced by Danckwerts [114] for instantaneous and irreversible reactions will be adopted. Sulphur dioxide diffuses through the interface from the gas to the liquid phase and has concentration $c^\ell_{SO_2,i}$ at the interface of the liquid film. Then it diffuses into the liquid film, where its concentration is constantly reduced (see Figure 5.8). At a distance δ^r in the liquid film ($\delta^r < \delta^\ell$), it meets the OH^- molecules, that have diffused from the bulk of the liquid phase, where they had a concentration $c^\ell_{OH^-,b}$. The concentration of OH^- is also reducing while they diffuse in the liquid film. The area at δ^r is called the reaction plane and there reaction 5.22 takes place.

The diffusion in the liquid film follows Fick's law. To have a complete chemical reaction and not to have excess of SO_2 molecules in the liquid phase, reaction 5.22 indicates that the amount of OH^- ions, and thus the diffusion rate, must be twice of that of SO_2. By applying Fick's law the above statement becomes:

$$\frac{D^\ell_{OH^-} \cdot c^\ell_{OH^-,b}}{\delta^\ell - \delta^r} = 2 \cdot \frac{D^\ell_{SO_2} \cdot c^\ell_{SO_2,i}}{\delta^r} \tag{5.23}$$

Reaction 5.22 is assumed to be complete and is carried out in the reaction plane. This means that in the reaction plane SO_2 disappears and it does not reach the bulk of the liquid ($c^\ell_{SO_2,b} = 0$). In reality the chemical reaction is never complete and there is always an excess of SO_2 in the liquid, but because it is small compared to the other substances it can be neglected. So, the molar diffusion is:

$$J_{SO_2} = \frac{D^\ell_{SO_2}}{\delta^r} \cdot c^\ell_{SO_2,i} \tag{5.24}$$

The term δ^r is more challenging to be calculated than δ^ℓ. By using 5.23 and rearranging the terms, δ^r can be substituted by δ^ℓ. Then the term of k_c can be used as in the equations 5.14 and 5.15. Finally by following the same steps as them from equation 5.16 to 5.19:

$$J_{SO_2} = \frac{D^{\ell}_{SO_2} \cdot c^{\ell}_{SO_2,i}}{\delta^{\ell}} \cdot \left(1 + \frac{D^{\ell}_{OH^-} \cdot c^{\ell}_{OH^-,b}}{2 \cdot D^{\ell}_{SO_2} \cdot c^{\ell}_{SO_2,i}}\right) \xrightarrow{k^{\ell}_c = \frac{D^{\ell}_{SO_2}}{\delta^{\ell}}} \tag{5.25}$$

$$J_{SO_2} = k^{\ell}_c \cdot c^{\ell}_{SO_2,i} \cdot \left(1 + \frac{D^{\ell}_{OH^-} \cdot c^{\ell}_{OH^-,b}}{2 \cdot D^{\ell}_{SO_2} \cdot c^{\ell}_{SO_2,i}}\right) \xrightarrow{k^{\ell}_y = k^{\ell}_c \cdot \frac{\rho^{\ell}}{M^{\ell}}} \tag{5.26}$$

$$J_{SO_2} = k^{\ell}_y \cdot \left(y^{\ell}_{SO_2,i} + \frac{D^{\ell}_{OH^-} \cdot y^{\ell}_{OH^-,b}}{2 \cdot D^{\ell}_{SO_2}}\right) \tag{5.27}$$

Equation 5.27 is the new right hand part of equation 5.19 that includes the chemical reaction. The left hand part for the diffusion in the gas phase remains the same. Therefore, the relation for the two film model that will substitute 5.19 is:

$$J_{SO_2} = k^{g}_y \cdot \left(y^{g}_{SO_2,b} - y^{g}_{SO_2,i}\right) = k^{\ell}_y \cdot \left(y^{\ell}_{SO_2,i} + \frac{D^{\ell}_{OH^-} \cdot y^{\ell}_{OH^-,b}}{2 \cdot D^{\ell}_{SO_2}}\right) \tag{5.28}$$

In the new relation of the two film model there are two unknowns. These are concentrations of SO_2 in the interface of the gas and liquid phase. By applying Henry's law, these concentrations can be eliminated. Henry's law, is a gas law that states that the amount of dissolved gas in a liquid is proportional to its partial pressure above the liquid. The constants are strongly dependent on the temperature of the system and, secondarily, on the salinity of the aqueous phase [111]. In the simplified representation of solubility equilibrium data with Henry's law, the temperature dependence is contained in the constant $\mathbb{H}(T)$ [104]. For the case of SO_2 the Henry's law is:

$$y^{g}_{SO_2,i} \cdot p^{g} = y^{\ell}_{SO_2,i} \cdot \mathbb{H}^{\ell}_{SO_2} \tag{5.29}$$

The parameter $\mathbb{H}^{\ell}_{SO_2}$ is called Henry's constant. The explanation for the case used in this model can be found in Appendix C.1. Now, by using Henry's law the $y^{\ell}_{SO_2,i}$ is eliminated:

$$y^{\ell}_{SO_2,i} = y^{g}_{SO_2,i} \cdot \frac{p^{g}}{\mathbb{H}^{\ell}_{SO_2}} \tag{5.30}$$

Then by using equation 5.28 the SO_2 concentration in the interface of the gas phase $y^{g}_{SO_2,i}$ is:

$$k^{g}_y \cdot \left(y^{g}_{SO_2,b} - y^{g}_{SO_2,i}\right) = k^{\ell}_y \cdot \left(y^{g}_{SO_2,i} \cdot \frac{p^{g}}{\mathbb{H}^{\ell}_{SO_2}} + \frac{D^{\ell}_{OH^-} \cdot y^{\ell}_{OH^-,b}}{2 \cdot D^{\ell}_{SO_2}}\right) \Longrightarrow y^{g}_{SO_2,i} = \frac{k^{g}_y \cdot y^{g}_{SO_2,b} - k^{\ell}_y \cdot \frac{D^{\ell}_{OH^-} \cdot y^{\ell}_{OH^-,b}}{2 \cdot D^{\ell}_{SO_2}}}{k^{g}_y + k^{\ell}_y \cdot \frac{p^{g}}{\mathbb{H}^{\ell}_{SO_2}}} \tag{5.31}$$

Now there is a relation for the concentration of SO_2 at the interface of the gas film. The equation 5.31 will be used in relation 5.28 and by doing rearrangement of the terms, the flux of SO_2 can be calculated:

$$J_{SO_2} = \frac{y^{g}_{SO_2,b} + \frac{\mathbb{H}^{\ell}_{SO_2}}{p^{g}} \cdot \frac{D^{\ell}_{OH^-} \cdot y^{\ell}_{OH^-,b}}{2 \cdot D^{\ell}_{SO_2}}}{\frac{1}{k^{g}_y} + \frac{1}{k^{\ell}_y} \cdot \frac{\mathbb{H}^{\ell}_{SO_2}}{P^{g}}} \tag{5.32}$$

A difference in the absorption with chemical reaction compared to physical absorption (equation 5.32 and 5.19) is that in the case of physical absorption there is a SO_2 concentration difference between the bulk and the interface. In the chemical absorption this is not the case as SO_2 in not in pure form in the bulk of liquid phase. For this reason the concentration term in the bulk of the liquid has been replace by an another term called the enhancement factor.

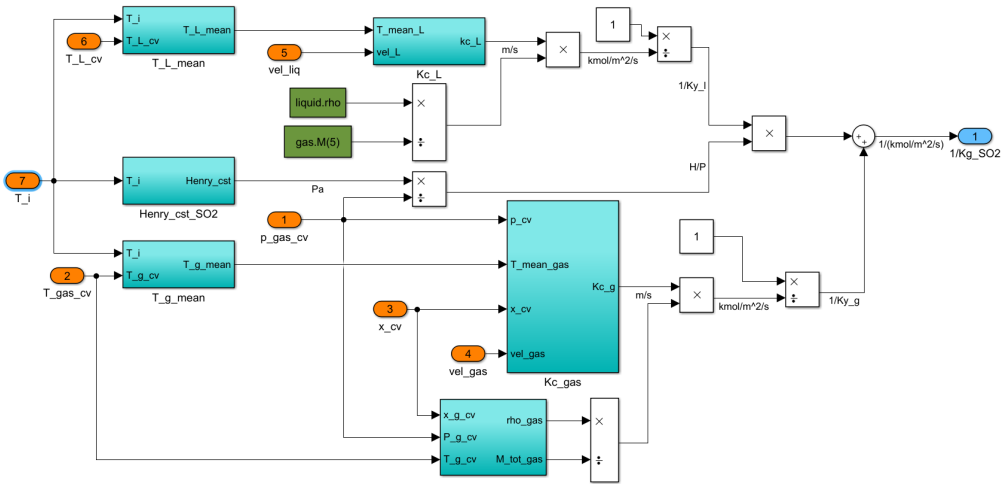

Figure 5.9: In the Simulink block of the total mass transfer coefficient

The denominator in equation 5.32, is referred in the literature as the total mass transfer coefficient K_g (Figure 5.9) and is given according to the following relation:

$$\frac{1}{K_g} = \frac{1}{k_y^g} + \frac{1}{k_y^\ell} \cdot \frac{\mathbb{H}_{SO_2}^\ell}{Pg} \tag{5.33}$$

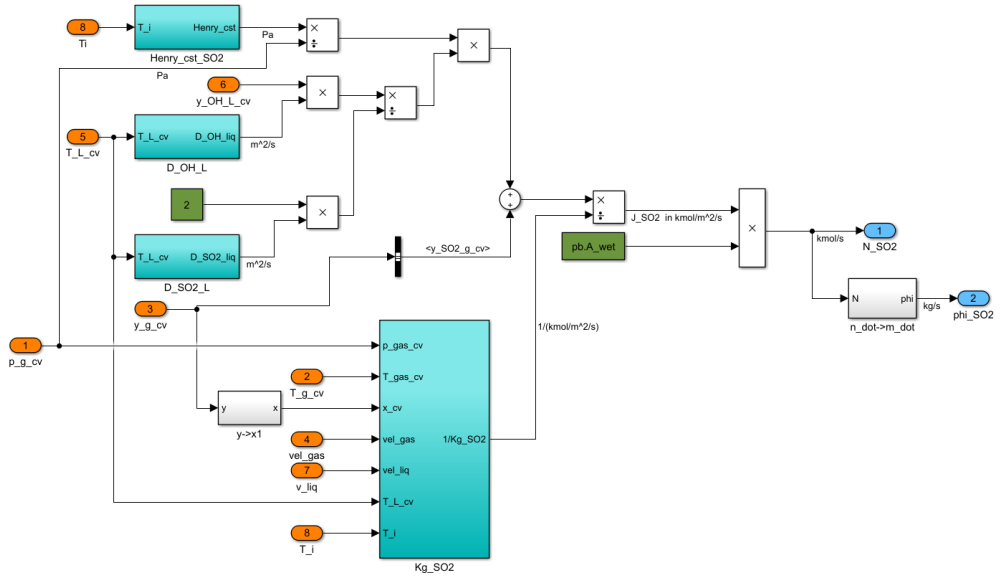

Figure 5.10: In the Simulink block of the sulphur dioxide mass transfer

To obtain the mass transfer of the SO_2 ($\mathbb{N}_{SO_2}$), the mass flux J_{SO_2} will be multiplied by the surface area that the mass transfer will occur (Figure 5.10). In a scrubber with a packed bed this surface area has irregular shape due to the packing material. A widely used approach is to multiply the interfacial surface area with the total volume of the column. The interfacial surface area a_i is a parameter dependent on the packing characteristic and the hydraulics inside the scrubber, and has unit of area per free column volume. So, the mass transfer $\mathbb{N}_{SO_2}$ is:

$$\mathbb{N}_{SO_2} = J_{SO_2} \cdot a_i \cdot V_{tot} \tag{5.34}$$

MODEL OF EVAPORATION OF H_2O

For the flux of H_2O, is assumed that the concentration in the liquid phase (in the bulk and stagnant liquid film region) is the same, $c^{\ell}_{H_2O,b} = c^{\ell}_{H_2O,i}$ (Figure 5.7). In the gas phase the approach of H_2O is the same like that of SO_2 with the only difference that the concentration in the interface is grater than that in the bulk phase, $c^{g}_{H_2O,b} < c^{g}_{H_2O,i}$.

The mass transfer of H_2O in the gas phase is like in the form of pure absorption since there is no chemical reaction in the gas phase. Following the same step as in the case of pure absorption of SO_2 the mass transfer of H_2O is

$$J_{H_2O} = \frac{D^{g}_{H_2O}}{\delta g} \cdot \left(c^{g}_{H_2O,b} - c^{g}_{H_2O,i} \right) \tag{5.35}$$

Instead of the term $\frac{D^{g}_{H_2O}}{\delta^{g}}$, the terms k^{g}_{c,H_2O} will be used due to the difficulty to calculate δ^{g}. Equation 5.35 then is converted to:

$$J_{H_2O} = k^{g}_{c,H_2O} \cdot \left(c^{g}_{H_2O,b} - c^{g}_{H_2O,i} \right) \tag{5.36}$$

Then follows the conversion of concentration to mole fraction.

$$c_{H_2O} = \frac{n_{H_2O}}{V} \xrightarrow[(V=\frac{m}{\rho})]{(n_{H_2O}=y_{H_2O}\cdot n_{tot})} c_{H_2O} = \frac{y_{H_2O} \cdot n_{tot} \cdot \rho}{m} \tag{5.37}$$

Molecular mass is, $M = \frac{m}{n_{tot}}$.

$$c_{H_2O} = \frac{y_{H_2O} \cdot \rho}{M} \tag{5.38}$$

By substituting the terms of concentration in equation 5.36 with the relation of equation 5.38, the molar flux can be written in terms of mole fraction:

$$J_{H_2O} = k^{g}_{c,H_2O} \cdot \left(y^{g}_{H_2O,b} - y^{g}_{H_2O,i} \right) \cdot \frac{\rho^{g}}{Mg} \tag{5.39}$$

The product $k^{g}_{c,H_2O} \cdot \frac{\rho^{g}}{Mg}$ is substituted and is equal to k^{g}_{y} and 5.39 is written as:

$$J_{H_2O} = k^{g}_{y,H_2O} \cdot \left(y^{g}_{H_2O,b} - y^{g}_{H_2O,i} \right) \tag{5.40}$$

Then the model is lead again in the problem to define the concentration of the interface. When there is a two phase mixture, in the interface water goes from the liquid to the gas phase, so the interface can be approached as an area of the two phase mixture [104]. In this case instead of using the Henry's law the law of Raoult will be used (Henry's law is a simplification of Raoult's law for very small concentrations). Raoult's law is also convenient to calculate saturation pressure that will be used later on for the indication of the saturation conditions. The explanation for the case used in this model can be found in Appendix C.2.

Raoult's law states that the partial pressure of each component of an ideal mixture of liquids is equal to the vapour pressure of the pure component multiplied by its mole fraction in the mixture [104]. The mathematical expression is given below:

$$y^{\ell}_{H_2O,i} \cdot p^{\ell}_{sat} = y^{g}_{H_2O,i} \cdot p^{g} \tag{5.41}$$

Raoult's law (equation 5.41) will be applied at equation 5.40 to eliminate the molar concentration of water in the interface of the gas phase ($y^{g}_{H_2O,i}$). Also, because it is assumed that the interfacial concentration in the liquid phase is equal to that of the liquid bulk ($c^{\ell}_{H_2O,b} = c^{\ell}_{H_2O,i}$) the Raoult becomes.

$$y^{g}_{H_2O,i} = y^{\ell}_{H_2O,b} \cdot \frac{p^{\ell}_{sat}}{p^{g}} \tag{5.42}$$

5

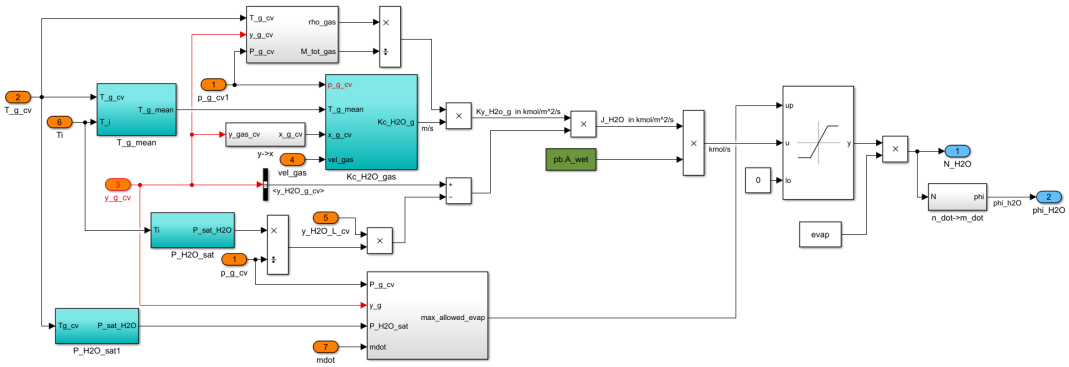

Figure 5.11: The inside of the Simulink block of the water evaporation

Then 5.42 is implemented in 5.40:

$$J_{H_2O} = k^g_{y,H_2O} \cdot \left(y^g_{H_2O,b} - y^\ell_{H_2O,b} \cdot \frac{p^\ell_{sat}}{p^g} \right) \tag{5.43}$$

The Simulink block the mass transfer of water is given in Figure 5.11 and the equation is:

$$\mathbb{N}_{H_2O} = J_{H_2O} \cdot a_i \cdot V_{tot} = k^g_{y,H_2O} \cdot \left(y^g_{H_2O,b} - y^\ell_{H_2O,b} \cdot \frac{p^\ell_{sat}}{p^g} \right) \cdot a_i \cdot V_{tot} \tag{5.44}$$

5.5.2. MOLE BALANCE

In the analysis of the packed bed the mass flow will be converted to its equivalent molar flow, because absorption process is generally described with molar quantities. Each phase will be described separately.

GAS PHASE

For the gas phase the total mole balance in the control volume is:

$$\frac{dn^g_{cv}}{dt} = \dot{n}^g_{in} - \dot{n}^g_{out} - \dot{\mathbb{N}}_{SO_2} + \dot{\mathbb{N}}_{H_2O} \tag{5.45}$$

In the above expression the left hand side accounts for the net mole transport in the control volume. In the right hand side the first two terms account for the net accumulation due to convection, the third term for the mass transfer of SO_2 from the gas to the liquid phase while the last term accounts for the mass transfer of water in the gas phase from the liquid phase. The sign convention is that the mass transfer considered to be positive for the transfer from the gas phase to the liquid phase. This convention should not be confused with the sign convention of the control volume. For example, everything that goes in the gas control volume has a positive sign and anything that goes out has negative sign. This is why $\dot{\mathbb{N}}_{SO_2}$ has a negative sign as it gets out of the control volume of the gas phase, but $\dot{\mathbb{N}}_{SO_2}$ is a positive quantity because SO_2 moles are transferred from gas to liquid and $\dot{\mathbb{N}}_{H_2O}$ is a negative quantity as H_2O moles are transferred from liquid to gas.

The main species of interest are the moles of SO_2 and H_2O and so the total mole balance can be split up into partial mole balance of these species. For SO_2:

$$\frac{dn^g_{SO_2,cv}}{dt} = \dot{n}^g_{SO_2,in} - \dot{n}^g_{SO_2,out} - \dot{\mathbb{N}}_{SO_2} \tag{5.46}$$

By using the definition of the partial mole balance, equation 5.46 can be written:

$$\frac{d(y^g_{SO_2,cv} \cdot n^g_{cv})}{dt} = y^g_{SO_2,in} \cdot \dot{n}^g_{in} - y^g_{SO_2,out} \cdot \dot{n}^g_{out} - \dot{\mathbb{N}}_{SO_2} \tag{5.47}$$

Differentiating the first part of the equation 5.47 results in:

$$y^g_{SO_2,cv} \cdot \frac{dn^g_{cv}}{dt} + n^g_{cv} \cdot \frac{dy^g_{SO_2,cv}}{dt} = y^g_{SO_2,in} \cdot \dot{n}^g_{in} - y^g_{SO_2,out} \cdot \dot{n}^g_{out} - \dot{\mathbb{N}}_{SO_2} \tag{5.48}$$

The first term of the left hand side the total mole balance can be recognised. By substituting it in equation 5.48 and moving it to the right hand side:

$$n^g_{cv} \cdot \frac{dy^g_{SO_2,cv}}{dt} = y^g_{SO_2,in} \cdot \dot{n}^g_{in} - y^g_{SO_2,out} \cdot \dot{n}^g_{out} - \dot{\mathbb{N}}_{SO_2} - y^g_{SO_2,cv} \cdot (\dot{n}^g_{in} - \dot{n}^g_{out} - \dot{\mathbb{N}}_{SO_2} + \dot{\mathbb{N}}_{H_2O}) \tag{5.49}$$

One of the most important assumption that defines this model is that of perfect mixing, meaning that the properties of the gas leaving the control volume are the same with them in the control volume ($y^g_{SO_2,out} = y^g_{SO_2,cv}$). Implementing this assumption, making rearrangement and calculations of the terms and dividing both sides with n^g_{cv} the equation 5.49 of the partial mole balance of SO_2 in the gas phase will be written:

$$\frac{dy^g_{SO_2,cv}}{dt} = \frac{(y^g_{SO_2,in} - y^g_{SO_2,cv}) \cdot \dot{n}^g_{in} - (1 - y^g_{SO_2,cv}) \cdot \dot{\mathbb{N}}_{SO_2} - y^g_{SO_2,cv} \cdot \dot{\mathbb{N}}_{H_2O}}{n^g_{cv}} \tag{5.50}$$

Now for the H_2O entering the gas phase:

$$\frac{dn^g_{H_2O,cv}}{dt} = \dot{n}^g_{H_2O,in} - \dot{n}^g_{H_2O,out} + \dot{\mathbb{N}}_{H_2O} \tag{5.51}$$

Working in a same way as in the equations 5.47, 5.48, 5.49 the procedure leads to an expression for H_2O which is similar to that of the dynamic of the mass transfer of SO_2 (5.50). So, the dynamic of the mass transfer of H_2O in the gas phase is:

$$\frac{dy^g_{H_2O,cv}}{dt} = \frac{(y^g_{H_2O,in} - y^g_{H_2O,cv}) \cdot \dot{n}^g_{in} + (1 - y^g_{H_2O,cv}) \cdot \dot{\mathbb{N}}_{H_2O} + y^g_{H_2O,cv} \cdot \dot{\mathbb{N}}_{SO_2}}{n^g_{cv}} \tag{5.52}$$

The other species of the exhaust gasses are assumed not be absorbed in the liquid phase. There is only mass transfer of SO_2 in the liquid phase, through absorption, and of H_2O in the gas phase, through evaporation. The other species are assumed to continue staying in their preexisting phase. Also, moles of SO_2 disappear from the gas phase and the moles of H_2O enter the gas phase. In general the amount of moles SO_2 disappearing and H_2O entering the gas phase is not the same, the mole fraction of the other elements will change. Actually, there is no need to differentiate for each single element because the number of moles of the element j in the control volume is a fraction of the SO_2 leaving the volume and H_2O getting in the control volume. So, for each component j in the control volume is:

$$y^g_{j,cv} = \frac{y^g_{j,in}}{1 - (y^g_{SO_2,in} - y^g_{SO_2,cv}) - (y^g_{H_2O,in} - y^g_{H_2O,cv})} \tag{5.53}$$

LIQUID PHASE

The procedure for the liquid phase is the same. In this case equations 5.45, 5.46 and 5.51 become:

$$\frac{dn^\ell_{cv}}{dt} = \dot{n}^\ell_{in} - \dot{n}^\ell_{out} + \dot{\mathbb{N}}_{SO_2} - \dot{\mathbb{N}}_{H_2O} \tag{5.54}$$

$$\frac{dn^\ell_{SO_2,cv}}{dt} = \dot{n}^\ell_{SO_2,in} - \dot{n}^\ell_{SO_2,out} + \dot{\mathbb{N}}_{SO_2} \tag{5.55}$$

$$\frac{dn^\ell_{H_2O,cv}}{dt} = \dot{n}^\ell_{H_2O,in} - \dot{n}^\ell_{H_2O,out} - \dot{\mathbb{N}}_{H_2O} \tag{5.56}$$

Following the same analysis like in the gas phase the dynamic of the mass transfer of SO_2 and H_2O are respectively:

$$\frac{dy^\ell_{SO_2,cv}}{dt} = \frac{(y^\ell_{SO_2,in} - y^\ell_{SO_2,cv}) \cdot \dot{n}^\ell_{in} + (1 - y^\ell_{SO_2,cv}) \cdot \dot{\mathbb{N}}_{SO_2} + y^\ell_{SO_2,cv} \cdot \dot{\mathbb{N}}_{H_2O}}{n^\ell_{cv}} \tag{5.57}$$

$$\frac{dy^\ell_{H_2O,cv}}{dt} = \frac{(y^\ell_{H_2O,in} - y^\ell_{H_2O,cv}) \cdot \dot{n}^\ell_{in} - (1 - y^\ell_{H_2O,cv}) \cdot \dot{\mathbb{N}}_{H_2O} - y^\ell_{H_2O,cv} \cdot \dot{\mathbb{N}}_{SO_2}}{n^\ell_{cv}} \tag{5.58}$$

This analysis of course is for pure absorption in the liquid phase. For the liquid phase the procedure is not as straightforward as in the gas phase because in the liquid phase there are the chemical reactants and products. An extensive analysis for the liquid phase will be done in the next section.

MOLE BALANCE OF LIQUID PHASE WITH CHEMICAL REACTION

Until this moment the only molar fraction that are used are them of the substances that compose the exhaust gas. In equation 5.32 it can be seen that the molar concentration of OH^- is also required. Therefore, the mole balance of OH^- is mandatory in for the model. For this reason the mole balances (equations 5.54 - 5.58) of the liquid phase needs do be redone so as to include the chemical reactions.

The total mole balance of the liquid phase including the chemical reaction is:

$$\frac{dn^{\ell}_{cv}}{dt} = \dot{n}^{\ell}_{in} - \dot{n}^{\ell}_{out} - \dot{\mathbb{N}}_{OH^-} + \dot{\mathbb{N}}_{SO_3^{2-}} + \dot{\mathbb{N}}^{r}_{H_2O} - \dot{\mathbb{N}}^{evap}_{H_2O} \tag{5.59}$$

The amount of water that is produced due to chemical reaction is different to that which evaporates ($\dot{\mathbb{N}}^{r}_{H_2O} \neq \dot{\mathbb{N}}^{evap}_{H_2O}$). This is why there are two different terms in the total mole balance. The chemical reaction (equation 5.22) gives the analogy of the amount of reactants and products compared to the amount of SO_2 which is supposed to have totally reacted and so there is none of it in the liquid phase. These analogies are given below:

$$\begin{aligned} \dot{\mathbb{N}}_{OH^-} &= 2 \cdot \dot{\mathbb{N}}_{SO_2} \\ \dot{\mathbb{N}}_{SO_3^{2-}} &= \dot{\mathbb{N}}_{SO_2} \\ \dot{\mathbb{N}}^{r}_{H_2O} &= \dot{\mathbb{N}}_{SO_2} \end{aligned} \tag{5.60}$$

By substituting these relation in the total mole balance of the liquid phase and making the calculations:

$$\frac{dn^{\ell}_{tot,cv}}{dt} = \dot{n}^{\ell}_{in} - \dot{n}^{\ell}_{out} - \dot{\mathbb{N}}^{evap}_{H_2O} \tag{5.61}$$

In the bulk of the liquid, the mole balance of OH^- is:

$$\frac{dn^{\ell}_{OH^-,cv}}{dt} = \dot{n}^{\ell}_{OH^-,in} - \dot{n}^{\ell}_{OH^-,out} - \dot{\mathbb{N}}_{OH^-} \tag{5.62}$$

By using the definition of the partial mole balance equation 5.62 can be written:

$$\frac{d(y^{\ell}_{OH^-,cv} \cdot n^{\ell}_{tot,cv})}{dt} = y^{\ell}_{OH^-,in} \cdot \dot{n}^{\ell}_{in} - y^{\ell}_{OH^-,out} \cdot \dot{n}^{\ell}_{out} - \dot{\mathbb{N}}_{OH^-} \tag{5.63}$$

In 5.60 was shown that the amount of OH^- ions that disappear from the bulk of the liquid must be two times higher than the amount of SO_2 entering the liquid phase with mass transfer. So, the partial mole balance of OH^- becomes:

$$\frac{d(y^{\ell}_{OH^-,cv} \cdot n^{\ell}_{tot,cv})}{dt} = y^{\ell}_{OH^-,in} \cdot \dot{n}^{\ell}_{in} - y^{\ell}_{OH^-,out} \cdot \dot{n}^{\ell}_{out} - 2 \cdot \dot{\mathbb{N}}_{SO_2} \tag{5.64}$$

Then, by applying the mathematical computations as it was also done in the gas phase and introducing again the important assumption of perfect mixing, the partial mole balance of the OH^- is:

$$\frac{dy^{\ell}_{OH^-,cv}}{dt} = \frac{\left(y^{\ell}_{OH^-,in} - y^{\ell}_{OH^-,cv}\right) \cdot \dot{n}^{\ell}_{in} - 2 \cdot \dot{\mathbb{N}}_{SO_2} + y^{\ell}_{OH^-,cv} \cdot \dot{\mathbb{N}}^{evap}_{H_2O}}{n^{\ell}_{tot,cv}} \tag{5.65}$$

Working in the same way the mole balance for the water is:

$$\frac{dn^{\ell}_{H_2O,cv}}{dt} = \dot{n}^{\ell}_{H_2O,in} - \dot{n}^{\ell}_{H_2O,out} + \dot{\mathbb{N}}^{r}_{H_2O} - \dot{\mathbb{N}}^{evap}_{H_2O} \tag{5.66}$$

While the partial mole balance of water in the liquid phase is:

$$\frac{dy^{\ell}_{H_2O,cv}}{dt} = \frac{\left(y^{\ell}_{H_2O,in} - y^{\ell}_{H_2O,cv}\right)\cdot \dot{n}^{\ell}_{in} - \left(1 - y^{\ell}_{H_2O,cv}\right)\cdot \dot{\mathbb{N}}^{evap}_{H_2O} + \dot{\mathbb{N}}_{SO_2}}{n^{\ell}_{tot,cv}} \tag{5.67}$$

The mole balance needs to be written also for SO_3^{2-} that is formed due to the chemical reaction.

$$\frac{dy^{\ell}_{SO_3^{2-},cv}}{dt} = \frac{\left(y^{\ell}_{SO_3^{2-},in} - y^{\ell}_{SO_3^{2-},cv}\right)\cdot \dot{n}^{\ell}_{in} + \dot{\mathbb{N}}_{SO_2} + y^{\ell}_{SO_3^{2-},cv}\cdot \dot{\mathbb{N}}^{evap}_{H_2O}}{n^{\ell}_{tot,cv}} \tag{5.68}$$

5.5.3. ENERGY BALANCE

Thermal energy is exchanged between the (hot) exhaust gas and the (cold) liquid flow, cooling down the first while heating up the latter. The heat exchange between the two phases does not affect the operationability of the scrubber, but does affects the physical phenomena such as mass transfer, evaporation of water and the properties of both the liquid and gas phase.

The energy balance is based on the first thermodynamic principle. In the case of process devices, its form is applied to an open system, as there are almost always input-output currents. Conventional energy taken into consideration is the internal (thermal) energy and the mechanical (kinetic and potential) energy. Therefore, the total energy of the system is:

$$E = U + KE + PE \tag{5.69}$$

The energy balance is :

$$\Delta E = Q - W \tag{5.70}$$

The instantaneous time rate form of the energy balance is:

$$\frac{dE_{cv}}{dt} = \dot{Q} - \dot{W} \Longrightarrow \frac{U}{dt} + \frac{dKE}{dt} + \frac{dPE}{dt} = \dot{Q} - \dot{W} \tag{5.71}$$

The conservation of energy applied to a control volume states:

$$\frac{dE}{dt} = \dot{Q} - \dot{W} + \dot{m}_{in}\left(u_{in} + \frac{v^2_{in}}{2} + g\cdot z_{in}\right) - \dot{m}_{out}\left(u_{out} + \frac{v^2_{out}}{2} + g\cdot z_{out}\right) \tag{5.72}$$

The various project contributions can be divided into two main categories: the moving parts project, called the shaft or turbine project, $\dot{W}_s$, and the work from the pressure vector displacement at the inlets and outlets of the device (p-V work).

$$\dot{W} = \dot{W}_s + \dot{m}_{out}(p_{out}\cdot v_{out}) - \dot{m}_{in}(p_{in}\cdot v_{in}) \tag{5.73}$$

The terms of kinetic and potential energy are negligible in relation to enthalpy changes and are usually eliminated. Specific enthalpy is given from the relation $h = u + pv$. Also, spindle-shaft work is not interchangeable because the devices rarely have moving parts. So, relation 5.72 can be written as following:

$$\frac{dU}{dt} = \dot{Q} + \dot{m}_{in}\cdot h_{in} - \dot{m}_{out}\cdot h_{out} \tag{5.74}$$

The last relation (5.74) needs to be expanded for the case of the packed bed as the terms of the mass transfer of both SO_2 and H_2O needs to be included in the model. Further more the total change of internal energy U can be split to the amount of species in the control volume and the specific internal energy of the species in the control volume:

$$\frac{dm_{cv}\cdot u_{cv}}{dt} = \dot{m}_{in}\cdot h_{in} - \dot{m}_{out}\cdot h_{out} \pm \dot{Q} \pm \dot{\Phi}_{SO_2}\cdot h_{SO_2} \pm \dot{\Phi}_{H_2O}\cdot h_{H_2O} \tag{5.75}$$

The sign $\pm$ is associated to whether the control volume is the gas or the liquid control volume, so there is mass entering or leaving the one phase for the other. The same reasoning applies to the heat transfer.

ENERGY BALANCE OF GAS PHASE

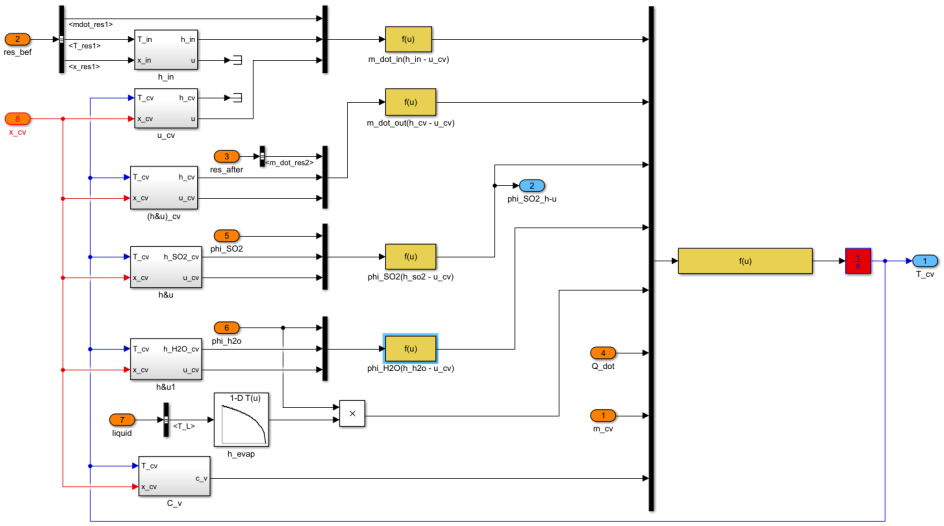

Figure 5.12: The inside of the Simulink block of gas temperature calculation

In the gas phase, there is mass transfer of SO_2 leaving the gas phase and H_2O getting into the gas phase due to evaporation. The sign of these mass transfers in 5.75 will be minus and plus respectively. Also, in the balance needs to be subtracted the enthalphy of evaporation of liquid as this energy is offered by the gas. Heat is transferred to the liquid phase from the gas phase because the gasses entering the wet scrubber are in high temperature and they will be in higher temperature than the liquid regardless of the stage ($T^g_{cv} > T^{\ell}_{cv}$).

$$\frac{dm^g_{cv} \cdot u^g_{cv}}{dt} = \dot{m}^g_{in} \cdot h^g_{in} - \dot{m}^g_{out} \cdot h^g_{out} - \dot{\Phi}_{SO_2} \cdot h^g_{SO_2} + \dot{\Phi}_{H_2O} \cdot h^g_{H_2O} - \dot{\Phi}_{H_2O} \cdot h^{evap}_{H_2O} - \dot{Q} \tag{5.76}$$

The left hand side of relation 5.76 can be analysed as in the case of equation 5.5 with the only difference that instead of mass flow, the mole flow will be used in the packed bed, due to its convenience.

$$\frac{d(m_{cv} \cdot u_{cv})}{dt} = m_{cv} \cdot \frac{du_{cv}}{dt} + u_{cv} \cdot \frac{dm_{cv}}{dt} \tag{5.77}$$

In the above equation, the total mass balance of the gas phase (equation 5.45) is the second term of the right hand side. Applying the same method as for the case of the mole balance and substituting from thermodynamics the term $du = c_v(T) \cdot dT$, then equation 5.76 becomes:

$$m^g_{cv} \cdot c_v \frac{dT^g_{cv}}{dt} = \dot{m}^g_{in} \cdot h^g_{in} - \dot{m}^g_{out} \cdot h^g_{out} - \dot{\Phi}_{SO_2} \cdot h^g_{SO_2} + \dot{\Phi}_{H_2O} \cdot h^g_{H_2O} - \dot{\Phi}_{H_2O} \cdot h^{evap}_{H_2O} - u^g_{cv} \cdot \left(m^g_{in} - m^g_{out} - \dot{\Phi}_{SO_2} + \dot{\Phi}_{H_2O}\right) - \dot{Q} \tag{5.78}$$

By introducing one of the most important assumptions used in this model, the perfect mixing the energy balance of the gas phase is:

$$m^g_{cv} \cdot c_v \frac{dT^g_{cv}}{dt} = \dot{m}^g_{in} \cdot \left(h^g_{in} - u^g_{cv}\right) - \dot{m}^g_{out} \cdot \left(h^g_{cv} - u^g_{cv}\right) - \dot{\Phi}_{SO_2} \cdot \left(h^g_{SO_2} - u^g_{cv}\right) + \dot{\Phi}_{H_2O} \cdot \left(h^g_{H_2O} - u^g_{cv}\right) - \dot{\Phi}_{H_2O} \cdot h^{evap}_{H_2O} - \dot{Q} \tag{5.79}$$

ENERGY BALANCE OF THE LIQUID PHASE

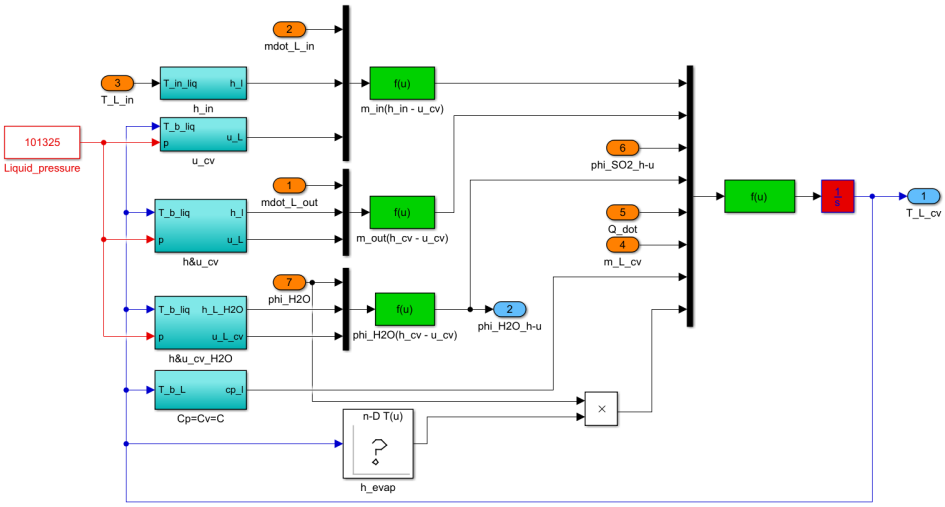

Figure 5.13: The inside of the Simulink block of liquid temperature calculation

To obtain the energy balance of the liquid phase the steps are the same as the one of the gas phase. Perfect mixing is also applied in the liquid phase. The difference here compared to the gas phase, is that the total mole balance to be used is that of the chemical reaction (equation 5.61). Sulphur oxides that go to the liquid phase carry their energy with them. Finally, the energy balance of the liquid phase is:

$$m^{\ell}_{cv} \cdot c \frac{dT^{\ell}_{cv}}{dt} = \dot{m}^{\ell}_{in} \cdot \left(h^{\ell}_{in} - u^{\ell}_{cv}\right) - \dot{m}^{\ell}_{out} \cdot \left(h^{\ell}_{cv} - u^{\ell}_{cv}\right) + \dot{\Phi}_{SO_2} \cdot \left(h^{g}_{SO_2} - u^{g}_{cv}\right) - \dot{\Phi}_{H_2O} \cdot \left(h^{\ell}_{H_2O} - u^{\ell}_{cv}\right) + \dot{\Phi}_{H_2O} \cdot h^{evap}_{H_2O} + \dot{Q} \tag{5.80}$$

The enthalpy and internal energy of the SO_2 in the liquid phase energy balance is the same with that of the gas phase. SO_2 reacts in the liquid film and disappears. It not part of the liquid phase. Energy balance requires this amount to exist in the equation because when it enters the liquid film it exists and can affect the properties. The heat of the chemical reactions is included in the enthalpies of the inflow and outflow of liquid, as it exists only in liquid phase.

5.5.4. HEAT TRANSFER

The heat flux between two fluids can be calculated using Fourier's law [115].

$$\dot{q}_x = -\lambda \cdot \frac{dT}{dx} \tag{5.81}$$

Similarly to mass transfer, conduction heat transfer is carried out at the interface and the driving force is the temperature difference between the bulk of the two fluids. The problem of defining the thickness of gas and liquid film is exist also for heat transfer. In the scrubber there are two moving liquids and so there is also heat convection. In most of the cases, heat convection overcomes heat conduction and the problem can be approached as in the case of mass transfer, assuming that the interface operates as a plate that separates the two flows. The term $\frac{\lambda}{dx}$ will be replaced for the case of convection by the heat transfer coefficient h_c. In the interface is assumed that there is no heat accumulation and that there are equilibrium conditions. In the case of heat transfer, equilibrium means that the temperature of the interface T_i is equal for both films (Figure 5.14). Thus heat flux for the gas phase can be described:

$$\dot{q}^{g} = h^{g}_{c} \cdot \left(T^{g}_{b} - T_i\right) \tag{5.82}$$

And heat flux in the liquid phase is:

$$\dot{q}^{\ell} = h^{\ell}_{c} \cdot \left(T_i - T^{\ell}_{b}\right) \tag{5.83}$$

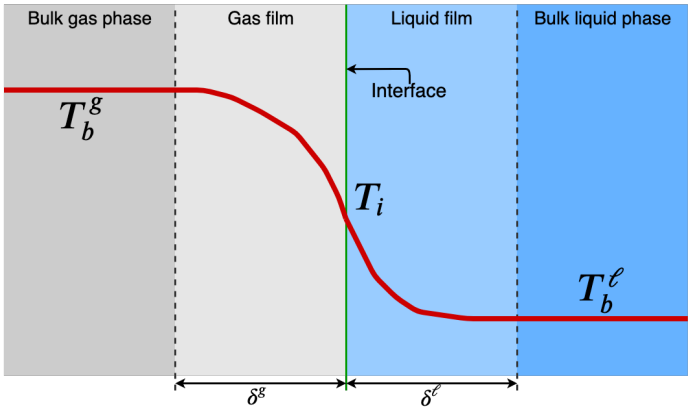

Figure 5.14: Temperature profile in the gas-liquid interaction

The convention used here is that heat flux is positive for heat flow from the hotter fluid to the cooler. The amount of heat going from the on phase to the other is equal:

$$\dot{q}^g = \dot{q}^\ell = \dot{q} \tag{5.84}$$

The above condition serves in the calculation of the interfacial temperature if heat transfer coefficient and the bulk temperatures of both phases are known. The bulk temperature can be obtained using the integrating the relations of energy balance (equations 5.79 and 5.80). The methodology to calculate heat transfer coefficients is the same as that of the mass transfer coefficient and will be presented in the Appendix D.3.

$$T_i = \frac{h_c^g \cdot T_b^g + h_c^\ell \cdot T_b^\ell}{h_c^g + h_c^\ell} \tag{5.85}$$

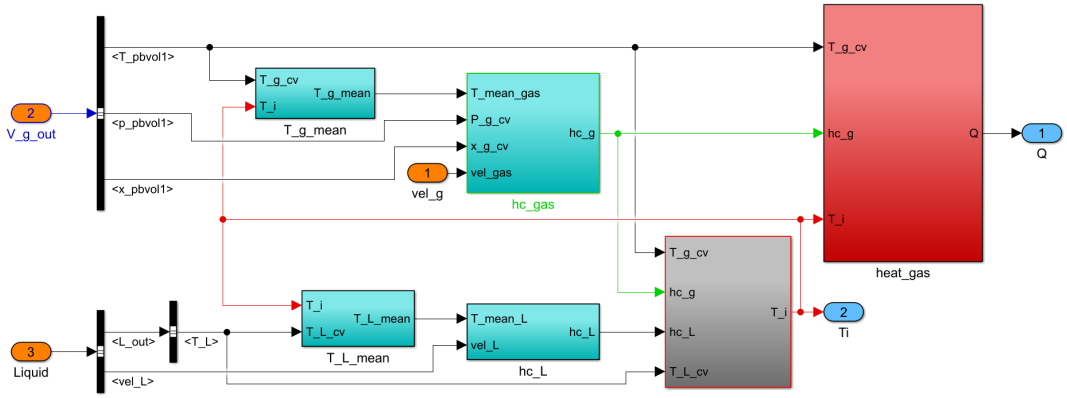

Figure 5.15: Simulink block for the calculation of temperature in the interface and the thermal energy flux.

Thermal energy flux, $\dot{Q}$, is the product of heat flux times the area (in this case the interfacial area) that heat transfer is carried out:

$$\dot{Q} = \dot{q} \cdot A_i = h_c^g \cdot A_i \cdot \left(T_b^g - T_i\right) = h_c^\ell \cdot A_i \cdot \left(T_i - T_b^\ell\right) \tag{5.86}$$

Relation 5.86 makes clear that the driving force of heat transfer is the temperature gradient. One of the most important factors affecting heat transfer is the interfactial area. Analytically the way to calculate the interfacial area is be provided in the section of the liquid phase model approach (paragraph 4.8). The simulink block is given in Figure 5.15.

6

MODEL VERIFICATION

"The man of science has learned to believe in justification, not by faith, but by verification"

Thomas Henry Huxley

6.1. INTRODUCTION

The designed model is the mathematical representation of the physical system. All the models before being used need to be verified and if possible to be validated. Verification and validation is an enabling methodology that is conducted during the development of a computational model with the ultimate goal of producing engineering predictions with quantified confidence.

Ideally, when building a model and make simulations with it, both verification and validation should be carried out. Although, in this thesis only verification was carried out. Validation was not possible to be accomplished because:

1. It was impossible to perform experiments and obtain results. The wet scrubber is an expensive device to be purchased by both TU Delft or Royal IHC and requires a lot of space and systems around it.
2. There is a lack of published data for the wet scrubbers, especially in the maritime sector where the technology is relatively new. The only available data were from industrial application, where the focus is on particulate matter removal and the dimensions and the packing material are not the same as of the maritime scrubbers.
3. Wet scrubber manufacturers were unwilling to share the results and other important information about their system because of competition.

The importance of the process parameters such as mass flow, temperature and composition was already described in chapter 5. Now the effects of these parameters is presented and verified in a static analysis, where these parameters have a constant value. Before presenting the results of the verification, the inputs of the system will be given together with the geometry of the system.

6.2. GEOMETRY OF THE SYSTEM

The prototype scrubber used for this project is the Alfa Laval PureSO$_X$ system (Figure 6.1). The system is in compliance with regulations set forth in Revised MARPOL Annex VI and it's guideline MEPC 184(59) "Scheme B". The design of the system covers the treatment of exhaust gasses from one four stroke 7.2 MW diesel engine. The scrubber can clean exhaust gasses of HFO with 3.5% sulphur to the equivalent of 0.1%, using fresh water and caustic soda. The data are from engine tests at 100% MCR. Alfa Laval does not provide all the required scrubber data, thus assumptions have been made and a sensitivity analysis has been used to define the remaining parameters. The provided data of the PureSO$_X$ that will be used are given in the Table 6.1.

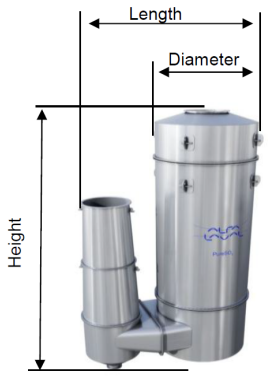

Figure 6.1: Alfa Laval $PureSO_X$ wet scrubber

Table 6.1: Dimensions of Alfa Laval $PureSO_X$ wet scrubber

Description	Size
Height	7.5 m
Diameter	2.8 m
Length	4.8 m
Venturi inlet diameter	1.1 m

6.2.1. PACKED BED

Alfa Laval provides no further information about the size, geometry and the type of the packing material. The total height of the scrubber is 7.5 meters and the packing material was chosen to be a section of 2 meters height and a diameter of 2.8 meters. The packing material used in the wet scrubber, can be a structure or dumped packing. Structured packing (Figure 6.2a) has high efficiency as it increases the contact surface between liquid and gas, but is rarely used in maritime application due to its high cost.

(a) Mellapack 250Y, of Sulzer [116]

(b) Hiflow ring 50, of RVT [117]

Figure 6.2: Structured packing (a) and dumped packing (b) material.

Marine wet scrubber for SO_X removal, mostly use dumped packing material. Billet and Schultes [108] have done extensive research on this topic and they provide a significant number of packing materilas and their characteristics. There are three choices of packing materials namely plastic, metallic or ceramic. Among these three materials, metallic seemed to be the worst option because of the corrosive properties of SO_X. The corrosive properties will be enhanced by the combination of the high temperatures of the exhaust gasses and the wet conditions in the scrubber. Plastic packing was also rejected for this application, as the exhaust

gasses coming from the diesel engine are at high temperature. Plastic will not be able to withstand these temperatures for a long period, resulting in a destroyed structure. Therefore, the material that best suits maritime applications is the ceramic material as it is resistant to both corrosion and high temperatures.

Table 6.2: Packing material used for the analysis

Dumped Packing	Size (mm)	Number (m^{-3})	a (m^2/m^3)	ε (m^3/m^3)
Hiflow ring	50	5120	89.7	0.809
	38	13241	111.8	0.788
Raschig ring	50	5990	95.0	0.830

The dumped ceramic packing material that were tested and their characteristic data are provided in Table 6.2. To chose among the available packing material an sensitivity analysis was carried out (Figure 6.3). The decision criteria for the choice was based on the price, the efficiency and the convergence of the results. Considering the price Hiflow ring-50 was the cheapest one, followed by Rasching ring-50 and the most expensive one was Hiflow ring-38.

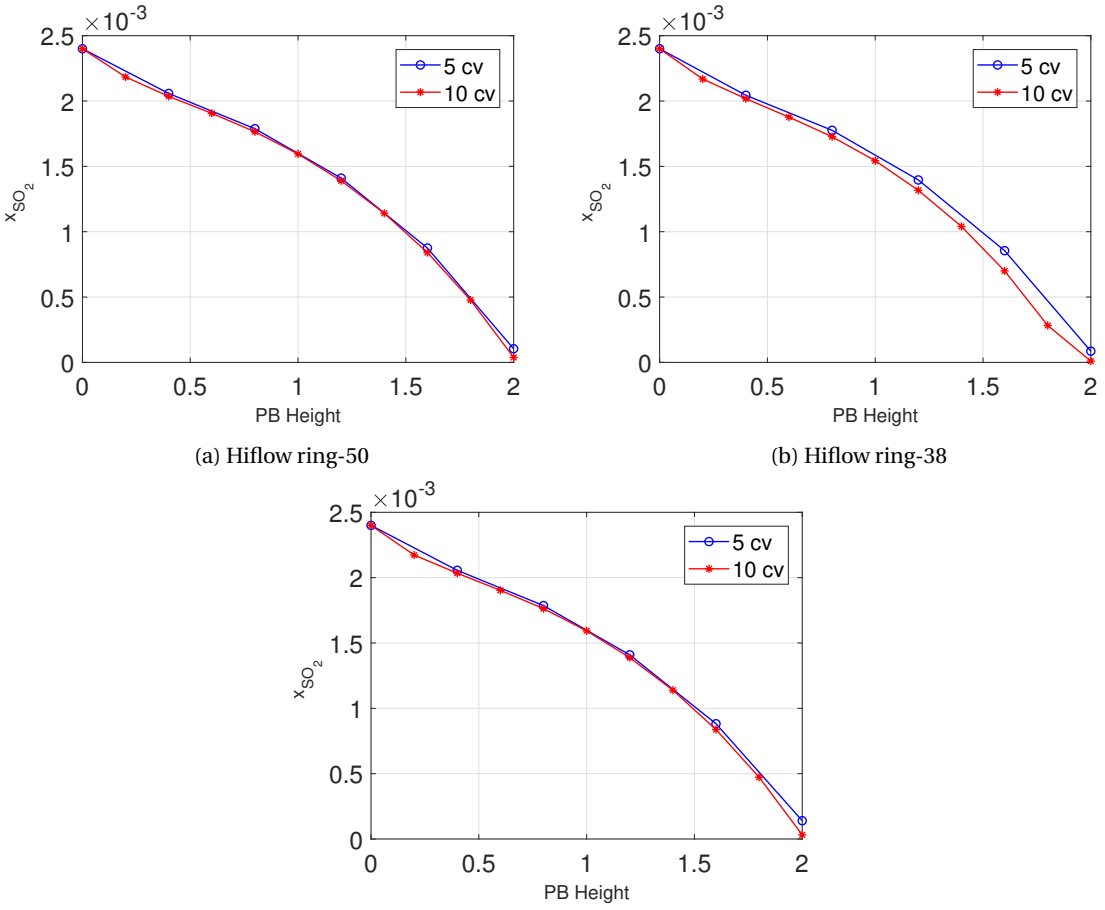

(a) Hiflow ring-50

(b) Hiflow ring-38

(c) Rasching ring-50

Figure 6.3: Sensitivity analysis for 5 and 10 control volumes in the packed bed of the three prospective packing material

A sensitivity analysis was done by adopting an initial discretisation between 5 and 10 control volumes and by using random values of mass flow and temperature for both gas and liquid. The highest removal efficiency is that of Hiflow ring-38, followed by Hiflow ring 50 and last Rasching ring-50. Hiflow ring-38 did not provide satisfactory results regarding convergence in contrast to Hiflow ring-50 (Figure 6.3). Taking into account the 3 parameters set for the analysis, the Hilflow ring 50 (Figure 6.2b) was chosen for its overall performance.

6.2.2. VENTURI, VOLUMES AND DEMISTER GEOMETRY

The exhaust gasses enter the scrubber through the venturi. The diameter of the venturi entrance is 1.1 m, given by Alfa Laval, while the diameter at the throat is assumed to be the half of it. The upper and lower volume have the same diameter as the scrubber diameter (2.8 meters) and is assumed that are of the same height. Their height is 2.75 m and results by subtracting from the total height the height of the packed bed and then divide by 2. In most of the scrubbers, the lower volume is slightly bigger than the upper because in the lower volume there is a section where the water is drained. The diameter of the demister is 0.9m and the height is small compared to the total height thus is not taken into account for the calculations.

6.3. PACKED BED DISCRETISATION

Prior doing the sensitivity analysis, discretisation of the packed bed section is required. All the other parts of the scrubber are considered to be one lumped control volume. The packed bed section, where the SO_X absorption mainly takes place needs to be discretised to have a better overview of the removal efficiency and the evaporation influence along the packed bed. A higher discretisation will give more accurate results.

The discretisation was made for 1, 2, 3, 5, 10 and 20 control volumes for a packed bed length of 2 meters height. The input values for mass flow and temperature of both gas and liquid were the same as them for the sensitivity analysis for the selection of the packing material. The packing material used is the Hiflow ring-50. The results of the discretisation analysis are provided in the Figure 6.4.

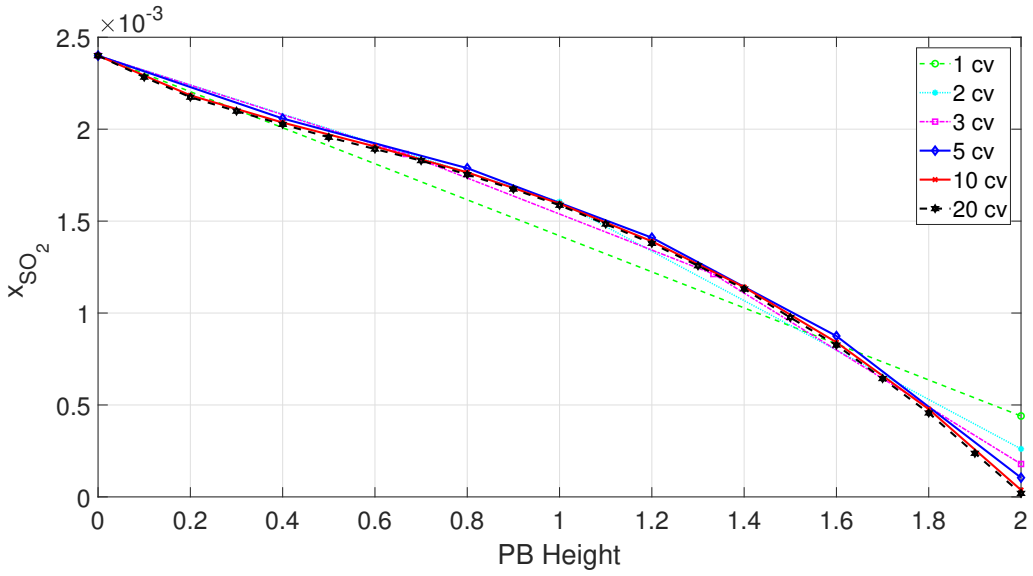

Figure 6.4: Discretisation of the packed bed (PB) section

The analysis show convergence between 5, 10, and 20 control volumes, but mainly between 10 and 20 control volumes. The more accurate results are obtained for 20 control volumes. Along the length of the packed bed the average difference of x_{SO_2} between 20 and 10 control volumes and between 20 and 5 control volumes is around 2% and 5% respectively. Another important parameter when modelling, is the simulation time. The simulation time for 20 control volumes is more than two hours, for 10 control volumes is around 25 minutes and for 5 control volumes is around 4 minutes. Due to the high difference in simulation time, the 5 control volumes will be adopted for the discretisation and will be used for the simulation of the model.

6.4. INPUT CONDITIONS

The inputs of the scrubber system are the exhaust gasses and the scrubbing liquid. Each flow can be characterised by the mass flow, temperature and composition. Exhaust gasses come from the diesel engine and are the product of combustion process in the cylinder. The scrubbing liquid is supplied from the liquid tank which normally is in the lower decks of the vessel. The scrubber is positioned at the end of the exhaust gas pipe system. A pump is used to overcome the height difference between the liquid tank and the scrubber.

6.4.1. EXHAUST GAS INFLOW

To carry out the simulation, a look up table was created with data taken from an existing diesel engine used in vessels. A version of it is used in the Diesel B model. This engine has a power of 10MW and a conversion to the equivalent 7.5 MW engine was performed so as to be in correspondence with its specifications of Alfa Laval for the maximum power of engine. The manufacturer's data provide the exhaust gas mass flow and temperature, but the data for the exhaust gas composition was not in line with the composition used for this thesis. Therefore, the file that provides the exhaust gas composition of the Diesel B model was used. Adjustment were applied in this file so as the composition of the exhaust gasses to be the same with the composition used in this report. Diesel B model complexity and the high requirement in computational power and time, made it feasible to carry out only one case. This is for air excess ratio value $\lambda = 2$ and the fuel sulphur content be $x_{S_{fuel}} = 0.035$. Table 6.3 provides the values of the look up tables that will be used as inputs for the simulations.

Table 6.3: Look up table values for the simulations

6 cylinder 7.5 MW Engine			
Power (%)	$\dot{m}_{gas}(kg/s)$	Temperature (K)	$x_{S_{fuel}}$ [-]
100	13.006	611	0.035
75	10.856	565	0.035
50	8.909	538	0.035
25	5.075	573	0.035

6.4.2. REQUIRED LIQUID MASS INFLOW

A parameter affecting the removal efficiency of the wet scrubber is the amount of the inflow wash-water [110]. To have the optimum efficiency of the scrubber the water inflow must be as high as possible. This amount is supplied by the pumping system. The operation of pumps consumes power which is provided by the diesel engine. To reduce the power consumption of the pumps the minimum required amount of water should be provided to the scrubber system. The sensitivity analysis is used to determine the least amount of water required to achieve the required scrubbing efficiency.

The sensitivity analysis carried out examines the influence of the gas mass flow, temperature and composition on the required amount of water flow in the scrubber. The values of gas mass flow and temperature are the same with Table 6.3. Exhaust gas composition is based on the values that the Diesel B model file provides for different sulphur composition. The effects of the evaporation and demister replenishment are included in the analysis. The upper limit of $\frac{ppmvSO_2}{y_{CO2}}$ in the SECA's defined by the IMO is 4.3 [118]. To operate a vessel in SECA, the scrubber output should be lower than that limit. The temperature of liquid water is constant and equal to 295K.

EXHAUST GAS MASS FLOW INFLUENCE

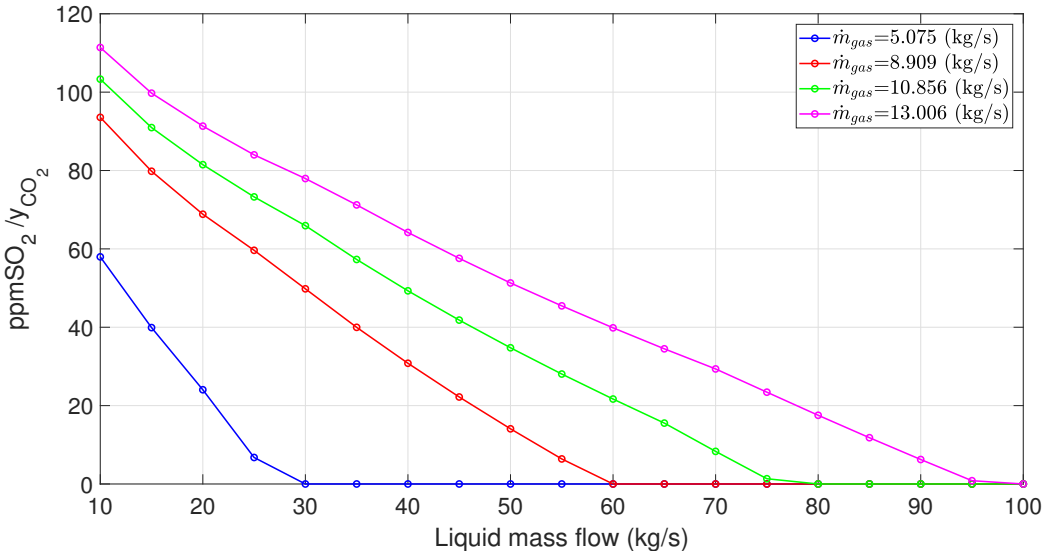

Figure 6.5: Liquid flow requirements for the different values of gas mass flow and fractions $\frac{ppmvSO_2}{y_{CO2}}$.

To examine the gas mass flow influence on the required amount of liquid supply, the inputs used are the mass flows from the look up table. The values of temperature and composition are them of the 100% engine load and are constant. For the different values of the gas mass flow, different values of liquid flow were examined and the fraction $\frac{ppmvSO_2}{y_{CO2}}$ was measured at the end of the scrubber. The results are shown in Figure 6.5.

The analysis showed that when the gas mass flow is low, then also the liquid requirements are low. When the gas flow becomes lower also the SO_X flow (that is part of the gas) is lower reducing also the requirements in liquid. Moreover, the volume of the scrubber is not changing and in lower gas mass flows for the same volume and temperature, the gas pressure in the volume is lower. The diffusion coefficient of a binary mixture is inversely proportional to the pressure and thus the diffusion coefficient increases, increasing also the mass transfer coefficient. The velocity of the gas is also lower for lower mass flows and thus the residence time in the scrubber is higher, giving more time for the gas-liquid interaction.

EXHAUST GAS TEMPERATURE INFLUENCE

The values of temperature that will be used in the analysis are the same with them of the different engine loads given in Table 6.3. In the analysis of temperature influence, gas mass flow and composition are constant and equal to the values of 100% MCR. Figure 6.6 provides the outcome of this investigation.

The temperature deviations of the exhaust gasses do not to have a significant influence on the required scrubbing liquid. The required scrubbing liquid is almost the same at any temperature and minor differences are observed at small liquid flows. Water has higher heat capacity than gas [119] and is at significant lower temperature. The direction of heat transfer is from the thermal body to the colder [115]. Heat is absorbed by liquid and as a result the temperature of the gas will drop from the first centimetres that will enter the scrubber. After some distance in the packed bed the temperatures are almost the equal, regardless of the temperature at the entrance making the effect of temperature insignificant, considering that the fraction $\frac{ppmvSO_2}{y_{CO2}}$ is calculated at the end of the scrubber. At the end of the packed bed (highest position), the water has the highest amount of $NaOH$ compared to the entrance in the packed bed, making the influence of the $NaOH$ more important. Higher heat capacity of liquid means that requires more energy to increase its temperature and thus can absorb more heat compared to the gas. If the amount of water increases for the same amount of gas, then these phenomena become intense, eliminating any temperature differences that may occur at the scrubber. This is why in Figure 6.6 at high liquid flows the values converge.

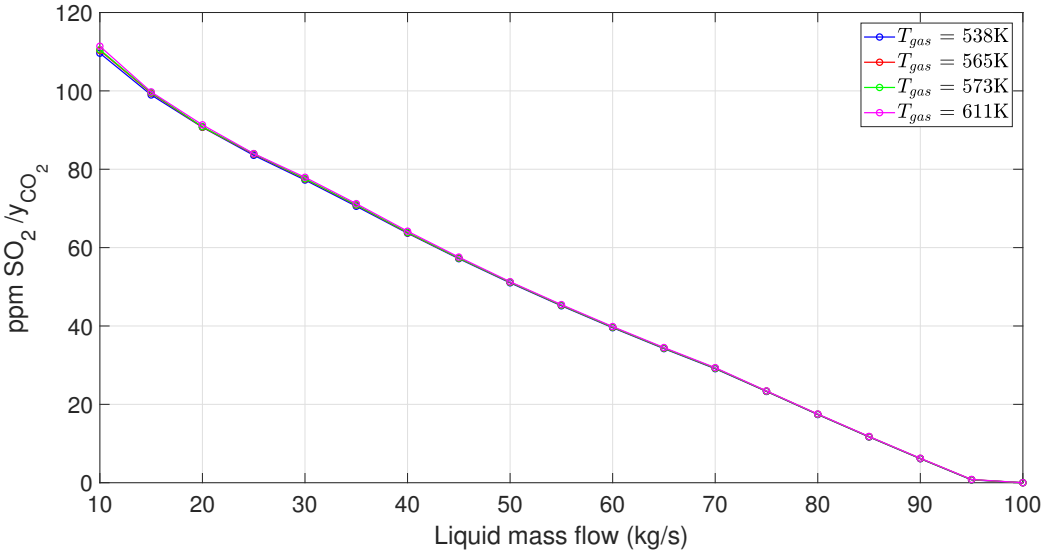

Figure 6.6: Liquid flow requirements for the different values of gas temperature and fractions $\frac{ppmvSO_2}{y_{CO2}}$.

EXHAUST GAS COMPOSITION INFLUENCE

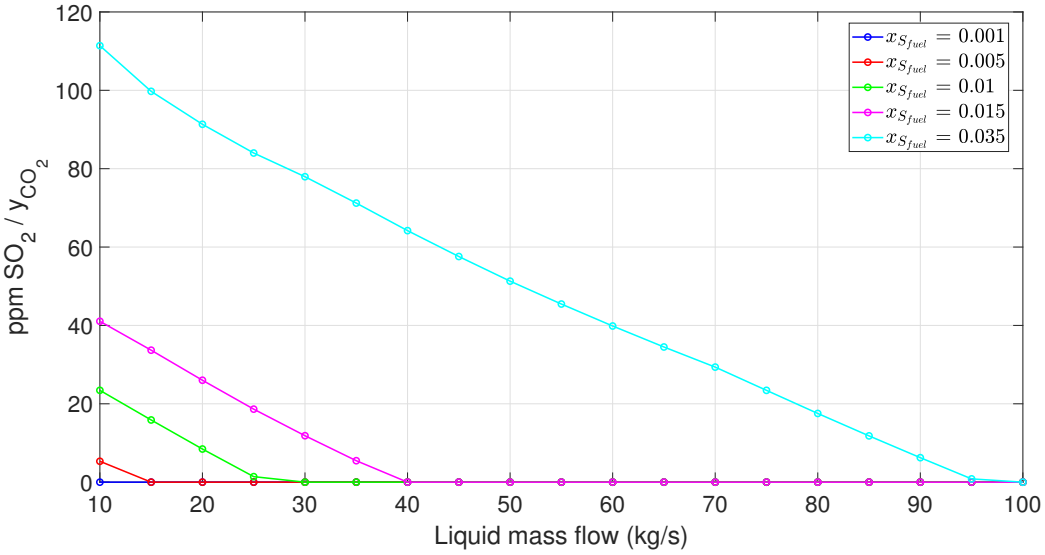

Figure 6.7: Liquid flow requirements for the different values of composition and fractions $\frac{ppmvSO_2}{y_{CO2}}$.

In this thesis, the exhaust gas composition is constant for all the engine loads. For the analysis, there are used different values of sulphur composition in the fuel that correspond to the available maritime fuels in the market. The gas mas flow and temperature are them of 100% MCR. The approach followed is the same with that in the two previous cases.

The results in Figure 6.7 demonstrate that the lower the sulphur concentration in the fuel, the lower the liquid requirements. When the fuel sulphur concentration was 0.1% the liquid requirements were always zero, as the sulphur content was already low enough to comply with the stringent SECA limit. This final result is also a verification of the designed model.

DECISIVE FACTOR

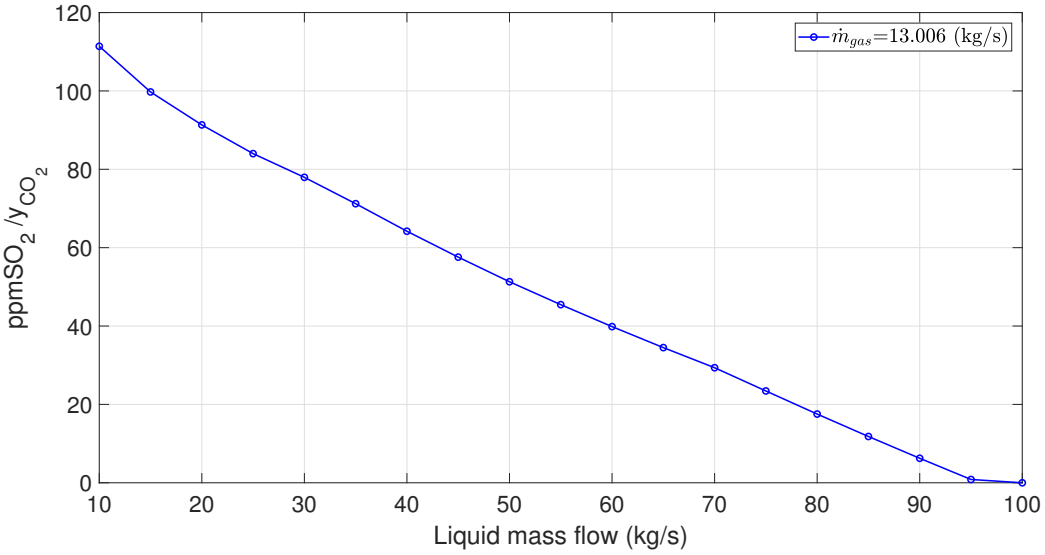

Figure 6.8: Liquid flow requirements at 100% MCR and different fractions $\frac{ppmvSO_2}{y_{CO2}}$.

The three analysis that were carried out provided the effects of each parameter of the gas flow, in the required amount of liquid that the pumping system will supply to the wet scrubber. Because the liquid flow is mainly water and the temperature is assumed to be constant, its effects were not investigated. Considering that the composition is constant and that the mass had greater influence compared to temperature the decision was to chose mass influence as the base to calculate the optimum liquid flow. The mass analysis showed that 100% MCR has the largest requirements in water. The results are projected in Figure 6.8. To comply with the SECA's limit the amount of liquid at 100% MCR should give a value of $\frac{ppmvSO_2}{y_{CO2}}$ lower than 4.3. From Figure 6.8 this corresponds to liquid requirements of $94 kg/s$. This is the value to be used for the static simulations because scrubber designers operate their systems continuously at the maximum required liquid flow.

6.5. STATIC VERIFICATION

The static verification examines the influence of the exhaust gas mass flow, temperature and the composition on the functional behaviour of the scrubber. The effect of the evaporation will be provided for all cases. In this section the value of the liquid flow obtained from section 6.4.2 is $\dot{m}_L = 94\frac{kg}{s}$ and the $NaOH = 0.013\frac{kg}{s}$ and combines sufficiently the scrubber efficiency and the power consumption of the flow. The $NaOH$ is not considered as an independent flow but as part of the liquid, because it is insignificant compared to the total amount of liquid. Therefore, the liquid flow refers to the combined flow of water and $NaOH$.

No experimental results are available to validate the present numerical model, that include the influence of evaporation on a wet scrubber with packing material. There are experimental results for wet scrubber but they are for small laboratory scale, do not use the same scrubbing liquid or do not use packing and the conditions of both phases are atmospheric. Therefore, a direct comparison of these results with the current computational model was not considered an accurate base of comparison.

To make a verification of the model, a literature research was carried out for the 3 examined parameters (gas mass flow, temperature and composition) and their influence on the evaporation. Attention was aminly paid to the range of these parameters and/or the trends that they follow in these cases and the analogies with the created model were examined. For example, if the temperature in the papers was in the desired range and the increase of temperature was causing an increase in the evaporation, and the same trend was also in the this model then the results were acceptable. The exact magnitude of the parameters can be examined only

with similar conditions and are also affected by the discretisation of the model. For the discretisation, the actual computational power imposes an upper limit.

A difference of this section compared to the next chapter is that here, only one parameter will change at every step while the rest remains constant. The values of the mass flow and temperature are the same with those of Table 6.3 and the values of the fuel sulphur concentration is the same used in the analysis to determine the liquid requirements.

6.5.1. MASS FLOW INFLUENCE

For the mass flow influence, the values used for the gas mass flow are them from the look up table 6.3 . In this analysis gas temperature is assumed to be constant at 611K and fuel composition of $x_{S_{fuel}} = 0.035$. The effect of the mass flows is examined upon the removal efficiency, evaporation, demister replenishment, gas and liquid temperature.

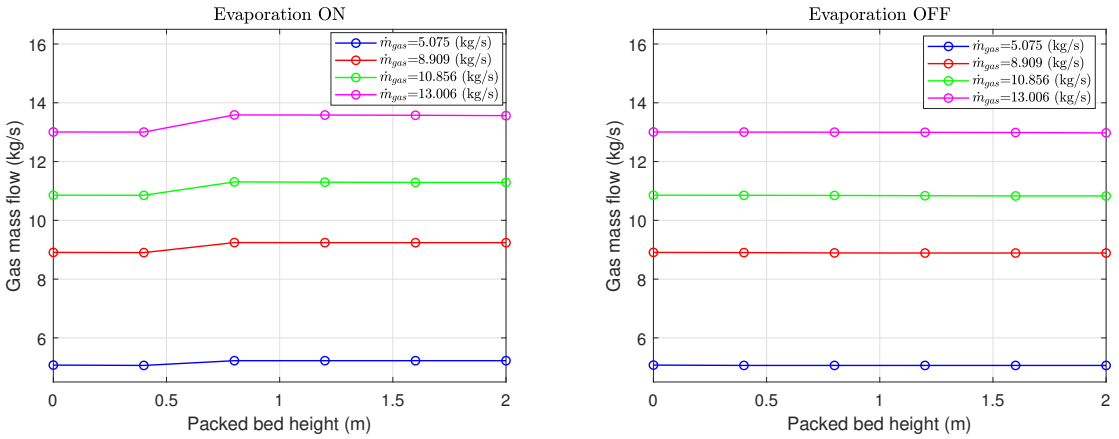

(a) Longitudinal mass flow including evaporation effect

(b) Longitudinal mass flow excluding evaporation effect

Figure 6.9: Longitudinal mass flow for the case that evaporation effect is taken into account (left) and for the case that evaporation effect is not taken into account (right)

The gas mass flow of the four engine loads along the packed bed for the case of evaporation is given in Figure 6.9a and in the case that evaporation is not considered in the analysis in Figure 6.9b. There are differences in the amount of gas that goes out of the packed bed in these two figures. In Figure 6.9b, the evaporation phenomena is not taken into account and the gas mass flow out of the packed bed is lower than the one entering the packed bed. The difference is equal to the amount of SO_2 absorbed from the liquid phase, which is small ($x_{SO_{2in}} = 0.0024 \cdot \dot{m}^g_{in}$) compared to the total amount of gas and this is why the values appear to be almost the equal in and out. In Figure 6.10b, at low engine load, the demister replenish an amount of water while at the higher engine load demister replenishment is zero. The conditions in the demister are almost atmospheric and are different compared to the inlet of the scrubber. Absolute humidity was considered for the humidity comparison and meaning that water amount does not change. Gas conditions in the demister, differ compared to the inlet of scrubber. The amount of water vapour is higher than the amount that gas flow can carry in these conditions in the demister and the gas appears to be saturated in water. In small gas flows the composition is the same with that of 100% MCR and absolute water capacity is also lower.

When evaporation is considered in the analysis (Figure 6.9a and 6.10a), then the amount exhaust gasses leaving of the packed bed is higher than the one entering. The increase is equal to the difference between the amount of water that evaporates (Figure 6.10a) minus the amount of SO_2 that is absorbed from the liquid. It is expected that evaporation should be higher in the first control volume and not in the second as it is happening here. This is a result of a limit imposed in the Simulink model, that controls the maximum amount of evaporation. This calculates the absolute humidity (w) and compares it with the absolute saturation humidity (w_{sat}). The maximum amount that can evaporate is relative to the difference between the saturation value of humidity and the actual ($\dot{m}^g \cdot (w_{sat} - w)$).

$$w = \frac{p_{H_2O}}{p^g - p_{H_2O}} \cdot \frac{M_{H_2O}}{M^g} \tag{6.1}$$

$$w_{sat} = \frac{p^{sat}_{H_2O}}{p^g - p^{sat}_{H_2O}} \cdot \frac{M_{H_2O}}{M^g} \tag{6.2}$$

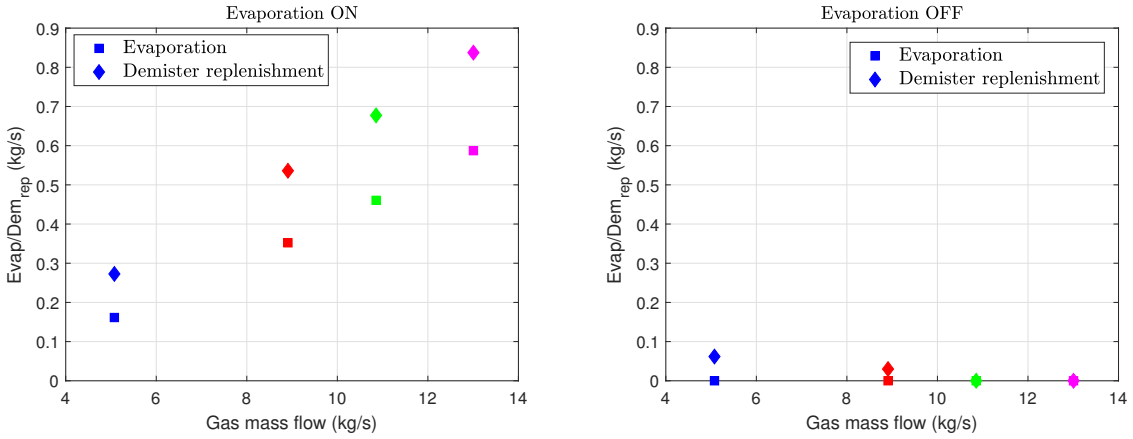

(a) Evaporation and demister replenishment for different mass flow, including evaporation effect

(b) Evaporation and demister replenishment for different mass flows, excluding evaporation effect

Figure 6.10: Evaporation and demister replenishment for the case that evaporation effect is taken into account (left) and for the case that evaporation effect is not taken into account (right), under the influence of the mass flow rates.

Vapour pressure, ($p^{sat}_{H_2O}$) is calculated by Antoine equation (Appendix C.2) and temperature has a significant effect. In Figure C.2 it can be seen that at high temperatures the vapour pressure increases significantly, making the value $w_{sat} < 0$ because the pressure of the gasses is close to atmospheric conditions. Gas cooling in the first stage of the scrubber reduces the $p^{sat}_{H_2O}$ and then w_{sat} is positive. The difference $w_{sat} - w$ should always be positive to have water evaporation. If it is negative, then evaporation is zero.

Figure 6.10a shows the dependence of the evaporation rate on the amount of gas flow. This is in accordance with the findings of other research. An increase in gas flow rate, at any temperatures of gas and liquid, implies a growth in evaporation rate [120]. This is because the exhaust gas that flows in the packed bed removes the vapour formed above the gas-liquid interface, were evaporation takes place. The vapour in the interfacial surface is transferred away due to forced convection and diffusion. An increase of the exhaust gas flow rate increases also the vapour concentration gradient in the gas phase [121] enhancing the evaporation of water. *He et al.* [122], measured the evaporation rate of water liquid film for different packing materials. They found that an increase in air velocity, in the same temperature, increases the evaporation rate. In packing material the flow volume is constant and the gas pressures close to atmospheric, meaning almost constant density, then the mass flow is proportional to velocity. The analogy of gas mass flow with the rate of evaporation is verified by other scientists that tested other gasses and liquids [120, 121, 123, 124]. For the same temperature and composition, an increase in gas mass flow also increases the water capacity the gas can carry. Moreover, the increase of exhaust gas flow rate will also grow the shear-stresses on the gas–liquid interface [123].

Demister replenishment focuses only in the water lost in the packed bed due to the evaporation and is not considering the water that is removed with the sludge at the bottom of the scrubber. Furthermore, there is an overestimation of the values of evaporation and demister replenishment, because in the scrubber except from evaporation also condensation takes place, but is not considered in this thesis.

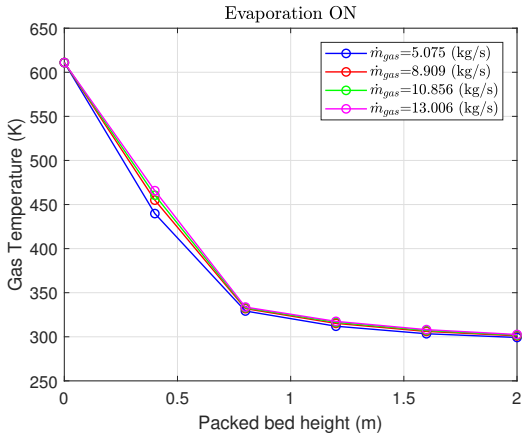

(a) Longitudinal gas temperature including evaporation effect

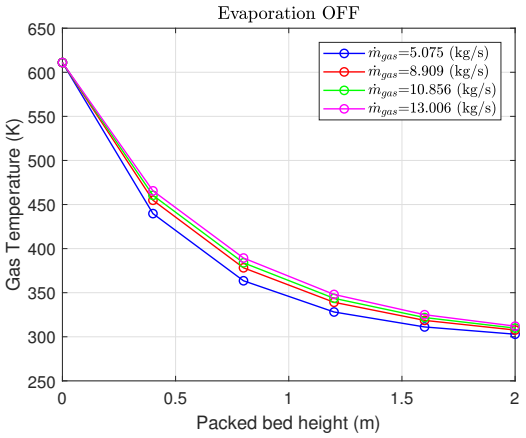

(b) Longitudinal gas temperature excluding evaporation effect

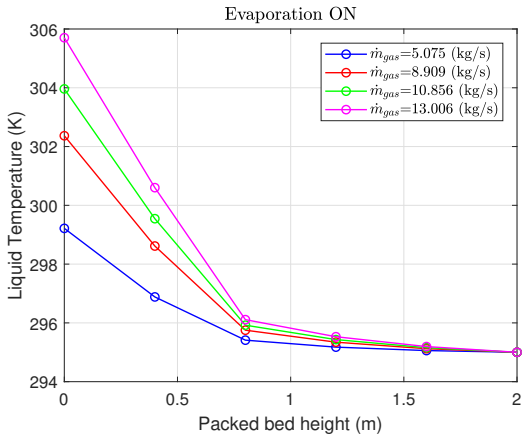

(c) Longitudinal liquid temperature including evaporation effect

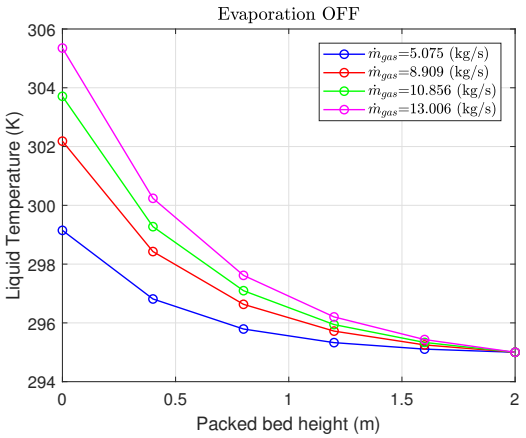

(d) Longitudinal liquid temperature excluding evaporation effect

Figure 6.11: Longitudinal gas and liquid temperature,under the influence of the mass flow rates, including and excluding the evaporation effect

The results of gas and liquid temperature along the packed bed height seem reasonable (Figure 6.11). The gas temperature is reduced and the liquid temperature is increased. At the top of the packed bed the gas temperature is higher than the liquid temperature and at the bottom of the packed bed liquid temperature is lower than that of the gas. There is no cross section where the liquid temperature is higher than that of gas, a situation resembling a heat exchanger in counterflow. Because of the assumption that liquid and gas phase do not mix in the packed bed and two films are formed, the section can be considered that operates as heat exchanger. In the case of evaporation, there is steep decrease of the gas phase temperature and an analogous increase of the liquid temperature, as the heat required to evaporate the water is taken from the gas phase. When evaporation is not taken into account the temperature profiles are smoother. In both cases (with or without evaporation), temperature decrease of the gas phase or increase of the liquid phase is inversely proportional or proportional respectively, to the gas mass flow in all the cross sections of the packed bed. For the same liquid flow rate and gas temperature, when the gas flow rate is low then there is a higher decrease of the gas temperature compared to when the mass flow is high. The gas velocity is lower and the residence time of the gas in the scrubber is higher leading to higher reduction of the gas temperature. For the liquid phase though low gas rates means that it will absorb less heat from it, as heat transfer is also linked to the amount of mass $\dot{Q} = \dot{m}^g \cdot c_p^g \cdot \Delta T^g = \dot{m}^\ell \cdot c_p^\ell \cdot \Delta T^\ell$.

The profile of the x_{SO_2} is affected by the gas flow rate. A reasonable outcome considering that high flow rates carry more SO_2 compared to the low flow rates. For the same liquid flow, less SO_2 means that it can be absorbed easily from the first stages that it enters the scrubber. When evaporation effect is considered, x_{SO_2}

is slightly lower compared to the non evaporation case, because the values of mass fraction are relative to each other so as their summation is equal to one. When water evaporates, then increases the x_{H_2O} in the gas phase lowering the mass fraction of the other substances. The blue, red and green lines as shown in Figure 6.12a and 6.12b do not have the same steep inclination as the magenta line before becoming zero due to the discretisation.

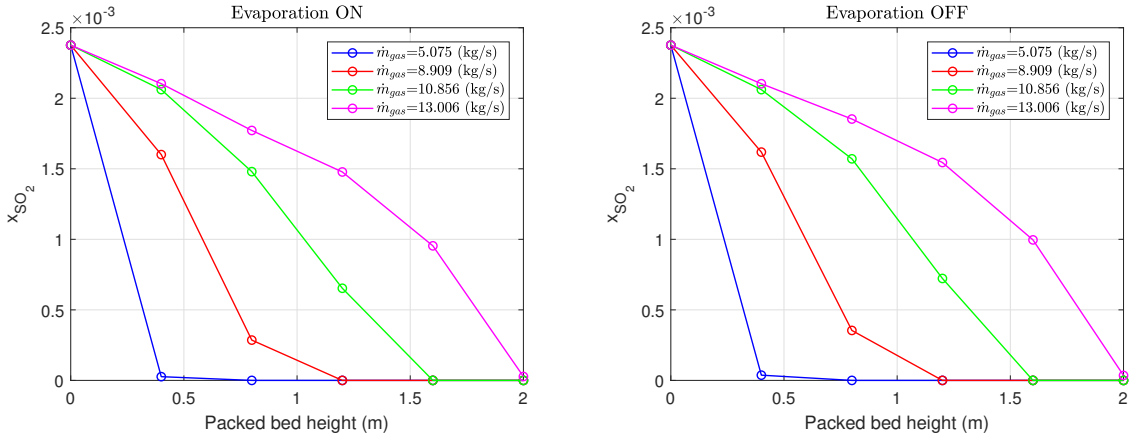

(a) Longitudinal x_{SO_2} including evaporation effect

(b) Longitudinal x_{SO_2} excluding evaporation effect

Figure 6.12: Longitudinal x_{SO_2}, under the influence of the mass flow rates, including and excluding the evaporation effect

6.5.2. TEMPERATURE INFLUENCE

To examine the influence of the exhaust gas temperature, the values used are them provided by the diesel engine for the four loading conditions. For this analysis the exhaust gas mass flow is constant and equal to 13.006 $\frac{kg}{s}$, the fuel sulphur content $x_{S_{fuel}} = 0.035$ and liquid flow is 94 $\frac{kg}{s}$.

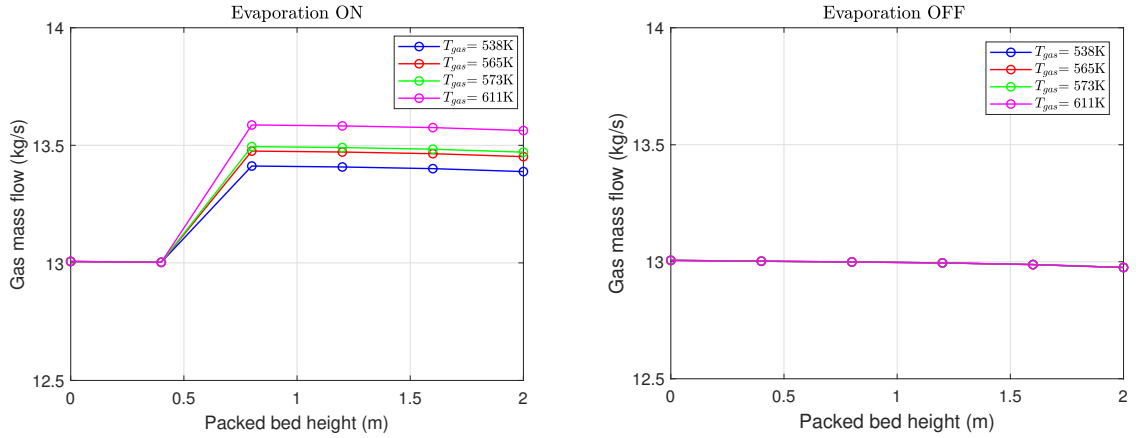

(a) Longitudinal mass flow including evaporation effect

(b) Longitudinal mass flow excluding evaporation effect

Figure 6.13: Longitudinal mass flow, for the case that evaporation effect is taken into account (left) and for the case that evaporation effect is not taken into account (right), under the influence of the temperature.

In Figure 6.13a, the increase of the gas temperature results to an increase of the exhaust gas mass flow at outlet of the scrubber compared to the inlet. That is the outcome of the water evaporation minus the SO_2 absorbed. Mass is an extensive property, so it is not directly affected by temperature. When evaporation is not accounted, the flow rate out of the scrubber is almost equal to that entering (Figure 6.13b).

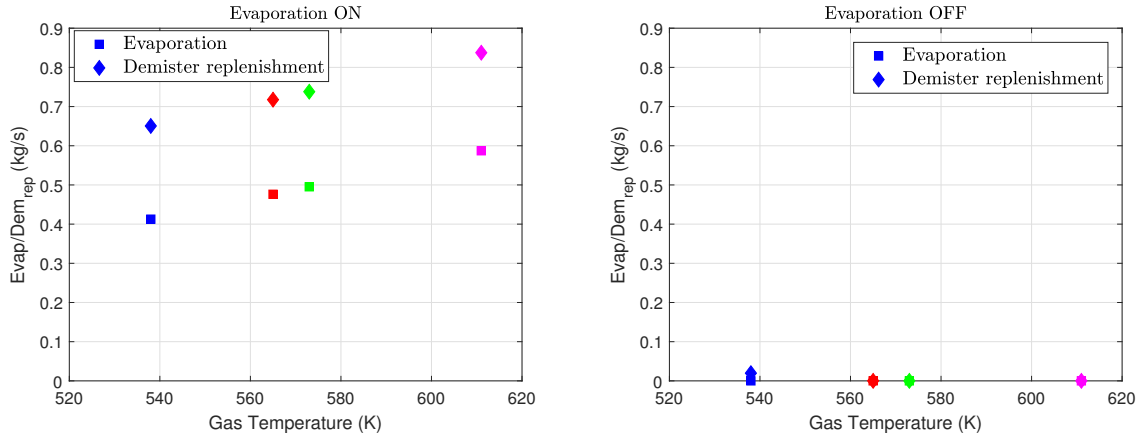

(a) Evaporation and demister replenishment for different temperature, including evaporation effect

(b) Evaporation and demister replenishment for different temperatures, excluding evaporation effect

Figure 6.14: Evaporation and demister replenishment for the case that evaporation effect is taken into account (left) and for the case that evaporation effect is not taken into account (right), under the influence of the temperature.

In the film theory, evaporation is governed by the simultaneous heat and mass transfer [125]. The direction of sensible heat needed for evaporation is from the gas flow to the interface [126]. For constant exhaust gas mass flow, composition and liquid temperature at the inlet, evaporation rate increases with the increase of the exhaust gas temperature (Figure 6.14a). When the gas temperature increases, the molar diffusion in the gas phase also increases, as the diffusion coefficient depends on the temperature (Appendix D.2). The temperature gradient between the gas and liquid increases, boosting heat transfer rate and in turn rising the temperature at the liquid-gas interface. Furthermore, an increase in the concentration difference can be observed due to the higher saturation pressure that come with the increase of gas temperature. The Mollier diagram shows that the absolute saturation humidity increases with temperature meaning that the warmer gasses require higher amount of vapour to saturate [104]. The physical outcome of the escalation of the T_i is an increase the average kinetic energy of the water molecules in the interface, and therefore more molecules of the water will have the sufficient kinetic energy to pass from the liquid to the gas phase [120, 121, 123].

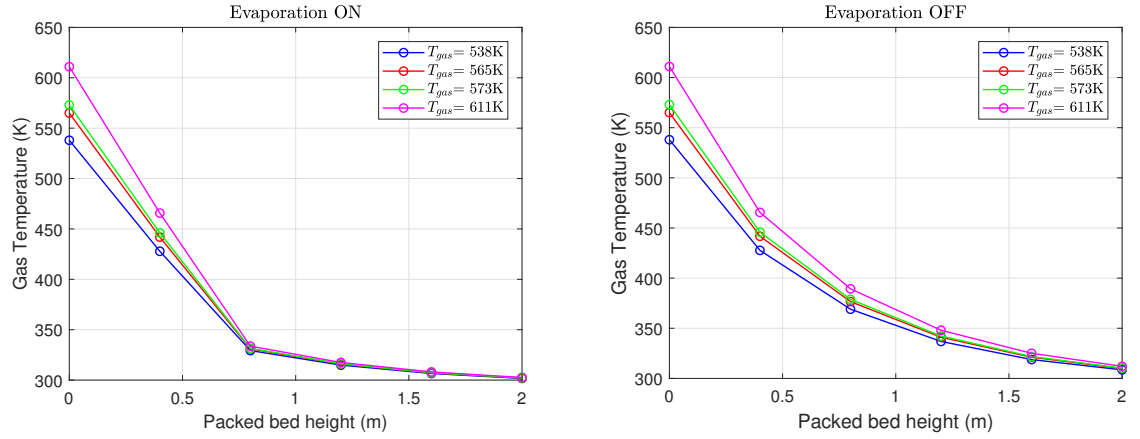

(a) Longitudinal gas temperature including evaporation effect

(b) Longitudinal gas temperature excluding evaporation effect

Figure 6.15: Longitudinal gas temperature including and excluding the evaporation effect, under the gas temperature influence

The gas temperature has similarities with the case of mass transfer influence. In Figure 6.15a the influence of evaporation on temperature profile can be observed, as at the first meter of the packed bed the inclination is steeper and the value lower, compared to the smoother profile of the non evaporative case (Figure 6.15b). The same characteristics can be observed also for the liquid temperature profile (Figures 6.16a and 6.16b).

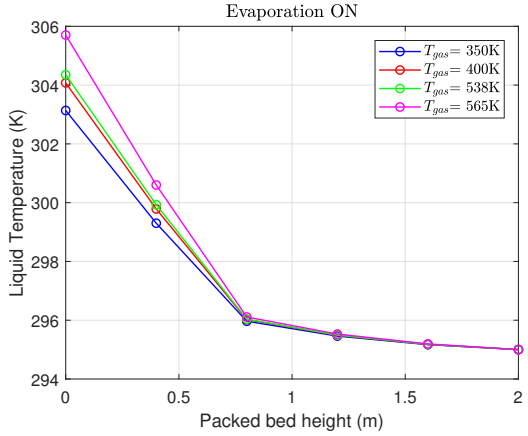

(a) Longitudinal liquid temperature including evaporation effect

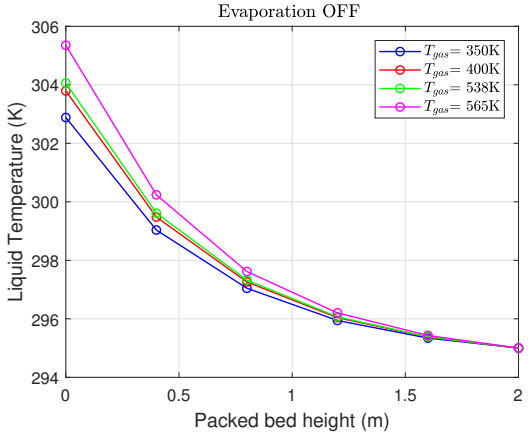

(b) Longitudinal liquid temperature excluding evaporation effect

Figure 6.16: Longitudinal liquid temperature, under the influence of gas temperature change, including and excluding the evaporation effect

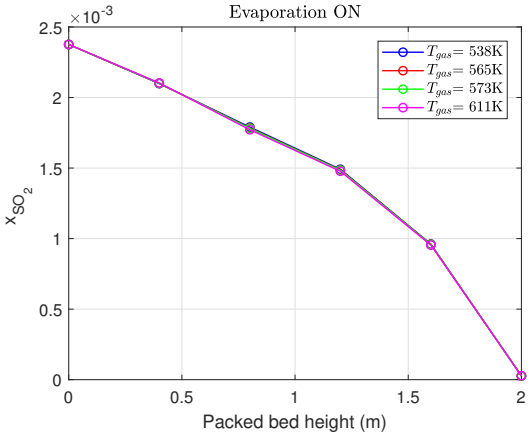

(a) Longitudinal x_{SO_2} including evaporation effect

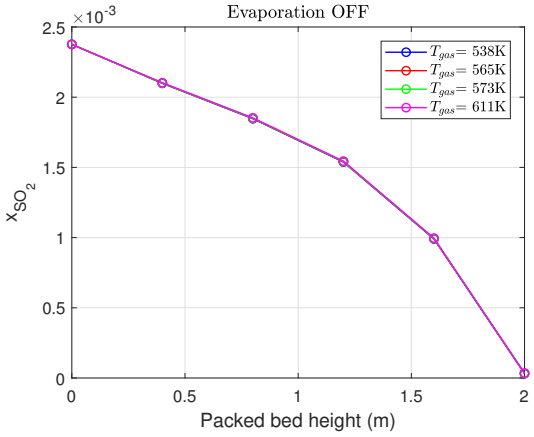

(b) Longitudinal x_{SO_2} excluding evaporation effect

Figure 6.17: Longitudinal x_{SO_2}, under the influence of gas temperature changes, including and excluding the evaporation effect

For the mass fraction of sulphur dioxide, temperature has no influence. Although, the situation here is complicated. Temperature increase, reduces the viscosity and viscosity appears in both Reynolds and Schmidt number and also in the diffusion coefficient in the liquid phase. Its influence is positive on the diffusion coefficient and Schmidt number and negative on Reynolds number. Also temperature has a positive effect on the diffusion coefficient, and this coefficient appears in the denominator of the Schmidt number but is also an enhancement factor in the mass transfer coefficient (Appendix D). From the ideal gas law, increase of the temperature has negative effect in the density under constant volume. A temperature increase, increases the kinetic energy of the gas and reduces the residence time in the scrubber vessel. This is one of the reasons of placing a venturi pre-scrubber. Zooming in the results of Figure 6.17 shows that the higher temperature results in higher x_{SO_2} in all cross sections.

6.5.3. COMPOSITION INFLUENCE

Changing the amount of sulphur in the fuel oil, will have as an outcome a different composition in the exhaust gas. In this case the exhaust gas mass flow and temperature will be the same with 100% MCR and the sulphur content the same as in the sensitivity analysis for the determination of required liquid flow.

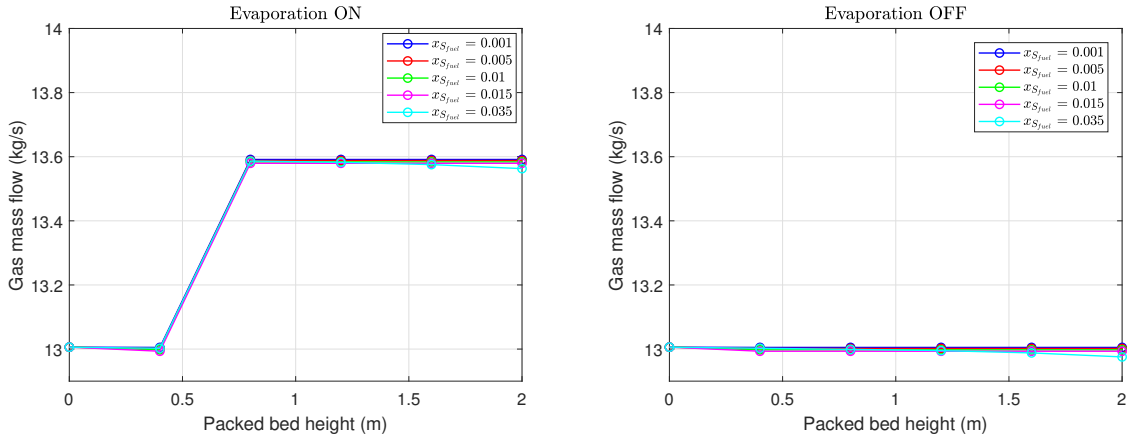

(a) Longitudinal mass flow including evaporation effect

(b) Longitudinal mass flow excluding evaporation effect

Figure 6.18: Longitudinal mass flow, for the case that evaporation effect is taken into account (left) and for the case that evaporation effect is not taken into account (right), under the influence of the fuel sulphur content.

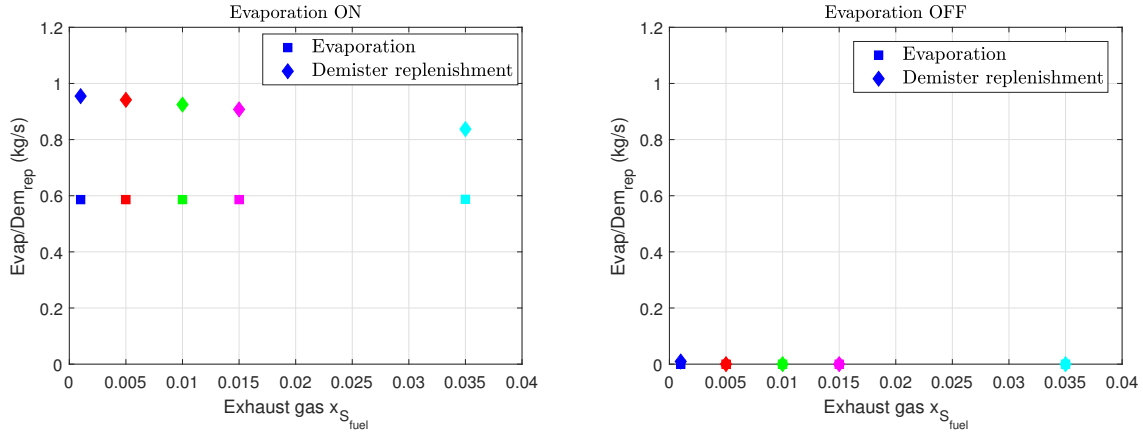

(a) Evaporation and demister replenishment for different mass flow, including evaporation effect

(b) Evaporation and demister replenishment for different mass flows, excluding evaporation effect

Figure 6.19: Evaporation and demister replenishment for the case that evaporation effect is taken into account (left) and for the case that evaporation effect is not taken into account (right), under the influence of the fuel sulphur content.

Fuel sulphur content variations do not have any influence on the evaporation rate (Figure 6.19). For the same gas mass flow and temperature, the amount of evaporation is decreasing as the mole fraction of steam is increasing [125]. Increasing of humidity induces a decreasing of gradient at interface because the gas will be closer to saturated conditions. While $x_{S_{fuel}}$ increases, the $x^g_{H2_O}$ decreases so as the sum of the mass fractions in the gas to be equal to one. Decrease of $x^g_{H2_O}$ will increase the gradient and thus increase the amount of evaporation. In this analysis the mass fraction of sulphur is meagre, does not imply any significant influence on the evaporation rate and thus the values seem to be the same.

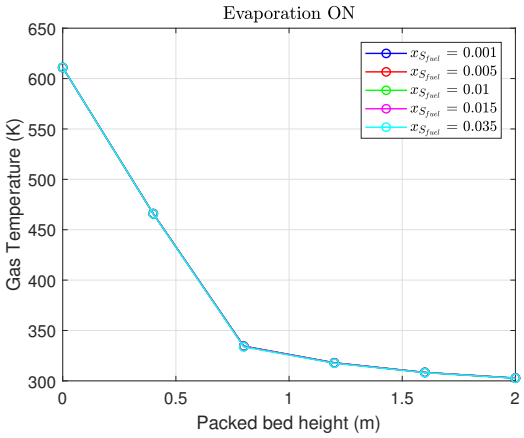

(a) Longitudinal gas temperature including evaporation effect

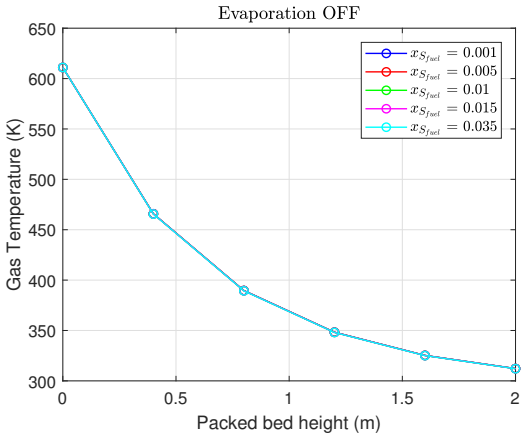

(b) Longitudinal gas temperature excluding evaporation effect

Figure 6.20: Longitudinal gas temperature, under the influence of the fuel sulphur content, including and excluding the evaporation effect

6

The above analysis is valid for the pre-inversion temperature regime in the gas phase [127]. When the gas temperature is above the inversion temperature, water evaporation increases, as the humidity of air increases and the evaporation rate is the highest for pure superheated steam [127]. For the analysis of the this project the effect after the inversion temperature is out of the scope and are not examined. In most of the papers [120, 122, 123, 125–127] the inversion temperature was more than 420K and the water temperature was close to 373K. In this project water temperature is 295 K and the temperature of the exhaust gasses after the second control volume is already below 400K. Therefore, it can safely stated that the evaporation is examined below the inversion temperature.

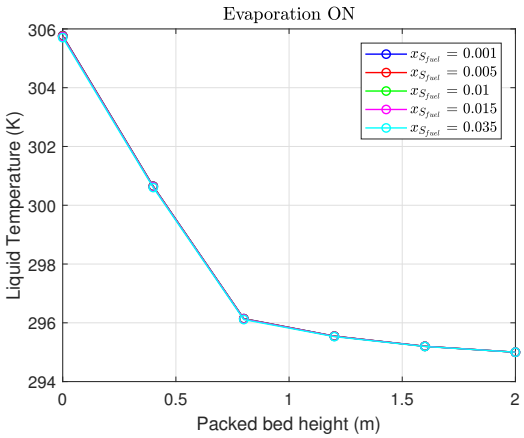

(a) Longitudinal liquid temperature including evaporation effect

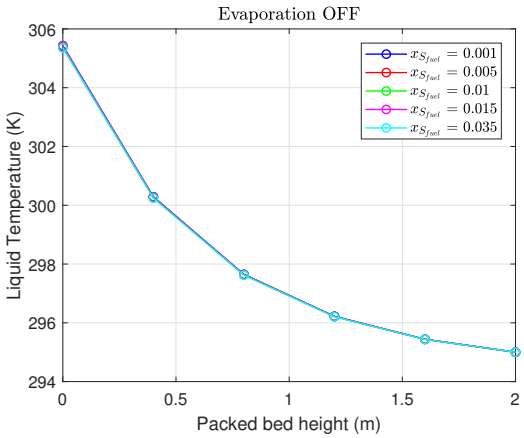

(b) Longitudinal liquid temperature excluding evaporation effect

Figure 6.21: Longitudinal liquid temperature, under the influence of the fuel sulphur content, including and excluding the evaporation effect

The other parameters demonstrate similar behaviour with the cases that were examined in the influence of gas mass flow rate and temperature. Their results are given in Figure 6.20 and 6.21. Exhaust gas and liquid temperature profile, including and excluding evaporation effect, is the same for all the five different compositions of exhaust gasses, because the amount of SO_2 is small compared to the other substances making its influence on the properties negligible.

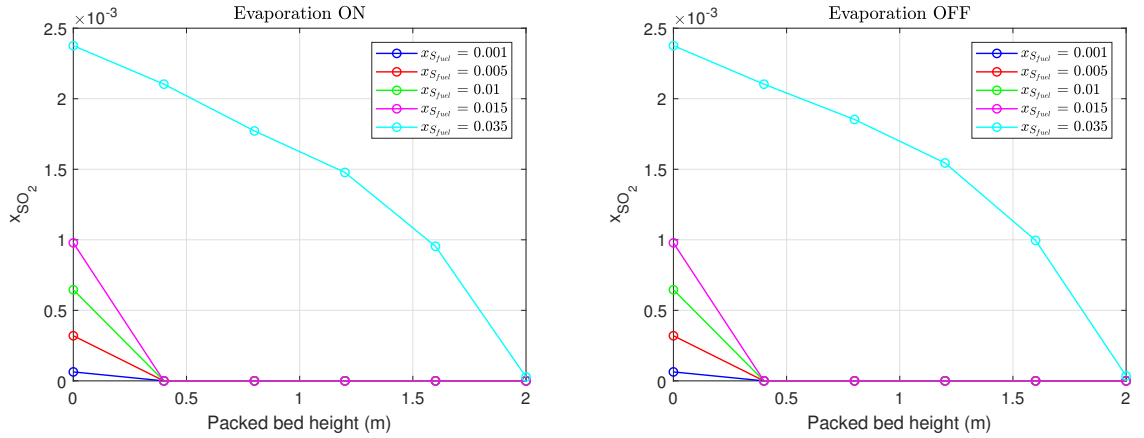

(a) Longitudinal x_{SO_2} including evaporation effect

(b) Longitudinal x_{SO_2} excluding evaporation effect

Figure 6.22: Longitudinal x_{SO_2}, under the influence of the fuel sulphur content, including and excluding the evaporation effect

Figure 6.22 for $x_{S_{fuel}} < 0.035$ shows that the scrubber removes sulphur oxides from the gas in the first half meter of the packed bed section.

The results from the static verification were satisfying as they are in line with the findings of other scientists. There were no unexpected results in the static verification which may place doubt on the validity of the used model approach. The precision of course of the values obtained can be validated only with experimental results, under the same operational conditions and with a higher discretisation of the packed bed system. Under the present conditions the outcome is acceptable and the next step consists of the static and dynamic simulations.

7

SIMULATIONS AND RESULTS

"If you do not expect the unexpected, you will not find it,
for it is not to be reached by search or trail."

Heraclitus

7.1. INTRODUCTION

In this chapter, the previously verified model will be used to perform both static and dynamic analyses. The input for these analyses will be based on the exhaust gas properties given in paragraph 6.4. The static analysis will be used to investigate the effect of evaporation on the scrubber operation and efficiency. The dynamic analysis will focus on the response and efficiency of the scrubber to changing exhaust gas conditions.

7.2. STATIC ANALYSIS

The static analysis will investigate the influence of evaporation on the sulphur dioxide removal efficiency of the scrubber. The investigation also includes the water replenishment in the demister and if this compensates for the evaporation in the packed bed. The simulations are carried out for the different engine loads. The following terminology will be used in the text and figures in this chapter:

- engine: refers to the conditions leaving the diesel engine (look up table data);
- scrubber: refers to the complete the scrubber system ;
- evap: means that the influence of evaporation is taken into account in the model;
- no evap: means that the influence of evaporation is not taken into account in the model (it is assumed that there is no evaporation in the packed bed).

The amount of scrubbing liquid required for cleaning the exhaust gasses for both the case that evaporation phenomena is taken into account and the case that is not taken into account is presented in Figure 7.1. The projected results reflect only 100%MCR. The required scrubbing liquid flow is lower when evaporation is not taken into account in the packed bed. This while achieving the same sulphur dioxide over carbon dioxide ratio. The lower requirements in liquid means lower power consumption by the pump and consequently lower fuel consumption of diesel engine. The only case that the opposite is happening is at a low liquid flow rate. The liquid flow rate is close to the gas flow rate and the heat transfer results in increase of the liquid temperature and affecting evaporation. Also, the gas temperature reduction is not as big as in the case of high liquid flow. The Simulink block, that imposes an upper limit to the amount of evaporation creates an instability in this case. Due to this instability, in the case of evaporation the value of liquid supply appears lower in this area.

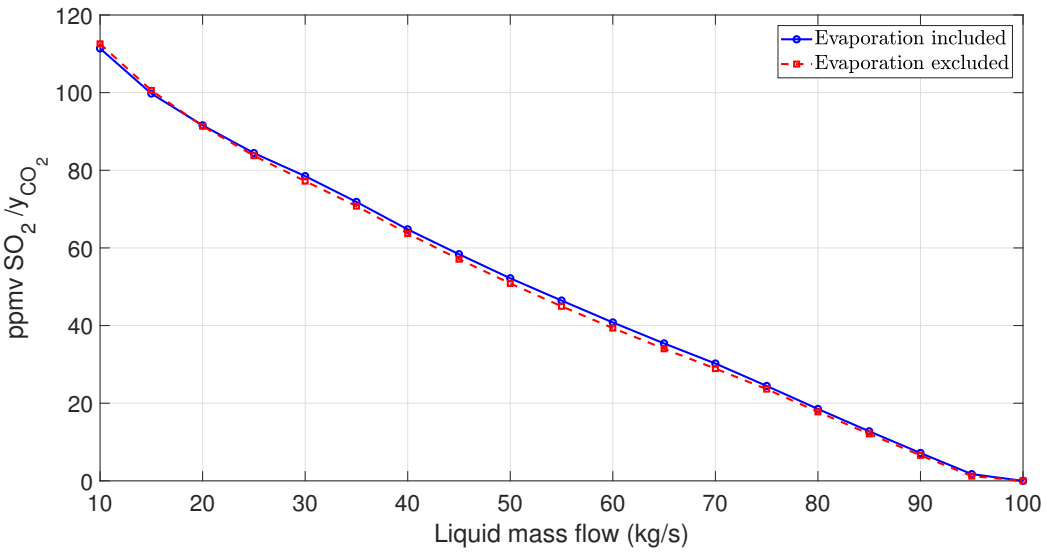

Figure 7.1: Required liquid flow in the scrubber, with and without the influence of evaporation.

The adequacy of the demister to replenish the water lost in the packed bed of the scrubber only focuses on the evaporation in the packed bed. The analysis does not include the water that is removed with the sludge at the bottom of the scrubber. Furthermore, it is assumed that the exhaust gasses leaving the demister have a relative humidity of 100%. No analytical design was made for the demister. Exhaust gasses leaving the packed bed section is supersaturated in vapour. Evaporation is taking place in the second control volume. Condensation in the packed bed is not taken into account and because the temperature at the output of the packed bed is lower than in the second control volume, exhaust gasses are supersaturated. Therefore, condensation that takes place in the demister has as an outcome a demister replenishment higher than the amount of evaporating water. The ambient condition effect on water consumption in the scrubber. In a very dry climate with a high seawater temperature, the evaporation will be higher than the replenishment.

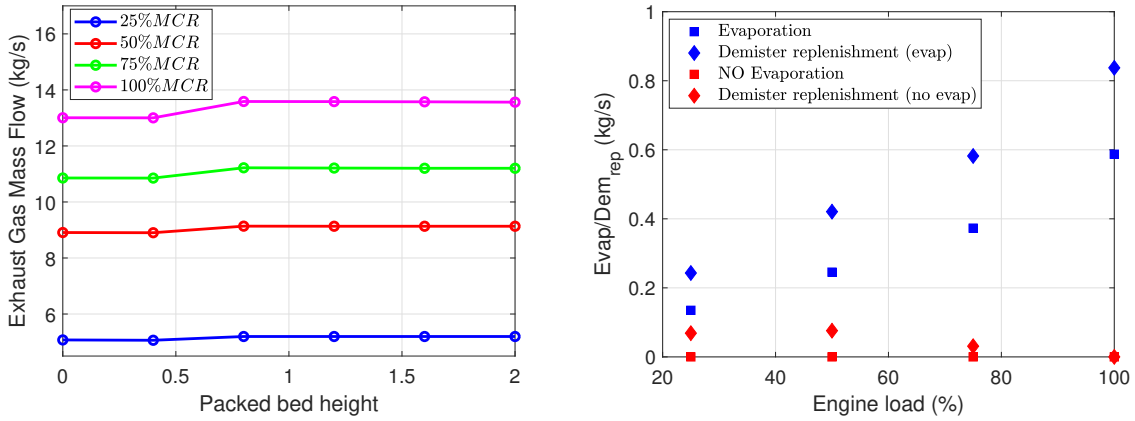

(a) Longitudinal gas mas flow in the packed bed at different engine loads for the evaporation case

(b) Evaporation in the packed bed and demister replenishment at different engine loads

Figure 7.2: Longitudinal gas mass flow rate (a) and evaporation and demister replenishment (b) at the four engine loads

The increase of the engine load implies an increase of the amount of evaporation as seen in Figure 7.2b. The sensitivity analysis in paragraph 6.5.1 and 6.5.2, showed that an individual increase of both mass flow and temperature has a positive effect on the evaporation rate. For the examined engine loads, the mass flow influence on evaporation rate seems to be higher than that of temperature.The evaporation rate is increasing as the engine load and gas mass flow increases. The increase trend of the evaporation rate is not affected by

the fluctuation of gas temperature. Figure 7.2b shows the evaporation and demister replenishment with and without taking evaporation into account for the four engine loads. If evaporation is not part of the analysis, the demister replenishes a small amount of water at low engine load. The temperature of the gasses leaving the scrubber is lower at 25, 50 and 75 $\%MCR$ compared to 100 $\%MCR$ (Figure 7.4). Lower temperature implies higher condensation rate. Therefore, at low engine load there is water condensation.

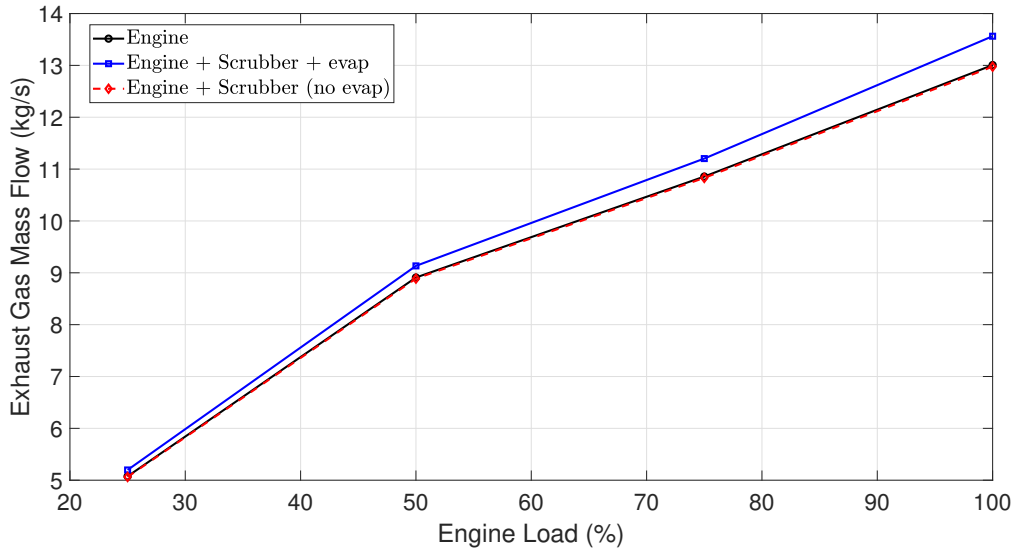

Figure 7.3: Exhaust gas mass flow leaving the packed bed section, for the cases of including and excluding the evaporation effect, at the different engine loads. These cases are compared to the case that no scrubber installed.

Figure 7.3 shows that the mass flow rate of the exhaust gasses leaving the packed bed is slightly lower than that of the flow leaving the engine if the evaporation is not taken into account. This difference is a result of the absorption of the sulphur oxides in the scrubber. If evaporation is taken into account the mass flow increases, because for the chosen engine outlet conditions, the amount of evaporation outweighs the absorbed sulphur oxides.

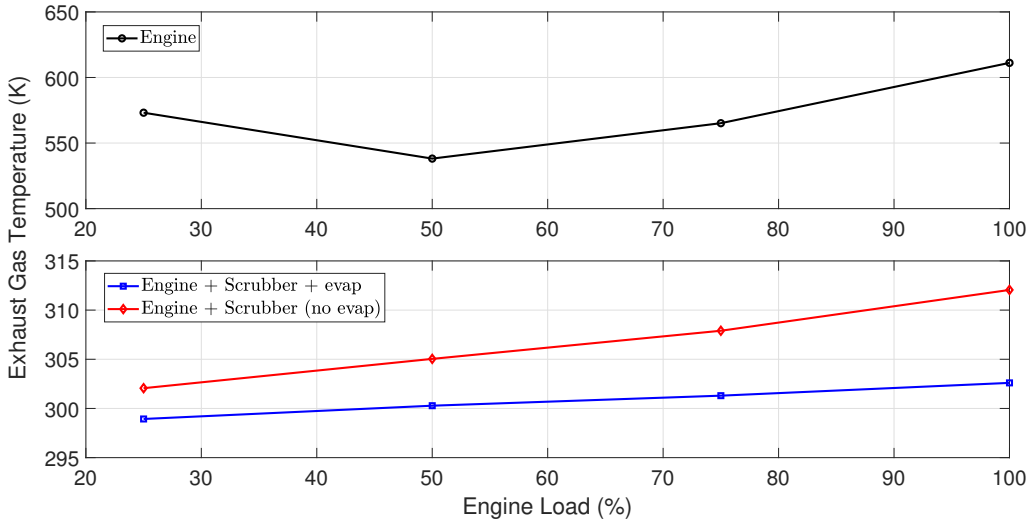

Figure 7.4: Exhaust gas temperature leaving the packed bed section, for the cases of including and excluding the evaporation effect, at the different engine loads. These cases are compared to the case that no scrubber installed.

Gas temperature, when evaporation effect is considered in the analysis, is lower compared to that when evaporation is ignored (Figure 7.4). Exhaust gas entering the packed bed has higher temperature compared to scrubbing liquid. Except form heat transfer that normally occurs between gas and liquid due to temperature difference, the required amount of energy for the evaporation is offered from the gas phase, reducing its temperature even more. Regardless of the temperature of the gas entering in the different engine loads, the high flows and heat capacity of water, stabilises the temperature at the outlet and forces it to follow the same trend of mass flow rate (higher engine load - higher temperature).

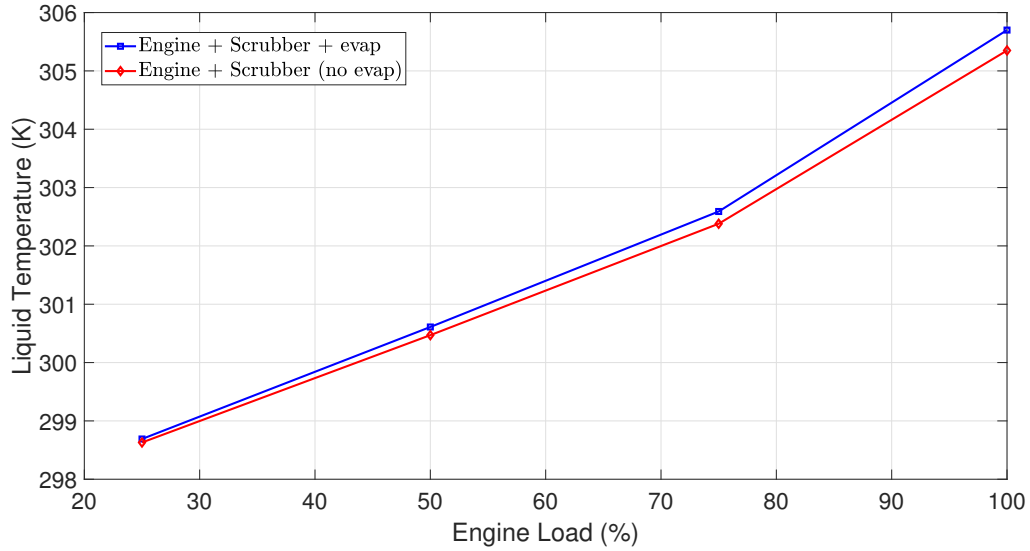

Figure 7.5: Liquid temperature leaving the packed bed section, for the cases of including and excluding the evaporation effect, at the different engine loads.

The high amount of the liquid phase and its high heat capacity (compared to gas phase), results in low temperature diverges at the bottom of the packed bed (outflow) for the different engine loads. In Figure 7.5 In the case that evaporation is included in the analysis the temperature of the liquid increases, in contrast to the gas phase that temperature that reduces due to evaporation effect.

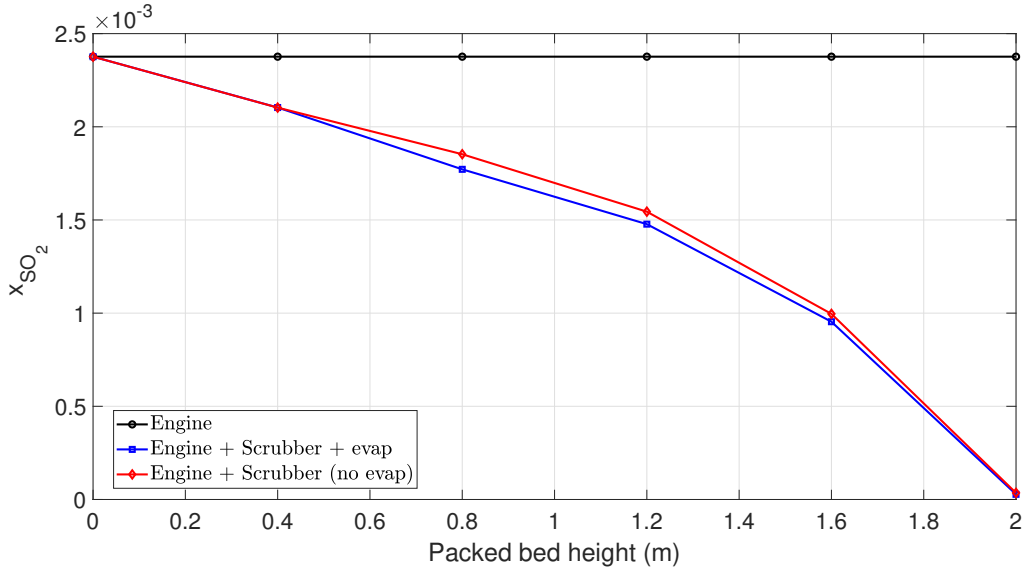

Figure 7.6: Sulphur dioxide mass fraction along the packed bed, for the cases of including and excluding the evaporation effect.

When evaporation effect is considered then, the x_{SO_2} is lower compared to the non evaporation case. The values of mass fraction are relative to each other so as their summation be equal to one. Water evaporation increases the x_{H_2O} in the gas phase and consequently reducing the mass fraction of the other substances. In Figure 7.6 three regions can be distinguished. Starting form the bottom of the packed bed, 0 - 0.4 m, the mass fraction of sulphur dioxide are identical for both cases and the reduction trend is low because most of $NaOH$ was consumed in the top of the packed bed. In the second and third control volume (0.4 - 1.2 m), the x_{SO_2} in the case of evaporation becomes lower, because the evaporation increases the water mass fraction in the gas and thus reduces the sulphur oxide fraction. In the last two control volumes (1.2 - 2 m) there is no evaporation and both lines follow a steeper diminish because the caustic soda is plenty in the top of the packed bed.

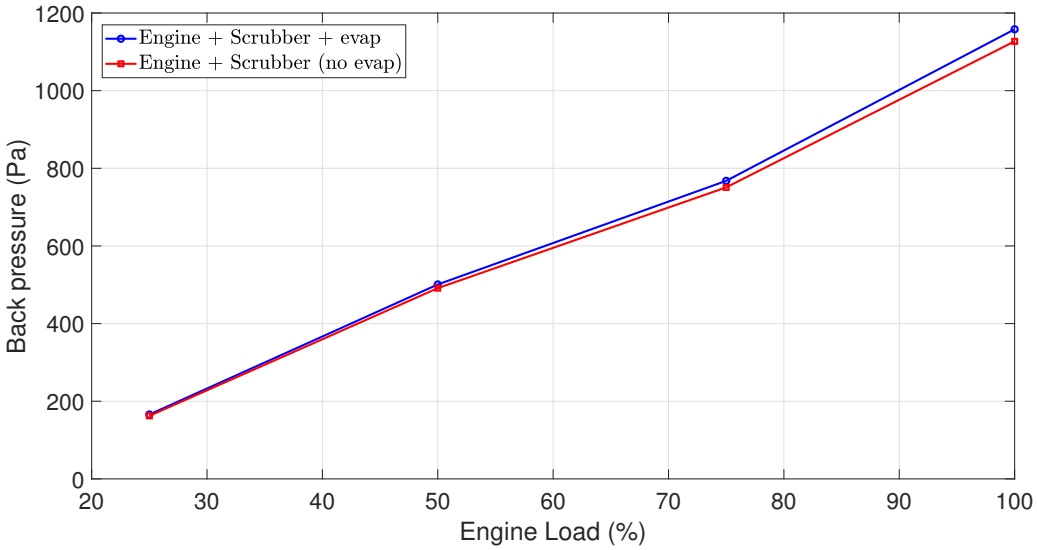

Figure 7.7: Back pressure created by the scrubber system.

The wet scrubber system imposes a back pressure on the diesel engine. The back pressure of the scrubber system as shown in Figure 7.7 is difference between the pressure before entering in venturi and the ambient pressure after the demister. In this model, the scrubber adds a back pressure of 1.158 kPa ("evap"). The data provided by Alfa Laval state that at 100% MCR the maximum pressure drop is 0.98 kPa. Although, their value is for lower mass flow, a different design, packing material and probably some other parameters. In the case of evaporation, mass flow is increases and thus the velocity is also higher. This explains the higher values of back pressure, as it is dependent on the velocity of the gasses. A higher back pressure results in a higher fuel consumption due to a slightly reduced engine efficiency [128].

7.3. DYNAMIC ANALYSIS

The operation conditions of vessels are not constant. On contrary, in heavy sea conditions (normally in deep sea sailing) or in manoeuvring in the ports, the engine power has fluctuations. These fluctuations provide also variations in the amount of sulphur oxides emitted. In a wet scrubber system, pumps are the components that consume a significant amount of energy. When the engine operates at low engine load, it would be more efficient to also reduce the power consumption of scrubber's pumps by reducing the water supplied in the scrubber tower. In the following sections, the design of the control system implemented in this thesis and 3 common sets of engine load variations will be examined to study the response of the scrubber system under transient conditions.

The input signal of the diesel engine is a cosine wave signal. The dynamic conditions to be investigated are them for dynamic load between 25% – 100%MCR, 50% – 100%MCR and 75% – 100%MCR. The influence of the evaporation and the influence of the input wave frequency will be examined.

7.3.1. DYNAMIC LOAD: 100% - 25% - 100%

The influence of evaporation will be examined, in the dynamic load in the range between 25% – 100%MCR. The exhaust gas properties as shown in Figure 7.8 are valid for both the case, with and without evaporation. In this analysis, the wave period is equal to 50 seconds.

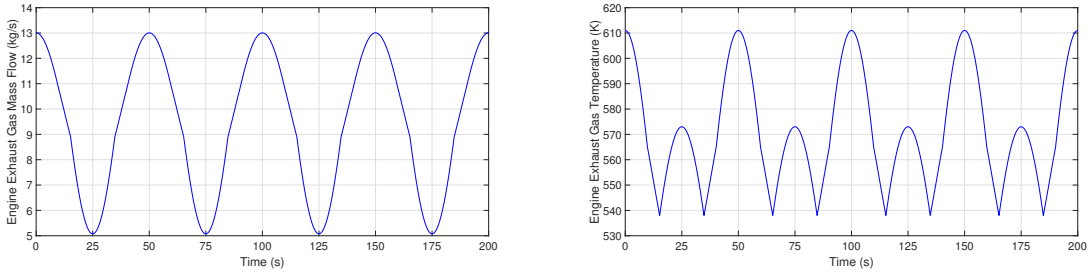

(a) Exhaust gas mass flow leaving the engine

(b) Exhaust gas temperature leaving the engine

Figure 7.8: Exhaust gas mass flow (a) and temperature (b) leaving the engine at the load condition 100% – 25% – 100%

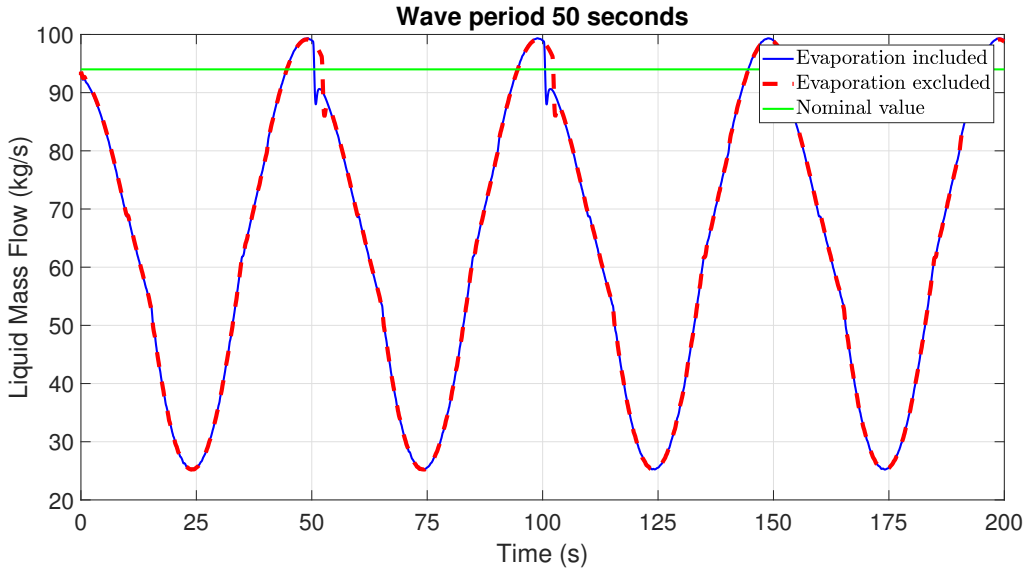

Figure 7.9: Liquid supply in the scrubber with and without evaporation influence.

To comply with the SECA limit and also to save energy from the operation of the pumps, the liquid supply needs to be adjusted at each engine load. In Figure 7.9, the transition from 25% MCR to 100% MCR the liquid supply exceeds the nominal value of 94$\frac{kg}{s}$ by 5.6% (or by 5.3 $\frac{kg}{s}$). The controller could not deal sufficiently with the sharp increase of the gas flow because the pump has time constant of 2 seconds and also there is I action of PI controller. The signal is measured at the output of the scrubber and then the pump flow is adjusted by a feedback control system. When the flow reaches the peak and then starts to reduces, the liquid supply is temporary higher than it should be due to the integration action of the PI controller and the time constant of the scrubber's balance of plant. Evaporation reduces the relative mass fraction of sulphur oxides and thus in the case of evaporation the reduction of the liquid supply is steeper than in the case that there is no evaporation in the scrubber. The problem of the higher liquid supply could be solved with the simultaneous operation of feedback and feed forward control approach. This control system will process the signal not only of the output of the scrubber, but also at the output of the diesel engine. Therefore, there will be two signals, one to measure the actual value of the sulphur oxides in the gas leaving the scrubber and one to make a prediction about the future values of the sulphur oxides that will enter the scrubber system.

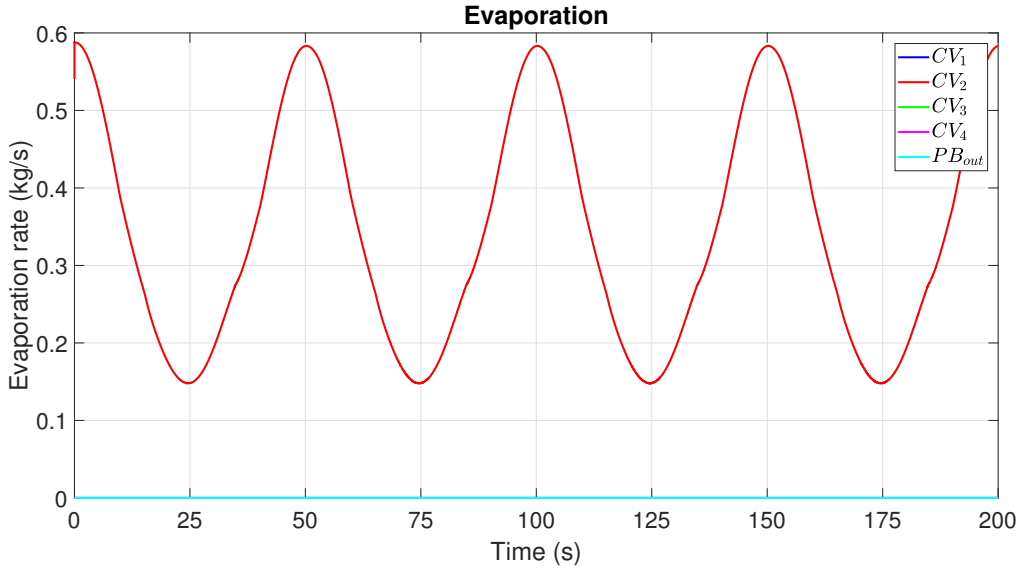

Figure 7.10: Rate of evaporation in the packed bed section.

The peaks and valleys of the evaporation rate in Figure 7.10 are in agreement with the values obtained from the respective engine loads in the static simulations. The output signal not a perfect sine due to the temperature at 50% MCR.

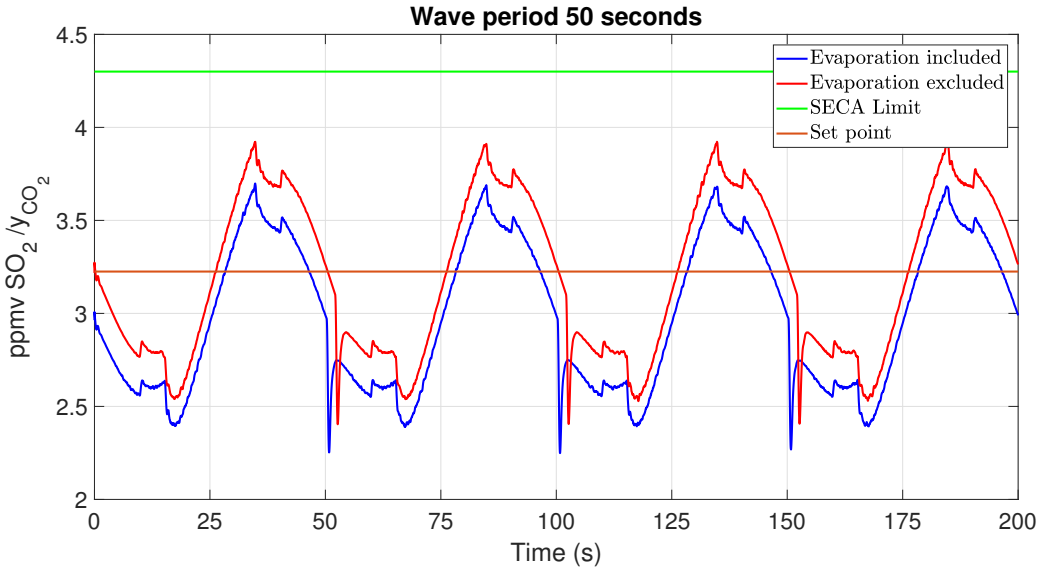

Figure 7.11: Fraction of $\frac{ppmvSO_2}{y_{CO_2}}$ at engine load fluctuations including and excluding the evaporation influence.

In both cases in Figure 7.11, the scrubber keeps the output of the sulphur oxides below the SECA limit by consuming more liquid, as Figure 7.9 shows. The steeper drop after the peak that liquid supply profile shows in the case of evaporation can be seen also in Figure 7.11. The profile of the evaporation case is enclosed in the profile of the non evaporation. Meaning that reaction of the pump is more rapid for the case of evaporation. Figure E.1 shows the amount of sulphur oxides is lower and more stable for the case of evaporation. This results are similar to the findings of the static simulations about the influence of evaporation on the removal efficiency.

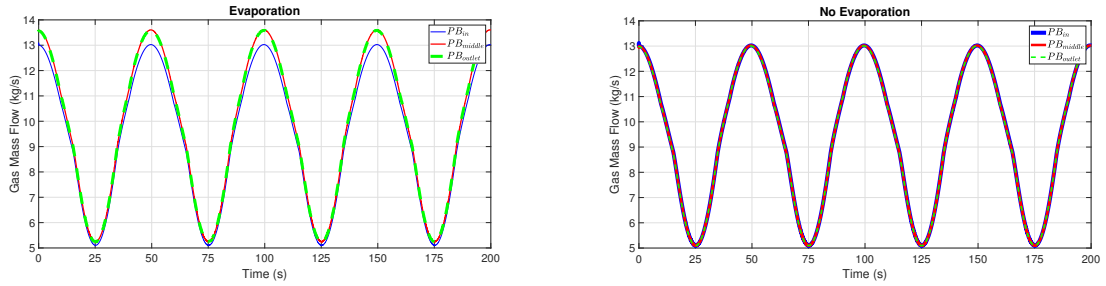

(a) Gas mass flow in the packed bed section in evaporative conditions

(b) Gas mass flow in the packed bed section in non evaporative conditions

Figure 7.12: Gas mass flow rate at engine load fluctuations in the packed bed section, including (a) and excluding (b) the effect of evaporation.

In Figure 7.12, the profile of the gas mas flow is in accordance with that of the engine load. In the case of evaporation there is an increase in the middle and the outlet of the of the scrubber that corresponds to the evaporation amount of water minus the SO_X removed.

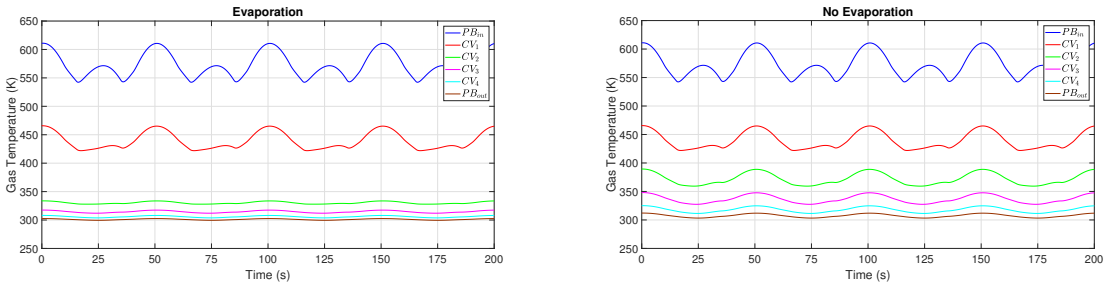

(a) Exhaust gas temperature in the packed bed section in evaporative conditions

(b) Exhaust gas temperature in the packed bed section in non evaporative conditions

Figure 7.13: Exhaust gas temperature at engine load fluctuations in the packed bed section, including (a) and excluding (b) the effect of evaporation.

Figure 7.13 shows the temperature profile along the scrubber for the different control volumes. After the second control volume, the temperature, in the case of evaporation, is lower and more stable compared to the non evaporative case.

The profile of water mass fraction in Figure 7.14, is mainly for the evaporation case. When evaporation is not taken into account, the water mass fraction leaving the control volumes of the packed bed is almost the same with the one entering. Therefore is not presented here. Only the profile leaving the demister for the non evaporative case is given (brown line). In the evaporative case the water concentration in the gas phase leaving the scrubber tower will be lower, because gas temperature is lower and therefore more water will condensate. The water leaving the demister section must have a relative humidity of 100%. The Mollier diagram shows that at a lower temperature, the water mass fraction is lower for the same relative humidity, thus more water will condensate at a lower temperature. The deviation of x_{H_2O} form the cosine profile under the evaporation influence is due to the input temperature profile.

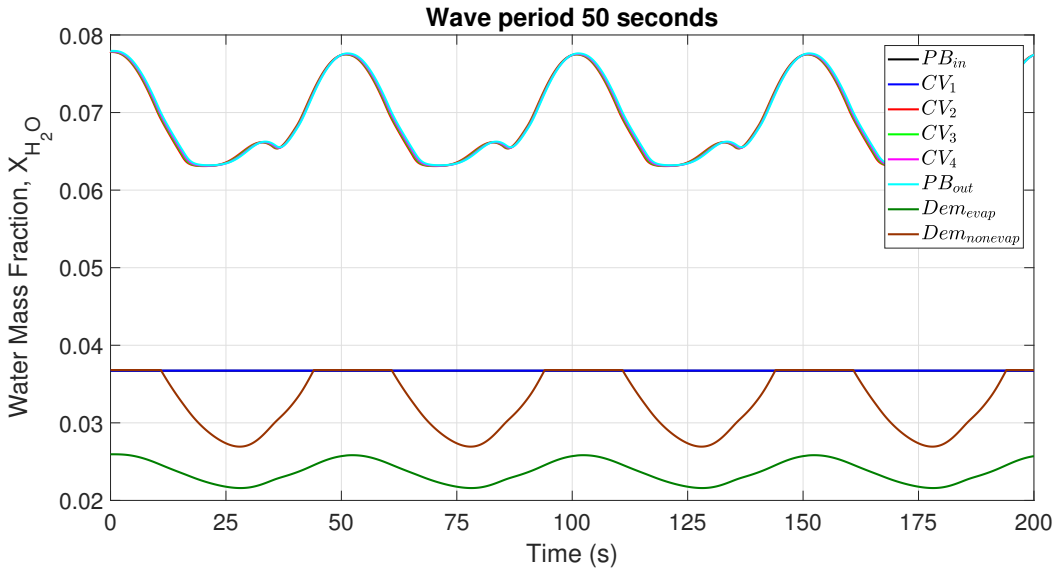

Figure 7.14: Water mass fraction along the control volumes of the packed bed section for the case of evaporation. For the non evaporation case only the water mass fraction leaving the demister is provided.

7.3.2. DYNAMIC LOAD: 100% - 50% - 100%

For the dynamic load between 50% – 100% the influence of wave period will be investigated. The examined periods are 25 and 50 seconds. Evaporation influence is taken into account for both cases. The input signal for gas mass flow and temperature is shown in Figure 7.15. Between the 25 and 50 seconds period no difference exists in the values of peak and valleys of the wave signal.

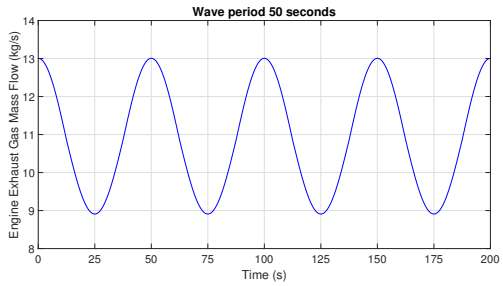

(a) Exhaust gas mass flow leaving the engine

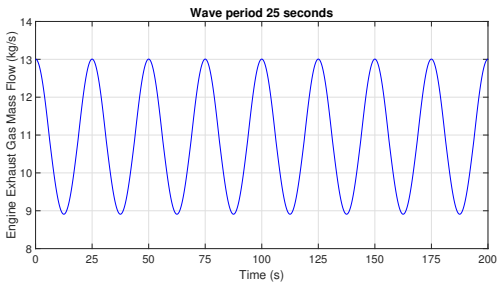

(b) Exhaust gas mass flow leaving the engine

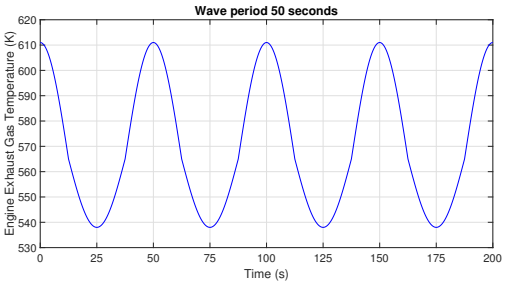

(c) Exhaust gas temperature leaving the engine

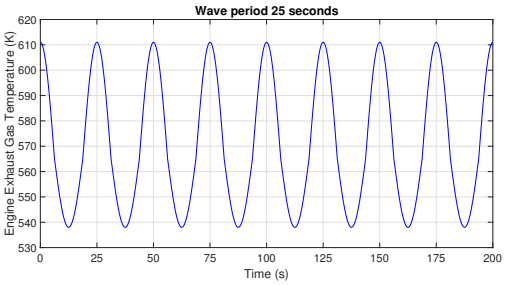

(d) Exhaust gas temperature leaving the engine

Figure 7.15: Exhaust gas mass flow and temperature leaving the engine for the wave period of 50 (left) and 25 (right) seconds

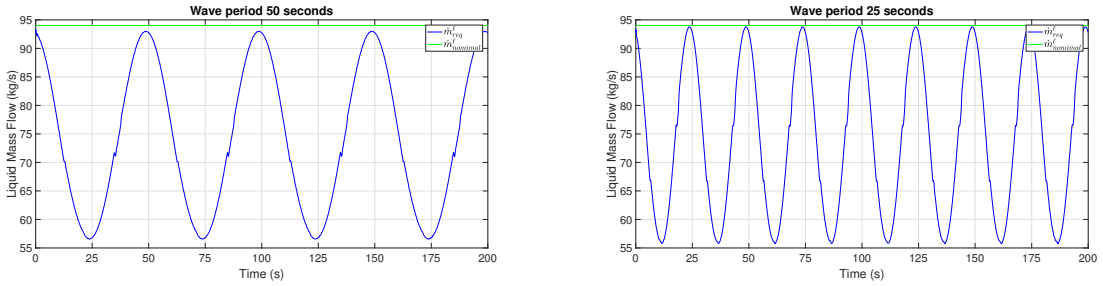

(a) Liquid flow rate for the wave period of 50 seconds

(b) Liquid flow rate for the wave period of 25 seconds

Figure 7.16: Liquid supply in the scrubber for the wave period of 50 (left) and 25 (right) seconds.

In both cases in Figure 7.16, to comply with the strict limit of SECA limit, the required liquid flow is below the nominal value. This is better response compared to the case between $25-100\%MCR$ where the values of the liquid supply where exceeding the nominal value.In Figure 7.16a and Figure 7.16b, there is an instability around $70\frac{kg}{s}$ because the input signal is a look up table. The delay of the control system explained in the previous case is also observed here. When the frequency is increased and thus the increase from 50 to 100% is more rapid, the maximum value of the liquid supply in 25 seconds period is higher ($93.8\frac{kg}{s}$) than that of the 50 seconds ($92.9\frac{kg}{s}$).

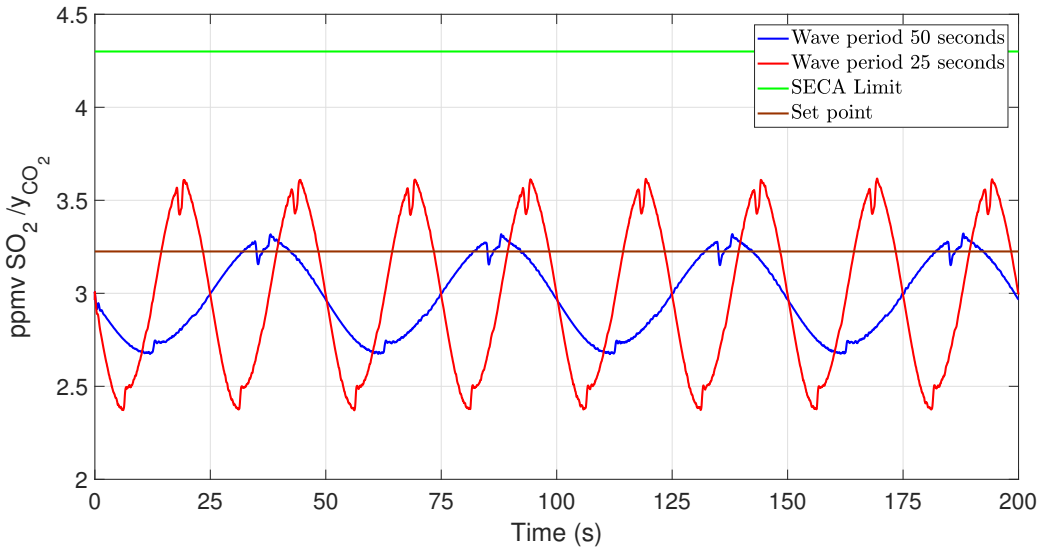

Figure 7.17: Fraction of $\frac{ppmvSO_2}{y_{CO_2}}$ leaving the scrubber at engine load fluctuations and wave periods of 50 and 25 seconds.

Figure 7.17 shows that compliance with SECA limit is achieved for both frequencies. When the wave period is 50 seconds and the wave amplitude is the same, the pump has more time to react to the fluctuations of the engine load. The controller has a better response to changes providing a more accurate amount of water. Therefore the values of output signal are slightly lower in the period of 50 seconds, but the difference is in the same order of magnitude. In both cases, the small fluctuation at the peaks are because of the variations in the water supply. These are not observable in Figure 7.17 as they are very small. Furthermore, in both frequencies, between 50-100%, the profile of the sulphur dioxide to carbon dioxide ratio leaving the scrubber approaches that of the wave signal and is more stable than the one obtained in for the load fluctuation from 25 to 100% MCR.

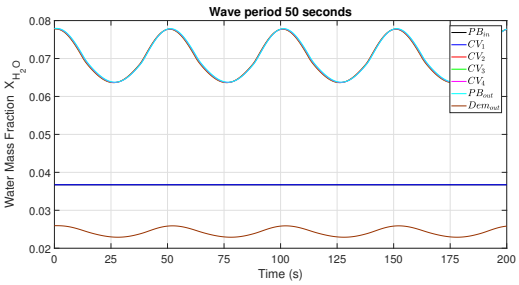

(a) Water mass fraction in the packed bed and the demister for the wave period of 50 second.

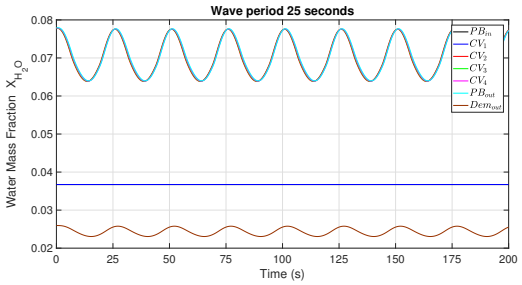

(b) Water mass fraction in the packed bed and the demister for the wave period of 25 second.

Figure 7.18: Water mass fraction along the control volumes of the packed bed for the case of evaporation and no evaporation

Comparing the profile of the water mass fraction between the two different periods no discrepancy is observed (Figure 7.18). But, when compared to 25 – 100% engine load case, then there are significant differences in the profile. In this case (50 – 100%), the temperature profile is monotonically increasing. The deviations of the upward trend shown in Figure 7.14 are not observable in Figure 7.18a and Figure 7.18b. Therefore the small fluctuation observed in the previous case does not occur here. As the temperatures in the output are close to each other for both cases, demister replenishment does not show any significant deviation.

In Appendix E.2, the profile of the gas mass flow, gas temperature, evaporation rate and sulphur dioxide to carbon dioxide ratio can be found. No significant differences were observed between the 2 wave frequencies.

7.3.3. DYNAMIC LOAD: 100% - 75% - 100%

For the dynamic load between 75% – 100% the influence of the wave period will be investigated. The examined periods are 10 and 50 seconds. Evaporation influence is taken into account for both cases. The input signal for gas mass flow and temperature is shown in Figure 7.19. Between the 10 and 50 seconds period no difference exists in the values of peak and valleys of the wave signal.

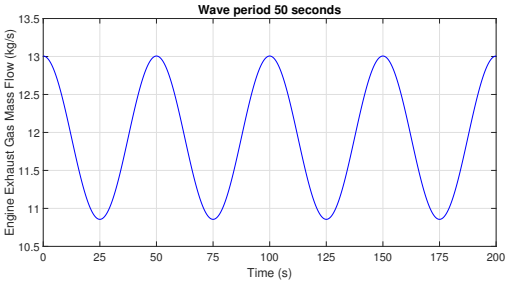

(a) Exhaust gas mass flow leaving engine section for the wave period of 50 seconds

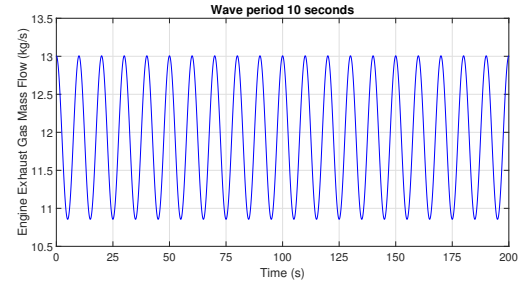

(b) Exhaust gas mass flow leaving engine section for the wave period of 10 seconds

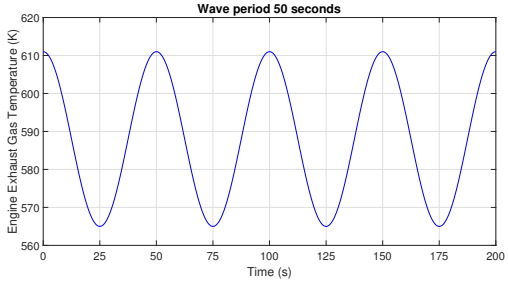

(c) Exhaust gas temperature leaving engine section for the wave period of 50 seconds

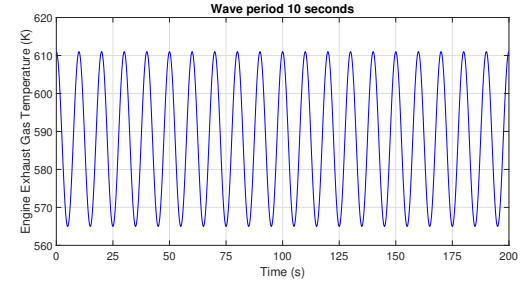

(d) Exhaust gas temperature leaving engine section for the wave period of 10 seconds

Figure 7.19: Exhaust gas mass flow and temperature leaving engine section for the wave period of 50 (left) and 10 (right) seconds

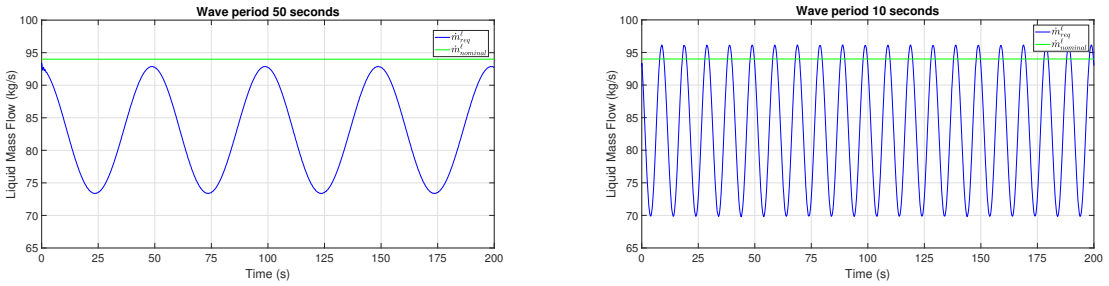

(a) Liquid flow rate for the wave period of 50 second

(b) Liquid flow rate for the wave period of 10 second

Figure 7.20: Liquid supply in the scrubber for the wave period of 50 and 10 seconds.

In contrast with the engine flow rate and temperature, the liquid supply seems to be affected by the change of frequency as shown in Figure 7.20. The control system and thus the pump, cannot respond with the same pace in the changes of the gas flow. The value of $\frac{ppmvSO_2}{y_{CO_2}}$ is changing rapidly for the case of 10 seconds period and there is no sufficient reaction time from the system. The I control creates overshoots in the pump operation and the peak exceeds the nominal value.

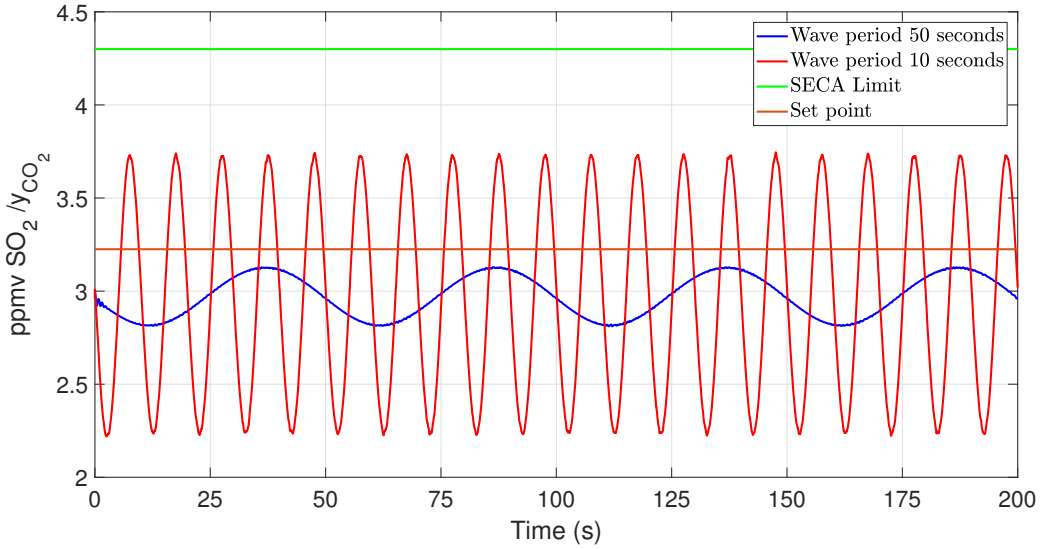

Figure 7.21: Fraction of $\frac{ppmvSO_2}{y_{CO_2}}$ leaving the scrubber at engine load fluctuations and wave periods of 50 and 10 seconds

The results obtained for the 10 second period are slightly higher than those of the 50 seconds, but still the output in both cases is below the required SECA limit (Figure 7.21). The value of the $\frac{ppmvSO_2}{y_{CO_2}}$ leaving the scrubber for the case of 50 and 10 seconds at their peaks, is 3.13 and 3.74 respectively but a small difference to be taken into account. The small deviations are the outcome of the inability of the control system to deal sufficiently with the rapid changes of the engine load. For the case of the 10 seconds, in order to remain below the SECA limit, the pump has to provide liquid flows higher than the nominal value.

In Appendix E.3, the profile of the gas mass flow, gas temperature, evaporation rate, sulphur dioxide to carbon dioxide ratio and water mass fraction along the packed bed and in the demister can be found. No significant differences were observed between the 2 wave frequencies.

8

CONCLUSIONS & RECOMMENDATIONS

"Wisdom begins in wonder."

Socrates

8.1. CONCLUSIONS

The objective of this thesis was to cover the knowledge gap of both evaporation and dynamic loads, on the operation of closed loop wet scrubber for maritime application. A dynamic model of a closed loop wet scrubber operating on fresh water and caustic soda was developed and verified. The packing material used the Hiflow ring-50. The value of the liquid supply from the sensitivity analysis is 94 kilogram per second and gives and sulphur dioxide to carbon dioxide ratio equal to 1.9. To clean exhaust gasses coming from fuel with 3.5%S to the equivalent 0.1%S, indicative values provided by scrubber manufactures, for the liquid requirements in an closed loop system are around 45 cubic meter per mega watt hour. For diesel engine of 7.5 mega watt and a scrubbing liquid with the same density as the fresh water, this is translated to 93.75 kilogram per second.

The inclusion of evaporation in the scrubber model leads to an increase of the scrubber efficiency. IMO does not provide and absolute value for the amount of sulphur oxides leaving the scrubber. But, gives a relation between the ppmv of sulphur oxides leaving the scrubber over the mole fraction of carbon dioxide leaving the engine. The increased vapour mass fraction in the gas phase reduced the sulphur dioxide mass fraction and consequently also the sulphur dioxide to carbon dioxide ratio.

A smaller difference in the engine load fluctuation results in a more stable scrubber response. A high engine load fluctuation results in overshoots on maximum amount of the required scrubbing liquid. An increase of the input frequency, for the same engine load fluctuation, results in a more unstable scrubber response and overshoots of the liquid supply, in order to keep the scrubber operate below the SECA limit and close to the setpoint. The sulphur dioxide to carbon dioxide ratio follows the same trend as the liquid supply. To have a safety margin, the setpoint was defined to be 75% of the SECA limit. The profile of the sulphur dioxide to carbon dioxide ratio is most of the times below the setpoint and not evenly distributed above and below the setpoint. This behaviour is because the values of numerator and denominator in the sulphur dioxide to carbon dioxide ratio are calculated at the outlet and inlet of the scrubber respectively. The applied control system relied on feedback PI control and the scrubber balance of plant was approached as a time constant.

The increase of evaporation rate in the packed bed is mainly influenced by the exhaust gas mass flow. The influence of the exhaust gas temperature is smaller than the influence of the mass flow because of the heat transfer phenomena tends to balance the gas temperature. The fuel sulphur content influence is insignificant.

The temperature of the exhaust gasses at the entrance of the packed bed does not have a significant impact on the sulphur dioxide absorption. Heat transfer significantly reduces gas temperature leaving the first control volume. Therefore, after the first control volume, temperature variations are close to each other. Although when evaporation is part of the analysis, temperature slightly affects the sulphur mass fraction leaving the packed bed, because temperature influences evaporation rate.

The exhaust gas leaving the packed bed is super saturated as condensation is not included in the packed bed model. Also, gas temperature leaving the packed bed is significantly lower than temperature entering, resulting in high humidity in the gas phase. Water condensation is proportional to temperature decrease. Water vapour in the gas phase will be condensed in the demister and will drop back in the packed bed. Demister replenishment is enough to compensate water evaporation in the packed bed, because there was also extra vapour in the gas phase that is the product of combustion in diesel engine. The reduction of temperature results in a small amount of condensation in the case that evaporation is not taken into account. The balance between evaporation and condensation were only tested for one condition of ambient temperature, humidity and seawater temperature. Changing any of these parameters may result in a different conclusion.

The wet scrubber is the most financially viable option to comply with the sulphur limits, while MGO is the most expensive option, but both can comply with the sulphur limit in SECA's. The cheapest option seems to be the open loop scrubber as it requires no additives, but prohibition of scrubber discharges in ports worldwide and the low alkalinity of some areas is a disadvantage for their usage. VLSFO is the second cheapest option, but it cannot be used in SECA's and so far it seems to emit more black carbon than HFO because it contain a large percentage of aromatic compounds. Closed loop scrubber are slightly more expensive than open loop and VLSFO, but allow to operate the vessel in SECA's, in all ports and in areas with low seawater alkalinity.

The wet scrubbers (open loop, closed loop and hybrid) are the most efficient systems for SO_X removal. They can deal sufficiently even with the stringent SECA limit and provide the advantage of using HFO. Dry scrubbers have lower operational cost than the wet scrubbers, but have high space requirements. There are other systems for SO_X removal in the market, but these still need approval from IMO.

8.2. RECOMMENDATIONS

During the thesis, a set of assumptions has been made in order to simplify the model that allowed to carry out the analysis. Therefore, further research is essential to improve the model accuracy.

The sensitivity analysis showed that a higher discretisation of the packed bed is required. This can be done by the same approach as used in this thesis, but it requires higher computational power. Another option is to use second order S-function for the discretisation.

The effect of integrating a wet scrubber, possibly combined with a selective catalytic reduction system, on the fuel consumption of a diesel engine should be investigated further. These devices, increase fuel consumption because of back pressure and the used satellite equipment (pumps). This will make it possible to compare this system to others capable of complying with the nitrogen oxide and sulphur oxide emission limits in emission control areas. Other solutions include among others the application of natural gas fuelled dual fuel engines.

The application of using seawater possibly in combination with caustic soda should be investigated for both open and closed loop systems. The water used in this model is fresh water which would have to be carried in the vessel or has to be made on board. Seawater is plenty around a ship and has higher alkalinity than pure water, meaning that amount of the caustic soda used will be reduced or even be zero in some cases. The exception is in areas with low seawater alkalinity.

An analytical model for condensation in the packed bed and in demister will provide a better indication of the water replenishment. In this model, the demister is approached as a lumped part of finite dimensions that operates in optimum conditions, using empirical formulas and values from literature. The balance between evaporation and condensation should be investigated further for other ambient temperatures, humidities and seawater temperatures as this may result in a different conclusion about the balance.

The application of a more advanced control system possibly with a combination of feed forward and feedback control may result in a more stable operation of the scrubber system and prevent the sulphur dioxide to carbon dioxide ratio from exceeding the allowed limit. The feedback will measure the value of the sulphur dioxide to carbon dioxide ratio leaving the scrubber system and will give the on time values to the control system. The feed forward will measure the gas flow entering the scrubber and will provide an indication (prediction) of what will be the future value of sulphur dioxide to carbon dioxide ratio. Then the pump flow will be adjusted to provide a more precise amount of water at each time step.

A model that will calculate the liquid properties as a mixture of water, $NaOH$, sulphite and SO_2 from the incomplete reaction, needs to be investigated. In this model, it is assumed that the only compounds absorbed is SO_2 and only water evaporates. It is possible that also other compounds are absorbed and/or that an amount of $NaOH$ is transferred to the gas flow.

A three phase flow analysis for the venturi is required, which will predict the size of the water droplets, temperature reduction due to heat transfer, SO_2 and particulate matter removal. The venturi is approached as a simple section, where only gas passes through it and there is no interaction with water. In the venturi the high speed of exhaust gasses leads to water atomisation and in unpredictable droplet sizes. Due to water atomisation, the exhaust gasses are cooled and a small part of SO_2 is removed. This is mainly the SO_2 attached to the particulate matter.

A model that uses a structure packing material can be investigated. Structured packing is not a common option for maritime scrubber due to its high cost. Researches from chemical engineering applications, indicate that is more efficient than the dumped packing. Structured packing require less space compared to dumped and if it is more efficient in maritime applications it may be an alternative to consider.

A model capable of approaching the mass transfer between the two (mixed) phases in turbulent conditions may produce more accurate results. In the model, the mass transfer is approached using the two film model. The turbulent conditions are approached as laminar flow, where the width of laminar film is extended. Although, due to turbulence, the liquid film collapses and droplets of different shape and size are formed. The gas and liquid phase are mixed and it is difficult to approach mass transfer in these conditions with analytical relations.

Finite elements analysis of the flow can improve the prediction of the output conditions from the control volume. One of the main assumptions in the model is that of perfect mixing, meaning that the properties of the fluids leaving the control volume are the same as the properties in the control volume. This uniformity of the phases is valid considering the turbulence in the scrubber, but this is not always the case. In areas close to the packed bed walls, mixing is not as intense as in the middle of the control volume, because flow is restricted by the friction that material is imposing on the fluids.

The effect of sulphur trioxide (SO_3) and nitrogen oxides (NO_X) on the scrubber efficiency should be investigated further. Exhaust composition is neglecting the SO_3 and NO_X, because they are in small amounts. Including them in the analysis will increase the precision of the efficiency of the scrubber and is important for future integration of the scrubber model, with a diesel engine and selective catalytic reduction model.

A

FINANCIAL ESTIMATION

The predictions for the differences in prices between MGO and HFO in the next years according to S.E.B are given in the Figure A.1a. Based on this prediction between 2020-2022 there will be still a surplus of HFO 3.5% keeping its price low and the difference with MGO high. After this period predictions conclude to stable conditions as HFO will be gradually substituted by MGO and MGO availability in the market will increase.

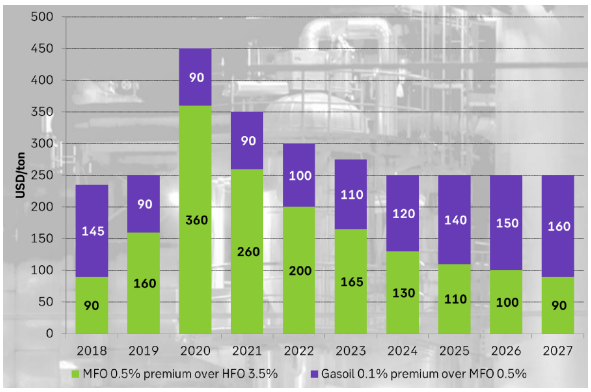

(a) SEB fuel price estimation [99]

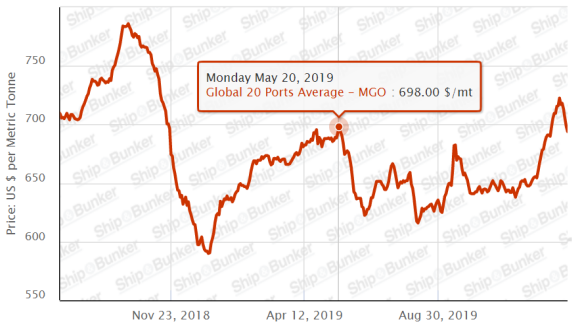

(b) MGO price [100]

Figure A.1: on the left the SEB projection for yearly average product price spreads. Gasoil 0.1% to MFO 0.5% and MFO 0.5% to HFO 3.5% in USD/ton. On the right the MGO average price of global 20 ports.

For the calculation of paragraph 3.6 the reference was MGO price on 20 May 2019 in Global average of 20 ports (Figure A.1b) [100] . On that day in the exchange market 1$ was equal to 0.894266411€. Table A.1 provides price difference of MGO and IFO-380, as long as the relative price of IFO-380 per year.

The value of NaOH on 7 May 2019, was 300 $\frac{\$}{ton}$. This values is assumed to be constant during the 10-year analysis. The density of NaOH 50% solution is $\rho = 1.5\frac{g}{cm^3}$=1500$\frac{g}{\ell}$. So, the price of NaOH per litter is 0.4$\frac{€}{\ell}$.

A

Table A.1: Ten year prediction of the prices of MGO and IFO according to SEB

Year	MGO-IFO	MGO-VLSFO	Unit	MGO-IFO	MGO-VLSFO	MGO	VLSFO	IFO	Unit
2019	250	90	$/ton	223.57	80.48	549.08	543.7	325.51	€/ton
2020	450	90	$/ton	402.42	80.48	549.08	543.7	146.66	€/ton
2021	350	90	$/ton	312.99	80.48	549.08	543.7	236.09	€/ton
2022	300	100	$/ton	268.28	89.43	549.08	534.8	280.80	€/ton
2023	275	110	$/ton	245.92	98.37	549.08	525.8	303.16	€/ton
2024	250	120	$/ton	223.57	107.31	549.08	516.9	325.51	€/ton
2025	250	140	$/ton	223.57	125.20	549.08	499	325.51	€/ton
2026	250	150	$/ton	223.57	134.14	549.08	490.1	325.51	€/ton
2027	250	160	$/ton	223.57	143.08	549.08	481.1	325.51	€/ton
2028	250	160	$/ton	223.57	143.08	549.08	481.1	325.51	€/ton

The net present value method helps to transform the future value, to an equal value of today considering the interest rate or depreciation. It can be calculated by applying the formulaA.1. The data used for the calculation are given in TableA.2

$$NPV = \sum_{i=0}^{n} \frac{FCF}{(1+r)^i} \tag{A.1}$$

where,

- i is the referred time period-year (i=0...n)
- n is the total length of the time period. In the examined case is 10 years
- r is the interest or depreciation rate. In the examined case is 5%, according to European Commission.
- FCF is the free cash flow per year

Table A.2: NPV values for the 3 different cases

Year	NPV open/year	NPV closed/year	NPV VLSFO/year	NPV MGO
2018	3000000	3000000	0	0
2019	1663574	1984194	2154143	2473013
2020	877054	1186462	2051565	2355250
2021	1172100	1464843	1953871	2243096
2022	1276672	1554555	1830224	2136281
2023	1292252	1556465	1713922	2034554
2024	1303454	1554668	1604546	1937670
2025	1241385	1480636	1475263	1845400
2026	1182271	1410130	1379833	1757524
2027	1125972	1342981	1290146	1673832
2028	1072355	1279029	1228710	1594126
NVP	15207089	17813962	16682223	20050747

B

THERMODYNAMIC PROPERTIES

B.1. THERMODYNAMIC PROPERTIES OF THE GAS PHASE

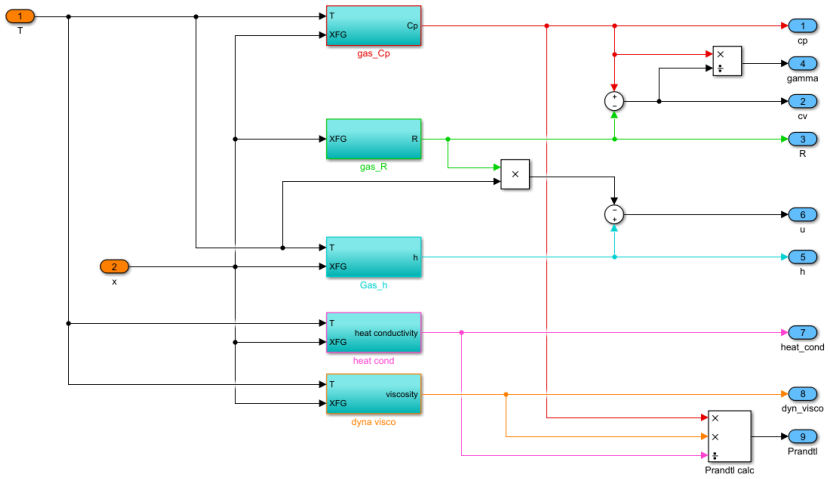

Figure B.1: Inside the Simulink block of the calculation of the gas properties

The gas properties are continuously calculated as the temperature, the pressure and the compositions of the gas is constantly changing. The characteristics of the exhaust gasses are close to that of the ideal gas and as such it will be approached. So, the exhaust gasses will follow the ideal gas law:

$$p \cdot V = n \cdot R_u \cdot T \tag{B.1}$$

Where $R_u = 8.314 \left[\frac{J}{mol \cdot K}\right]$ is the international gas constant [13]. The gas constant R on a mass basis is calculated as:

$$R_j = \frac{1000 \cdot R_u}{M_j} \tag{B.2}$$

The gas constant of the gas mixture is

$$R^g = \sum_{j=1}^{nc} x_j \cdot R_j \tag{B.3}$$

M^g is the molar mass of the gas mixture given by mole fraction:

$$M^g = \sum_{j=1}^{nc} y_j \cdot M_j \tag{B.4}$$

while the mass fraction is given by:

$$x_j = \frac{M_j}{M^g} \tag{B.5}$$

j refers to each one of the component of the gas, $j = 1...nc$ and nc stands for the number of the components that in this report are six.

Table B.1: Molar masses of the gasses used in the west scrubber model [12]

	Substance					
	N_2	O_2	Ar	CO_2	H_2O	SO_2
Molar mass [kg/kmol]	28.0134	31.999	39.948	44.0097	18.0152	64.064

The specific heat at constant pressure, c_p, and the specific heat at constant volume, c_v, depend only on temperature because the specific internal energy and thus the specific enthalpy is a function of temperature alone [13]. For an ideal gas the c_p is:

$$c_p(T) = \frac{dh}{dT} \tag{B.6}$$

The ideal gas specific heat c_p, of every component j, can be obtained by an empirical expression in polynomial form as a function of temperature. These polynomial forms are common in the engineering literature. Moran and Shapiro [13] propose the following form for pure substance:

$$\frac{c_{p_j}(T)}{R} = A + B \cdot T + C \cdot T^2 + D \cdot T^3 + E \cdot T^4 \tag{B.7}$$

For the gasses used in this thesis the values of A, B, C, D and E (see values in Table B.2) are valid for a temperature range between 300 to 1000 Kelvin. The temperature of the gasses of this model will not exceed these values, making them appropriate for usage.

The c_p of the gas mixture is:

$$c_p^g = \sum_{j=1}^{nc} x_j \cdot c_{p_j} \tag{B.8}$$

The enthalpy difference between two states (two different temperatures) can be calculated by separating the variables and integrating equation B.6.

$$\Delta h = h(T_2) - h(T_1) = \int_{T_1}^{T_2} c_p(T)\,dT \tag{B.9}$$

The polynomial form of c_p can be integrated in the equation B.9.

$$h(T_2) - h(T_1) = \left(A \cdot (T_2 - T_1) + \frac{B}{2} \cdot (T_2^2 - T_1^2) + \frac{C}{3} \cdot (T_2^3 - T_1^3) + \frac{D}{4} \cdot (T_2^4 - T_1^4) + \frac{E}{5} \cdot (T_2^5 - T_1^5) \right) \cdot R \tag{B.10}$$

In this form of the enthalpy calculation is valid for pure substances/stable elements and when there is no chemical reaction. However, in reacting systems, reactants disappear and products are formed. An enthalpy datum for the study of reacting systems can be established by assigning arbitrarily a value of zero to the enthalpy of the stable elements at a state called the standard reference state and defined by T_{ref} = 298.15 K and p_{ref} = 100000 Pa (1 atm) [13]. Only the enthalpy of the stable elements (like N_2,O_2 and H_2) is assigned a value zero at standard state (Table B.2).

The enthalpy of the compounds (CO_2, H_2O and SO_2) at a standard state is equal to the enthalpy of formation (h_{fg}). At a state other than the standard state the specific enthalpy is found by the specific adding enthalpy

change between the standard state and the state of interest to the enthalpy of formation [13].

$$h(T) = \Delta h + h_{fg} = \left[h(T) - h(T_{ref})\right] + h_{fg}(T_{ref}) \tag{B.11}$$

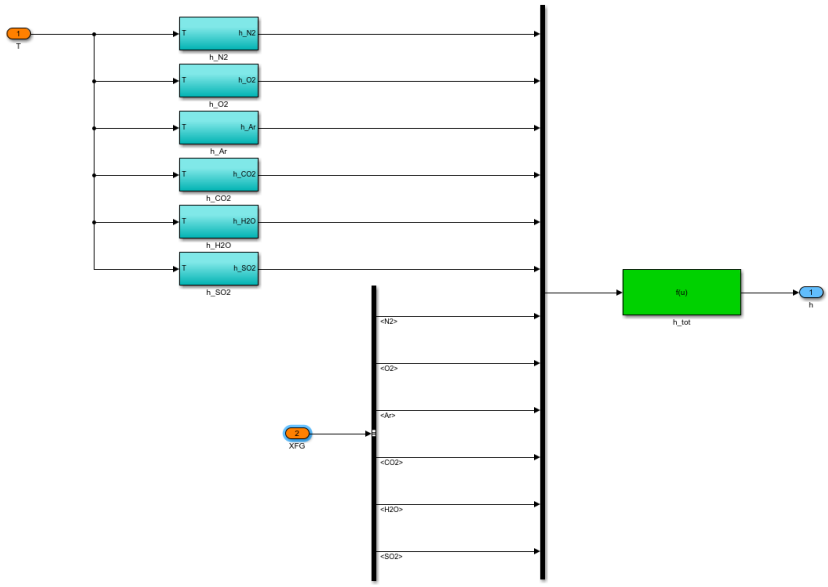

Figure B.2: Simulink block for the calculation of gas enthalpy

By integrating equation B.10 to the last relation (equation B.11) and substituting the temperatures T_2 and T_1 with T and T_{ref} the following relation for the specific enthalpy of each substance can be used:

$$h_j(T) = \left(A \cdot (T - T_{ref}) + \frac{B}{2} \cdot (T^2 - T_{ref}^2) + \frac{C}{3} \cdot (T^3 - T_{ref}^3) + \frac{D}{4} \cdot (T^4 - T_{ref}^4) + \frac{E}{5} \cdot (T^5 - T_{ref}^5)\right) \cdot R + h_{fg_j}(T_{ref}) \tag{B.12}$$

and the total enthalpy of the gas is given:

$$h^g(T) = \sum_{j=1}^{nc} x_j \cdot h_j(T) \tag{B.13}$$

Table B.2: Values of the parameters used for the calculation of C_p and enthalpy, and the values of enthalpy of formation of the gasses used in the model [13].

Gas	A	$B \times 10^3$	$C \times 10^6$	$D \times 10^9$	$E \times 10^{12}$	$h_{fg}[kJ/kmol]$
N_2	3.675	-1.208	2.324	-0.632	-0.226	0.000
O_2	3.626	-1.878	7.055	-6.764	2.156	0.000
Ar	2.500	0.000	0.000	0.000	0.000	0.000
CO_2	2.401	8.735	-6.607	2.002	0.000	-393,520
H_2O	4.070	-1.108	4.152	-2.964	0.807	-241,820
SO_2	3.267	5.324	0.684	-5.281	2.559	-296,830

Now that the specific enthalpy is known, the specific internal energy can be calculated by the following formula:

$$u^g(T) = h^g(T) - R^g \cdot T \tag{B.14}$$

Thermodynamics provide a relation that associates the specific heat at constant pressure with the specific heat at constant volume.[1]

[1]The reader can refer to the book of Moran and Shapiro [13] for the detailed proof of the relationship.

$$c_v^g = c_p^g(T) - R \tag{B.15}$$

Temperature has a strong effect on viscosity while the effect of pressure is moderate. Especially for gasses, viscosity increases slowly with pressure, only a few percent up to 100 atm [14]. In this model the pressures will not exceed the value 100 atm so the effect of pressure in viscosity will be neglected. For the calculation of dynamic viscosity for different temperatures two common approximations the power law and the Sutherland law [14]. As both approximations provide valid results, the method chosen for this model is the power law due to its simplicity.

$$\frac{\mu_j(T)}{\mu_{ref_j}(T_{ref})} = \left(\frac{T}{T_{ref}}\right)^n \tag{B.16}$$

The power law curve fits to these gasses to within ±4 % in the temperature range $250 \leq T \leq 1000K$ [14].

Table B.3: Properties of the viscosity of common gasses at 1 atm and 298.15K [14]

Gas	μ_{ref} $(N \cdot s/m^2)$	Power law exp. n
N_2	1.77 E-05	0.67
O_2	2.05 E-05	0.69
Ar	2.27 E-05	0.72
CO_2	1.50 E-05	0.79
H_2O	1.04 E-05	0.15
SO_2	1.27 E-05	0.97

While the viscosity of the gas mixture is again the sum of the viscosity of individual components times the mass fraction.

$$\mu^g(T) = \sum_{j=1}^{nc} x_j \cdot \mu_j(T) \tag{B.17}$$

Table B.4: Coefficients of the polynomial form of the heat conductivity equation [15]

Gas	A	B	C	D
N_2	3.919 E-04	9.816 E-05	-5.067 E-08	1.504 E-11
O_2	-3.273 E-04	9.996 E-05	-3.743 E-08	9.732 E-12
Ar	2.714 E-03	5.540 E-05	-2.178 E-08	5.528 E-12
CO_2	-7.215 E-03	8.015 E-05	5.477 E-09	-1.053 E-11
H_2O	7.341 E-03	-1.013 E-05	1.801 E-07	-9.100 E-11
SO_2	-8.086 E-03	6.344 E-05	-1.382 E-08	2.303 E-12

White [14] proposes the calculation of heat conductivity to be done in a same way as the calculation of the dynamic viscosity, by using a power law. [2] On the other hand, Reid [15] proposes an polynomial approach for better accuracy.

$$\lambda_j(T) = A + B \cdot T + C \cdot T^2 + D \cdot T^3 \tag{B.18}$$

And the total heat conductivity of the gas substances is:

$$\lambda^g(T) = \sum_{j=1}^{nc} x_j \cdot \lambda_j(T) \tag{B.19}$$

[2] For further details on the power law for the heat conductivity or for the Sutherland law, the reader can refer to the book of White [14].

In Table B.4 are given the values of the constants A, B, C, D that are used in the polynomial equation B.18 for the calculation of the heat conductivity relative to temperature.

Now that the dynamic viscosity and heat conductivity is known the Prandtl number can be calculated according to the following relation.

$$Pr^g = \frac{c_p^g \cdot \mu^g}{\lambda^g} \tag{B.20}$$

B.2. THERMODYNAMIC PROPERTIES OF THE LIQUID PHASE

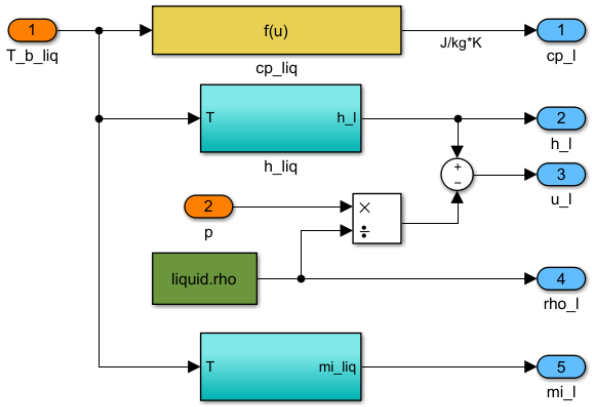

Figure B.3: Simulink block for the calculation of liquid properties

The liquid that is used to clean the exhaust gasses from the sulphur oxides is composed mainly by fresh water and caustic soda. Considering that the amount of caustic soda is small compared to the amount of water, the concentration of the alkali is also negligible in the liquid phase. For this reason the properties of the liquid phase will be calculated as being a pure homogeneous water. This is one of the most important assumptions made for in this thesis.

For liquids that are not near their critical point the incompressible substance model can be adopted. For these liquids specific internal energy and specific volume changes little with pressure at a fixed temperature. For this reason it is consider that this variables are a function of temperature alone [119]. To simplify evaluations it is assumed that specific volume, and thus density, is assumed to be constant and the specific internal energy is assumed to vary only with temperature [13]. The density of the liquid phase will be constant and equal to 998 kg/m^3.

It can be proved [3] that for incompressible liquids the specific heat at constant pressure is equal to specific heat at constant volume.

$$c_p(T) = c_v(T) = c(T) \tag{B.21}$$

It is important to define a relation for the calculation of the specific heat as a function of temperature. Again, as in the case of the gas phase, a calculation using polynomial data will be adopted.

$$c(T) = A + B \cdot T + C \cdot T^2 + D \cdot T^3 + E \cdot T^4 \tag{B.22}$$

The relation B.22 as well as the constant used in it are provided in Perry's chemical engineering handbook [16]. The constant A, B, C, D and E used in this model are:

[3] See Moran and Shapiro [13]

Table B.5: Constants of the polynomial equation of specific heat of water [16]

Substance	A	B	C	D	E
H_2O	2.7637 E+05	-2.0901 E+03	8.1250 E+00	-1.4116 E-02	9.3701 E-06

The calculation of the enthalpy of water using a polynomial form, for different values of temperature, was not as straightforward as it was the case gas. The data available were for particular temperature range and there were temperature taps between the one model and the other. For this reason it was chosen to approach the enthalpy of the liquid using the Mollier diagram. In Mollier diagram, for a particular pressure, the difference in the enthalpy between liquid and vapour is the vaporisation enthalpy.

$$h_{H_2O,\ell}(T) = h_{H_2O,gas}(T) - h_{evap}(T) \tag{B.23}$$

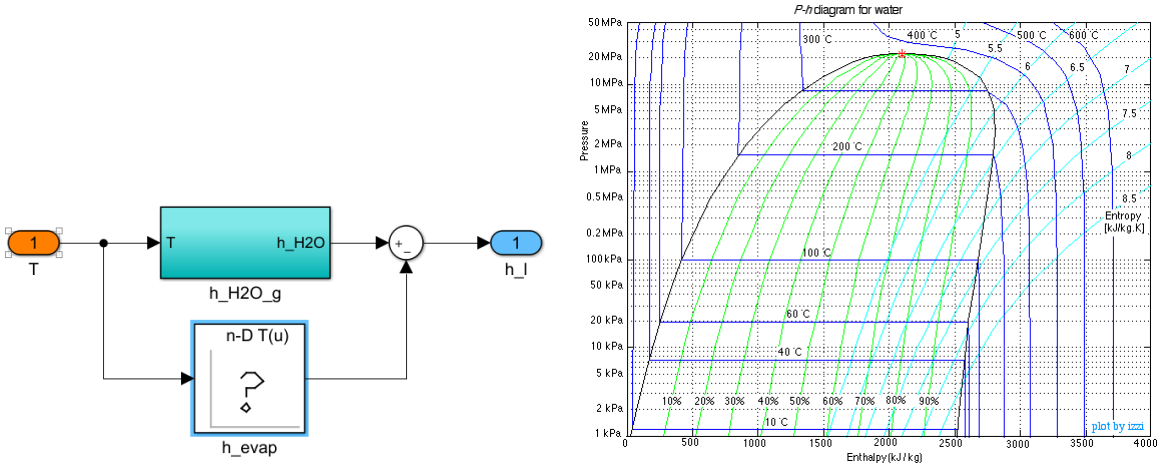

(a) Liquid enthalphy

(b) Mollier diagram for water

Figure B.4: Simulink block of liquid enthalphy (a) and the Mollier diagram (b).

A look up table was created in Simulink that contains the evaporation enthalpies of water in a temperature range from 0°C to 374°C. The values used in the look up table were obtained from Moran and Shapiro [13].

Now that the enthalpy of water is known, the specific internal energy can be calculated.

$$u(T) = h(T) - p \cdot v = h(T) - \frac{p}{\rho_\ell} \tag{B.24}$$

Liquid viscosity decreases with temperature and is roughly exponential, $\mu \approx a \cdot e^{bT}$, but a better fit is the empirical result that $ln\mu$ is quadratic in $1/T$, where T is absolute temperature [14]

$$ln\frac{\mu}{\mu_0} \approx a + b \cdot \frac{T_0}{T} + c \cdot \left(\frac{T_0}{T}\right)^2 \tag{B.25}$$

For water, with $T_0 = 273.15K$, $\mu = 0.001792kg/(m \cdot s)$, suggested values are $a = -1.94$, $b = -4.80$ and $c = 6.74$ with accuracy about ±1% [14].

C

HENRY'S AND RAOULT'S LAW

C.1. HENRY'S LAW

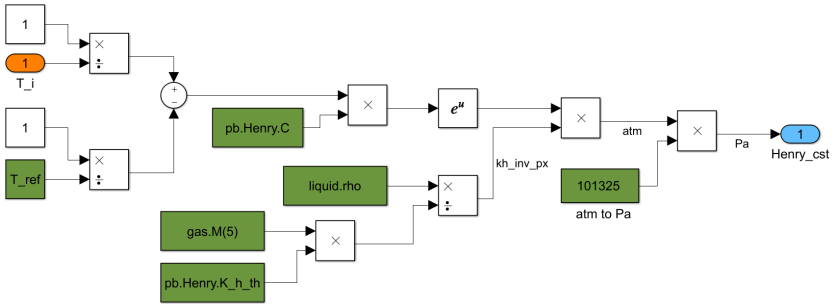

Figure C.1: Simulink block for Henry's constant

The parameter $\mathbb{H}^{\ell}_{SO_2}$ is called Henry's constant. Extensive research for that is carried out by Sander [129]. A simple way to describe Henry's law as a function of temperature is:

$$K_{H,SO_2}(T) = K^{ref}_{H,SO_2}(T_{ref}) \cdot \exp\left[\frac{-\Delta_{soln}H}{R} \cdot \left(\frac{1}{T} - \frac{1}{T_{ref}}\right)\right] \tag{C.1}$$

Where $\Delta_{soln}H$ is the enthalpy of the solution.

$$-\frac{d\ln \mathbb{H}^{\ell}_{SO_2}(T)}{d(1/T)} = \frac{\Delta_{soln}H}{R} \tag{C.2}$$

For SO_2 at the reference temperature of $T_{ref} = 298.15K$ there are tabulated values for K^{ref}_{H,SO_2} and $-\frac{d\ln \mathbb{H}^{\ell}_{SO_2}(T)}{d(1/T)}$. The chosen values are 1.2 $\frac{mol}{dm^3 \cdot atm}$ and 3100 K respectively. These two parameters appear always in pairs. Sander [129][130] provides multiples values for the above parameters. The reasoning behind these two options is that the value 1.2 appears 11 times out of 16. Between the pairs that had value K^{ref}_{H,SO_2} 1.2 the value $-\frac{d\ln \mathbb{H}^{\ell}_{SO_2}(T)}{d(1/T)} = 3100k$ is the most common. Another reason for choosing this pair of values was because they were the only to be verified both thermodynamically and experimentally [1].

For this model the Henry's constant needs to be expressed in pressure units. The units of C.1 are $\frac{mol}{dm^3 \cdot atm}$. For that Sander [129] proposes to use the volatility instead of solubility. The usual definition is:

$$K^{inv,P.X}_{H,SO_2}(T) = \frac{\rho_{H_2O}}{M_{H_2O} \cdot K_{H,SO_2}(T)} \tag{C.3}$$

[1] For more information regarding this topic is recommended to the reader to refer to the papers of Sander [129][130]

Where $K^{inv,P.X}_{H,SO_2}(T)$ is actually $\mathbb{H}^{\ell}_{SO_2}(T)$. For $T = T_{ref}$, equation C.3 becomes:

$$K^{inv,P.X,ref}_{H,SO_2}(T_{ref}) = \frac{\rho_{H_2O}}{M_{H_2O} \cdot K^{ref}_{H,SO_2}(T_{ref})} \tag{C.4}$$

The unit of $K^{inv,P.X,}_{H,SO_2}$ is atm. Also $K^{inv,P.X,ref}_{H,SO_2}(T_{ref})$ is $\mathbb{H}^{L,ref}_{SO_2}$. So, equation C.1 takes the desired form:

$$\mathbb{H}^{\ell}_{SO_2}(T) = \mathbb{H}^{L,ref}_{SO_2} \cdot \exp\left[\frac{-\Delta_{soln}H}{R} \cdot \left(\frac{1}{T} - \frac{1}{T_{ref}}\right)\right] \tag{C.5}$$

The units of C.5 are in atm and they are converted to Pa in the Simulink model.

C.2. RAOULT'S LAW

Raoult's law is applied for ideal mixtures. In this model there are two mixtures; the one of the gas phase and the other of the liquid phase. The gas mixture is mainly the exhaust gasses and the water that evaporates. One of the main assumptions of this model is that the exhaust gasses are approached as ideal gas [109]. An ideal gas can be considered as an ideal mixture since its thermodynamic properties depend only on the properties of the pure substances of its components. So, the gas phase has an ideal "behaviour". The same applies for the liquid phase that is which is not a mixture, since it is assumed that the properties of the liquid phase are them of pure water. Thus, Raoult's law can be applied for liquid phase.

Moreover, Raoult's law requires equilibrium conditions. The liquid and the gas phase are in thermodynamic equilibrium since in the interface they both have the same temperature T_i. Also, the concentrations of the substances in the interface are in equilibrium.

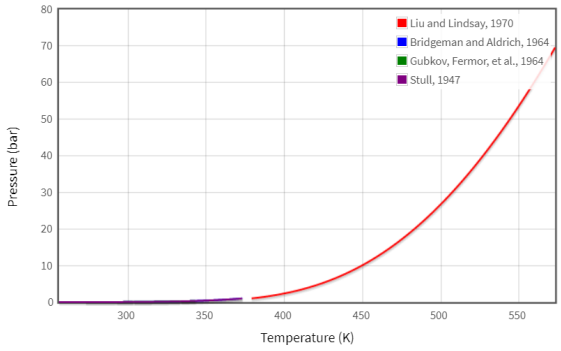

Figure C.2: Concentrations of the substances that are engaged in the instantaneous reaction [11]

Models		
Parameters	Stull	Liu and Lindsay
A	4.6543	3.55959
B	1435.264	643.748
C	-64.848	-198.043

Table C.1: Parameters of Antoine equation developed by Stull and Liu and Lindsay

Calculation of the saturation pressure of water in each step will be carried out by using the Antoine equation. Antoine equation is a empirical formula. The parameters A,B and C for Antoine equation are obtained from NIST Chemistry WebBook [11]. They are derived by experimental data for different temperature range. For the model used in this thesis the values of the parameters that will be used are them proposed by Liu and Lindsay [131] and Stull [132].

$$log_{10}(p_{sat}(T_i)) = A - \frac{B}{C + T_i} \tag{C.6}$$

Other values for the parameters of Antoine equation are developed by other scientists that corer a small temperature range or temperature ranges that do not match with this thesis. The parameters of Liu and Lindsay, and Stull were chosen because cover the temperature range between 379 - 573 K and the range 255.9 - 373K. For the small gap between 373 - 379 K both ranges were expanded by some degrees K. The range of Stull is expanded to 255.9 - 376K and the range of Liu and Lindsay 376 - 573K. This expansion of the ranges can be consider as reasonable because as it can be seen in Figure C.2 there is linearity in this area. In the Simulink Block an "if statement" is used that depending on the value of the T_i it chooses the one range or the other to calculate the saturation pressure.

D

COEFFICIENTS

D.1. MASS TRANSFER COEFFICIENT

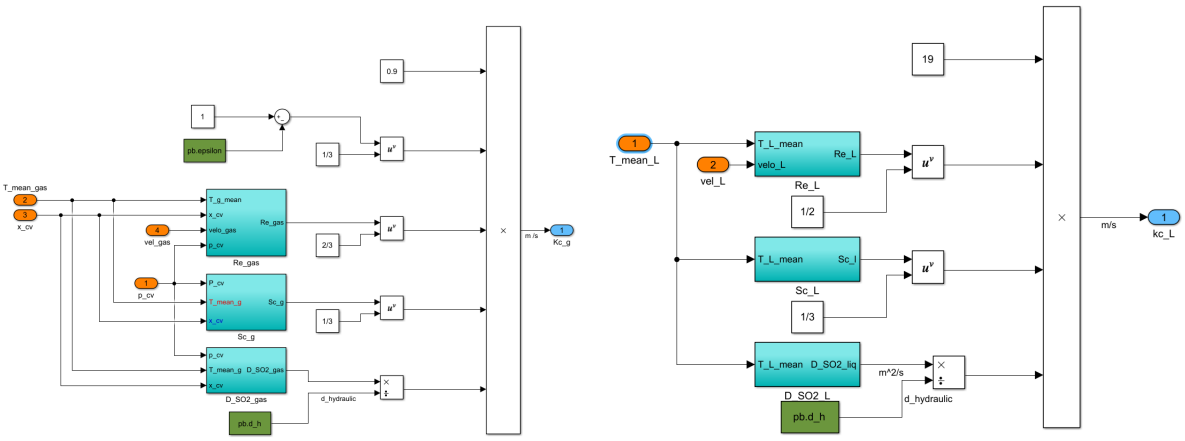

(a) Mass transfer coefficient of the gas phase

(b) Mass transfer coefficient of the liquid phase

Figure D.1: Simulink blocks for mass transfer coefficient of the gas phase (a) and the liquid phase(b) according to the model proposed by Krishna and Wesseling.

The packed bed is the place were the gas absorption is mainly carried out. The liquid flows downwards over the packed bed and the gas flows upwards with high speed through the packing material.The flow that governs the both phases can be characterized as turbulent. In turbulent flow is difficult to approach mass transfer with analytical relations. So, the mass transfer coefficient are taken from experimental data. Another method, less costly, is to apply dimensional analysis [14]. The dimensionless numbers used in this model are the Reynolds number; Sherwood number; Schmidt number and Prandtl number.

Turbulent flow on its own is difficult to be approached. The case of mass transfer in packed bed makes it more difficult. Research has been made that provide correlations for different types of packing. The equations developed by Krishna and Wesseling [133] will be used in this model. The correlation that they provide for the Sherwood number in relation to the other dimensionless numbers is:

$$Sh^{\ell} = 19 \cdot (Re^{\ell})^{1/2} \cdot (Sc^{\ell})^{1/3} \tag{D.1}$$

$$Sh^{g} = 0.9 \cdot (1-\varepsilon)^{1/3} \cdot (Re^{g})^{2/3} \cdot (Sc^{g})^{1/3} \tag{D.2}$$

The three dimensionless numbers that are used in the above relations can be defined as:

$$Sherwood \quad number \quad Sh = \frac{k_c \cdot d_h}{D^{g/\ell}} \tag{D.3}$$

$$Reynolds \quad number \quad Re = \frac{v \cdot \rho}{a \cdot \mu} \tag{D.4}$$

$$Schmidt \quad number \quad Sc = \frac{\mu}{\rho \cdot D^{g/\ell}} \tag{D.5}$$

Now by substituting the definition of the Sherwood number in the equations D.1 and D.2 and making the appropriate rearrangement of the terms the mass transfer coefficient can be calculated by the dimensionless numbers:

$$k_c^{\ell} = 19 \cdot (Re^{\ell})^{1/2} \cdot (Sc^{\ell})^{1/3} \cdot \frac{D^{g/\ell}}{d_h} \tag{D.6}$$

$$k_c^{g} = 0.9 \cdot (1-\varepsilon)^{1/3} \cdot (Re^{g})^{2/3} \cdot (Sc^{g})^{1/3} \cdot \frac{D^{g/\ell}}{d_h} \tag{D.7}$$

The properties of the fluid in the dimensionless numbers are calculated using the average temperature between the bulk of the fluid and the interface. The method - relation to calculate of the interface temperature will be provided in the next sections.

The term d_h in the above relations is the hydraulic diameter of the packing system and is dependent of the packing parameters a and ε. The hydraulic diameter is:

$$d_h = \frac{4 \cdot \varepsilon}{a} \tag{D.8}$$

D.2. DIFFUSION COEFFICIENTS

The diffusion coefficient is a measure of the resistance that a molecule encounters as it moves into a medium under the influence of "pushing force", that is, the concentration gradient.

The gas from the cylinder is lead to the turbine. In the turbine expansion of gasses occurs and the pressures becomes low. In a binary gas mixture there are several empirical formulas proposed by Poling [17] and by Brodkey and Hersey [134] for gasses in low to moderate pressures. Poling proposes the Wilke and Lee equation (1955), and Fuller, Schetter & Giddings equation (1966) for calculating the binary gas diffusion coefficient. Brodkey and Hersey add to the above the a method that uses the kinetic gas theory and The Chapman-Enskog method. All these equations generally agree with experimental values within 5 to 10%, although discrepancies of more than 20% are possible. Moreover, these equations show to be inversely proportional to pressure and at low pressures, the binary diffusion coefficient is essentially independent of composition [17].

Among the above proposed methods the one that will be adopted in this thesis is the Fuller, Schetter & Giddings equation. The reasoning behind this choice is that yielded the smallest average error (an average error of around 4%), it is the method recommended for use by Poling and it can be used when no data is available for Lennard - Jones parameters (σ and Ω) [1].

The Fuller et all. equation for a binary gas A and B is described in the following relation:

$$D_{AB} = \frac{0.00143 \cdot T^{1.75}}{p \cdot M_{AB}^{1/2} \left[(\Sigma v)_A^{1/3} + (\Sigma v)_B^{1/3} \right]^2} \tag{D.9}$$

The molecular weight of the binary mixture is defined as:

$$M_{AB} = \frac{2}{\frac{1}{M_A} + \frac{1}{M_B}} \tag{D.10}$$

The summation of diffusion volumes (v) for each component used in the model is found in Table D.1:

[1] An extensive explanation of the methods and the parameters used on them is provided in the books of Poling [17] and Brodkey and Hersey [134]

Table D.1: Diffusion volumes of the exhaust gas molecules [17]

	Substance					
	N2	O2	Ar	CO2	H2O	SO2
Diffusion volume	18.5	16.3	16.2	26.9	13.1	41.8

Of course in the present model there is no binary mixture but a multicomponent gas mixture. The diffusion coefficient for a multicomponent mixture is given by Blanc's law:

$$D_{Am} = \left(\sum_{\substack{B=1 \\ B \neq A}}^{n} \frac{x_B}{D_{AB}} \right)^{-1} \tag{D.11}$$

DIFFUSION IN LIQUIDS

Diffusion of a solute A (SO_2 or OH^-) in a solvent B (H_2o), implies that each molecule of A is in an environment of essentially pure B. In engineering applications D_{AB} is assumed to be a representative diffusion coefficient for concentrations of A of 5 to 10% mole.

Several trials were carried out by scientist to calculate the diffusion coefficient in liquids. The most accurate of them with and average error of less or equal than 10% were the methods of Wilke and Chang (1955), Tyn and Calus (1975), Hayduk and Minhas (1982), and Nakanishi (1978). To use the Tyn-Calus and Hayduk-Minhas form, however, the parachors, and thus the surface tension, of both the solute and the solvent must be known. These two methods were mostly tasted when the solvent were parafins. The Nakanishi method is applicable at 298K and gives poor result when the solute is gas. On the other hand Wilke and Chang method, which is an empirical modification of the Stokes-Einstein equation, is the oldest, easiest and still the widely used method to calculate the diffusion coefficient [17]. In this model the Wilke and Chang method will be used.

$$D_{AB} = \frac{7.4 \cdot 10^{-8} \cdot (\phi \cdot M_B)^{1/2} \cdot T}{\mu_B \cdot V_A^{0.6}} \tag{D.12}$$

Wilke and Chang recommend that ϕ be chosen as 2.6 if the solvent is water. The molar volume of SO_2 is 44.8. For OH^- the molar volume at its normal boiling temperature couldn't be found from experimental data. Poling recommends in these cases the Le Bas and Schroeder additive method to be used so as to calculate the molar volume. According to Le Bas:

$$V_A = \sum N_i \cdot V_i \tag{D.13}$$

For the case of OH^- there is one molecule of O and one of H with molar volumes 7.4 and 3.7 respectively [17]. So, D.13 gives,

$$V_{OH^-} = 1 \cdot 7.4 + 1 \cdot 3.7 = 11.1 \tag{D.14}$$

D.3. HEAT TRANSFER COEFFICIENTS

The English Osborne Reynolds (1842-1912) was the first to observe the analogy between turbulent momentum and heat transfer (with convection). The transfer coefficients can be written as the sum of two components: the molecular transport effect and the turbulent flow effect [111]. Transfers are because of vortexes, where inside the vortex the transfer is by molecular means.

It has already been stated the analogy of the laws of Newton, Fourier and Fick, that is, the relationships that describe molecular transport. These three equations have the same form. It can be proved that [2]:

[2] The explanations falls out of the scope of this thesis project and is requested by the reader to refer to the book of Incropera [115] for the analytical theory

$$C_f \frac{Re_L}{2} = Nu = Sh \tag{D.15}$$

Where C_f is the skin friction factor. Replacing Nu and Sh by the Stanton number (St) and the mass transfer Stanton number (St_m), respectively,

$$St = \frac{h_c}{\rho \cdot v \cdot c_p} = \frac{Nu}{Re \cdot Pr} \tag{D.16}$$

$$St_m = \frac{k_c}{v} = \frac{Sh}{Re \cdot Sc} \tag{D.17}$$

Combing the last three equations :

$$\frac{C_f}{2} = St = St_m \Longrightarrow \frac{k_c}{v} = \frac{h_c}{\rho \cdot v \cdot c_p} \tag{D.18}$$

The above analogy is known as the Reynolds analogy. Experimental data for gaseous systems are roughly in agreement with this "ratio", since the numbers Pr and Sc are close to 1 (generally when $Pr = Sc = 1$) and there is only friction on the surface (i.e there is no drag resistance). It obviously does not apply to liquids for which $Sc \sim 1000$ and $Pr \sim 10$. It is noted that many researchers, including Prandtl and von Kármán, have made efforts to modify, extend and improve the above ratio[111].

Reynolds analogy can be applied in a wide range of Pr and Sc numbers if certain correction are made. Many efforts have been made to extend the Reynolds ratio to liquids. Perhaps the most useful analogy is the empirical one by Chilton and Colburn (1934), which was based on the analysis of a large number of experimental data (fluid + air, turbulent + laminar flow). The Chilton-Colburn analogy is given:

$$\frac{C_f}{2} = \frac{k_c}{v} \cdot Sc^{2/3} = \frac{h_c}{\rho \cdot v \cdot c_p} \cdot Pr^{2/3} \tag{D.19}$$

With Chilton-Colburn analogy and using the values obtained from mass transfer coefficient that were calculated in section D.1, the heat transfer coefficient can be calculated.

The model required for this thesis is for packed bed. In section D.1 the equations from Wesselingh and Krishna [133] were used for mass transfer in the packed bed. They give Sherwood number in relation to Reynolds and Schmidt number. In equation D.15 is given that $Nu = Sh$. Fick's and Fourier's have the same form and the mechanism of convective heat and mass transfer has the same form. So, from all the above and for consistency reasons, the same equations from Wesselingh and Krishna will be used. Now the Nusselt number will substitute the Sherwood number and the Schmidt number will be substituted by Prandtl number. The new relations are as follow:

$$Nu^{\ell} = 19 \cdot (Re^{\ell})^{1/2} \cdot (Pr^{\ell})^{1/3} \tag{D.20}$$

$$Nu^{g} = 0.9 \cdot (1-\varepsilon)^{1/3} \cdot (Re^{g})^{2/3} \cdot (Pr^{g})^{1/3} \tag{D.21}$$

The Nusselt number definition is given in the formula below:

$$Nu = \frac{h_c \cdot d_h}{\lambda} \tag{D.22}$$

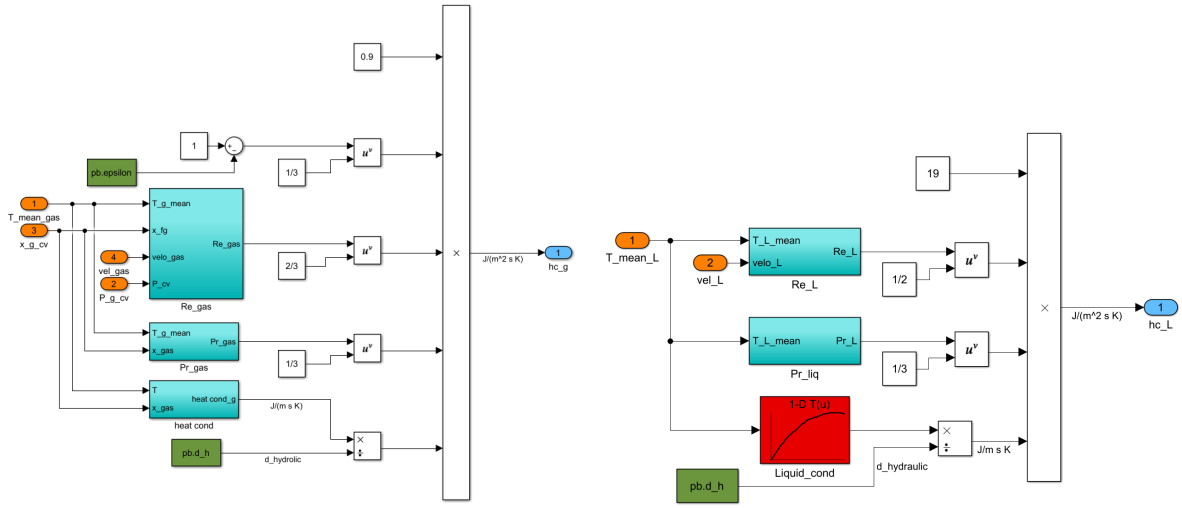

(a) Heat transfer coefficient of the gas phase

(b) Heat transfer coefficient of the liquid phase

Figure D.2: Simulink blocks for Heat transfer coefficient of the gas phase (a) and the liquid phase(b) adapted to the model of mass transfer coefficient proposed by Krishna and Wesseling.

Substituting the definition of Nusselt number (equation D.22) in the relations D.20 and D.21 and making the appropriate rearrangement of the terms the heat transfer coefficient for the liquid and the gas phase is respectively:

$$h_c^{\ell} = 19 \cdot (Re^{\ell})^{1/2} \cdot (Pr^{\ell})^{1/3} \cdot \frac{\lambda^{\ell}}{d_h} \tag{D.23}$$

$$h_c^{g} = 0.9 \cdot (1-\varepsilon)^{1/3} \cdot (Re^{g})^{2/3} \cdot (Pr^{g})^{1/3} \cdot \frac{\lambda^{g}}{d_h} \tag{D.24}$$

The properties of the liquid and gas phase in the dimensionless numbers are calculated for the average temperature between the bulk of the fluids and the interface.

E

DYNAMIC ANALYSIS

E.1. DYNAMIC LOAD: 100% - 25% - 100%

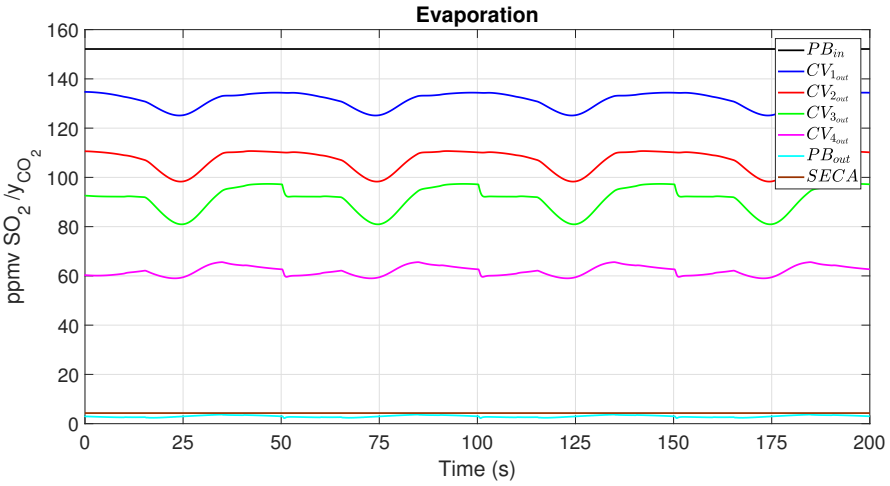

(a) Fraction of $\frac{ppmvSO_2}{y_{CO_2}}$ along the control volumes at load variations (evap)

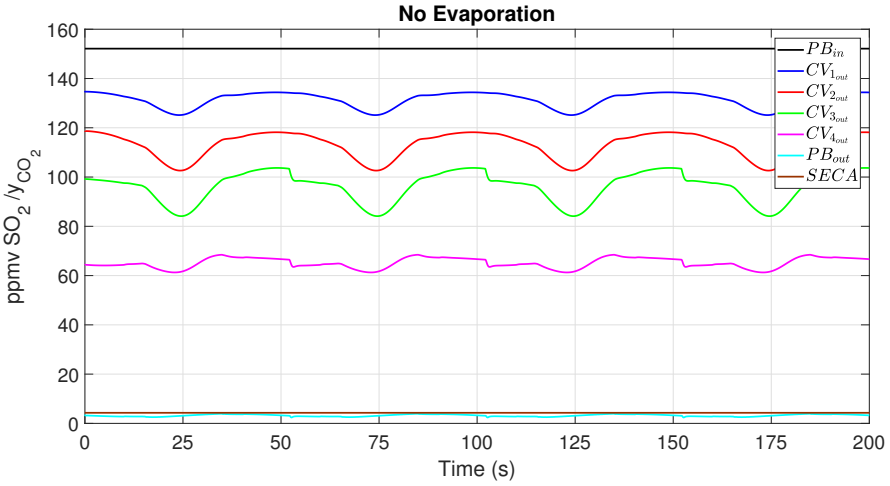

(b) Fraction of $\frac{ppmvSO_2}{y_{CO_2}}$ along the control volumes at load variations (no evap)

Figure E.1: Fraction of $\frac{ppmvSO_2}{y_{CO_2}}$ along the control volumes at load variations in evaporation (a) and non evaporation (b) influence.

Figure E.1 demonstrates that in both cases the scrubber manages to keep the output of the sulphur oxides below the SECA limit. Excluding the first control volume where the profile is identical in both cases, in the remaining control volumes, the amount of sulphur oxides is lower and more stable for the case of evaporation. This results are verifying the findings of the static simulations about the influence of evaporation in the removal efficiency.

E.2. DYNAMIC LOADING: 100% - 50% - 100%

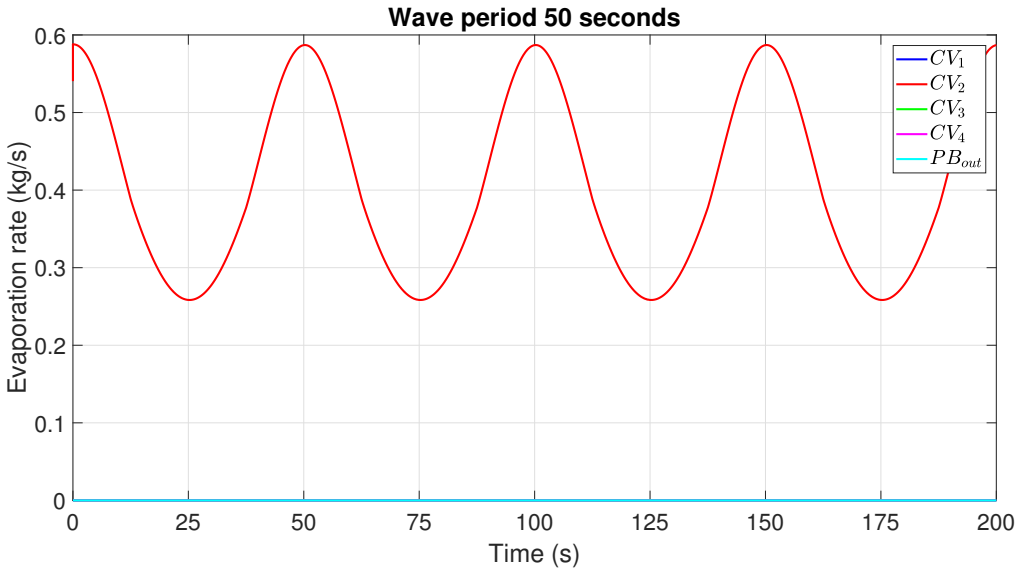

(a) Evaporation rate in the scrubber for a wave period of 50 seconds.

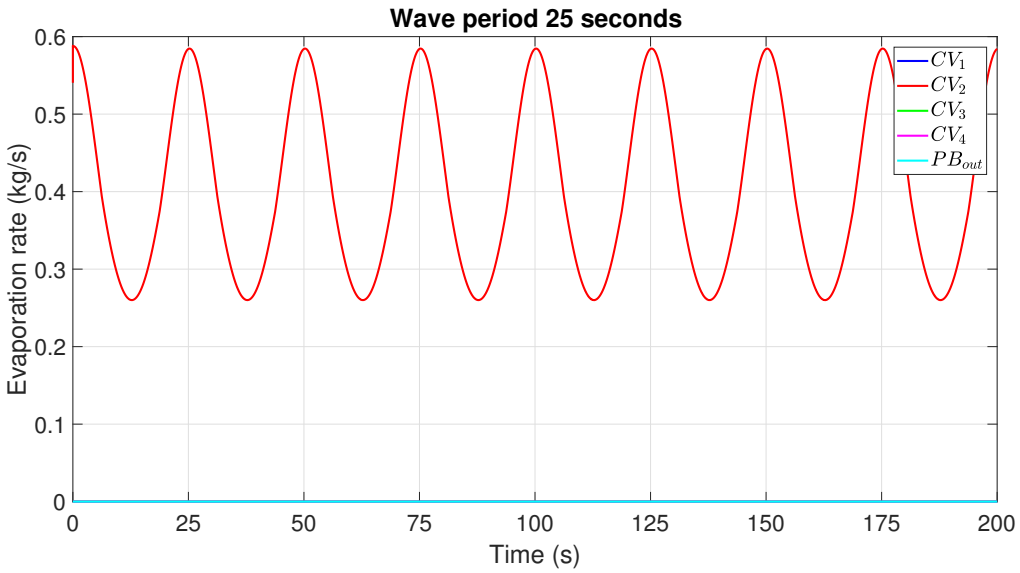

(b) Evaporation rate in the scrubber for a wave period of 25 seconds.

Figure E.2: Rate of evaporation in the wet scrubber system in two different wave periods.

The evaporation rate is around 0.6 grams higher of the case of 50 seconds, but considering the overall magnitude of the evaporation rate this difference can be considered insignificant. The values at the peak are the same and in accordance with the findings of static simulation and the previous dynamic load.

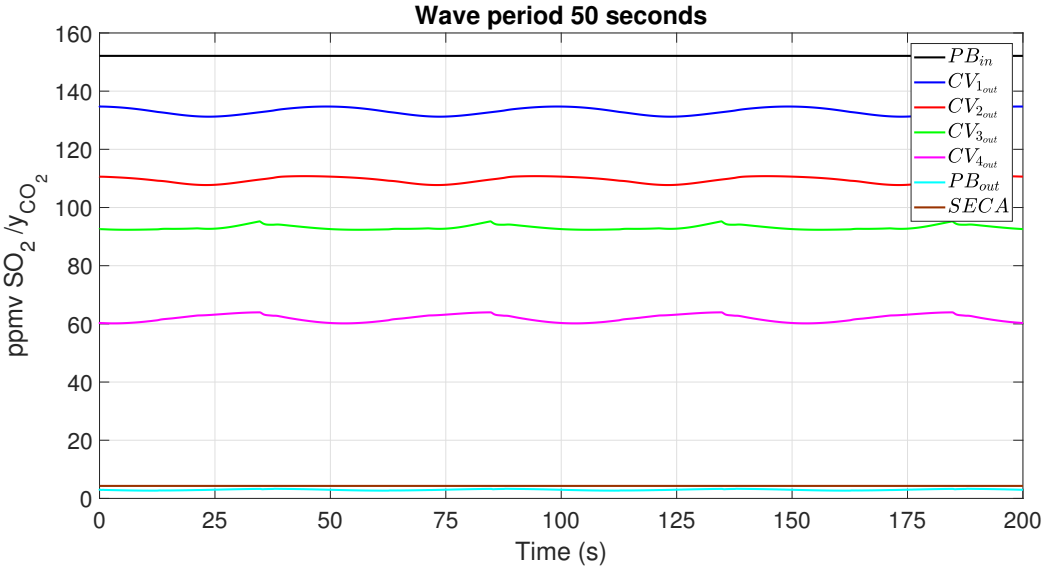

(a) Fraction of $\frac{ppmvSO_2}{y_{CO_2}}$ along the control volumes at load variations for a wave period of 50 second.

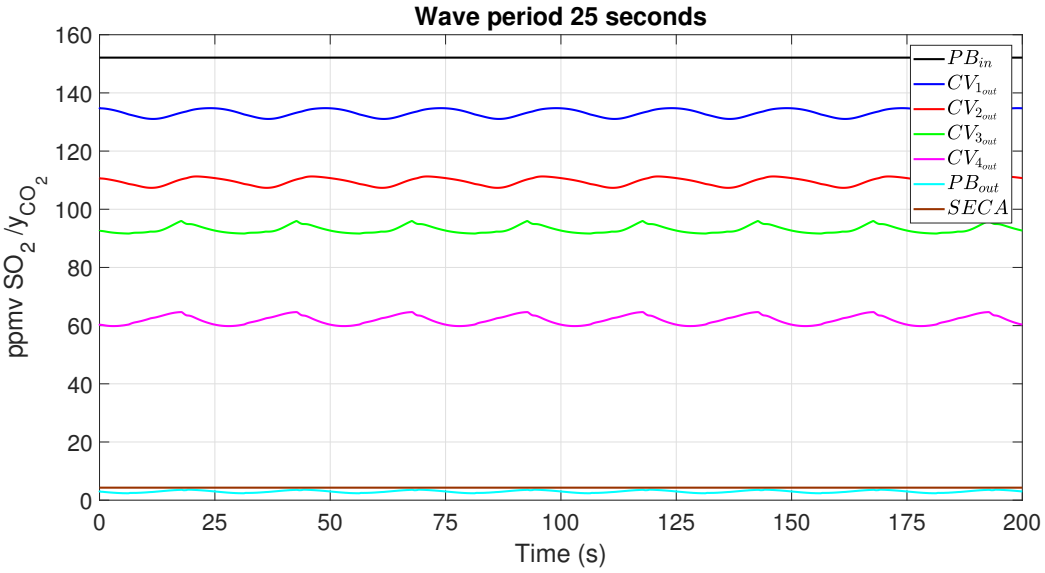

(b) Fraction of $\frac{ppmvSO_2}{y_{CO_2}}$ along the control volumes at load variations for a wave period of 25 second.

Figure E.3: Fraction of $\frac{ppmvSO_2}{y_{CO_2}}$ along the control volumes at load variations in two different wave periods.

When the wave period is 50 seconds the output signal of each control volume is smoother and the values are slightly lower. The difference is in the same order of magnitude. Compliance with SECA is achieved in both cases. The profile approaches that of the wave signal, which is better than the one obtain in the previous engine load.

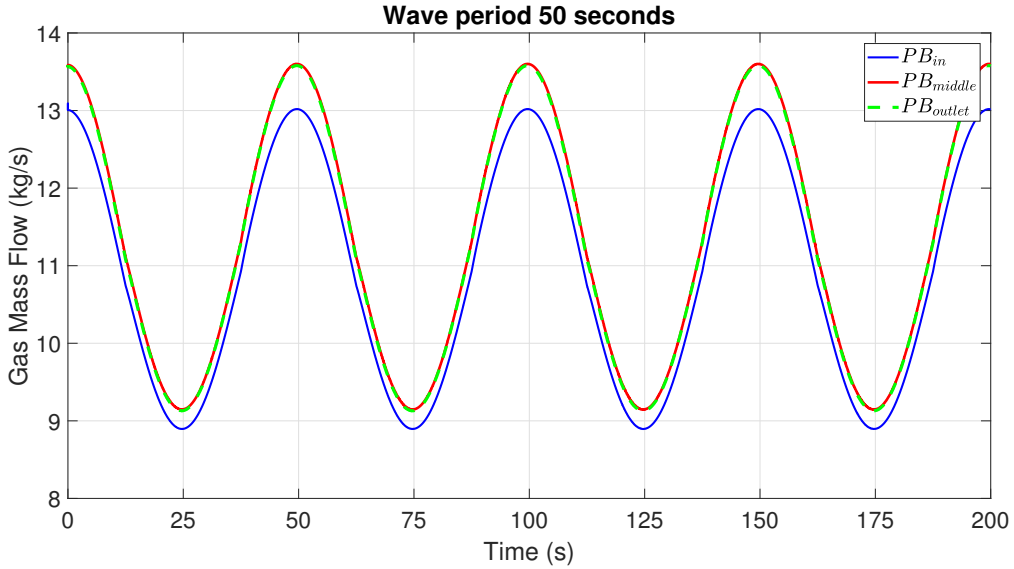

(a) Gas mass flow at loading variations in the scrubber system for a wave period of 50 second.

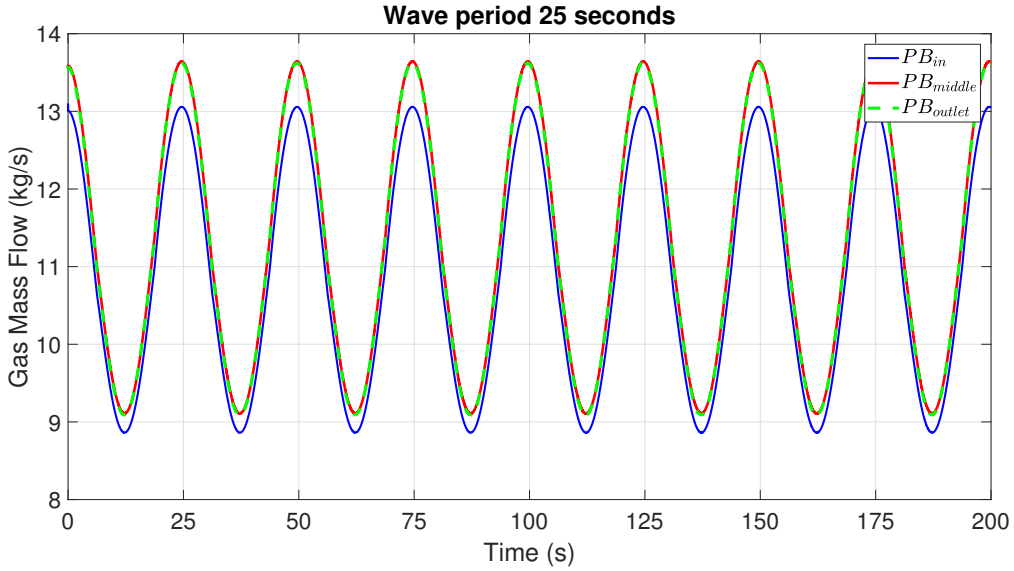

(b) Gas mass flow at loading variations in the scrubber system for a wave period of 25 second.

Figure E.4: Gas mass flow rate at loading variations in the scrubber system in two different wave periods.

The values of the peak and valleys are of the exhaust gas mass flow are almost identical and the minor differences that occur are the result of the small differences in the evaporation rate and the amount of sulphur removed in each step. Comparing them with the 25 – 100% engine load, their peaks show a deviation of less than 1%.

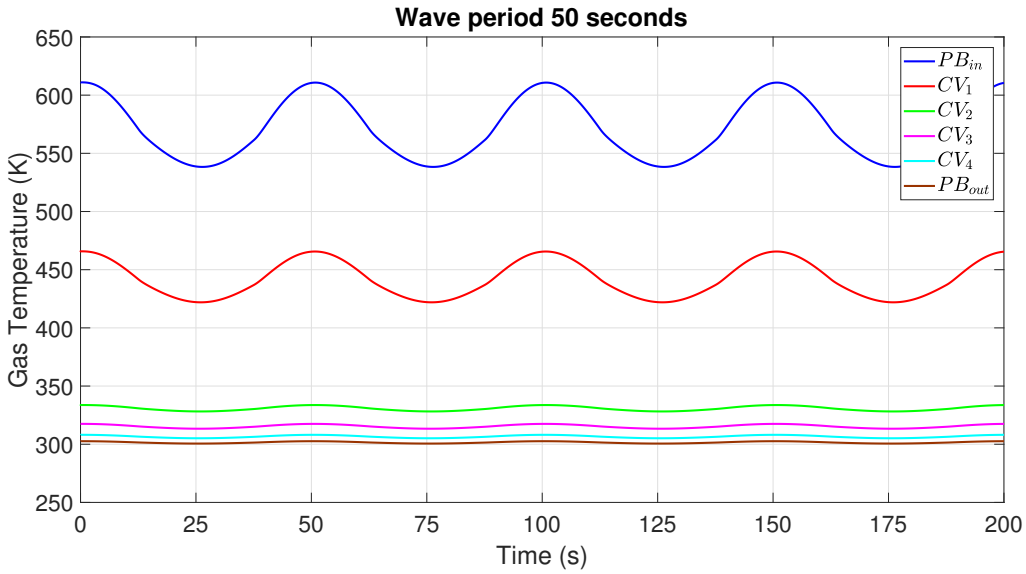

(a) Exhaust gas temperature in the scrubber sections for a wave period of 50 second.

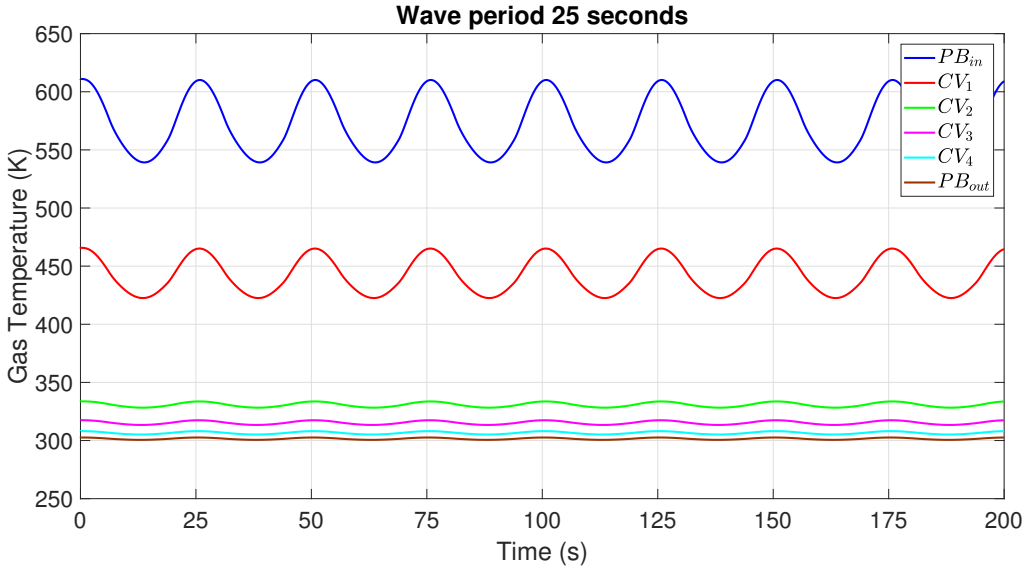

(b) Exhaust gas temperature in the scrubber sections for a wave period of 25 second.

Figure E.5: Temperature at loading variations in the scrubber system in two different wave periods.

The temperature profile of the both cases is almost identical considering the values of temperature at each step. The only thing changing as it was expected is frequency, which is not associated with scrubber. Comparing these results with the previous engine load, they do not show inconsistencies.

E.3. DYNAMIC LOADING: 100% - 75% - 100%

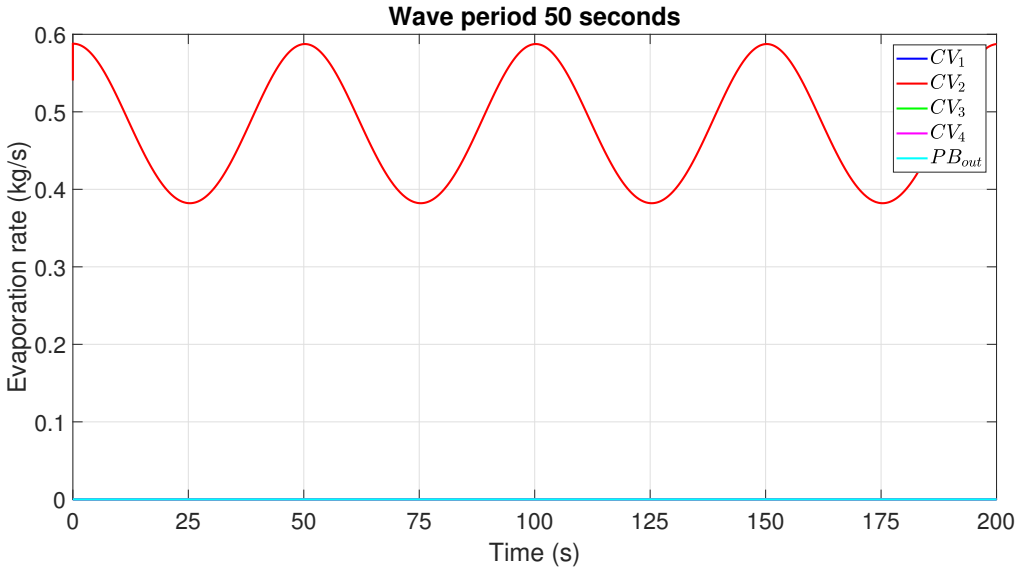

(a) Evaporation rate in the scrubber for a wave period of 50 second.

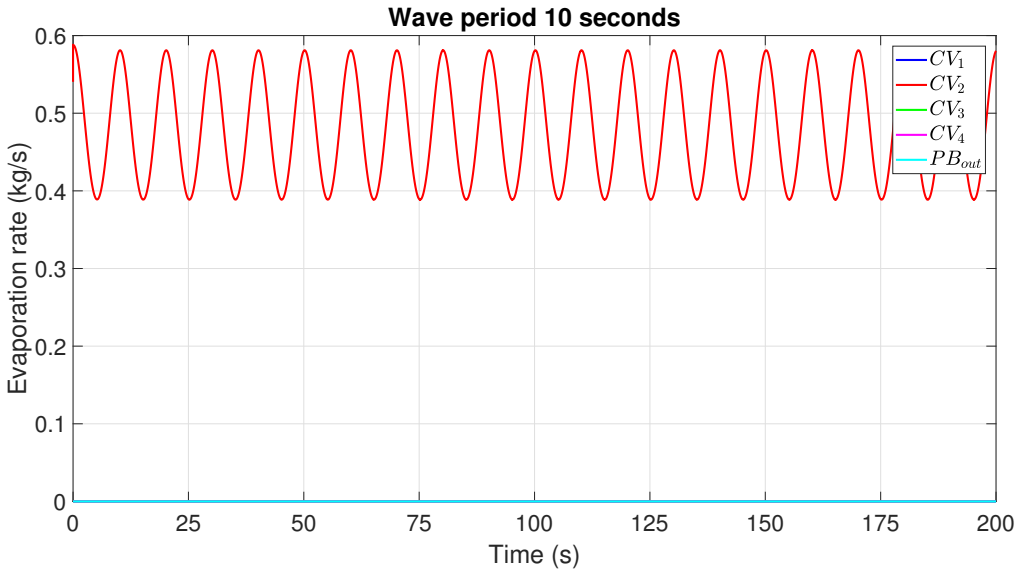

(b) Evaporation rate in the scrubber for a wave period of 10 second.

Figure E.6: Rate of evaporation in the wet scrubber system in two different wave periods.

The results of the evaporation rate are almost identical between the two cases and are in accordance with the values obtained from the static simulations. Comparing their peak with the previous loads they seem to be in agreement.

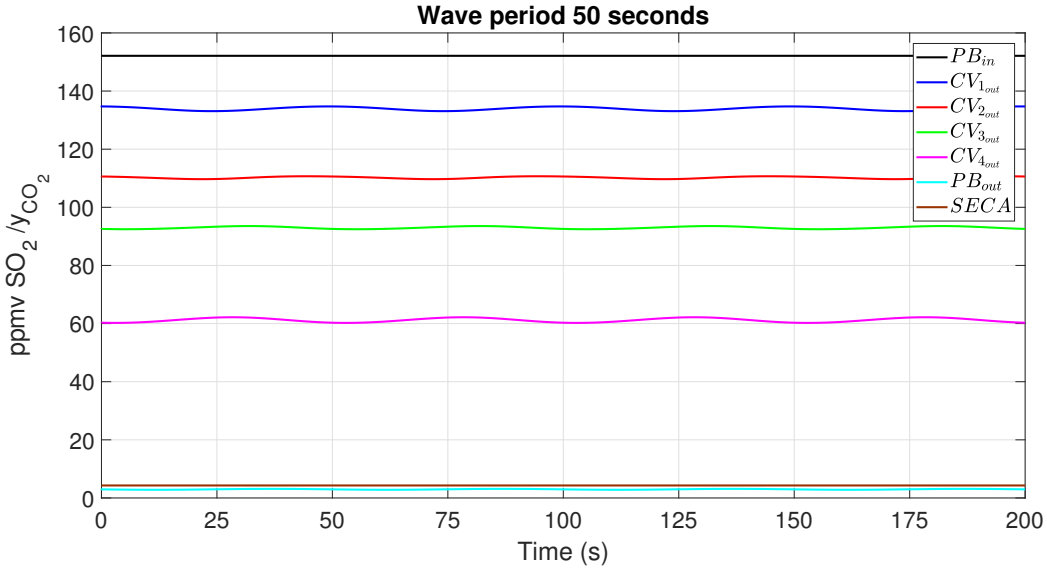

(a) Fraction of $\frac{ppmvSO_2}{y_{CO_2}}$ along the control volumes at load variations for a wave period of 50 second.

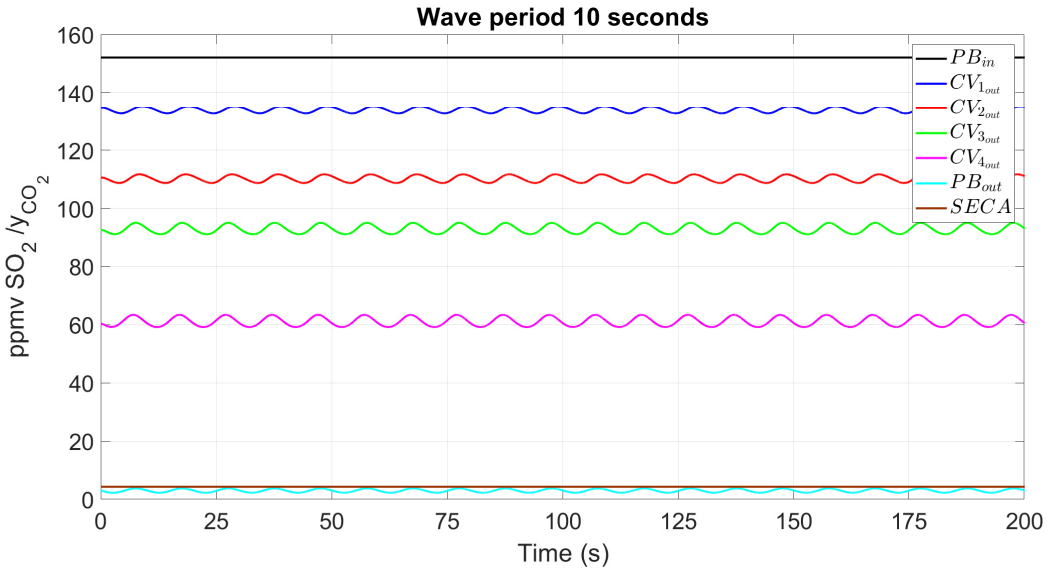

(b) Fraction of $\frac{ppmvSO_2}{y_{CO_2}}$ along the control volumes at load variations for a wave period of 10 second.

Figure E.7: Fraction of $\frac{ppmvSO_2}{y_{CO_2}}$ along the control volumes at load variations in two different wave periods.

The results obtained when the period is 10 seconds are slightly higher than that of the 50 seconds but still the output in both cases is below the required SECA limit. Characteristically for the differences of in the value of the $\frac{ppmvSO_2}{y_{CO_2}}$ leaving the scrubber for the case of 50 and 10 seconds at their peaks is 3.22 and 3.75 respectively, that is a small difference to be taken into account. This difference is representative for all the control volumes. Also, for the case of 10 seconds, the deviations between of the values in the same control volume is higher than that of the 50 seconds, making the system a little more unstable. The effect of this instability is minor to affect significantly the final outcome.

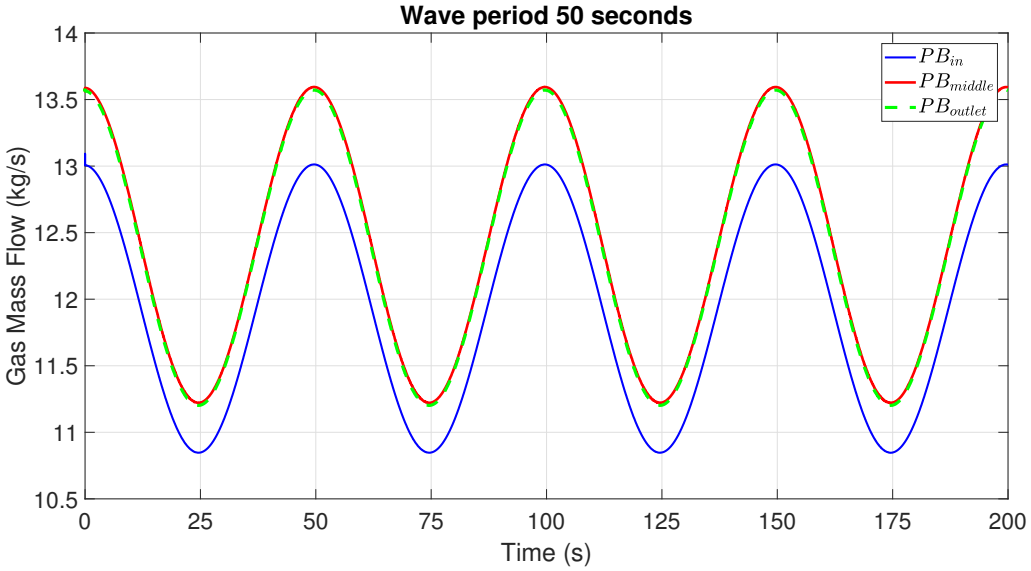

(a) Gas mass flow at loading variations in the scrubber system for a wave period of 50 second.

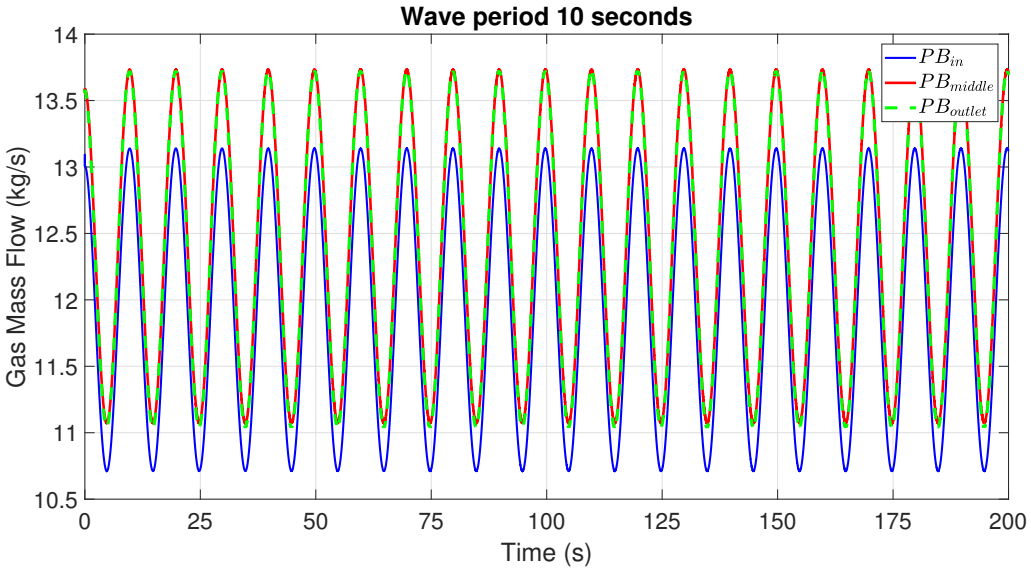

(b) Gas mass flow at loading variations in the scrubber system for a wave period of 10 second.

Figure E.8: Gas mass flow rate at loading variations in the scrubber system in two different wave periods.

The small differences of the values at the peaks of the exhaust mass flow rate between the case of the 50 and 10 seconds derive from the minor deviations at the values of evaporation rate and SO_2 absorbed at each control volume. These values are in close relation with the previous loading.

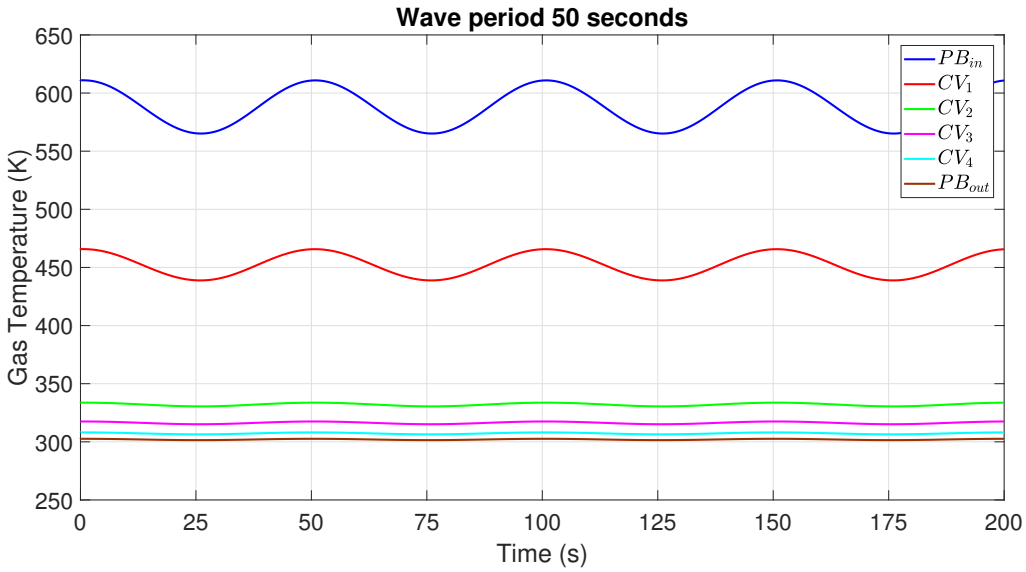

(a) Exhaust gas temperature in the scrubber sections for a wave period of 50 second.

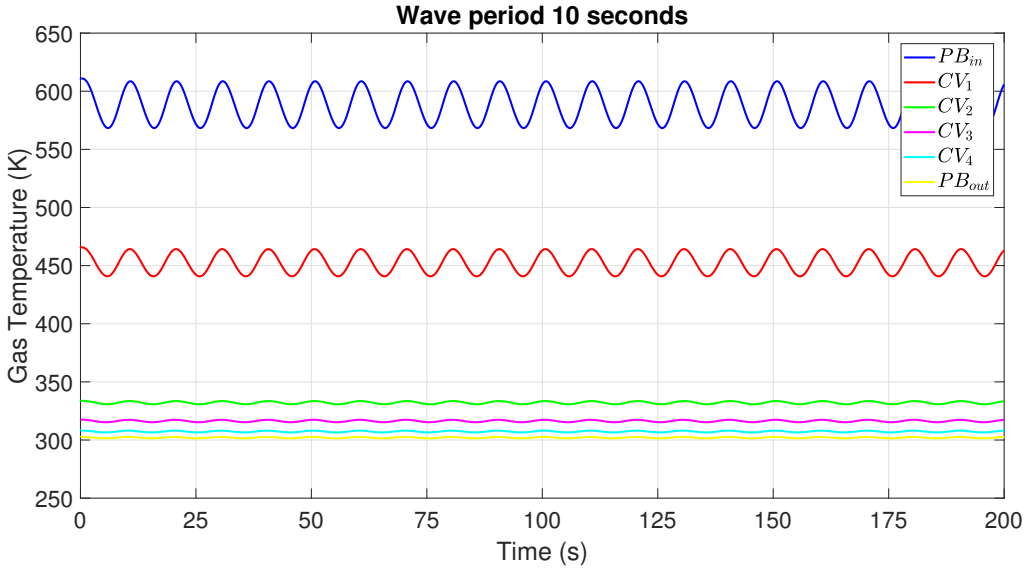

(b) Exhaust gas temperature in the scrubber sections for a wave period of 10 second.

Figure E.9: Temperature at loading variations in the scrubber system in two different wave periods.

The temperatures in the control volumes between the two cases are almost identical. There are slightly higher fluctuations for the case of the 50 second period. In overall the response when the frequency is increased is acceptable, considering that it does not provide any inconsistencies.

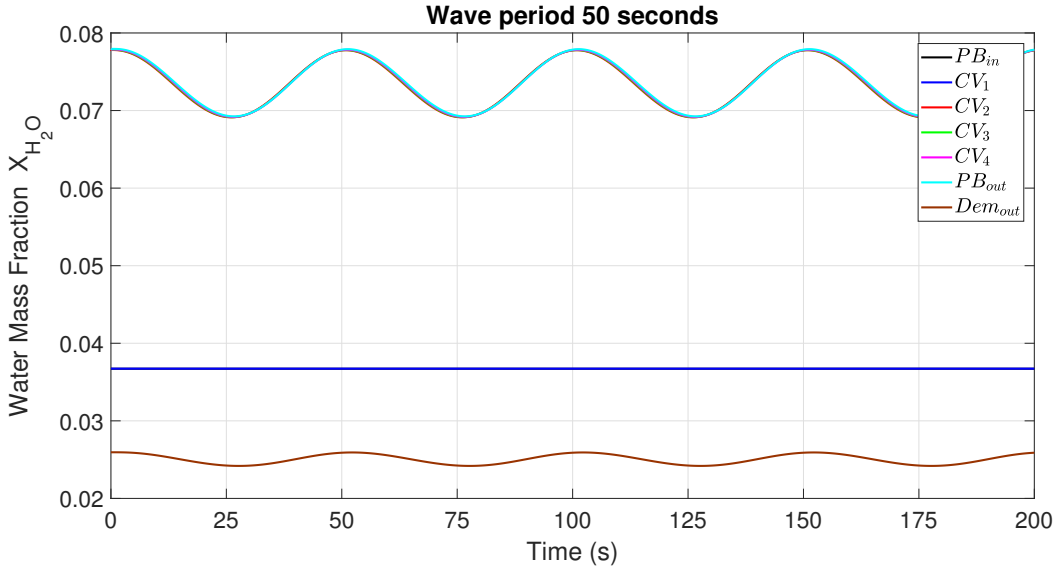

(a) Water mass fraction in the PB and the demister for a wave period of 50 second.

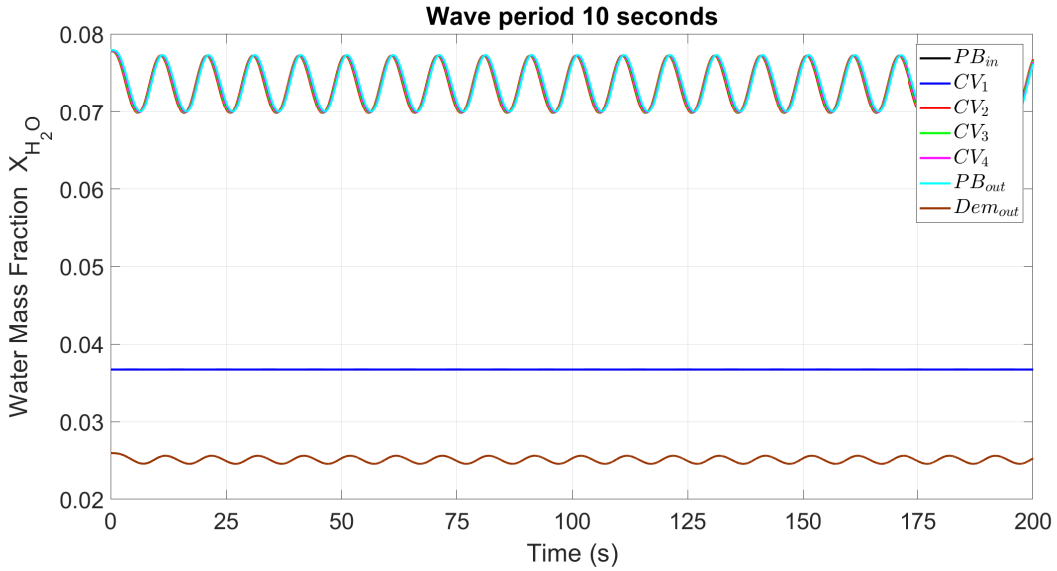

(b) Water mass fraction in the PB and the demister for a wave period of 10 second.

Figure E.10: Water mass fraction along the control volumes of the packed bed for the case of evaporation and no evaporation

There are small differences between the values of the x_{H_2O}, where them of the 50 second case seem to have higher deviation between the peak and the valleys compared to the second case. All these deviations are small and are the outcome of the other smaller deviations in the system, like temperature, $\frac{ppmvSO_2}{y_{CO_2}}$ and other. The model is designed in such a way, that is control volume oriented and the changes of every parameter in the control volume affect also the other parameters.

BIBLIOGRAPHY

REFERENCES

[1] European Environment Agency, (EEA), *Air pollutant emissions data viewer (gothenburg protocol, lrtap convention) 1990-2016,* (July 12, 2018), last accessed 09 April 2019.

[2] European Environment Agency, (EEA), *Emissions of the main air pollutants in europe,* (October 16,2018), last accessed 5 April 2019.

[3] International Council on Clean Transportation (ICCT), *Air pollution and greenhouse gas emissions from ocean-going ships,* (2007), last accessed 15 April 2019.

[4] L. Johansson, J.-P. Jalkanen, and J. Kukkonen, *Global assessment of shipping emissions in 2015 on a high spatial and temporal resolution,* Atmospheric environment **167**, 403 (2017).

[5] International Maritime Organization (IMO), *Sulphur oxides (sox) and particulate matter (pm) – regulation 14,* (2019), last accessed 10 April 2019.

[6] International Maritime Organization (IMO), *AIR POLLUTION AND ENERGY EFFICIENCY: Study on effects of the entry into force of the global* 0.5% *fuel oil sulphur content limit on human health, Submitted by Finland,* (2016), last accessed 14 April 2019.

[7] G. Joseph and D. Beachler, *Scrubber systems operation review: self-instructional manual,* Prepared for the United States Environmental Protection Agency under Cooperative Assistance Agreement CT-902765 by North Carolina State University, Raleigh, NC1998 (1998).

[8] B. Mestemaker, *Exhaust gas after treatment, technology assessment,* MTI Holland B.V. **DIV 217A** (2013).

[9] N. Atkinson and O. Lejeune, *Oil 2019 – analysis and forecasts to 2024,* (26 March, 2019), international Energy Agency (IEA), Last accessed 06 May 2019.

[10] L. Jiang, J. Kronbak, and L. P. Christensen, *The costs and benefits of sulphur reduction measures: Sulphur scrubbers versus marine gas oil,* Transportation Research Part D: Transport and Environment **28**, 19 (2014).

[11] NIST Chemistry WebBook, SRD 69, *Antoine equation parameters for water,* (2018), last accessed 02 September 2019.

[12] NIST Chemistry WebBook, *Molar mass of gases,* (2019), last accessed 04 August 2019.

[13] M. J. Moran and H. N. Shapiro, *Fundamentals of engineering thermodynamics*, 5th ed. (John Wiley & Sons, 2006).

[14] F. M. White, *Fluid Mechanics*, 7th ed. (Mcgraw-Hills, 2011).

[15] R. C. Reid, J. M. Prausnitz, and B. E. Poling, *The properties of gases and liquids,* (1987).

[16] H. Perry Robert, W. Green Don, and O. Maloney James, *Perry's chemical engineers' handbook,* Mc Graw-Hills New York (1997).

[17] B. E. Poling, J. M. Prausnitz, J. P. O'connell, *et al.*, *The properties of gases and liquids*, Vol. 5 (Mcgraw-hill New York, 2001).

[18] European Environment Agency, (EEA), *International chamber of shipping,* (2015), last accessed 09 April 2019.

[19] K. Zavitsas, T. Zis, and M. G. Bell, *The impact of flexible environmental policy on maritime supply chain resilience,* Transport Policy **72**, 116 (2018).

[20] K. Cullinane and S. Cullinane, *Policy on reducing shipping emissions: implications for "green ports",* in *Green Ports* (Elsevier, 2019) pp. 35–62.

[21] L. Van Biert, *Solid oxide fuel cells, System integration concepts with reforming and thermal cycles* (Phd dissertation, 2020).

[22] D. Flagiello, A. Erto, A. Lancia, and F. Di Natale, *Experimental and modelling analysis of seawater scrubbers for sulphur dioxide removal from flue-gas,* Fuel **214**, 254 (2018).

[23] K. Brown, W. Kalata, and R. Schick, *Optimization of so2 scrubber using cfd modeling,* Procedia Engineering **83**, 170 (2014).

[24] C. Brogren and H. T. Karlsson, *Modeling the absorption of so2 in a spray scrubber using the penetration theory,* Chemical Engineering Science **52**, 3085 (1997).

[25] S. Darake, M. Hatamipour, A. Rahimi, and P. Hamzeloui, *So2 removal by seawater in a spray tower: Experimental study and mathematical modeling,* Chemical Engineering Research and Design **109**, 180 (2016).

[26] X.-J. Tang, T. Li, H. Yu, and Y.-M. Zhu, *Prediction model for desulphurization efficiency of onboard magnesium-base seawater scrubber,* Ocean Engineering **76**, 98 (2014).

[27] Y. Zhu, X. Tang, T. Li, Y. Ji, Q. Liu, L. Guo, and J. Zhao, *Shipboard trials of magnesium-based exhaust gas cleaning system,* Ocean Engineering **128**, 124 (2016).

[28] I. Boscarato, N. Hickey, J. Kašpar, M. V. Prati, and A. Mariani, *Green shipping: Marine engine pollution abatement using a combined catalyst/seawater scrubber system. 1. effect of catalyst,* Journal of Catalysis **328**, 248 (2015).

[29] S. Yang, X. Pan, Z. Han, D. Zhao, B. Liu, D. Zheng, and Z. Yan, *Removal of nox and so2 from simulated ship emissions using wet scrubbing based on seawater electrolysis technology,* Chemical Engineering Journal **331**, 8 (2018).

[30] A. M. Dashliborun, F. Larachi, and S. M. Taghavi, *Gas-liquid mass-transfer behavior of packed-bed scrubbers for floating/offshore co2 capture,* Chemical Engineering Journal **377**, 119236 (2019).

[31] R. Brouwer, *Dynamic Modelling of a SO2 - NaOH Scrubber System for Marine Applications* (Master Thesis Report, TU Delft, 2011).

[32] International Maritime Organization (IMO), *REDUCTION OF THE IMPACT ON THE ARCTIC OF BLACK CARBON EMISSIONS FROM INTERNATIONAL SHIPPING, Initial results of a Black Carbon measurement campaign with emphasis on the impact of the fuel oil quality on Black Carbon emissions, Submitted by Finland and Germany ,* (2019), last accessed 14 January 2019.

[33] Clarksons, *Sox scrubber fleet (fitted and pending),* (2020), last accessed 14 January 2020.

[34] E. Borsos, L. Makra, R. Béczi, B. Vitányi, and M. Szentpéteri, *Anthropogenic air pollution in the ancient times,* Acta climatológica et chorologica **36**, 5 (2003).

[35] J. J. Lennon, *Pollution and religion in ancient Rome* (Cambridge University Press, 2014).

[36] W. H. Te Brake, *Air pollution and fuel crises in preindustrial london, 1250-1650,* Technology and Culture , 337 (1975).

[37] F. Uekötter, *The age of smoke: environmental policy in Germany and the United States, 1880-1970* (University of Pittsburgh Pre, 2009).

[38] C. D. Cooper and F. C. Alley, *Air pollution control: A design approach* (Waveland Press, 2010).

[39] A. Petzold, E. Weingartner, J. Hasselbach, P. Lauer, C. Kurok, and F. Fleischer, *Physical properties, chemical composition, and cloud forming potential of particulate emissions from a marine diesel engine at various load conditions,* Environmental science & technology **44**, 3800 (2010).

[40] J. Colls and A. Tiwary, *Air pollution: measurement, modelling and mitigation* (CRC Press, 2017).

[41] B. I. Yentekakis, *Air pollution: Impacts, control and alternative technologies* (Klidarithmos Publications, 2010).

[42] F. Popescu and I. Ionel, *Anthropogenic air pollution sources* (INTECH Open Access Publisher, 2010).

[43] C. Hewitt, *Sulphur and nitrogen chemistry in power plant plumes,* Atmospheric Environment **35**, 1155 (2001).

[44] European Environment Agency, (EEA), *Industrial pollution in europe,* (August 06,2018), last accessed 5 April 2019.

[45] European Environment Agency, (EEA), *Sulphur dioxide (so2) emissions,* (September 4, 2015), last accessed 08 April 2019.

[46] R. Colvile, E. Hutchinson, J. Mindell, and R. Warren, *The transport sector as a source of air pollution,* Atmospheric environment **35**, 1537 (2001).

[47] K. F. Jensen and L. S. Dochinger, *Response of eastern hardwood species to ozone, sulfur dioxide and acid precipitation,* JAPCA **39**, 852 (1989).

[48] Z. L. Yang, D. Zhang, O. Caglayan, I. Jenkinson, S. Bonsall, J. Wang, M. Huang, and X. Yan, *Selection of techniques for reducing shipping nox and sox emissions,* Transportation Research Part D: Transport and Environment **17**, 478 (2012).

[49] Baltic Exchanges, *The shipping markets,* (April 09, 2019), last accessed 09 April 2019.

[50] V. Matthias, I. Bewersdorff, A. Aulinger, and M. Quante, *The contribution of ship emissions to air pollution in the north sea regions,* Environmental Pollution **158**, 2241 (2010).

[51] M. Viana, P. Hammingh, A. Colette, X. Querol, B. Degraeuwe, I. De Vlieger, and J. Van Aardenne, *Impact of maritime transport emissions on coastal air quality in europe,* Atmospheric Environment **90**, 96 (2014).

[52] D. Grewal and H. Haugstetter, *Capturing and sharing knowledge in supply chains in the maritime transport sector: critical issues,* Maritime Policy & Management **34**, 169 (2007).

[53] H. Ma, K. Steernberg, X. Riera-Palou, and N. Tait, *Well-to-wake energy and greenhouse gas analysis of sox abatement options for the marine industry,* Transportation Research Part D: Transport and Environment **17**, 301 (2012).

[54] V. Eyring, H. Köhler, J. Van Aardenne, and A. Lauer, *Emissions from international shipping: 1. the last 50 years,* Journal of Geophysical Research: Atmospheres **110** (2005).

[55] European Environment Agency, (EEA), *Emissions of air pollutants from transport,* (November 22, 2018), last accessed 09 April 2019.

[56] D. Stapersma, *Diesel Engines, A fundamental approach to performance analysis, turbocharging, combustion, emissions and heat transfer, Part II, Combustion, emissions and heat transfer, Volume 4, Emissions and Heat transfer,* (Royal Netherlands Naval College, 12 April 2010).

[57] I. Komar and B. Lalić, *Sea transport air pollution,* in *Current Air Quality Issues* (IntechOpen, 2015).

[58] T. Smith, J. Jalkanen, B. Anderson, J. Corbett, J. Faber, S. Hanayama, E. O'keeffe, S. Parker, L. Johanasson, L. Aldous, *et al., Third imo ghg study,* IMO (2015).

[59] H. Lindstad, *Strategies and measures for reducing maritime co2 emissions,* NTNU: Trondheim, Norway (2013).

[60] V. Duran, Z. Uriondo, and J. Moreno-Gutiérrez, *The impact of marine engine operation and maintenance on emissions,* Transportation research Part D: Transport and environment **17**, 54 (2012).

[61] H. Lindstad, G. S. Eskeland, H. Psaraftis, I. Sandaas, and A. H. Strømman, *Maritime shipping and emissions: A three-layered, damage-based approach,* Ocean Engineering **110**, 94 (2015).

[62] V. Eyring, I. S. Isaksen, T. Berntsen, W. J. Collins, J. J. Corbett, O. Endresen, R. G. Grainger, J. Moldanova, H. Schlager, and D. S. Stevenson, *Transport impacts on atmosphere and climate: Shipping,* Atmospheric Environment **44**, 4735 (2010).

[63] J. J. Corbett and P. Fischbeck, *Emissions from ships,* Science **278**, 823 (1997).

[64] C.-h. Han, *Strategies to reduce air pollution in shipping industry,* The Asian Journal of Shipping and Logistics **26**, 7 (2010).

[65] H. E. Lindstad and I. Sandaas, *Emission and fuel reduction for offshore support vessels through hybrid technology,* Journal of Ship Production and Design **32**, 195 (2016).

[66] International Maritime Organization (IMO), *Sulphur 2020 – cutting sulphur oxide emissions,* (2019), last accessed 10 April 2019.

[67] S. Bengtsson, K. Andersson, and E. Fridell, *A comparative life cycle assessment of marine fuels: liquefied natural gas and three other fossil fuels,* Proceedings of the Institution of Mechanical Engineers, Part M: Journal of Engineering for the Maritime Environment **225**, 97 (2011).

[68] MARPOL, *Annex vi- regulations for the prevention of air pollution from ships,* (2019), last accessed 10 April 2019.

[69] Hielscher Ultrasound Technology, *Ultrasonic marine fuel desulphurization,* (2019), last accessed 21 December 2019.

[70] Tecnoveritas, *Fuel desulphurisation,* (2019), last accessed 21 December 2019.

[71] Green Framework, *On board sulphur filtering,* (2019), last accessed 21 December 2019.

[72] A. Lauer, V. Eyring, J. Hendricks, P. Jöckel, and U. Lohmann, *Global model simulations of the impact of ocean-going ships on aerosols, clouds, and the radiation budget,* Atmospheric Chemistry and Physics **7**, 5061 (2007).

[73] P. Gilbert, *From reductionism to systems thinking: How the shipping sector can address sulphur regulation and tackle climate change,* Marine Policy **43**, 376 (2014).

[74] H. E. Lindstad, C. F. Rehn, and G. S. Eskeland, *Sulphur abatement globally in maritime shipping,* Transportation Research Part D: Transport and Environment **57**, 303 (2017).

[75] J. Kjølholt, S. Aakre, C. Jürgensen, and J. Lauridsen, *Assessment of possible impacts of scrubber water discharges on the marine environment,* København: Environmental Protection Agency, Danish Ministry of Environment (2012).

[76] N. Andritsos, *Lecture notes in Industrial Pollution Abatement Technology, Scrubbers,* (November, 2018), University of Thessaly, Department of Mechanical Engineers.

[77] H. Ülpre and I. Eames, *Environmental policy constraints for acidic exhaust gas scrubber discharges from ships,* Marine pollution bulletin **88**, 292 (2014).

[78] M. Koski, C. Stedmon, and S. Trapp, *Ecological effects of scrubber water discharge on coastal plankton: potential synergistic effects of contaminants reduce survival and feeding of the copepod acartia tonsa,* Marine environmental research **129**, 374 (2017).

[79] United States Environmental Protection Agency, (U.S. EPA) , *Sulfur dioxide basics,* (April 2,2019), last accessed 4 April 2019.

[80] United States Environmental Protection Agency, (U.S. EPA) , *Exhaust gas scrubber washwater effluent, epa-800-r-11-006,* (November,2011), last accessed 17 April 2019.

[81] R. M. Key, A. Kozyr, C. L. Sabine, K. Lee, R. Wanninkhof, J. L. Bullister, R. A. Feely, F. J. Millero, C. Mordy, and T.-H. Peng, *A global ocean carbon climatology: Results from global data analysis project (glodap),* Global biogeochemical cycles **18** (2004).

[82] J. Knutzen, *Effects of decreased ph on marine organisms,* Marine Pollution Bulletin **12**, 25 (1981).

[83] R. Jürgens, M. Mikaelsen, J. Heslop, and H. Oudman, *Technologies and Scenarios For Low Emissions Shipping, Project Number: SCP0-GA-2010-266126, Document ID: RJ-WP2- D2.1-V07-07/2011,* European Commission, CORDIS EU research results (2011).

[84] Exhaust Gas Cleaning Systems Association (EGCSA), *Dry exhaust gas cleaning system,* (2009), last accessed 23 April 2019.

[85] Exhaust Gas Cleaning Systems Association (EGCSA), *A practical guide to exhaust gas cleaning systems for the maritime industry,* (2012), last accessed 24 April 2019.

[86] O. Bockman, A. Tokerud, P. Gramme, S. Terjesen, and E. Thurmann-Nielsen, *Process for removal of sulphur dioxide from flue-gases by absorption in sea-water,* in *AFIPS Conference Proceedings* (1974).

[87] M. A. Borowitzka and A. W. Larkum, *Calcification in the green alga halimeda: Iii. the sources of inorganic carbon for photosynthesis and calcification and a model of the mechanism of calcification,* Journal of Experimental Botany **27**, 879 (1976).

[88] European Parliament and the Council of the European Union, *Directive on environmental quality standards (directive 2008/105/ec),* (December 16, 2008), last accessed 23 April 2019.

[89] CE Delft, *The impacts of egcs washwater discharges on port water and sediment,* (December 2019), last accessed 14 January 2020.

[90] I.-M. Karle and D. Turner, *Seawater scrubbing-reduction of sox emissions from ship exhausts,* AGS Office at Chalmers, GMV, Chalmers University of Technology, SE-41296 Gothenburg, Sweden , 26 (2007).

[91] N. Bialystocki and D. Konovessis, *On the estimation of ship's fuel consumption and speed curve: a statistical approach,* Journal of Ocean Engineering and Science **1**, 157 (2016).

[92] I. Panasiuk and L. Turkina, *The evaluation of investments efficiency of sox scrubber installation,* Transportation Research Part D: Transport and Environment **40**, 87 (2015).

[93] L. M. Abadie, N. Goicoechea, and I. Galarraga, *Adapting the shipping sector to stricter emissions regulations: Fuel switching or installing a scrubber?* Transportation Research Part D: Transport and Environment **57**, 237 (2017).

[94] A. Halff, L. Younes, and T. Boersma, *The likely implications of the new imo standards on the shipping industry,* Energy Policy **126**, 277 (2019).

[95] J. Antturi, O. Hänninen, J.-P. Jalkanen, L. Johansson, M. Prank, M. Sofiev, and M. Ollikainen, *Costs and benefits of low-sulphur fuel standard for baltic sea shipping,* Journal of environmental management **184**, 431 (2016).

[96] D. Osler, *Sox scrubber on vessels,* (2020), last accessed 14 January 2020.

[97] H. E. Lindstad and G. S. Eskeland, *Environmental regulations in shipping: Policies leaning towards globalization of scrubbers deserve scrutiny,* Transportation Research Part D: Transport and Environment **47**, 67 (2016).

[98] B. Mestemaker, *Exhaust gas after treatment, ocean going vessel application,* MTI Holland B.V. **DIV 217B** (2013).

[99] B. Schieldrop, SEB| Macro research, *Imo 2020 report 2,* (25 October, 2018), last accessed 07 May 2019.

[100] Ship and Bunker, *Global 20 ports average bunker price,* (19 May, 2019), last accessed 15 January 2020.

[101] European Commission, *Guide to Cost-Benefit Analysis of Investment Projects, Economic appraisal tool for Cohesion Policy 2014-2020,* (2014), last accessed 07 May 2019.

[102] V. Dabbaghian and V. K. Mago, *Theories and simulations of complex social systems* (Springer, 2014).

[103] D. M. Himmelblau and J. B. Riggs, *Basic Principles and Calculations in Chemical Engineering*, 7th ed. (Pearson Education, 2006).

[104] V. Bontozoglou, *Introduction to Physical Processes, Theoretical Background and Basic Applications (Εισαγωγή στις Φυσικές Διεργασίες)* (Kallipos Publications, 2015).

[105] W. L. McCabe, J. C. Smith, and P. Harriott, *Unit operations of chemical engineering*, 6th ed. (McGraw-hill New York, 2008).

[106] P. J. M. Schulten, *The interaction between diesel engines, ship and propellers during manoeuvring* (DUP Science, 2005).

[107] D. Stapersma, *Diesel Engines, A fundamental approach to performance analysis, turbocharging, combustion, emissions and heat transfer, Part I, Performance analysis and turbocharging, Volume 2, Turbocharging,* (Royal Netherlands Naval College, 12 April 2010).

[108] R. Billet and M. Schultes, *Prediction of mass transfer columns with dumped and arranged packings: Updated summary of the calculation method of billet and schultes,* Chemical Engineering Research and Design **77**, 498 (1999).

[109] D. Stapersma, *Diesel Engines, A fundamental approach to performance analysis, turbocharging, combustion, emissions and heat transfer, Part I, Performance analysis and turbocharging, Volume 1, Performance Analysis,* (Royal Netherlands Naval College, 12 April 2010).

[110] J.R. Richards (United States Environmental Protection Agency) , *Control of gaseous emissions, apti course 415, third edition, ices ltd. epa contract no. 68d99022,* (January 2000), last accessed 23 July 2019.

[111] N. Andritsos and V. Bontozoglou, *Mass Transfer Phenomena, Lecture notes in Transport Phenomena, University of Thessaly, Department of Mechanical Engineers,* (University of Thessaly Publications, April, 2019).

[112] J. A. Dean, *Lange's handbook of chemistry* (New york; London: McGraw-Hill, Inc., 1999).

[113] G. Vázquez, G. Antorrena, F. Chenlo, and F. Paleo, *Absorption of so2 by aqueous naoh solutions in the presence of a surfactant,* Chemical engineering & technology **11**, 156 (1988).

[114] P. Danckwerts, *Gas-liquid reactions. 1970,* New York: McGraw-Hill **147**, 115.

[115] F. P. Incropera, A. S. Lavine, T. L. Bergman, and D. P. DeWitt, *Fundamentals of heat and mass transfer* (Wiley, 2007).

[116] Sulzer, *Structured packings for distillation, absorption and reactive distillation,* (2004), last accessed 28 December 2019.

[117] RVT, *Tower packings for high performance,* (2012), last accessed 28 December 2019.

[118] International Maritime Organization (IMO), *ANNEX 1,RESOLUTION MEPC.259(68),(adopted on 15 May 2015),2015 GUIDELINES FOR EXHAUST GAS CLEANING SYSTEMS ,* (2015), last accessed 11 October 2019.

[119] Y. A. Çengel and M. A. Boles, *Thermodynamics: an engineering approach,*, 7th ed. (McGraw-Hill, 2010).

[120] Y. V. Lyulin and O. A. Kabov, *Measurement of the evaporation mass flow rate in a horizontal liquid layer partly opened into flowing gas,* Technical physics letters **39**, 795 (2013).

[121] E. G. Orlova, A. G. Islamova, and O. A. Kabov, *Evaporation rate of a liquid layer streamlined by gas flow in minichannel,* in *MATEC Web of Conferences*, Vol. 91 (EDP Sciences, 2017) p. 01028.

[122] S. He, Z. Guan, H. Gurgenci, K. Hooman, Y. Lu, and A. M. Alkhedhair, *Experimental study of film media used for evaporative pre-cooling of air,* Energy conversion and management **87**, 874 (2014).

[123] Y. Lyulin and O. Kabov, *Evaporative convection in a horizontal liquid layer under shear–stress gas flow,* International Journal of Heat and Mass Transfer **70**, 599 (2014).

[124] P. Gandhidasan, *Quick performance prediction of liquid desiccant regeneration in a packed bed,* Solar Energy **79**, 47 (2005).

[125] J. Schwartze and S. Bröcker, *The evaporation of water into air of different humidities and the inversion temperature phenomenon,* International journal of heat and mass transfer **43**, 1791 (2000).

[126] C. Debbissi, J. Orfi, and S. B. Nasrallah, *Evaporation of water by free or mixed convection into humid air and superheated steam,* International journal of heat and mass transfer **46**, 4703 (2003).

[127] L. Chow and J. Chung, *Evaporation of water into a laminar stream of air and superheated steam,* International Journal of Heat and Mass Transfer **26**, 373 (1983).

[128] H. Sapra, M. Godjevac, K. Visser, D. Stapersma, and C. Dijkstra, *Experimental and simulation-based investigations of marine diesel engine performance against static back pressure,* Applied Energy **204**, 78 (2017).

[129] R. Sander, *Compilation of henry's law constants for inorganic and organic species of potential importance in environmental chemistry,* (1999).

[130] R. Sander, *Compilation of henry's law constants (version 4.0) for water as solvent.* Atmospheric Chemistry & Physics **15** (2015).

[131] C.-T. Liu and W. T. Lindsay Jr, *Vapor pressure of deuterated water from 106 to 300. deg.* Journal of Chemical and Engineering Data **15**, 510 (1970).

[132] D. R. Stull, *Vapor pressure of pure substances. organic and inorganic compounds,* Industrial & Engineering Chemistry **39**, 517 (1947).

[133] J. Wesselingh, R. Krishna, *et al.*, *Mass transfer in multicomponent mixtures* (Delft University Press Delft, 2000).

[134] S. Brodkey Robert and C. Hersey Harry, *Transport Fenomena* (Mc. Graw-Hill, Inc. New York).

NOMENCLATURE

Abbreviations

CAPEX	Capital Expenditure
CLRTAP	Convention on Long-range Transboundary Air Pollution
ECA	Emission Control Areas
EEA	European Environment Agency
EU	European Union
GHG	Green House Gases
HFO	Heavy Fuel Oil
ICCT	International Council on Clean Transportation
IEA	International Energy Agency
IMO	International Maritime Organization
KE	Kinetic Energy
LSFO	Low Sulpfur Fuel Oil
MARPOL	International Convention for the Prevention of Pollution from Ships
MCR	Maximum continuous rating
MDO	Marine Diesel Oil
MEPC	Marine Environment Protection Committee
NECD	National Emission Ceilings Directive
NPV	Net Present Value
OPEX	Ooperational Expenses
PE	Potential energy
SEB	Skandinaviska Enskilda Banken
SECA	Sulphur Emission Control Areas
UVR	Ultraviolet radiation
VLSFO	Very Low Sulphur Fuel Oil

Greek symbols

Symbol	Name	Unit
α	speciffic surface area	m^2/m^3
γ	ratio of speciffic heat	[-]
δ	liquid film thickness	m
ε	void fraction	[-]
ζ	resistance factor in the inlet	[-]
λ	air excess ratio	[-]
λ	heat conductivity	$J/(s \cdot m \cdot K)$
μ	Dynamic viscosity	$kg/m \cdot s$
π	pressure ratio	[-]
π	number pi	[-]
ρ	Density	kg/m^3
υ	velocity	m/s
Φ	mass transfer (mass based)	kg/s
ϕ	association factor of solvent B	[-]
Ψ	pressure function	[-]

Roman symbols

Symbol	Name	Unit
A	Surface	m^2
c	molar concentration	$mole/m^3$
C	cost	Euro
c_p	Specific heat at constant pressure	J/kg/K
c_v	Specific heat at constant volume	J/kg/K
d	diameter	m
D	difussion coefficient	m^2/s
g	gravitational acceleration	m/s^2
GT	Gross tonage	ton = 1000kg
$\mathbb{H}$	Henry's constant	Pa
H	Enthalpy	J
h	specific enthalphy	J/kg
h	holdup	[-]
h_c	heat transfer coefficient	$J/(m^2 \cdot s \cdot K)$
J	Flux	$kmole/m^2 \cdot s$
k_c	mass transfer coefficient, cocentration based	m/s
K_g	Total mass transfer coefficient	$kmol/m^2/s$
k_y	mass transfer coefficient, molar fraction based	$kmol/m^2/s$
L	liter	m^3
m	mass	kg
M	Molar mass	kg/kmole
$\dot{m}$	mass flow	kg/s
mt	million tones	mt
$\mathbb{N}$	Mass transfer (mole based)	kmole/s
$\dot{n}$	molar flow	kmole/s
P	power	W or J/s
p	pressure	Pa
ppm	parts per million	ppm
Pr	Prandtl number	[-]
$\dot{Q}$	Heat flow	J/s
$\dot{q}$	heat flux	$J/(m^2 * s)$
R	Gas constant	J/kg/K
R_u	Universal Gas Constant	J/mole/K
Re	Reynolds number	[-]
Sc	Schmidt number	[-]
sfc	specific fuel consumption	g/kWh
Sh	Sherwood number	[-]
t	time	s
T	Temperature	K
U	Internal energy	J
u	speciffic internal energy	J/Kg
V	Volume	m^3
W	watt	W
w	absolute humidity	kg/kg
$\dot{W}$	work	J/s
x	mass fraction	[-]
y	molar fraction	[-]
V_A	molar volume of solute A at its normal boiling temperature	$m^3/mole$
St	Stanton number	[-]
Nu	Nusselt number	[-]

Subscripts

Symbol	Name
b	bulk of the phase
crit	critical
cv	control volume
dem	demister
eff	effective
evap	evaporation
f	flow
g	gas
h	hydraulic
i	interface
in	inflow
ℓ	liquid
loss	quantity losses
lv	lower volume
nc	number of components
net	net flow/net accumulation
out	outflow
p.a	projected area
pb	packed bed
r	reaction
ref	reference
s	superficial
sat	saturation
sc	scrubber
tot	total
uv	upper volume
vent	venturi
vs	vertical surface
w	wet